THESIS

This is to certify that the

thesis entitled

AN EXPERIMENTAL STUDY OF THREE-DIMENSIONAL STRAIN AROUND COLDWORKED HOLES AND IN THICK COMPACT TENSION SPECIMENS

presented by

Somnuek Paleebut

has been accepted towards fulfillment
of the requirements for

Ph.D. degree in Mechanics

Gary Lee Cloud
Major professor

Date 24 Feb 1982

O-7639

RETURNING MATERIALS:
Place in book drop to remove this checkout from your record. FINES will be charged if book is returned after the date stamped below.

AN EXPERIMENTAL STUDY OF THREE-DIMENSIONAL STRAIN AROUND COLDWORKED HOLES AND IN THICK COMPACT TENSION SPECIEMNS

By

Somnuek Paleebut

A DISSERTATION

Submitted to
Michigan State University
in partial fulfillment for the requirements
for the degree of

DOCTOR OF PHILOSOPHY

Department of Metallurgy, Mechanics and Materials Science

1982

ABSTRACT

AN EXPERIMENTAL STUDY OF THREE-DIMENSIONAL
STRAIN AROUND COLDWORKED HOLES AND
IN THICK COMPACT TENSION SPECIMENS

By

Somnuek Paleebut

This research investigated and developed a new three-dimensional multiple Embedded Grid Moire Method for measuring the strain field in the interior and on the surface of specimens in order to study currently important problems in mechanics and structural design. Coldwork specimens and compact tension specimens which were made from transparent material were used. Specimens were fabricated with multiple embedded grids. These grids were photographed for each specimen state. Moire fringe photographs were extracted from the replicas by coherent optical processing. Digital analysis of the fringes gave the desired strain maps.

The three-dimensional nature of radial, hoop, and transverse strains which are created by drawing a tapered mandrel through a cylindrical hole were measured. The residual radial strain after coldwork inside the specimen was found to be smaller than on the surface. The transverse strain changes from tension near the top surface where the mandrel enters to maximum compression at the mid-plane, where it begins to decrease. The hoop strain is minimum at the mid-plane. The change in this component is only

about four percent of maximum value. Potential problems in the use of such a coldworking process might arise from the low value of the interior residual strain in comparison with the surface value and the existance of tensile transverse normal strain near the surface.

The static strain distribution near the crack tip on the surface plane and three interior planes of polycarbonate compact tension specimens were studied. The strains results that were obtained from the moire method are in good agreement with strain measurement from similar specimens with embedded strain gages. Near the crack tip strain ε_y (perpendicular to the crack line) was found to be much larger than strain ε_x on any plane along the specimen thickness. Therefore, strain ε_y is more important. Strain ε_y on the mid-plane was found to be larger than on the surface, and it causes the fracture to start on the mid-plane. The maximum strain ε_y on the mid-plane lies along the crack plane, but on the surface it starts from the crack tip and lies along two separate lines.

ACKNOWLEDGEMENTS

This research was supported by the National Science Foundation under grant ENG 78-02530. The author is grateful to National Science Foundation and Program Director Dr. Clifford Astill.

The author would like to give grateful thanks to The Royal Thai Air Force which sponsored my graduate program.

The author wishes to express my sincerest appreciations and gratitude to his advisor, Professor Gary Lee Cloud, for his encouragement and many valuable guidances during the course of this work. Thanks are also extended to the other members of his guidance committee, Dr. N. Altiero, Dr. J. Martin and Dr. N. Hills. Special thanks are due to Dr. N. Altiero and Dr. R. Abeyaratne for their suggestions during the course of this investigation.

Finally the author wishes to thank his wife, Arasiri, and son, Ayudh, for their understanding, help, patience and encouragement.

TABLE OF CONTENTS

LIST OF TABLES

LIST OF FIGURES

CHAPTER 1

INTRODUCTION

Methods derived from linear elasticity are not in general sufficient to complex problems involving plastic deformation, fatigue and fracture. It is important to consider nonlinear elastic, plastic, viscoelastic, and viscoplastic responses as well as the nonhomogeneous and nonisotropic responses of material.

Experimental and theoretical three-dimensional strain analysis can be accomplished by only a few methods. Few problems have been solved completely by the theory of elasticity. Three-dimensional photoelasticity, on the other hand, has found widespread application in its many forms. Methods involving locking-in stress in a photoelastic model are common one. All of these techniques are destructive in that they require slicing of the model. A nondestructive photoelastic technique uses scattered light. The photoelastic technique, in general, suffers from the limitation that it is not sufficient in itself, and it requires complementary methods for the separation of stresses. Another approach is the embedded grid moire method, which might be easier to implement. The moire method is basically

two-dimensional. Three dimensional analysis is accomplished through successive applications of the technique to various planes of a specimen. The moire technique is no different in this respect from most other methods, including three-dimensional photoelasticity, which requires optical or physical slicing of the specimen. The embedded grid moire method is similar to layered model photoelasticity in that only one plane or, in certain cases, a few planes can be analyzed for any one specimen. The application of a cross-grid to analyze a two-dimensional strain field was discussed by Post (1), while applications for three-dimension strain analyses using an embedded grid in clear epoxy-resin and urethane-rubber models were made by Durelli and Daniel (2) and by Sciammarella and Chiang (3).

1.1 Purpose and Motivation

The purpose of this research are:

a) to develop a new three-dimensional moire method using multiple embedded and surface grating. The method requires that interior gratings be photographed through an intervening surface grating.

b) to measure strain around a coldworked hole through the thickness of a polymeric specimen and;

c) to measure the strain components near a crack tip on the surface and in the interior of a thick specimen.

1.2 Coldworked Specimens

Crack initiation and growth are major causes of failure of high performance structural components and source of difficulty to the designer. A 1971 review of aircraft structure failure showed that cracks which began at fastener holes were preliminary causes of one-third of early failures (4). One class of techniques for improving the fatigue performance of fasteners is to plastically deform the hole prior to or during installation of the fastener. This deformation is accomplished by preexpansion of the holes with an oversize mandrel.

The surface strains and stresses around coldworked holes have been studied by many researchers. The nature of the strain fields around a coldworked hole was studied experimentally by Adler and Dupree (5) and by Sharpe (6). Sharpe and Chandawanich (7) studied the change of the residual strain field around coldworked holes during the initiation of cracks. Sharpe and Poolsuk (8) studied the elastic-plastic boundary and thickness changes around the coldworked hole. Cloud (9) investigated and described the nature of surface strain near the coldworked hole. Cloud and Tipton (10) and Cloud and Sulaimana (11) observed the strain distributions and effects of a row of holes which

were parallel to and near a straight edge after coldworking. No experimental work has been done concerning the change of residual strains along the thickness of coldworked specimens, and no theory of coldworked holes is available which accounts for interior behavior.

Given the nature of the mandrelizing process, the strain field near a coldworked hole is probably three-dimensional. The degree and direction of residual strains might change from one side to the other side of the specimen.

The three-dimensional nature of the radial, hoop, and transverse strains created by mandrelizing were explored to establish whether the interior value of the strain correlated well with surface measurements. The embedded grid moire method was developed to measure interior values of the strain in both vertical and radial directions on a plane of symmetry through the hole center.

A transparent specimen with a grating plane (nickel mesh) at the center was coldworked by loading in four steps. A data plate was recorded at each step. The strains in the radial and vertical directions were obtained by using the fringe data reduction method developed by Cloud (9). It was expected that the strain field would not be symmetrical on both sides of the hole and not uniform along the thickness. The strain field along the thickness was measured to within 0.01 inches (0.254 mm) of the hole boundary.

1.3 Thick Compact Tension Specimens

Many researchers have measured surface stress and strain states in the vicinity of a crack by various methods, primarily as a step towards obtaining stress intensity factors (12, 13, 14, 15), although some have been interested in exploring the fundamental assumptions and limitations of fracture mechanics (16, 17, 18). Post (19) pointed out the need for an experimental study of the three-dimension character of the crack tip stress state. Baker and Fourney (20) investigated the stress intensity factor along the crack front by using an interferometric method. Cases where yielding is involved have not been investigated. Pitoniak, Grandt, Montulli and Packman (23) observed crack retardation and crack closure in polymethylmethacrylate, and found that the crack tip opening displacement (COD) values in the interior could be much different from the surface values. Hahn and Rosenfield (21) and Underwood and Kendall (22) found a difference in the shape of the plastic zone on the surface plane and the mid-plane of a crack specimen.

In this investigation polycarbonate compact tension specimens with gratings on the surface, quarter and mid-plane were studied. Strains (ε_x and ε_y) on the surface and in the interior were measured by using the multiple embedded grid moire method; results were compared with strain measurements that were obtained from the specimens with strain gages. The results from both methods were in good agreement. Near the crack tip along the crack line strain

ε_y was found to be much greater than ε_x both on the surface and in the interior. Strain ε_y was maximum on the mid-plane. On the mid-plane the maximum strain ε_y starts from the crack tip and lies on the crack plane. On the surface plane, however, the maximum strain ε_y lies on two separate lines radiating from the crack tip.

1.4 Organization of the Dissertation

The experimental technique for grid deposition is described in the beginning of Chapter 2. The multiple embedded grid moire method is also described in Chapter 2.

Description of the material used in this investigation, their properties, and details on specimen preparation are given in Chapter 3.

Chapter 4 describes and discusses the results from coldworked specimens. A summary of results is given at the end of this chapter.

Chapter 5 describes and discusses the results from crack specimens. The first experimental results from crack specimens are described and discussed in the beginning of this chapter. The final results are compared with the results that were obtained from strain gages. A discussion and summary of the results are also given at the end of this chapter.

This dissertation concludes with Chapter 6 which summarizes the findings of the investigation.

CHAPTER 2

SUMMARY OF MOIRE TECHNIQUE

2.1 Fundamentals of the Moire Method

Moire fringes are produced by the interference of two grids; they are formed by two grills of parallel lines that are slightly different in pitch and/or orientation (64). Figure 2.1 illustrates the basic idea. It is possible to measure displacements and strains with this method by recording a specimen grid twice, once in the undeformed state and once in the deformed state. Superposition of the two images formed will produce moire fringes. Displacement can then be determined directly from the fringe patterns. Differentiation of the displacement data establishes the strains.

There are three simple ways to perform the superposition and obtain moire fringes. One method is to bring a reference grill, which is often on a glass plate, directly into contact with the specimen grill. The interference between these two grills gives moire fringes. In this case, intimate contact is essential to produce satisfactory results.

In the second method, the image of the model grill is projected onto the reference grill on a glass plate with a precision camera. The interference fringe formed on the

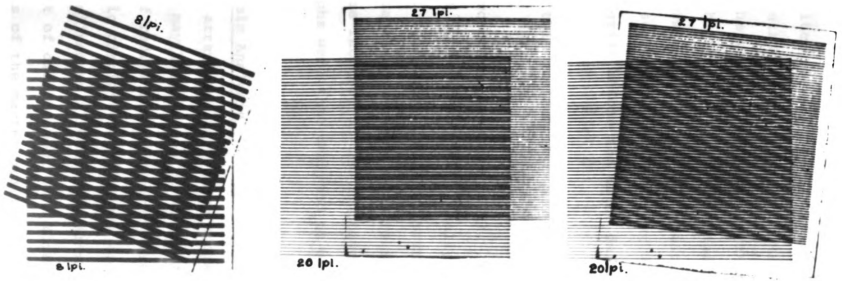

(a) (b) (c)

Figure 2.1 Moire Fringe Patterns Formed by (a) Rotation, (b) Difference in Pitch and (c) Combination of Rotation and Difference in Pitch.

glass plate are then recorded by a second camera. With this method, pitch mismatch and rotational mismatch can be readily introduced. The slight change of the magnification of the camera introduces pitch mismatch.

In the third method, the image of the model grill before deformation and after deformation can be recorded on photoplates. The interference of the two images of the same grill before and after deformation give moire fringes.

For this project, two photoplates were used for each specimen. One plate records the undeformed grill and the other records the deformed grill. Then the photoplates were each superimposed individually with the same submaster to form moire fringe patterns. By using an optical data processing system, the moire fringe patterns from each plate were recorded on the negative film. The moire fringe photographs were then analyzed to obtain displacements and strains.

2.2 Strain Analysis

The array used to produce moire fringes for strain analysis may be a series of straight parallel lines, a series of radial lines eminating from a point, a series of concentric circles, or a pattern of dots. A moire fringe can be defined as a locus of points which have the same component of displacement in a direction perpendicular to the lines of the master grating.

A simple moire fringe pattern can be obtained by using transmitted light through a deformed moire grill and an undeformed master as shown in Figure 2.2. In certain areas, the light is blocked, causing a moire fringe. Examination of the sketch will show that one dark band appears every time eight grill lines on the model have been stretched to fill the space of nine on the undistorted master array. One may number the moire fringes consecutively starting anywhere. Then, beginning from the corresponding point on the model, the relative displacement between the model and the master is easily calculated to be

$$U = Np$$

where U = component of displacement

N = moire fringe order

p = pitch of master

from

$$\varepsilon_x = \frac{\partial U}{\partial x} = \frac{\partial (Np)}{\partial x}$$

where ε_x = strain in x-direction.

From the above, it can be seen that strain in a direction perpendicular to the orientation of the specimen grating is simply the pitch of the analyzer grating multiplied by the slope of the fringe order plot at the point in question. The steps from moire fringe pattern to strain distribution are illustrated in Figure 2.3.

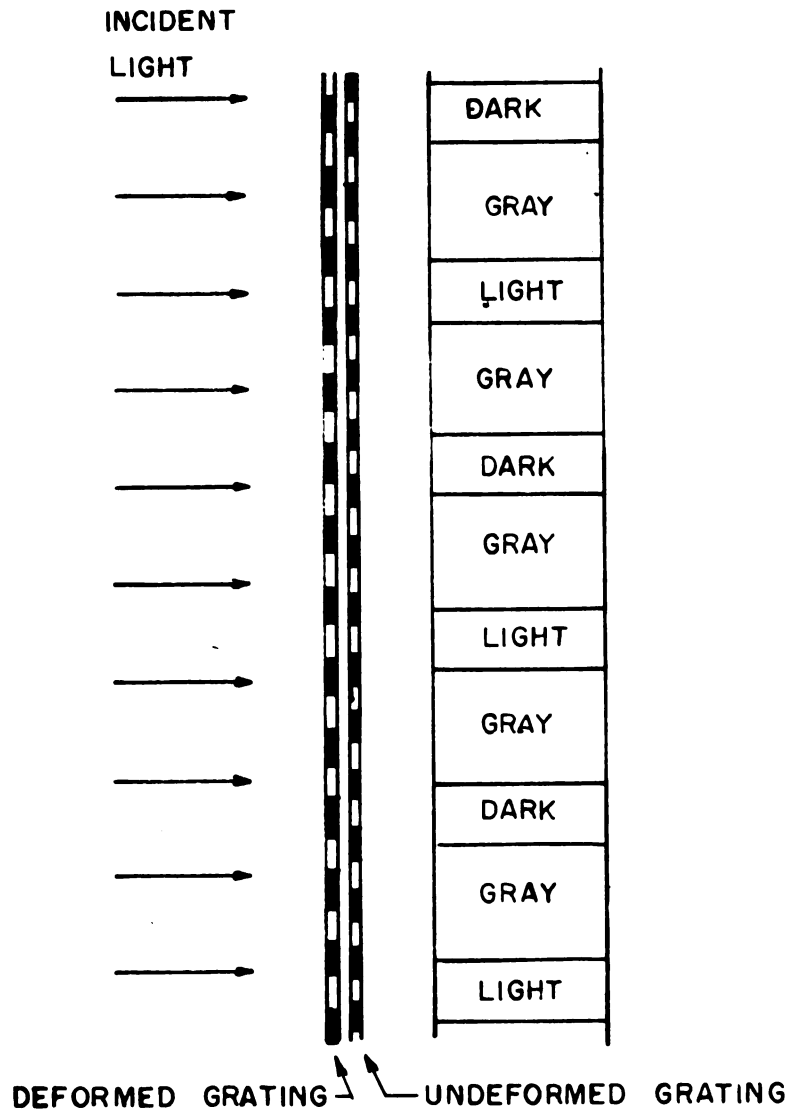

Figure 2.2. Formation of a Moire Fringe.

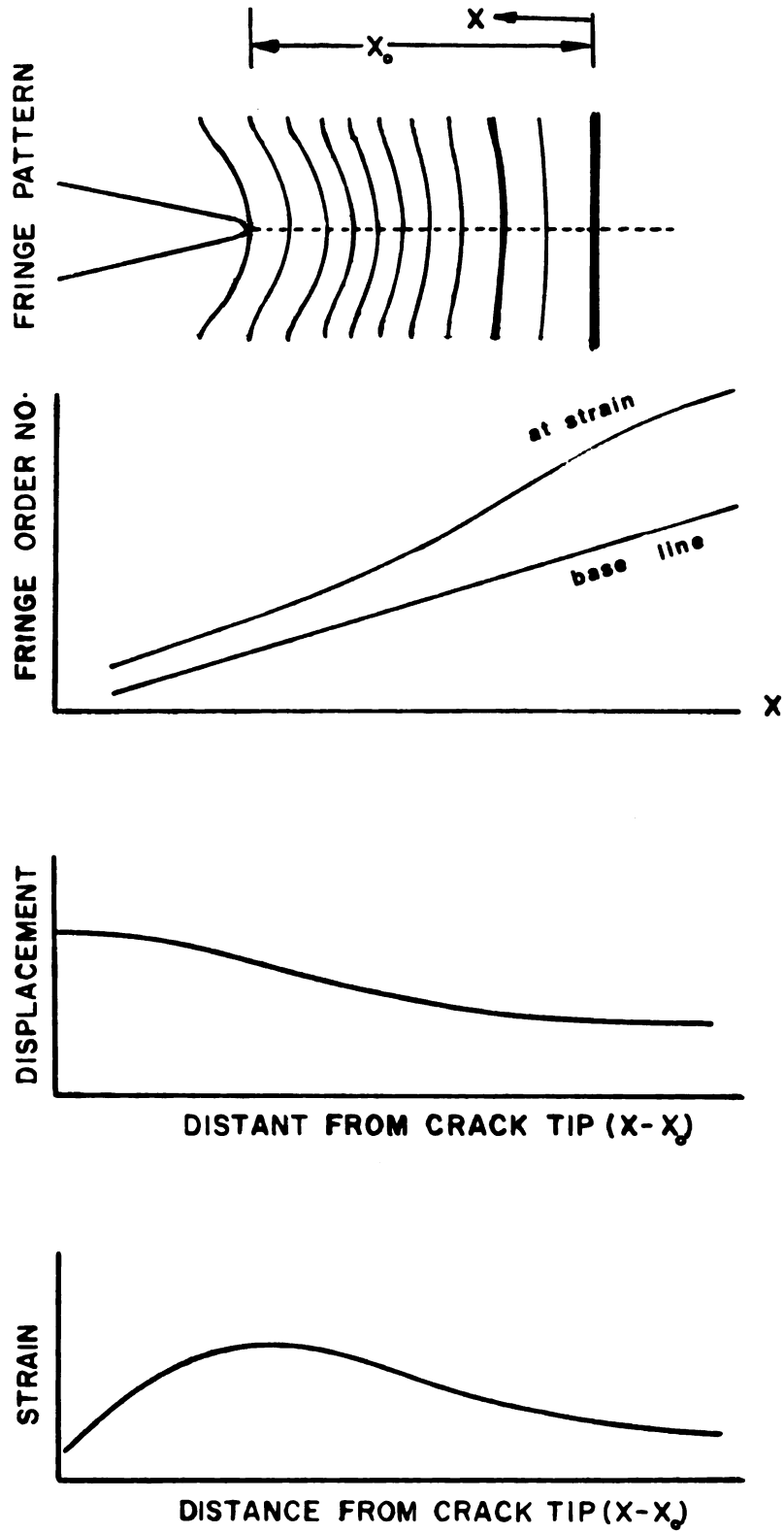

Figure 2.3 Progression of the Data Reduction Procedure Required in Moire Strain Analysis.

For any displacement field, as grating frequency is increased, so also is the number of moire fringes. Increasing fringe density gives better definition to the displacement field. This results in increased efficiency in the differentiation of the experimental data from which the strains are determined. The use of high density moire gratings is sometimes not wise in that there tends to be problems in handling and application.

2.3 Producing Submaster Gratings

Direct photographic reproduction was employed in the manufacture of the several submaster gratings required for the optical data processing of the specimen grating photographs. Several of each gratings having spatial frequencies of 125, 215, 230, 260, 266, and 270 lines per inch were produced. These values are ½ and ¼ times the fundamental spatial frequency of the master grating photographs (500 or 1000 lpi divided by magnification used) plus or minus various frequency mismatches.

Figure 2.4 shows a sketch of the apparatus used. The 1000 lpi (or 500 lpi) master grating was held in a laboratory clamp base and backlit with light from a slide projector. A ground glass plate was placed about 3-5 inches behind the grating to scatter the incident light. The lens and camera were the same as those used in photographing the specimen grating (see section 4.2.2). The whole set-up rested upon an optical bench. The camera to subject

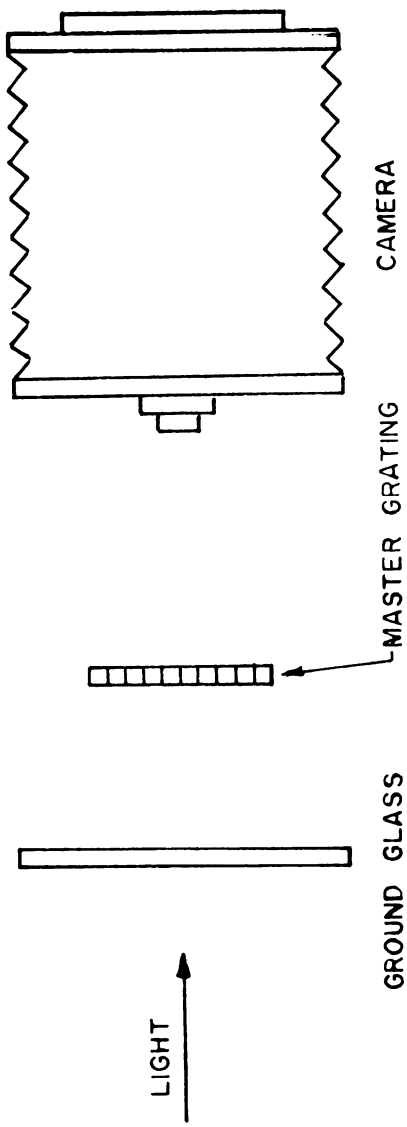

Figure 2.4. Sketch of a set-up for Photographically Producing a Submaster Grating.

grating distances were estimated by calculation and finalized by trial and error to give the correct submaster grating frequency on the photographic plate. The focus of the grating image on the emulsion side of the focus plate was checked to see that the critical dimensions were maintained over the field. The focus plate was made of a developed and a fixed unexposed film plate of the same type that was used in the photography.

In theory, it is best to use a large lens opening for greatest sharpness and resolution in such a demanding situation, and this was done for most of the grating copies. For this study white light was used as a light source, and Kodak Highspeed Holographic plates, type 131-02, were used to make all submasters.

2.4 Specimen Grid Deposition

Application of the moire effect to any problem depends on the successful deposition of line grids (or dots) on the specimen material.

Several methods were developed for this study. The measurement required a two-way grating to obtain the strain in two directions (vertical and horizontal direction), and the grid on the specimen surface had to be useable after the other piece of transparent material was glued over it. It was found that photoresist could not be used to make a grating on the specimen surface because it would be destroyed

when the other piece was glued over it. Therefore, copper gratings were used throughout of this study. The specimen with a copper grating inside gave fairly good results. In this study, two methods were used to make a copper grating, the etching method and the stencil method.

With the etching method, after the specimen was cleaned, a thin film of copper was deposited on the area of interest by using a Denton D.V.-502 High Vacuum Evaporator. The specimen was sprayed with photoresist to cover the thin copper film. The two way grating was printed by using a submaster grating having 1000 lpi (40 lpmm). Finally, the copper was etched with P.C. Board Etching Solution diluted with water 1:3 and brushed one way. The specimen was then washed by water. This grating application process is summarized in Figure 2.5. A photograph of the copper grating made by the etching method is shown in Figure 2.6a.

In the stencil method, a fine metal mesh with an orthogonal array of holes was used. In this study, nickel mesh with 500 lpi (20 lpmm) was used. First, a nickel mesh was held in close contact with a specimen by spreading soap solution over it and then removing the surplus with filter paper. This procedure removed the solution from the holes but left the mesh secured by a thin liquid layer under the lines. The specimen and mesh were then placed in a vacuum unit, and copper was deposited through the holes of the mesh.

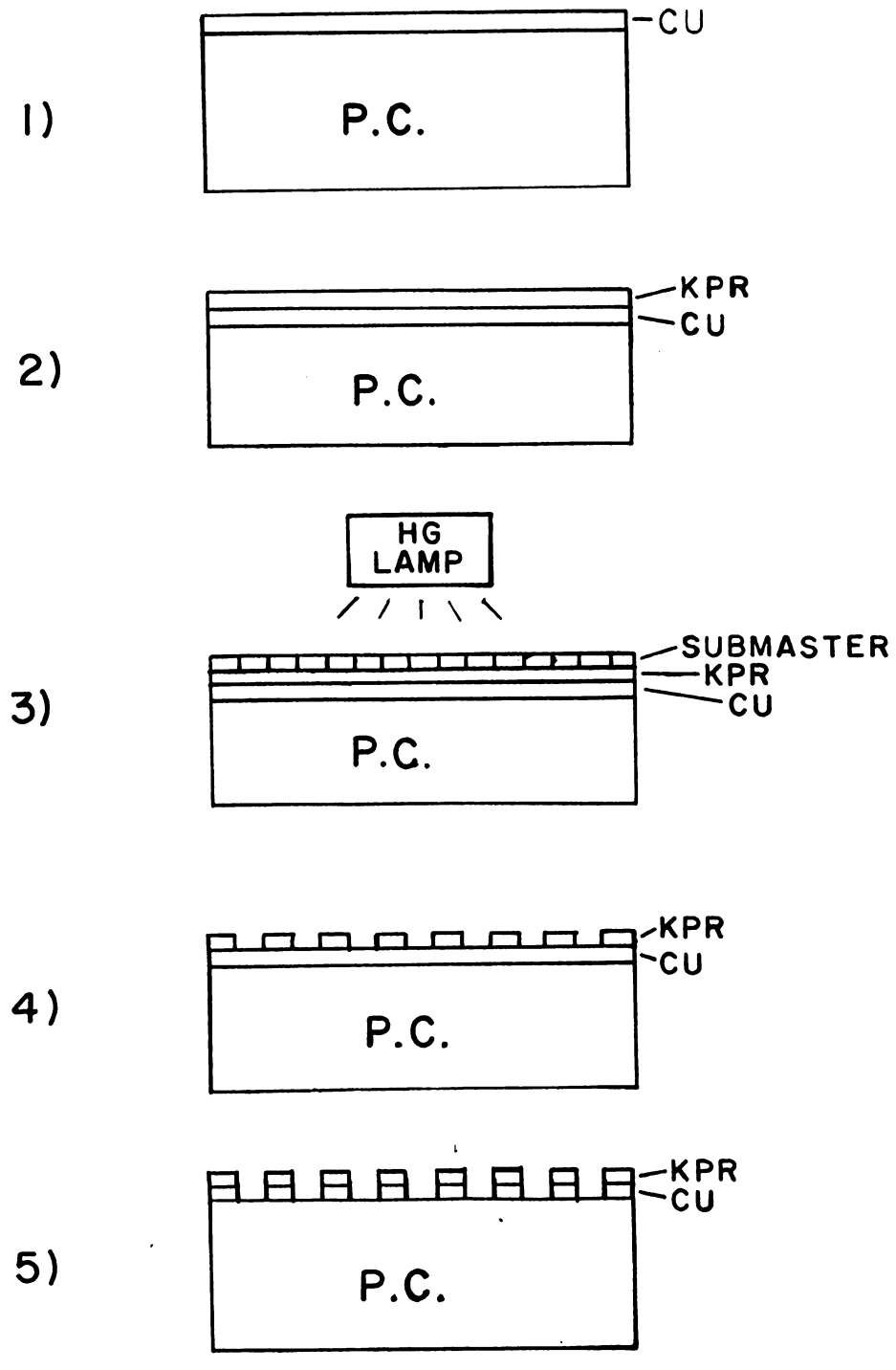

Figure 2.5 The Copper Grating Etching Process.

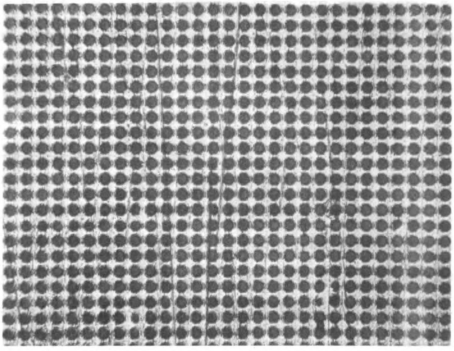

Figure 2.6a A Copper Grating by the Etching Method.

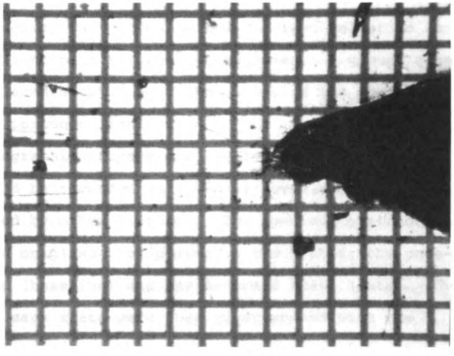

Figure 2.6b A Copper Grating by the Stencil Method.

Finally, the nickel mesh was removed from the specimen. A photograph of such a copper grating near the crack tip on the surface of a compact tension specimen is shown in Figure 2.6b.

2.5 Specimen Grating Photographs

The complete state of strain throughout an extended field can be determined from moire fringe photographs obtained through superposition of a submaster grating with deformed and undeformed (baseline) specimen grating replicas. Such a superposition yields baseline moire fringes and data (at strain) fringe patterns.

In this project, transparent material was used to make all specimens. Copper grating (or Nickle mesh) was printed on one (or two) planes in the interior of the specimen. The test specimen was placed on the specimen holder so as to let the light pass through the specimen. A ground glass plate was placed about 3 to 5 inches behind the specimen to scatter the incident light.

A photographic process was developed so that each grating could be recorded individually even though it might be obstructed by other gratings. The specimen grating was photographed on glass photoplates in two states; the undeformed state (baseline) and the deformed state (data). The plates from each state were then superimposed with the submaster plate in turn to produce the moire fringe photographs. The moire fringe patterns obtained from the data

plates of the interior grating are almost as good as those obtained from the data plates of the surface grating.

Three types of specimens were used for this study. The grating recording systems for each type of test specimens are described in section 4.2.2, 4.3.2, and 5.3.

2.6 Optical Data Processing System

Coherent optical data processing is an optical spatial filtering process that enables the experimentalist to bypass some of the pitfalls of real-time interferometry. The direct superposition of photoplates does not exploit the full potential of the information that is stored in the photoplates. Increased sensitivity and control of the measurement process is obtained by utilizing the basic procedures of optical data processing. The function and the theory behind optical data processing are outlined in papers and reports by Cloud (9,65). Physical phenomenon used by Cloud (9) to explain the optical filtering processes are the diffraction of light by a grating and the Fourier transform properties of lens. These two physical phenomena can both be used to explain moire fringe formation and fringe multiplication. As noted, both treatments can be used as the single explanatory model: or the two approaches can be combined and pursued to a single consistent model (9). The diffraction model is presented here.

Figure 2.7 illustrates the behavior of a single beam as it passes through a sinusoidal amplitude or phase grating.

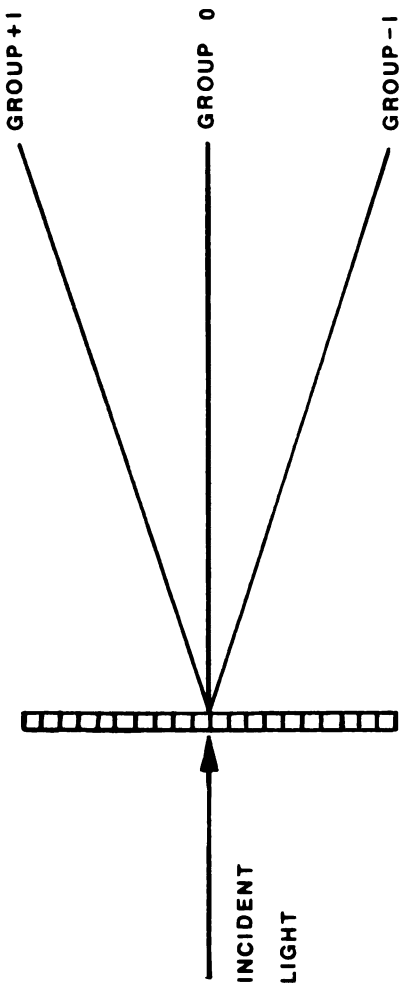

Figure 2.7 Diffraction of a Single Beam Passing Through a Sinusoidal Amplitude Grating.

The beam is divided into three parts or diffraction orders. The zero diffraction order is the undisturbed portion of the beam that passes directly through the grating and undergoes no diffraction. The other diffraction orders are numbered consecutively, either positive or negative, as they increase in their angular separation from the path of the incident beam. The angle of diffraction, θ, is dependent upon the spatial frequency (lines/inch) of the grating, the angle of incidence, and the wavelength of the light used for illumination.

When two sinusoidal amplitude gratings of nearly equal spatial frequency are superimposed, diffraction of the incident beam occurs at each of the grating as illustrated in Figure 2.8. It can be seen that one beam passing through the two gratings gives rise to five diffraction orders. As illustrated, the second ray group contains beam diffracted at both the gratings, while the first ray group is composed of beam diffracted from either of the two gratings. The two beams that comprise this first ray group diverge slightly from each other. The angular separation is due to pitch and orientational differences that occur between the two gratings.

A lens or imaging system (as in Figure 2.9) can be inserted into the path of the beams, and this causes the rays of one group to converge and overlap. From the rays of group 1, the imaging system constructs two separate images

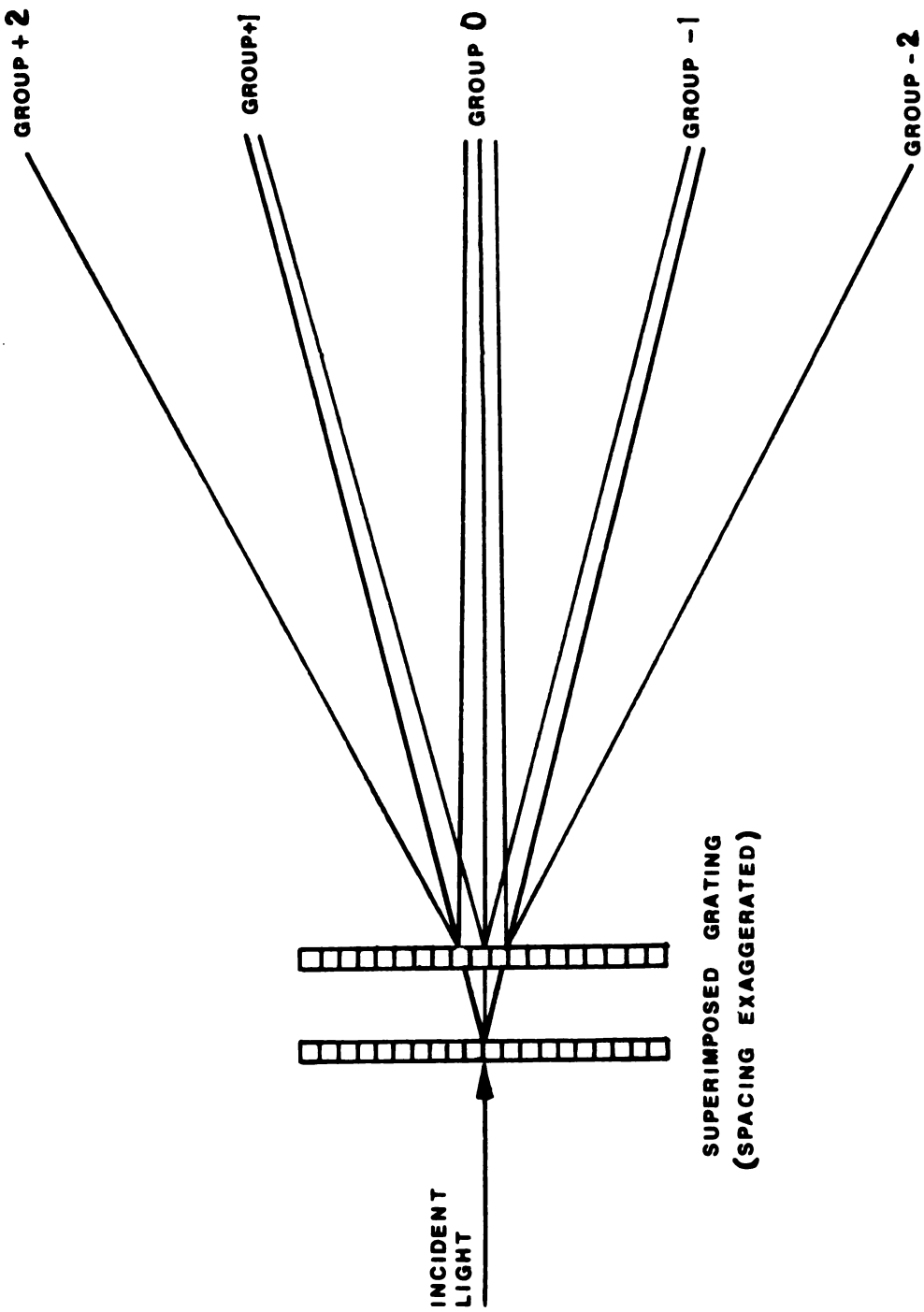

Figure 2.8 Diffraction of a Single Beam Passing Through two Superimposed Sinusoidal Gratings of Nearly Equal Spatial Frequency.

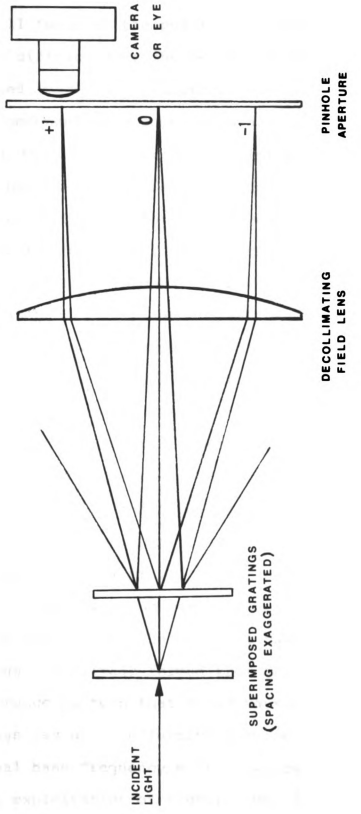

Figure 2.9 Imaging System used in the Formation of Moire Interference Patterns (Reference 9).

that lie atop one another. Rays diffracted from the first grating will focus at the position slightly displaced from those rays diffracted at the second grating. The two superimposed images will interfere with one another provided that the component beam comes from a source with sufficient coherence potential. The resulting interference pattern is a classic example of two beam interferometry. The degree of interference between the two images is dependent upon the spatial frequencies of the two gratings. A pattern of interference fringes becomes visible if the eye or a camera is placed at the focal plane of the imaging system and is used to view the image formed in a ray group.

The concept of the variability of moire sensitivity arises when consideration is given to the higher order of diffractions at the two superimposed gratings. Higher order diffractions lead to numerous ray groups or clusters of diffraction orders at the focal plane of the imaging system. Figure 2.9 illustrates that at the focal plane, these ray groups are oriented in a symmetrical distribution about the zero ray group. Each ray group corresponds to a grating frequency that is the multiple of the original base frequency of the two gratings. The image formed from any ray group contains an interference pattern that could have been obtained from two gratings having an effective grating frequency equal to the original base frequency multiplied by the ray group number. Such exploitation of higher order diffractions lead to moire sensitivity multiplication. There are some

difficulties with this multiplication technique. For example, the fringe pattern formed in each of the ray groups are not identical in overall clarity or intensity. Background noise caused by other diffractions can sometimes obscure and render useless the interference pattern formed in the image.

Consideration must be given to a common experimental situation in which the two superimposed gratings are very different in spatial frequency. This occurs when one grating is a multiple of the other, plus some small additional mismatch. The diffractions occurring at the two gratings are now somewhat more complicated, as is the composition of the various ray groups. Figure 2.10 illustrates the diffractions occurring at the gratings and the rays that comprise each of the associated ray groups, for the case when the fine grating is twice the frequency of the coarse grating. Given the natural attenuation of the higher order diffractions, only two of the component rays in any ray group will usually interact to form an interference pattern. The interference pattern so generated will correspond to an interference pattern constructed from two gratings of the higher spatial frequency. Again, general background noise that is present in some ray groups can serve to obscure the interference pattern. Since the interference in all ray groups is identical, it is best to use the ray group that provides the best fringe visibility. Throughout the study, this method of mismatched gratings was utilized as the means of moire fringe multiplication.

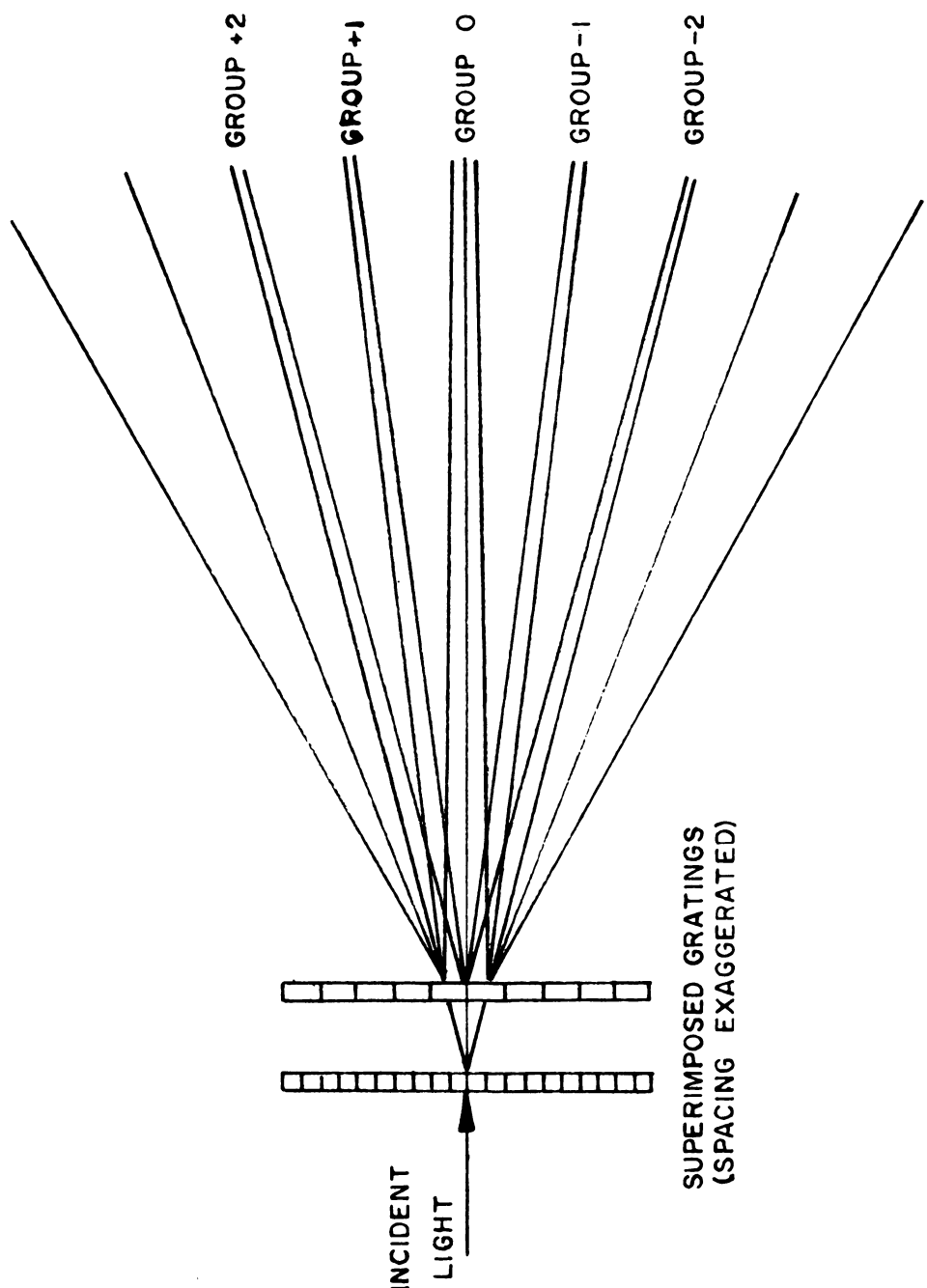

Figure 2.10 Diffraction of a Single Beam Passing Through Two Superimposed Gratings of Different Spatial Frequency.

Application of the diffraction models to moire analysis requires only that the previous models be applied to a whole field. In whole field analysis, specimen grating after deformation are not uniform, but vary in pitch and orientation from point to point. Superposition of a uniform analyzer grating with the nonuniform specimen grating will result in fringes which will also vary in their orientation and spacing.

Another approach to understanding the creation of moire fringes by superimposing specimen and master gratings in a coherent optical system is based on the fact that a simple lens acts as a Fourier transforming device. Consider the system shown in Figure 2.11. The first lens is a collimating lens. Two superimposed gratings (as shown in Figure 2.9) act as an optical signal to the collimated light that passes through. The light is modulated by diffraction at the two gratings and is brought to a focus by the decollimating lens. The focal plane of the lens is termed the Fourier transform plane. It is at the transform plane that there appears a diffraction pattern of the Fourier transform of the optical signal (superimposed gratings). As in the diffraction model, at the transform plane this diffraction pattern appears as a row of dot (ray groups); the position and brightness of these dots is indicative of the various harmonics of the grating. This occurs because a lens acts as a simple Fourier transform device (9).

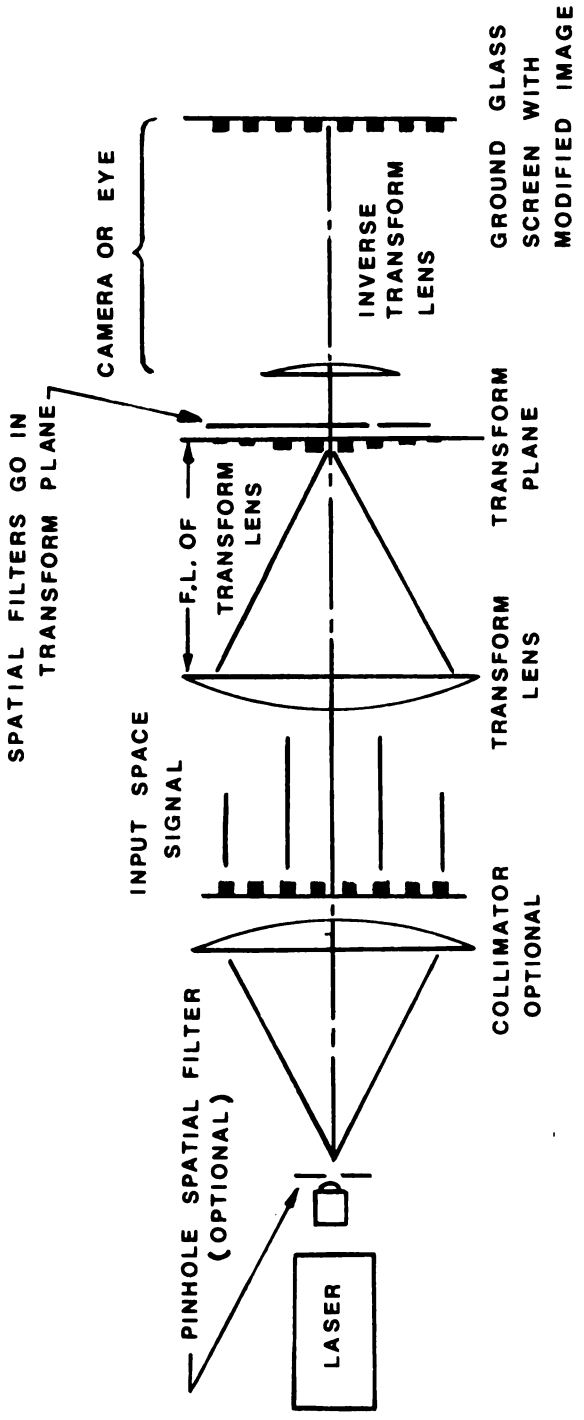

Figure 2.11 Optical System for Spatial Filtering in Fourier Transform Plane and Creation of Inverse Transform in Filter Image (Reference 9).

Coherent optical data processing, or spatial filtering, is the alteration of the light distribution at the transform plane. In moire analysis, spatial filtering is accomplished by the elimination of all frequency components undesirable in the formation of the moire interference pattern. In reference to the diffraction model, this filtering process is analogous to the elimination of all diffraction orders except the one of interest. Filtering at the transform plane is accomplished with an opaque mask with a single pinhole aperture. When the eye or a camera is placed at this aperture, its lens system serves to form the inverse Fourier transform and to recover the moire interference pattern carried in the signal.

In this study, all the specimen gratings were made of a rectangular dot array and the submaster grating used was unidirectional. The moire fringes of each family are obtained separately by rotation of the master grating through an angle of 90°. The center dot in the Fourier transform plane designated as the (0,0) order is the direct current output signal, and any one order along the central horizontal array of orders contains only the u-field fringes. Any one order along the central vertical array or dots contains only v-field fringes. Therefore, if a black paper mask with a hole is placed at the transform plane to let through the optical system one order along the central horizontal (or vertical) array, the u-field (or v-field) fringes will be obtained, again making sure that the order

allowed to pass has the least entanglement with the spectrum of noise.

2.7 Moire Fringe Photographs

As stated previously, moire fringe patterns are formed by the superposition of a specimen grating photoplate and a submaster grating. A schematic of the optical processing system developed to perform the superposition and create the fringe patterns is shown in Figure 2.12. The light source was a 15 mw Helium-Neon Laser made by Jodon Engineering Associates. The laser beam passed through a spatial filter which converted it to a moderately clean diverging beam. This beam was then directed through a simple lens to produce a parallel light field. The moire submaster grating and photoplate of the specimen gratings were placed, emulsion sides together, in the optical path normal to the light beam. After passing through the photoplate, the beam which now contained diffraction components was decollimated by a second simple lens. Both lens were 13 inches (330 mm) in diameter with focal length 39 inches (1000 mm). The focal plane of the system was found by trial. This focal plane is the transform plane of the field lens combination. A black paper screen containing a hole of approximately 3/32 inches (2.38 mm) diameter was then placed in the focal plane. This screen was actually held in the filter mount of a zoom lens with a focal length range of 95-205 mm which fitted a Nikon F camera. The camera was

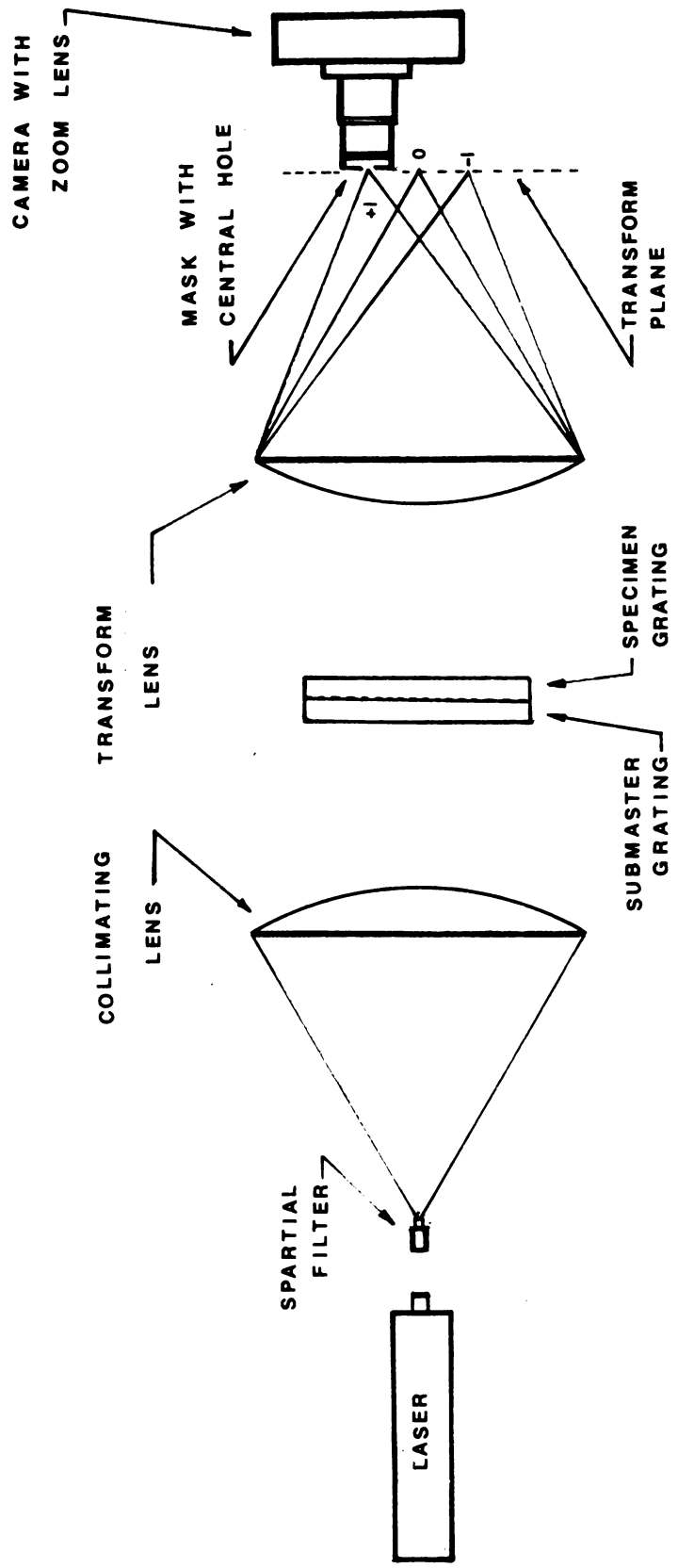

Figure 2.12 Schematic of the Optical Processing System used for Obtaining Moire Fringe Photograph from Specimen Grating Photoplates.

placed on a moveable holder so that the hole in the filter mask could be made to coincide with the chosen ray group. A series of these ray groups appear as bright spots in the diffraction pattern. Selection of the proper bright patch must be accomplished with the camera pointed so as to focus an image of the specimen grating plate on the camera film. All equipment used in this system were set up on an iron optical bench that was designed and built at Michigan State University.

The camera was focused in the apparent plane of the data plates as seen through the field lens. After proper adjustment of the grating photoplates, a moire pattern was visible in the image of the specimen seen in the camera viewfinder. After final adjustment of the plates to eliminate rigid body rotation effects in the fringe pattern, the pattern was photographed. The fringe photograph negatives were made on Kodak Plus-X film. Exposures were worked out by trials.

The baseline (zero strain) and deformed grating data are permanently stored on glass photographic plates. It is possible to superimpose these plates with different submaster gratings in order to gain maximum useful sensitivity multiplication and to improve subsequent fringe reading and data analysis by optimizing the spatial frequency mismatch of the superimposed gratings. For this study submasters were selected which had density and diffraction characteristics which balanced with the properties of the

specimen grating to produce the best fringe pattern and also, the ray group which gave best fringe visibility was selected. (Ray group no. 1 was used for most of this study.) All baseline and deformed grating data plates of the same specimen used the same submaster to form moire fringe patterns.

Finally the 35 mm negative of the fringe patterns were developed. Following normal development, the 35 mm negatives were developed in Kodak D-76, stop bath, fixer, then washed and dried. The best fringe patterns were selected, and most of them were enlarged and printed on 8 x 10 Kodabromide paper for numerical fringe analysis.

2.8 Digitizing Moire Fringe Data

The photograph of the moire fringe patterns were prepared for digital data reduction to obtain strain in a direction perpendicular (ε_y) and paralled (ε_x) to the crack line near the crack tip of a compact tension specimen as shown schematically in Figure 2.13a and Figure 2.13b. These patterns serve here as examples to explain the steps in the digital processing.

The negatives of the moire grating photography and optical data processing were enlarged showing the moire fringes in the area around the crack tip with the fiducial marks. In order to obtain the normal strain along the axis normal to the grating lines, it is first necessary

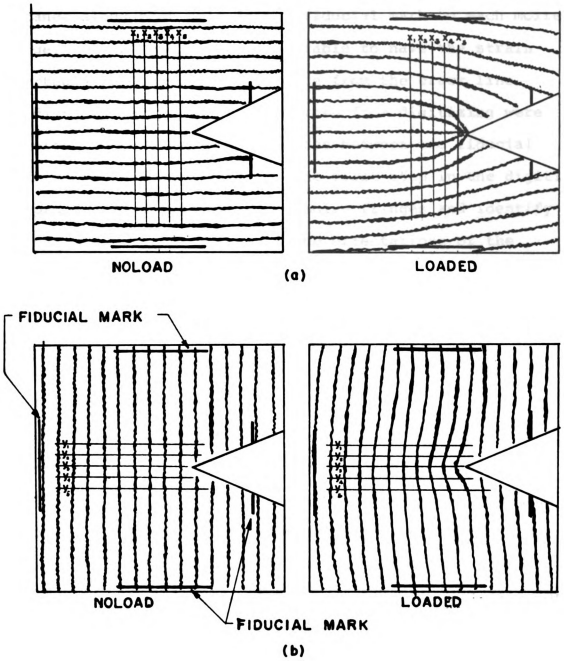

Figure 2.13 Schematic of the Photograph Preparation for Digitizing.

a) To Measure Strain ε_y
b) To Measure Strain ε_x

to obtain the record, in this case in digital form, of the distance along that axis from a fiducial mark to each moire fringe. In the end, it was desirable to have the strain reported as a function of distance from the crack line. The distance data that were obtained from digitizing were converted by measuring the distance between two fiducial marks on the specimen itself. The first step in the digitizing procedure was to number the moire fringes and identify the various fiducial marks and the orientations of the specimen in the pictures. An example of a fringe photograph so prepared for digitizing is shown in Figure 2.14. This preparation was done for each data photo and for its matching baseline fringe pattern. One can begin counting the fringe orders anywhere because the absolute fringe number is not important; it is very important, however, that the numbers of fringes not be repeated or skipped.

Digitizing moire fringe data for coldworked specimens is almost the same as the procedure described above. The coldworked specimen was studied on one plane along the specimen thickness. Because two-way gratings were used for coldworked specimens, moire fringe data in the radial and thickness directions were digitized to obtain radial strain, ε_r, and vertical strain, ε_z, along the specimen thickness. The radial strain was reported as a function of the distance from the hole edge, and vertical strain was reported as a function of the distance from the bottom surface of the specimen thickness. More details about digitizing

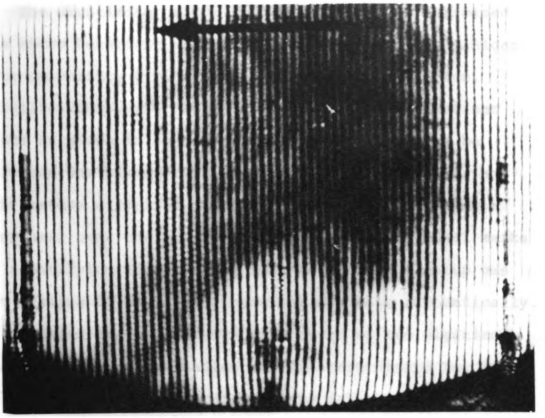

Figure 2.14 Sample Moire Fringe Photograph.

the moire fringe data for coldworked specimens have been described in reference (9).

The digitizing of the fringe patterns was performed on a Micro Datatizer (software specification for Michigan State University S.O. No. 178058 by GTCO Corporation, Rockville, Maryland). A schematic of the microdatatizer system is shown in Figure 2.15. The photograph to be digitized was placed firmly under a protective cover and digitization of points one-by-one was done by placing a cross-hair over the point or any one of the fiducial marks and identifying labels. One advantage of this setup was that scaling to specimen dimensions was done automatically. The required scaling factors were based on two digitized points and the corresponding specimen coordinate for each. The further away the fiducial points were from each other, the more accurate was the digitization procedure.

As mentioned above, the digitizing process was applied to a moire data photograph (loaded specimen) and a zero strain (noloaded specimen) baseline photograph. These two sets of digitized fringe data from a unit for the computation and plotting of the displacement component and the strain component. In several cases, the same photographs were digitized at least two times in order to analyze experimental errors derived from the digitizing process.

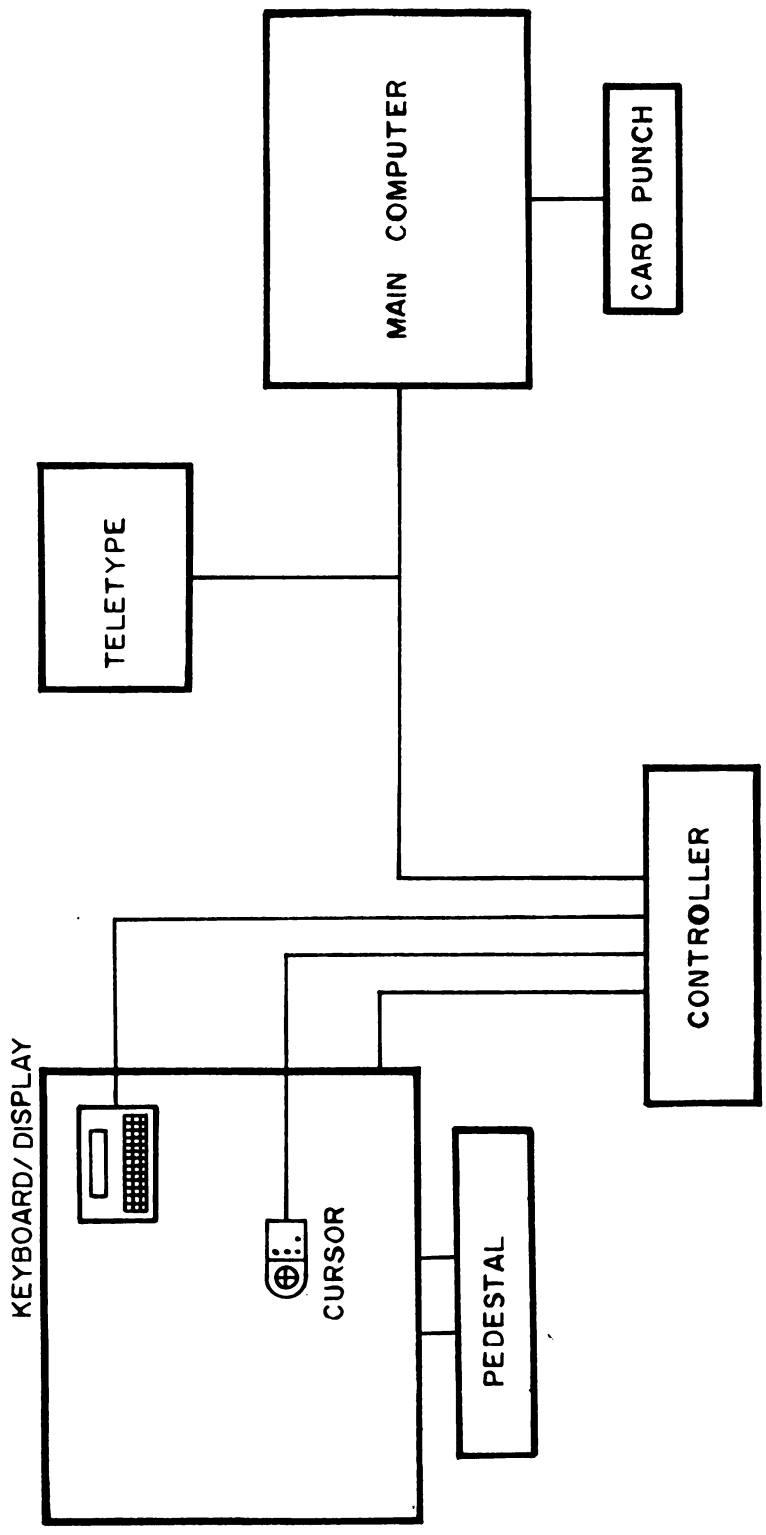

Figure 2.15 The Micro Datatizer System.

2.9 Data Reduction and Plotting Displacements and Strains

Three computer programs (named "Moire," "Cloud," and "Hoop") were used to reduce the data and plot the displacements and strains discussed in this study. They were specifically developed by Cloud and coworkers to use in this and similar projects. Details about the computer programs are given in Reference (9). Copies of all three programs are provided in the Appendix. Program Moire was used for single data sets. Programs Cloud and Hoop were used for composite plots. The later two programs will give the same strain results but they differ in the position of the strain plot. For this study, Program Cloud was used for the radial strain plot for the coldworked specimen and for the strain in the direction parallel to the crack line of the compact tension specimen. Program Hoop was used for the strain plot in the direction perpendicular to the crack line of the compact tension specimen and for the tangential strain near the hole edge of the coldworked specimen.

2.9.1 Detailed Analysis and Plot of Single Data Sets

Program "Moire" (Appendix) was used to obtain a detailed picture of moire fringe order, displacements and strains by printout and graphical output. This picture provided a means to study the original input, the computed displacement field, and the computed strain map. The operations performed by the detailed analysis routine (Appendix) are as follows:

1. Read in the data containing the set designation (specimen identifiers), the moire sensitivity multiplication factor from the optical fringe data processing and the moire grating spatial frequency. Then, for an "at strain" fringe pattern, the distance between two fiducial marks, the maximum fringe order to be entered, and the distances from the fiducial mark to the intersection of each moire fringe with the y-axis under study are entered. The maximum fringe order and the fringe locations for the baseline fringe pattern are also read into the computer.

2. Generate fringe order numbers to match each fringe location entered as data.

3. Fit the baseline and the "at load" data with two continuous smooth curves by means of a cubic spline fitting and smoothing routine.

4. Interpolate the calculated curves to obtain the fringe number as a function of the distance from the fiducial mark at 100 points on the data and baseline curves. The maximum range of the curves is sorted out and divided by 100 to establish the nodes, which must be common to both the data and the baseline curves.

5. Subtract the baseline fringe order (unloaded specimen) from the data fringe orders (loaded specimen) for each of the 100 points and multiply this difference by the pitch (the reciprocal of the spatial frequency) of the grating on the specimen, and then divide by the sensitivity multiplication factor to obtain the displacement function u_y for the

chosen y-axis.

6. Subtract the distance from the first fiducial mark to the hole edge or crack line from each nodal y-value, in order to have all result reported in the term of distance from the important specimen feature.

7. Compute by finite differences the first derivative of displacement with respect to distance along the appropriate axis. This result is the strain at each of the 100 nodes.

8. Print, if ordered by the input control cards, all values of input fringe orders, displacements, and strains.

9. Scale the data and generate a plot of the input data and baseline curves. This graph shows fringe data points and the smooth curves.

10. Plot vertical displacement, u_y, as a function of the distance along the choosen axis.

11. Plot vertical strain, ε_y, as a function of the distance along the axis.

12. Start over with the next complete set of data.

Samples of each of three graphs produced by this routine are shown in Figure 2.16.

The main purpose of this analysis program was to allow a detailed study of each set of data and the results it produced. Input errors, such as faulty card punching or skipping a fringe during digitizing, were immediately evident. As proficiency and accuracy increased, this routine was used only as a last resort for data sets which seemed

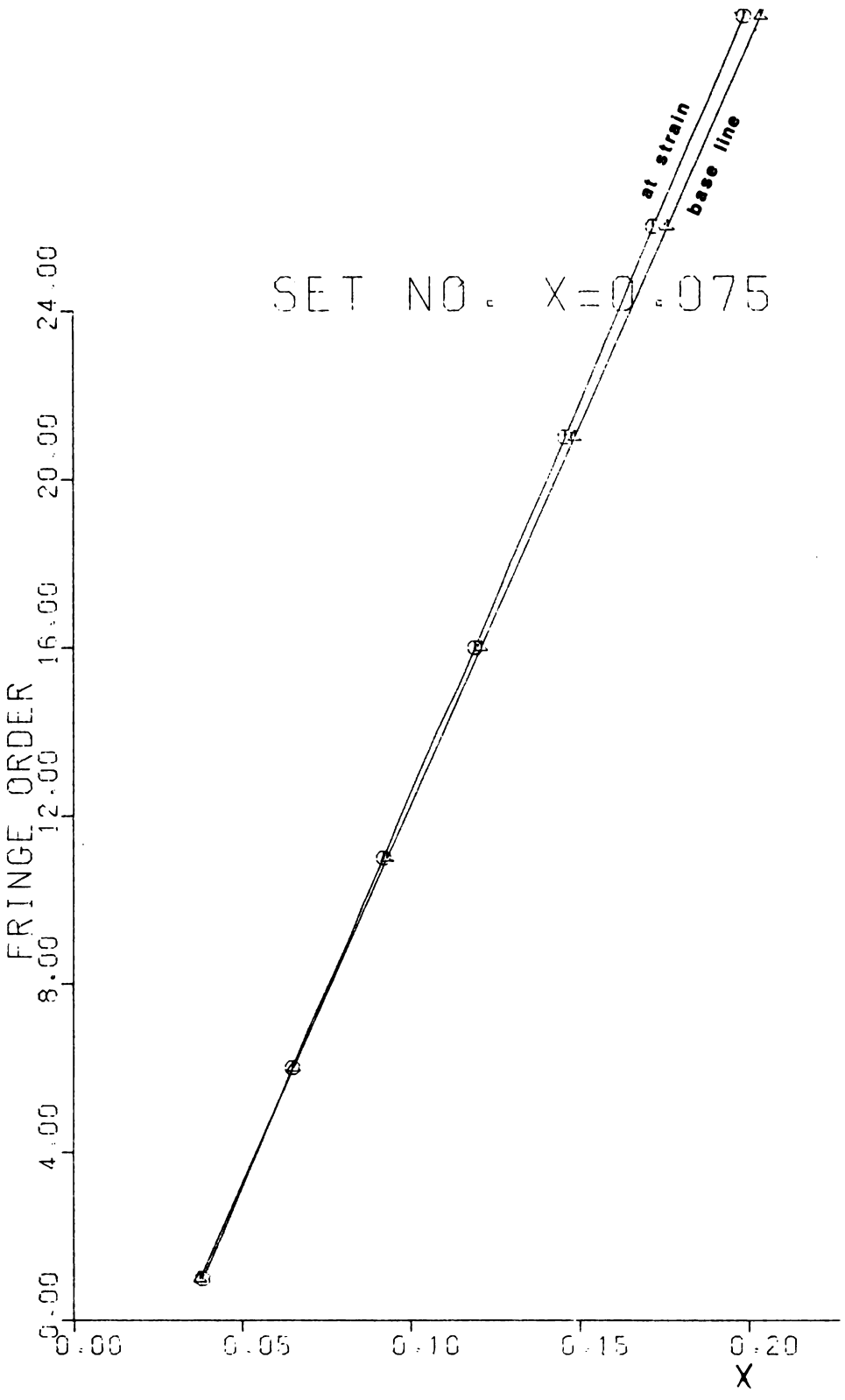

Figure 2.16a Plot of Distance Versus Fringe Order.

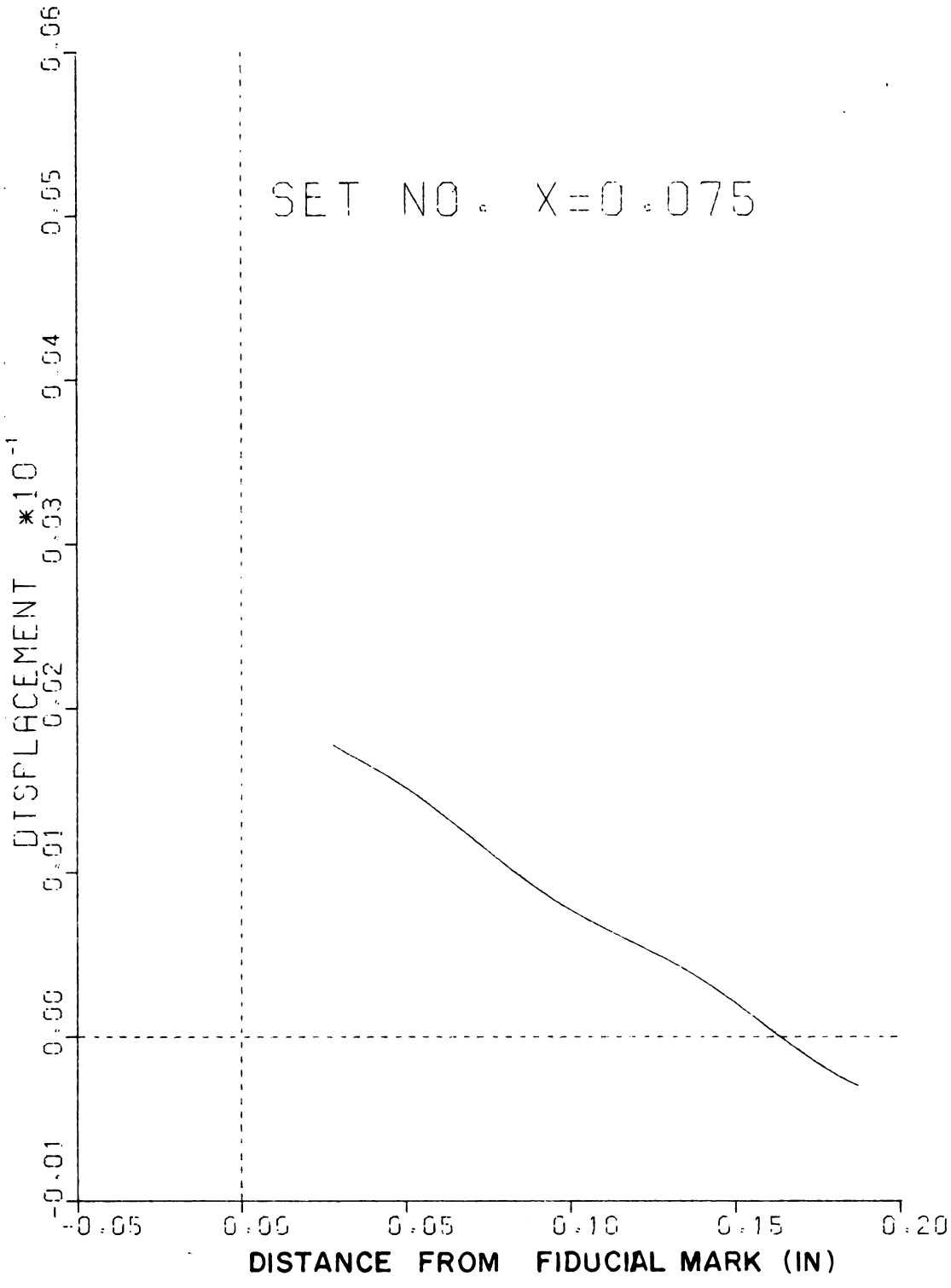

Figure 2.16b Plot of Distance from Fiducial Mark Versus Displacement.

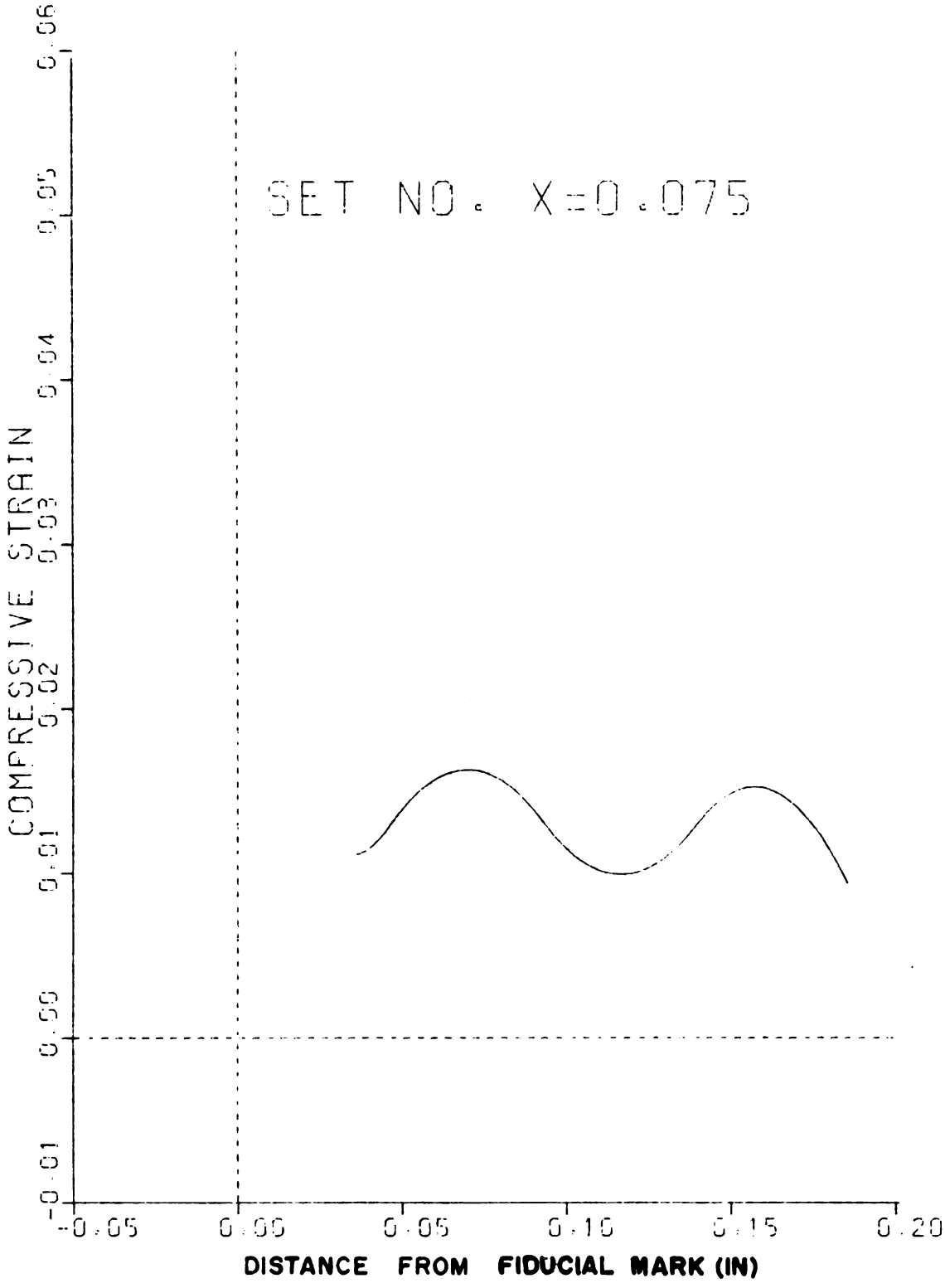

Figure 2.16c Plot of Distance from Fiducial Mark Versus Strain.

as if they might contain faults when processed by the less-detailed summary plotting routine.

2.9.2 Analysis and Summary Plotting of Multiple Data Sets

Program "Cloud" and "Hoop" (Appendix) were used to plot many results on a single graph. These two programs are very similar to the Moire Program discussed in the previous section. They differ in the input requirements and, obviously, in the output. The purpose of these two programs is to generate a single plot of the calculated strain versus distance which contains several sets of the data obtained for any one specimen. Two sets of strain results can be obtained on each plane of the specimen because two-way gratings were used. For each coldworked specimen, radial strain, ε_r, for several lines along the thickness were combined in a single plot, and transverse strain, ε_z, for several lines successively further from the edge of the hole were also plotted together. For each crack specimen, strain in the direction perpendicular to the crack line for several lines at increasing distance from the crack tip were produced in a single plot; and strain in the direction parallel to the crack line for several axes parallel to the crack line were combined in one single plot. Thus, the strain at any point on the same specimen can be seen on a single plot. An example of such a multiple data plot is given in Figure 2.17.

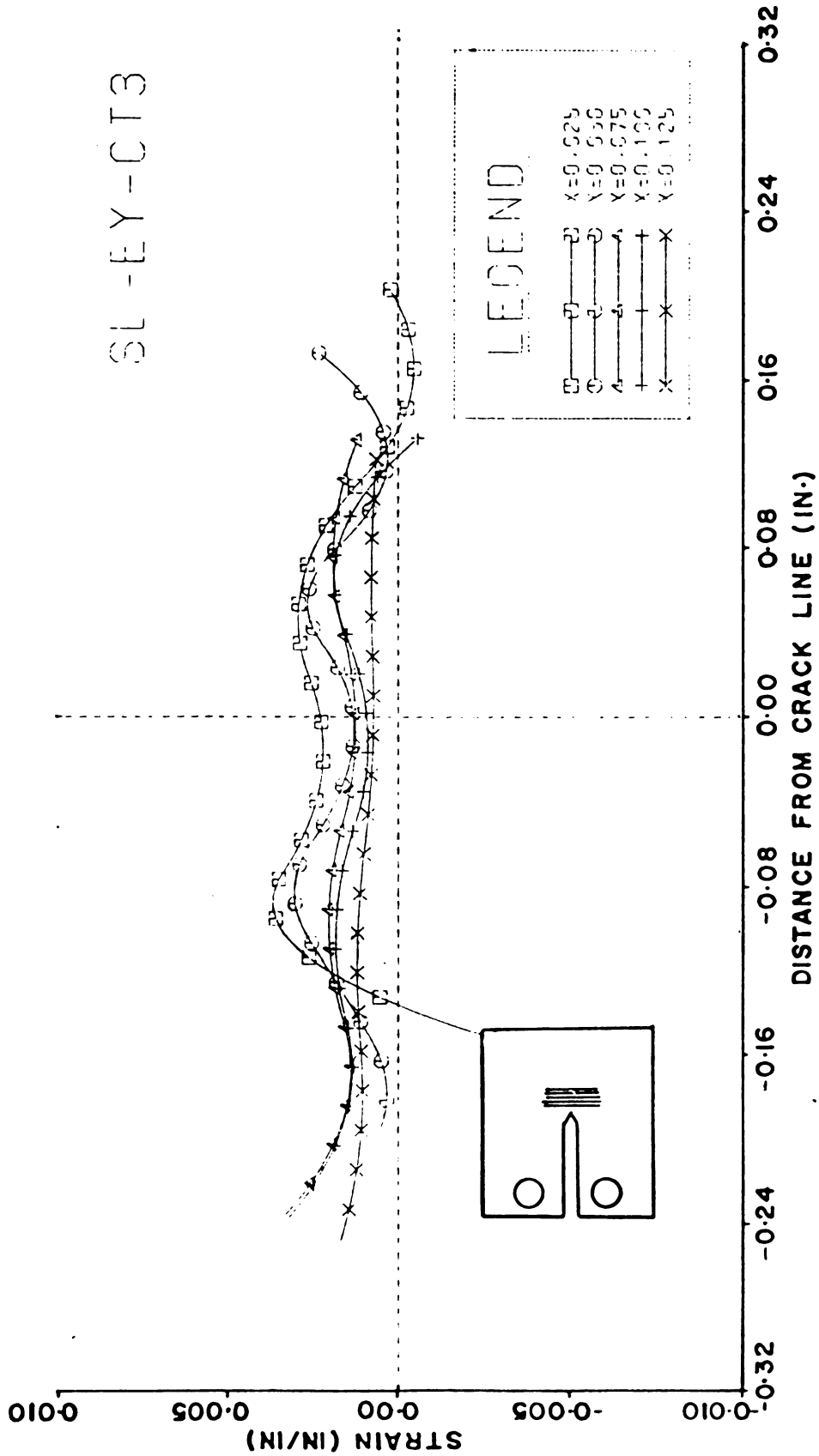

Figure 2.17 Plot of Multiple Data Set.

CHAPTER 3

MATERIAL SPECIFICATION

The material used for this investigation included polycarbonate resin and mixture of flexible and rigid polyester resins.

Polycarbonate is a very tough polymeric material. Because of its optical and mechanical properties including good transparency, small creep, high elastic modulus, and machinability, polycarbonate has been proposed by several researchers as a convenient material for in-plane photoelasticity study and for the study of stress fields in crack plates. Given the similarity of the stress-strain diagram of polycarbonate to that of mild steel, and the fact that it stays transparent during plastic deformation, Cloud (25) and Brinson (16) suggested that plasticity and photoplasticity experiments might be conducted with this material. In this study, the polycarbonate obtained from Mobay Chemical Company. Poisson's ratio of polycarbonate is 0.45. The curve of the modulus of elasticity as a function of temperature and a typical stress-strain curve are shown in Figure 3.1 and Figure 3.2. These curves are from an engineering handbook on Merlon Polycarbonate published by Mobay Chemical Company, Pittsburgh, Pennsylvania (24).

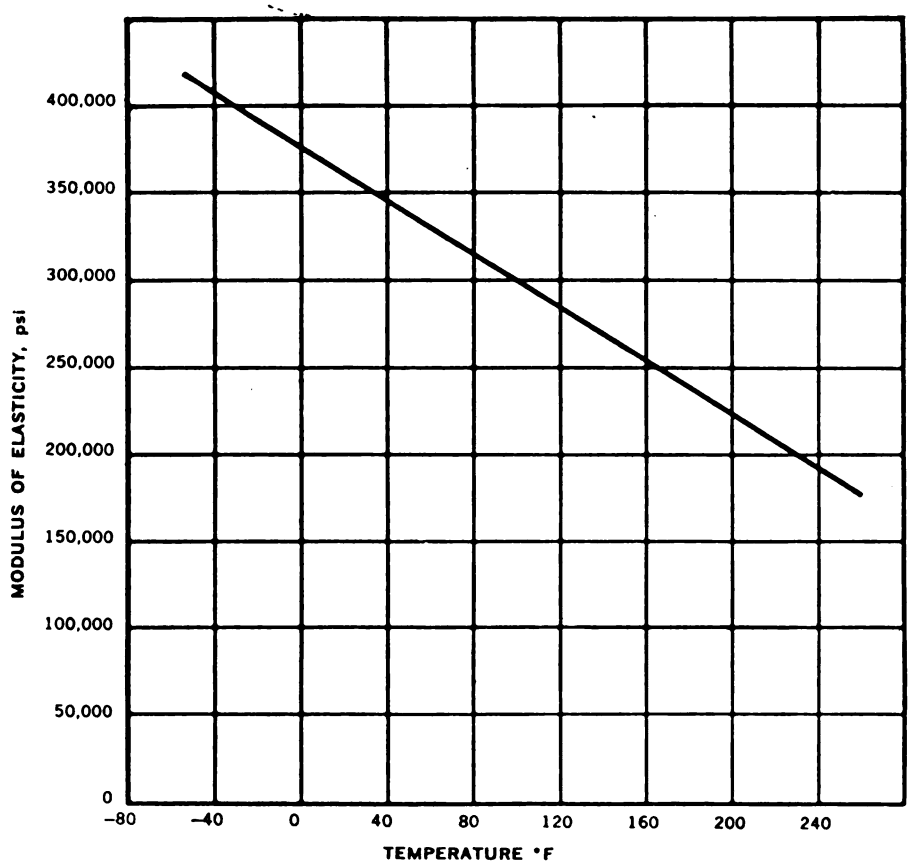

Figure 3.1 The Modulus of Elasticity Versus Temperature of Polycarbonate (Reference 24).

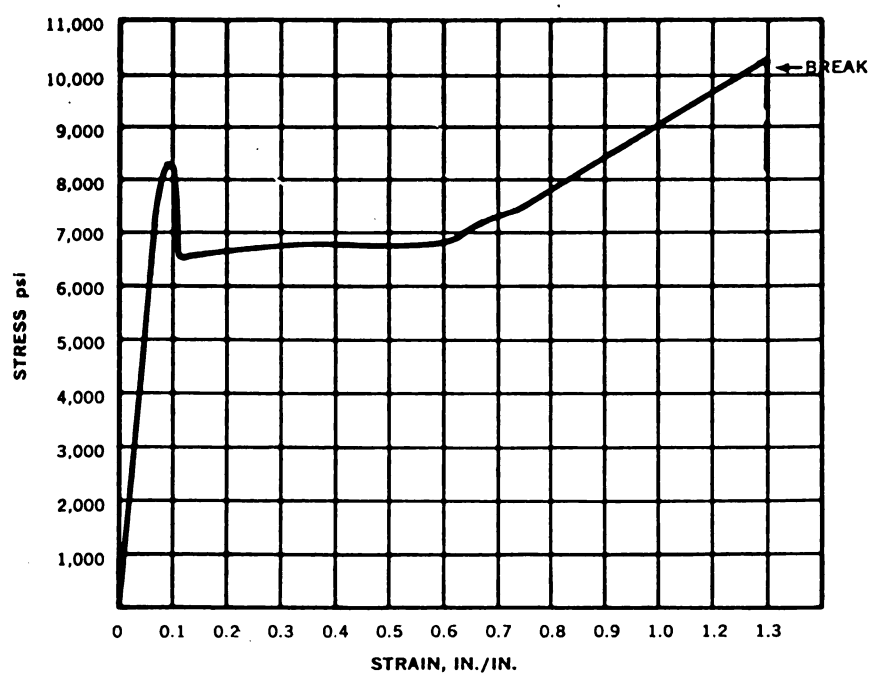

Figure 3.2 The Stress-Strain Curve of Polycarbonate (Reference 24).

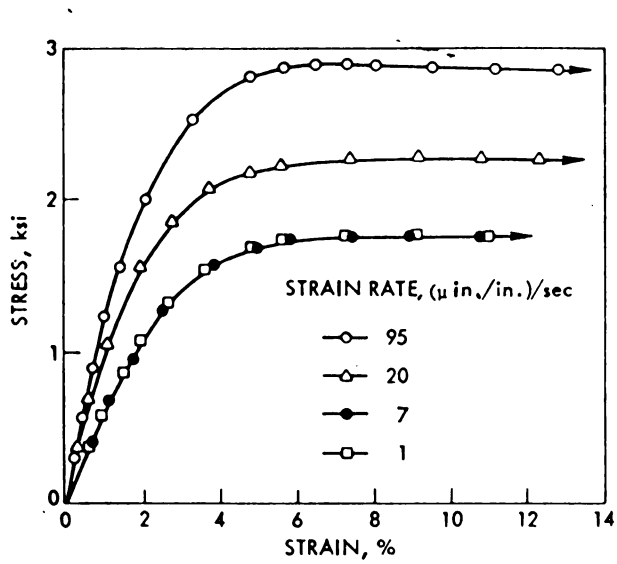

Figure 3.3 Stress-Strain Curve as a Function of the Strain Rate for a 60:40 Mixture of Laminac Polyester Resins (Reference 26).

A mixture of flexible and rigid polyster resins was used to make the other specimens. D. H. Morris and W. F. Riley (26) show that a mixture of 60% by weight flexible MR-9600 (previously designated EPX-126-3) and 40% by weight Laminac 4116 can be used to predict the behavior of an aluminum prototype. The Poisson's ratio was found by them to be 0.45. Their stress-strain curves, which depend on strain rate, are reproduced in Figure 3.3. These particular resins are now marketed by the USS Chemicals Division of United States Steel, Polyester unit.

CHAPTER 4

RESIDUAL STRAIN AROUND COLDWORK HOLES

Consider a thick plate with internal pressure on the boundary of a small hole as in Figure 4.1. Since stress is symmetrical with respect to hole axis and uniform along the thickness, no

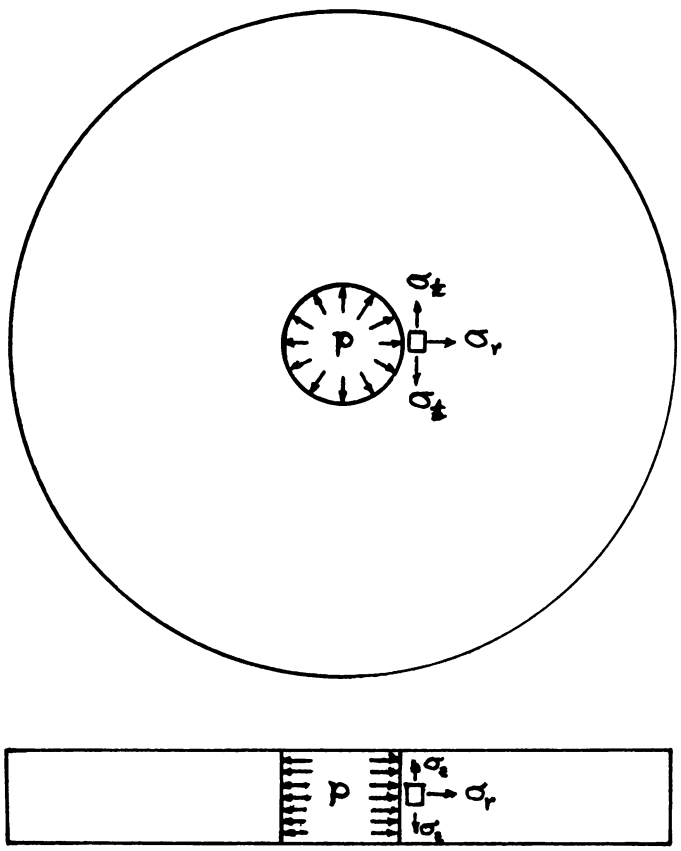

Figure 4.1 A Small Hole in a Thick Plate under Uniform Internal Pressure.

shearing stress will be transmitted along any plane which is perpendicular to the axis. The shearing stress components acting on these surfaces must hence vanish. The only stress around the edge of the hole along the thickness are:

i) a radial stress, σ_r, in a radial direction,

ii) a tangential stress, σ_t, in a circumferential direction,

iii) a transverse stress, σ_z, in a direction parallel to the axis of the hole.

Since everything is symmetrical with respect to the axis of the hole, all three stress components σ_r, σ_t and σ_z are principal stresses and depend only on one independent variable, the distance r, from the hole center.

The deformation of all points along a circle of radius r are displaced in the direction of the radius by the same amount. These small displacements will be designated by ρ. In the case of plane strain the cross section of the mid-plane of the plate remains plane, the transverse strain, ε_z, along the direction parallel to the axis of the hole is constant. During plastic flow the material will be stretched and the amount of the unit elongation in the radial and tangential directions will be denoted by ε_r and ε_t. The radial and tangential strains are:

$$\varepsilon_r = \frac{d\rho}{dr}$$

$$\varepsilon_t = \frac{\rho}{r}$$

Since the volume of any element is not changed by the plastic deformation the sum of the strain in all three directions is zero.

$$\varepsilon_r + \varepsilon_t + \varepsilon_z = 0$$

where the uniform internal pressure, p, is constant and independent of r.

For the coldworked problem, a tapered rod is used to expand a hole in the thick plate (see Figure 4.2). The force acting on the surface of the hole is not perpendicular to the hole surface. Vertical and horizontal forces act on the surface of the hole, and thus the strain will not be uniform along the plate thickness.

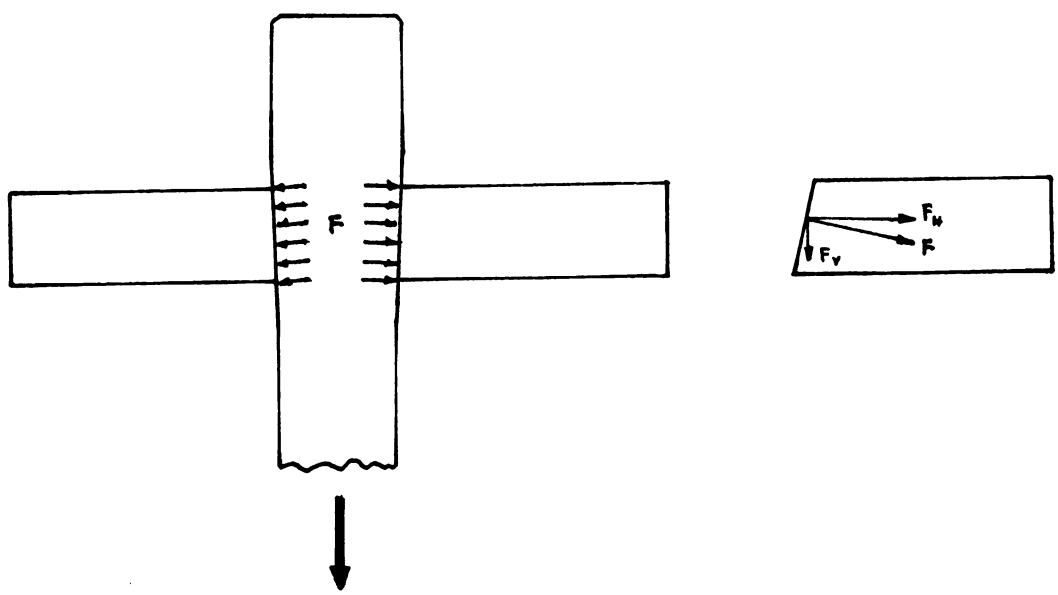

Figure 4.2 Expanding a Hole in the Thick Plate by Using a Tapered Rod.

4.1 Coldworking

The coldworking procedure is the one developed by J. O. King, Inc. 711 Trabert Avenue, N. W., Atlanta, Georgia 30318, and is described in the following paragraphs.

A thin-walled sleeve which carries an anvil on one end is inserted into the hole. A tapered mandrel is pulled through the hole to expand it while the anvil of the sleeve is supported to oppose the pulling force (see Figure 4.3) The mandrel enlarges the sleeve and expands the hole enough to cause plastic deformation around the hole. The sleeve remains in the hole but the anvil drops off. A machine incorporating a hand-operated hydraulic cylinder was constructed to pull the mandrel in the laboratory. The tapered mandrel used for this study had a maximum diameter of 0.2550 inch (6.4770 mm), the sleeve had a 0.2350 inch (5.9690 mm) inside diameter, a 0.2540 inch (6.4516 mm) outside diameter, and it was 0.0095 inch (0.2413 mm) in wall thickness.

The mandrelizing and testing sequence was accomplished in steps as follows:

1-a The tapered mandrel was pulled down until the top of the mandrel was at the same level as the top surface of specimen.

1-b A grating photograph was recorded.

2-a The tapered mandrel was pulled down about 1/3 of the thickness.

2-b A grating photograph was recorded.

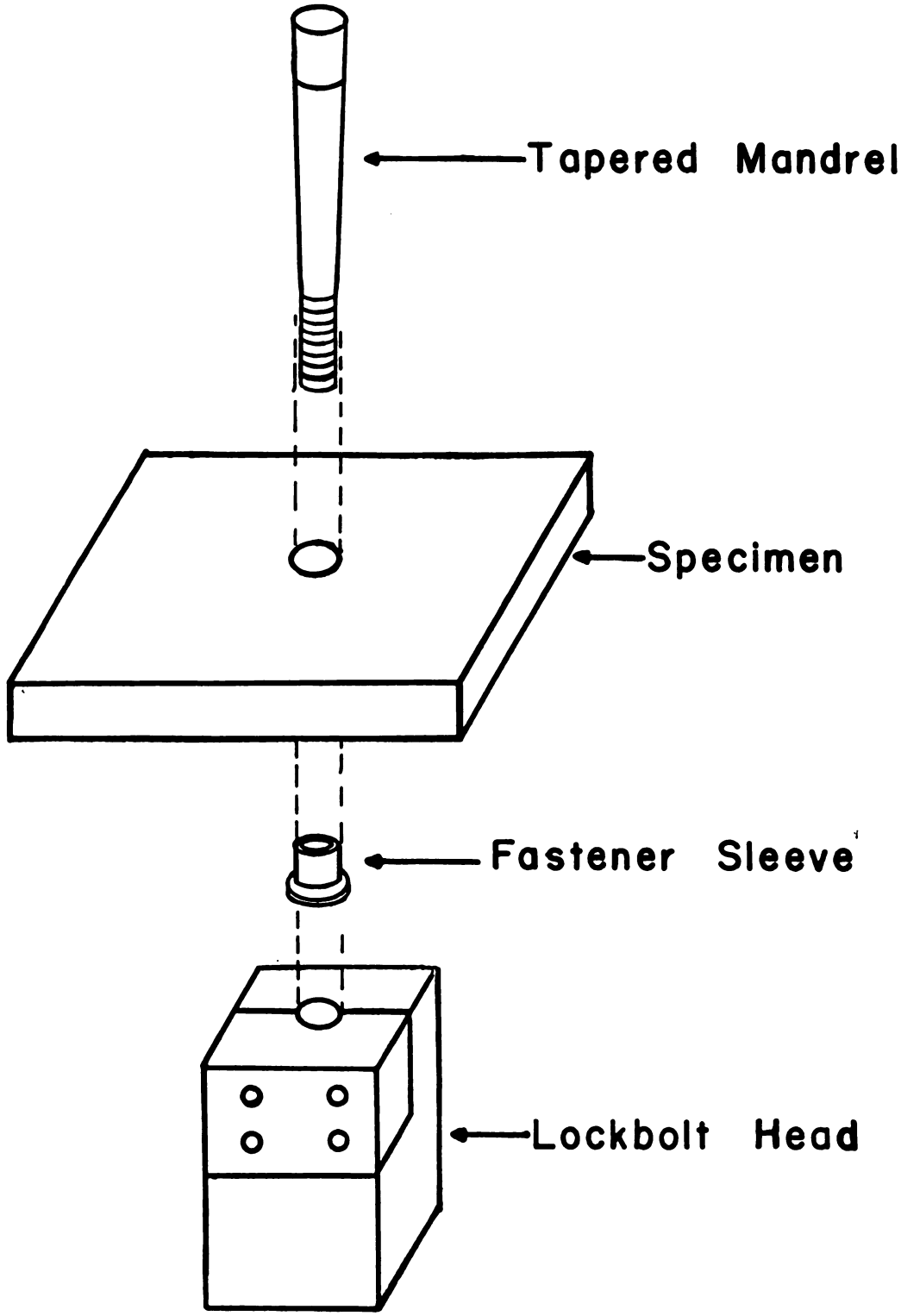

Figure 4.3 Schematic of the Coldworking Process.

3-a The tapered mandrel was pulled down about 2/3 of the thickness.

3-b A grating photograph was recorded.

4-a The tapered mandrel was pulled completely through.

4-b A grating photograph was recorded.

4.2 Residual Strain and Transverse Strain Measurement

4.2.1 Specimen Preparation

Both Polycarbonate resin and a mixture of flexible and rigid polyester resins were used to make coldworked specimens.

In the beginning, Polycarbonate was used. A polycarbonate sheet obtained from Mobay Chemical Company was cut into two rectangular pieces. A copper grating was printed on one of the surfaces. The blocks were then glued together to form the specimen block with the copper grating at the mid-plane.

The 60:40 mixture by weight of flexible resin (MR-9600) and rigid polyester resin (Laminac 4116) was used to make the other specimens. The two resins were first blended with 1% Methyl-Ethyl-Peroxide (marketed by Witco Chemical U.S. Peroxygen Division). The specimens were cast in aluminum mold. Nickel mesh with 500 lpi (20 lpmm) and 0.0008 inches (0.0203 mm) thickness (marketed by Buckbee Mears Company) was retained at the center of mold and the resin poured around it. The resin was allowed to cure at room temperature for 24 hours. The partially set specimen

was then removed from the mold, and left in an oven and post-cured at 80°C for 16 hours.

The dimensions of all specimens which were used for this investigation are shown in Figure 4.4. The hole with diameter of 0.25 inch (6.35 mm) was drilled and reamed at the center of the specimen for the coldworking process. The fiducial marks were made by drilling a small hole 1/32 inches (0.794 mm) in diameter on the grating line at a distance 0.5 inch (12.7 mm) from the center of the large hole as shown in Figure 4.4.

4.2.2 Photograph of Specimen Grating

The specimen was polished to get smooth, clear, and parallel surfaces which let the light pass through it without scattering or causing optical distortion of the embedded grating. The system devised for photographing the specimen grating is shown schematically in Figure 4.5.

The camera used was a Tech/ops 4x5 bellows module. The lens was a Schnieder Krueznach, Retinar-Xenar with a focal length of 50 mm and a maximum aperture of f2.8. The system rested upon a granite optical table. The camera was set up to give a magnification factor of 4. The specimen was placed on a specially designed holder. The light source for this work was a 150 W. General Electric Reflector Flood.

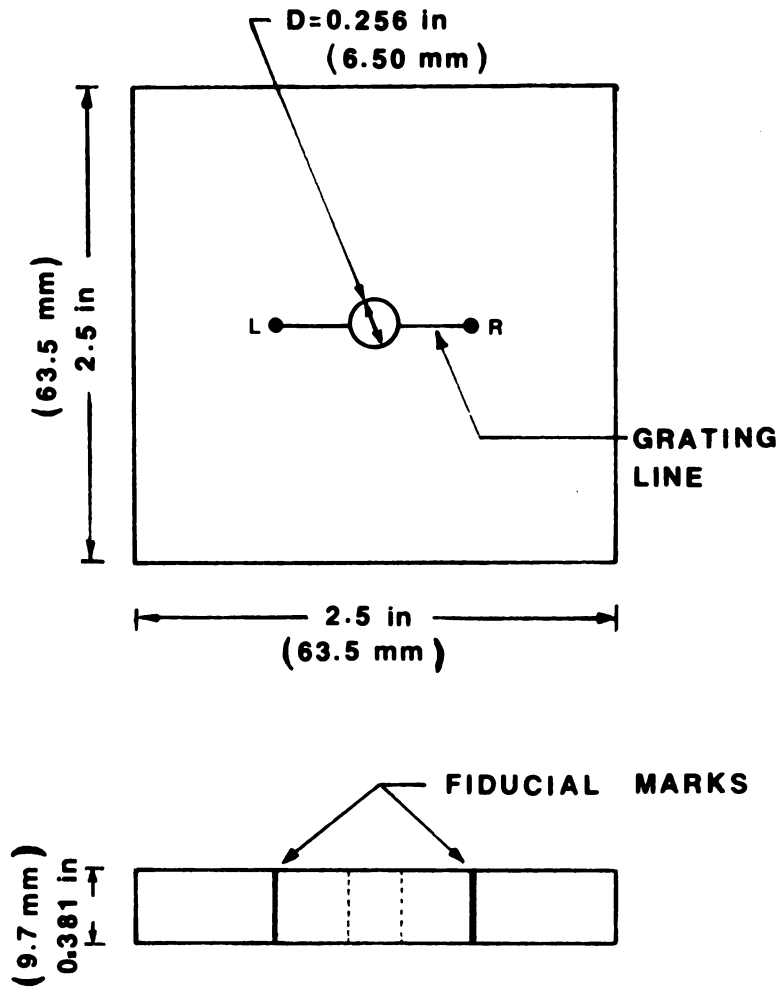

Figure 4.4. Specimen Dimensions.

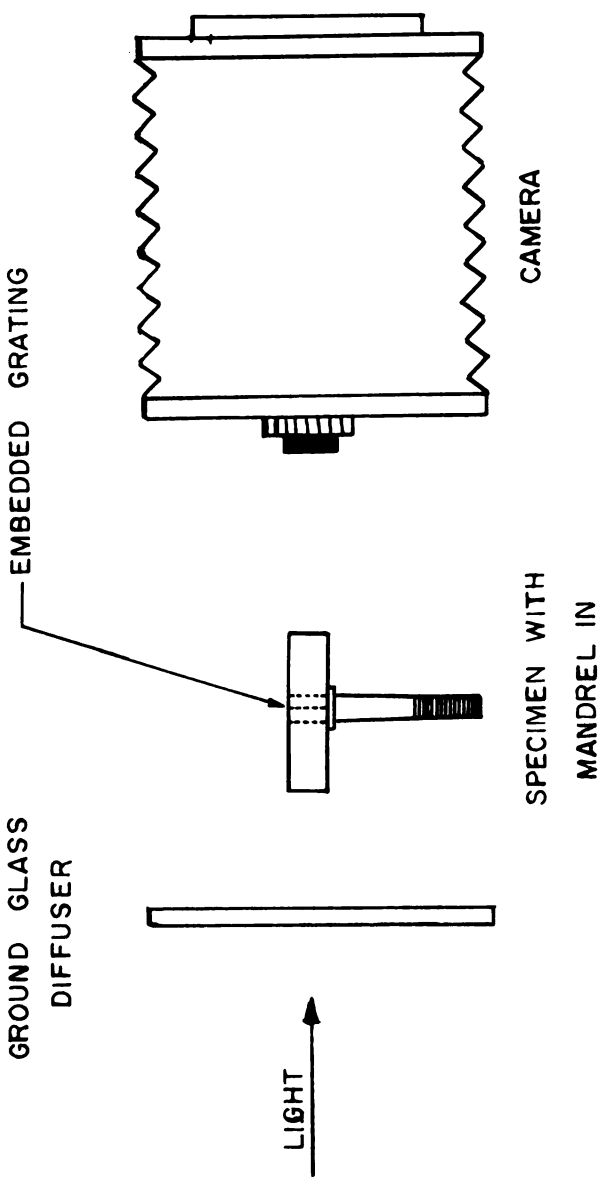

Figure 4.5 Schematic of Photography Process.

The image of the specimen grating in the emulsion of a test photoplate was examined with a Bausch and Lomb Optical Co. 10x magnifier, which had been adjusted to focus in the emulsion plane. The image of the specimen grating could be checked over the entire area near the edge of the hole along the thickness of the specimen for maximum sharpness and contrast. Kodak High Speed Holographic Film (SO-253, 4x5 in) was used to take test photographs of the specimen grating. After getting the best grating from Kodak film, the data plates were made by using Kodak High Speed Holographic Plate (Type 131-02, 4x5 in). Five data plates were made for each specimen loading:

1. The specimen with no load; this data plate was used as a base line to eliminate error which might be induced by deformations created during fabrication of the specimen as well as various optical distortions.
2. The specimen with the top of mandrel at the same level as the top surface of specimen.
3. The specimen with the top of mandrel at 0.13 inches (3.302 mm) from the top surface.
4. The specimen with the top of mandrel at 0.24 inches (6.096 mm) from the top surface.
5. The specimen without mandrel (the mandrel was pulled out).

4.2.3 Experimental Results and Discussion

The nature of the coldworking operation is to exert a force perpendicular to the specimen surface through the sleeve and thus create deformation of the hole. The diameter of the hole along the thickness was measured from the "unloaded" data plate and the "loaded" data plate (mandrel was passed through). Table 4.1 gives the results. Plots of the diameter of the hole before and after load and the diametral expansions along the thickness of the specimen are shown in Figure 4.6 and Figure 4.7 respectively. The deformation result shows that the hole is not uniformly expanded through the specimen by coldwork. The specimen has a minimum diametral expansion near its center.

Table 4.1 Diameter of Hole Before and After Load

Distance from the top (in)	Dia. of unloaded specimen (in)	Dia. of loaded specimen (in)	Dia. expansion (in)
0.000	0.2574	0.2708	0.0134
0.130	0.2563	0.2695	0.0132
0.240	0.2551	0.2679	0.0128
0.381	0.2564	0.2713	0.0149
Average	0.2563	0.2700	0.0137

In this investigation the specimen had a two way grating (that is an array of dots). By using the optical processor the Moire fringe pattern was formed separately for each direction. One was formed to get vertical fringes (direction

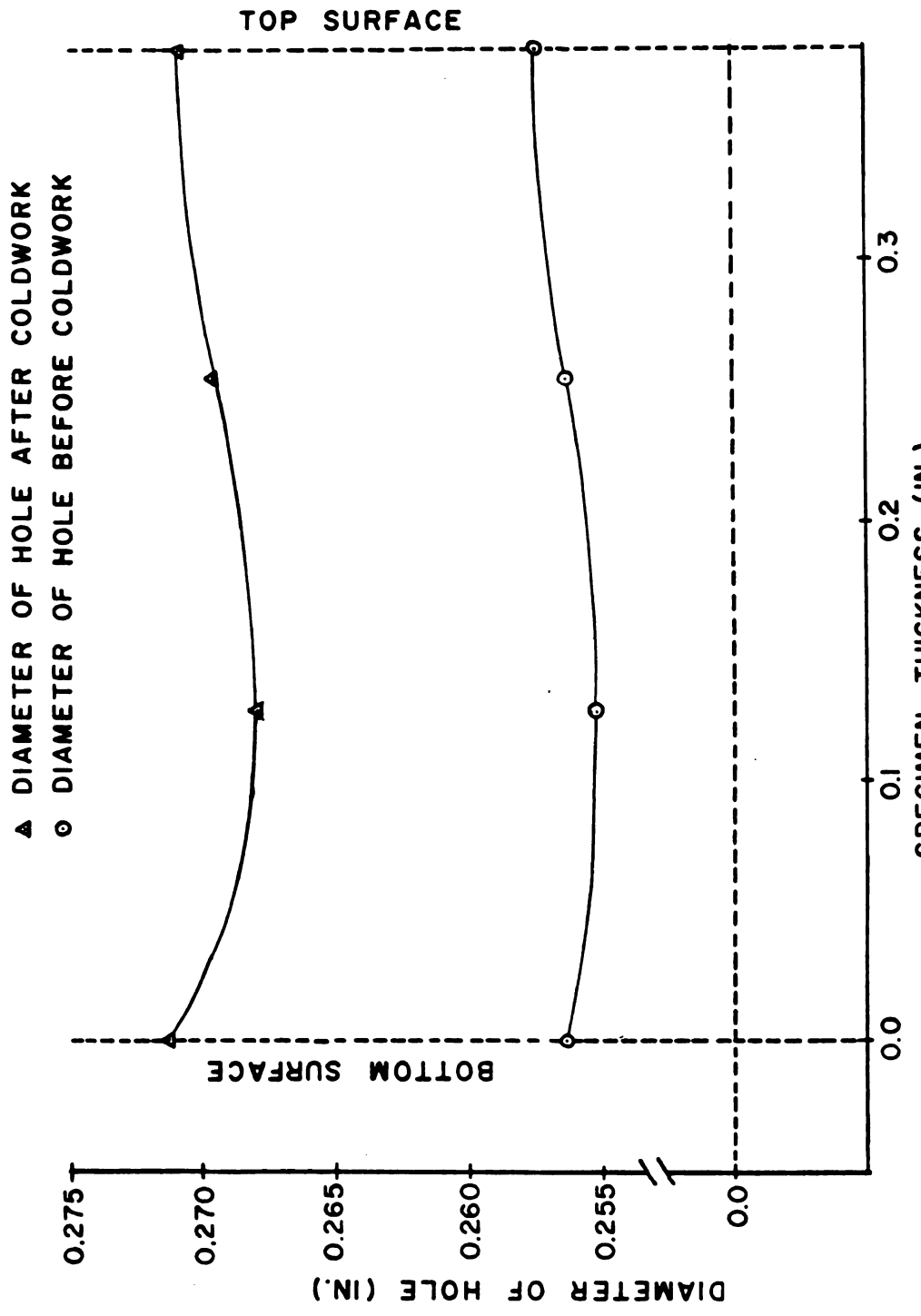

Figure 4.6 Diameter of the Hole Along the Thickness.

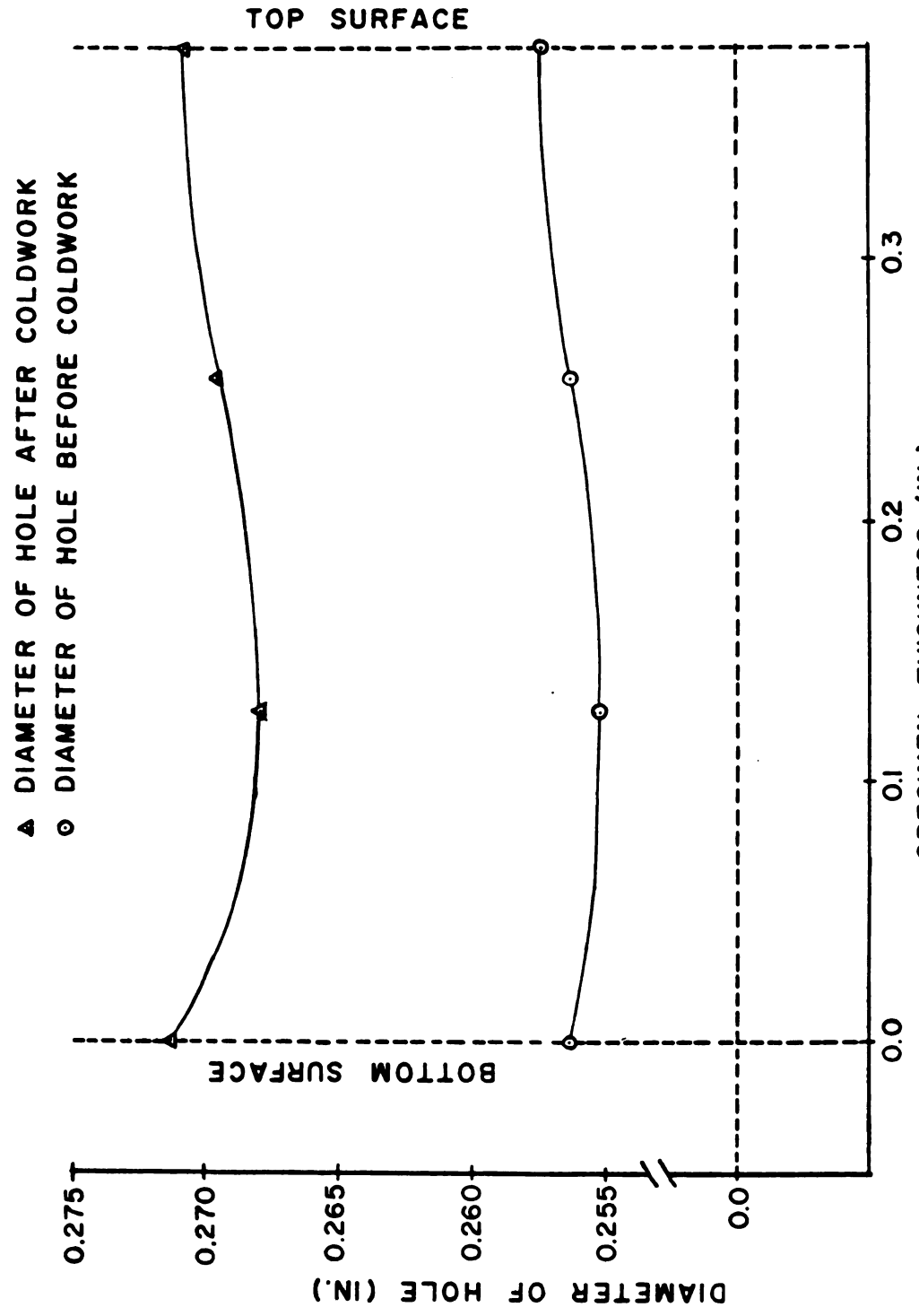

Figure 4.6 Diameter of the Hole Along the Thickness.

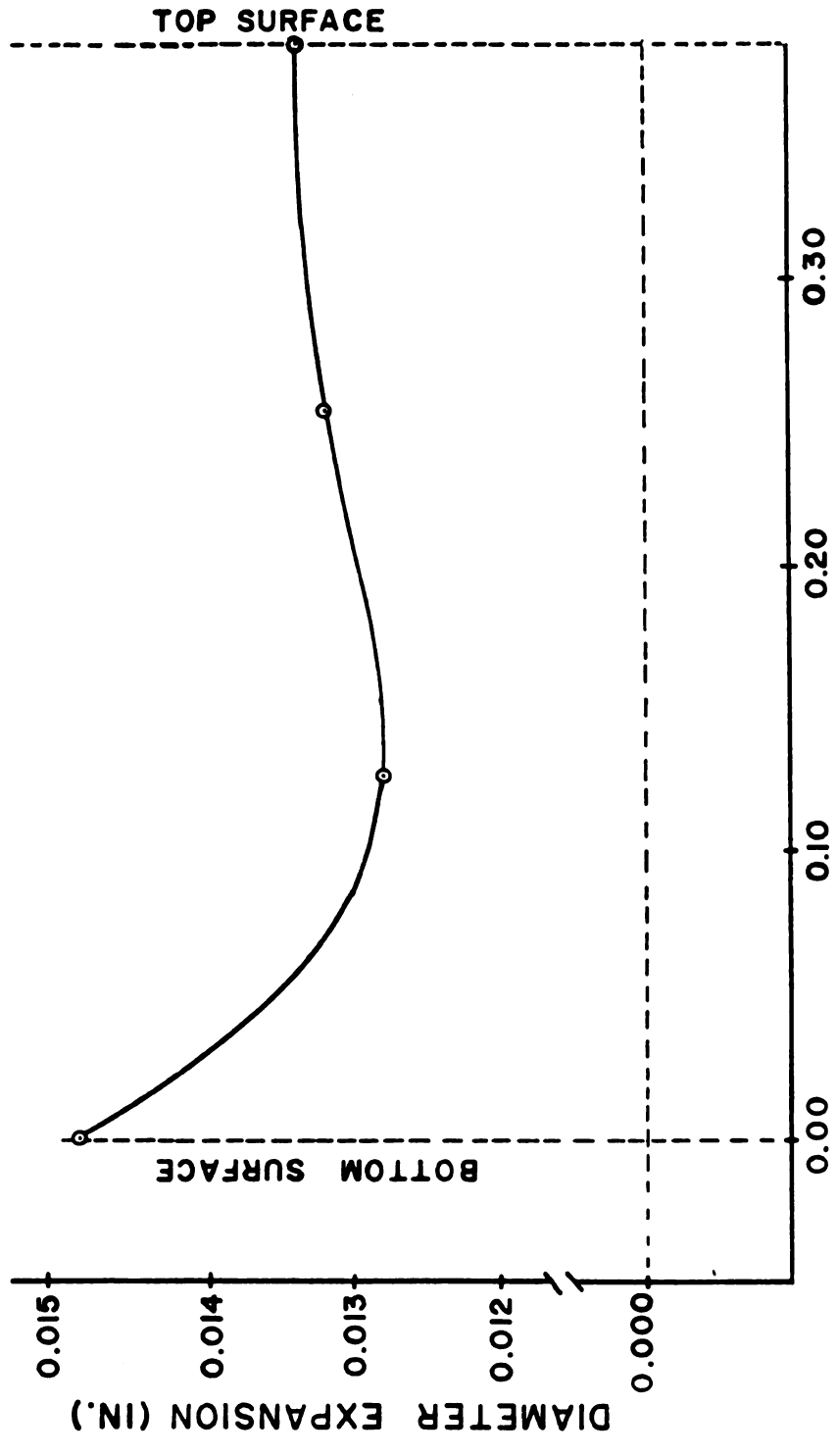

Figure 4.7 Diametral Expansions Along the Thickness.

parallel to the hole) and this fringe pattern was used to measure strain in the radial direction (direction perpendicular to the hole). The other pattern was formed with horizontal fringes (direction perpendicular to the hole); fringes in this direction were used to measure strain in the z-direction (direction parallel to the hole). The photograph of the fringe pattern was recorded separately for each direction and for each loading step.

Photographs of the moire fringe patterns obtained from polycarbonate for vertical and horizontal directions are shown in Figure 4.8 and Figure 4.9 respectively. Because the polycarbonate specimen was found to be partly split along the grating plane after coldwork, the moire fringe patterns are not entirely valid for the region near the hole. Because of the splitting that occurred, the analysis of the fringe data from the polycarbonate specimen was not completed.

The photographs of vertically-oriented (from the vertical grating) fringe patterns at each loading step obtained from the mixed polyester specimen are shown in Figures 4.10.1 to 4.10.5. The strain on the left and right sides at each loading step are shown in Figures 4.11.1 to 4.11.4 and Figures 4.12.1 to 4.12.4 respectively. At the first step, the top of the mandrel was pulled down to the level of the top surface of the specimen. The maximum expansion occurred at the top of the specimen, as shown in figure 4.10.2 because the shape of the mandrel is a taper. The strain in

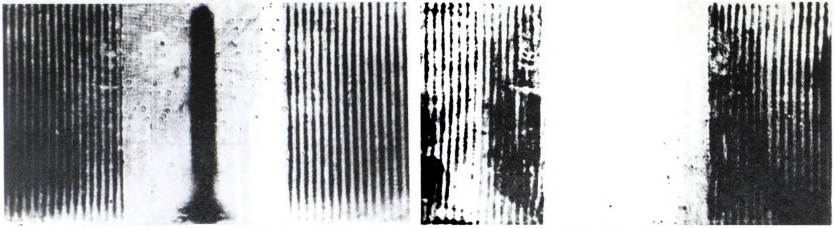

Figure 4.8 Photographs of the Moire Fringe Pattern with Noloaded and Loaded in the Direction Perpendicular to the Hole of the Polycarbonate Test Specimen.

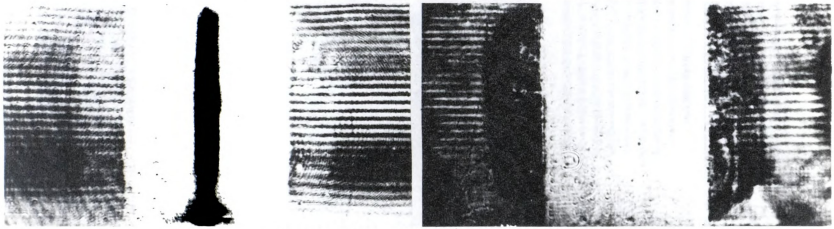

Figure 4.9 Photographs of the Moire Fringe Pattern with Noloaded and Loaded in the Direction Parallel to the Hole of the Polycarbonate Test Specimen.

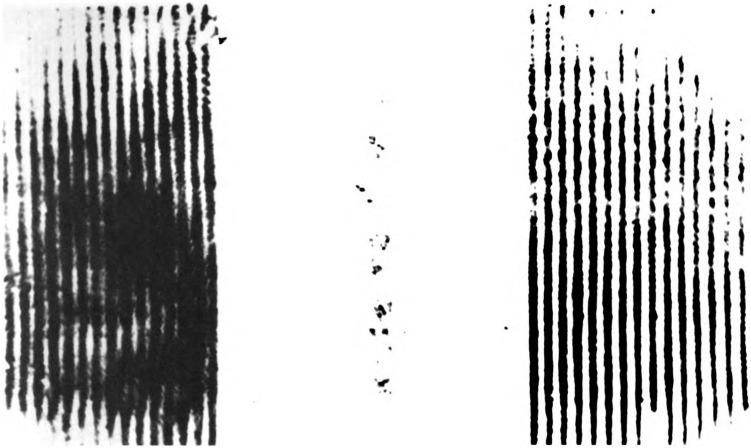

Figure 4.10.1 Photograph of Moire Fringe Pattern with Noloaded on Test Specimen of Mixed Polyester 60:40.

Figure 4.10.2 Photograph of Moire Fringe Pattern with 1st-Step Load on Test Specimen of Mixed Polyester 60:40.

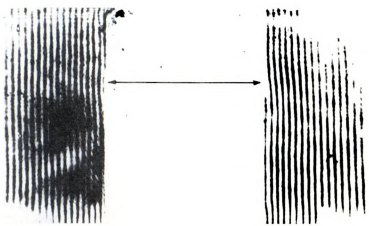

Figure 4.10.3 Photograph of Moire Fringe Pattern with 2nd-Step Load on Test Specimen of Mixed Polyester 60:40.

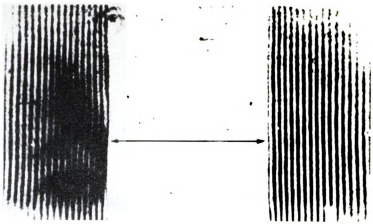

Figure 4.10.4 Photograph of Moire Fringe Pattern with 3rd-Step Load on Test Specimen of Mixed Polyester 60:40.

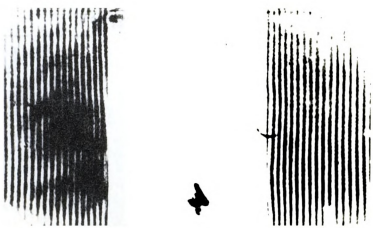

Figure 4.10.5 Photograph of Moire Fringe Pattern with 4th-Step Load on Test Specimen of Mixed Polyester 60:40.

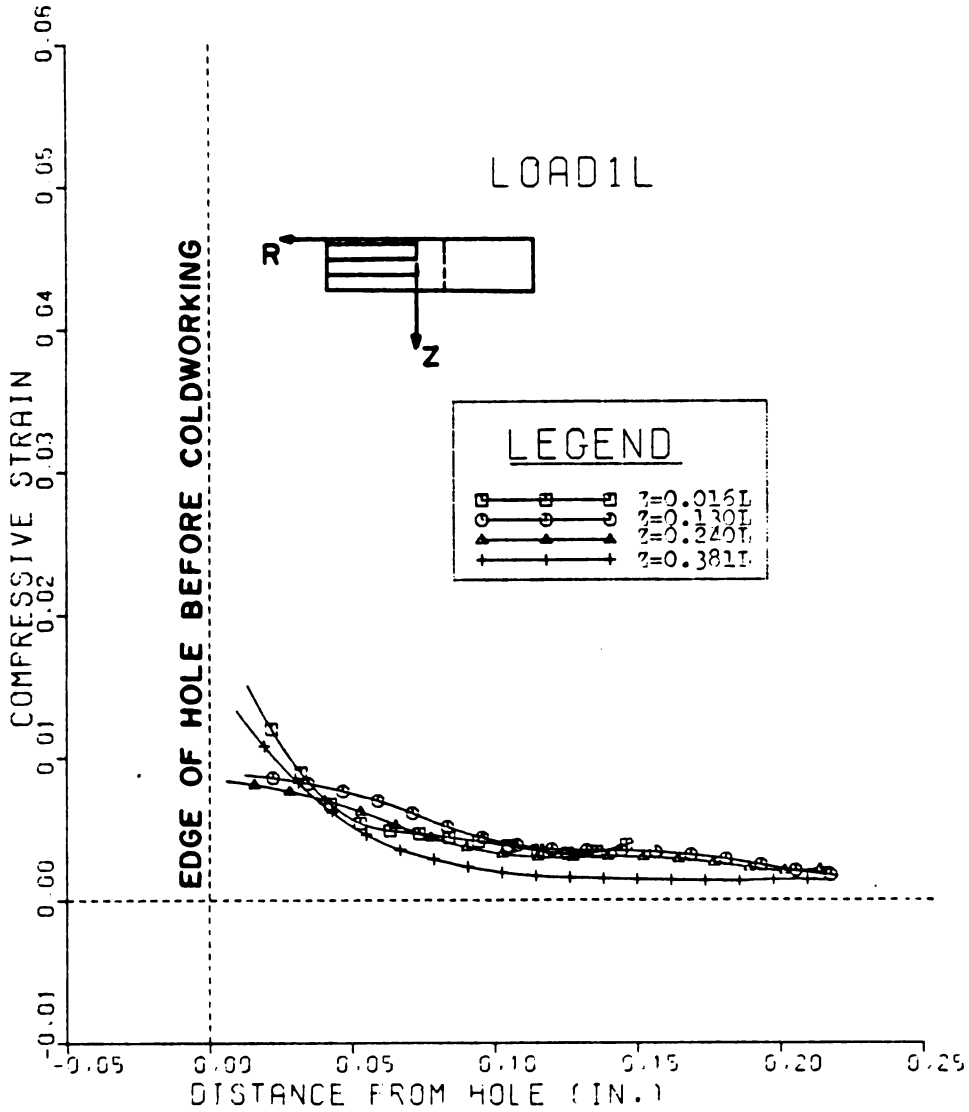

Figure 4.11.1 Radial Strain at Different Planes Along the Thickness on Left Side of Hole at 1st Step.

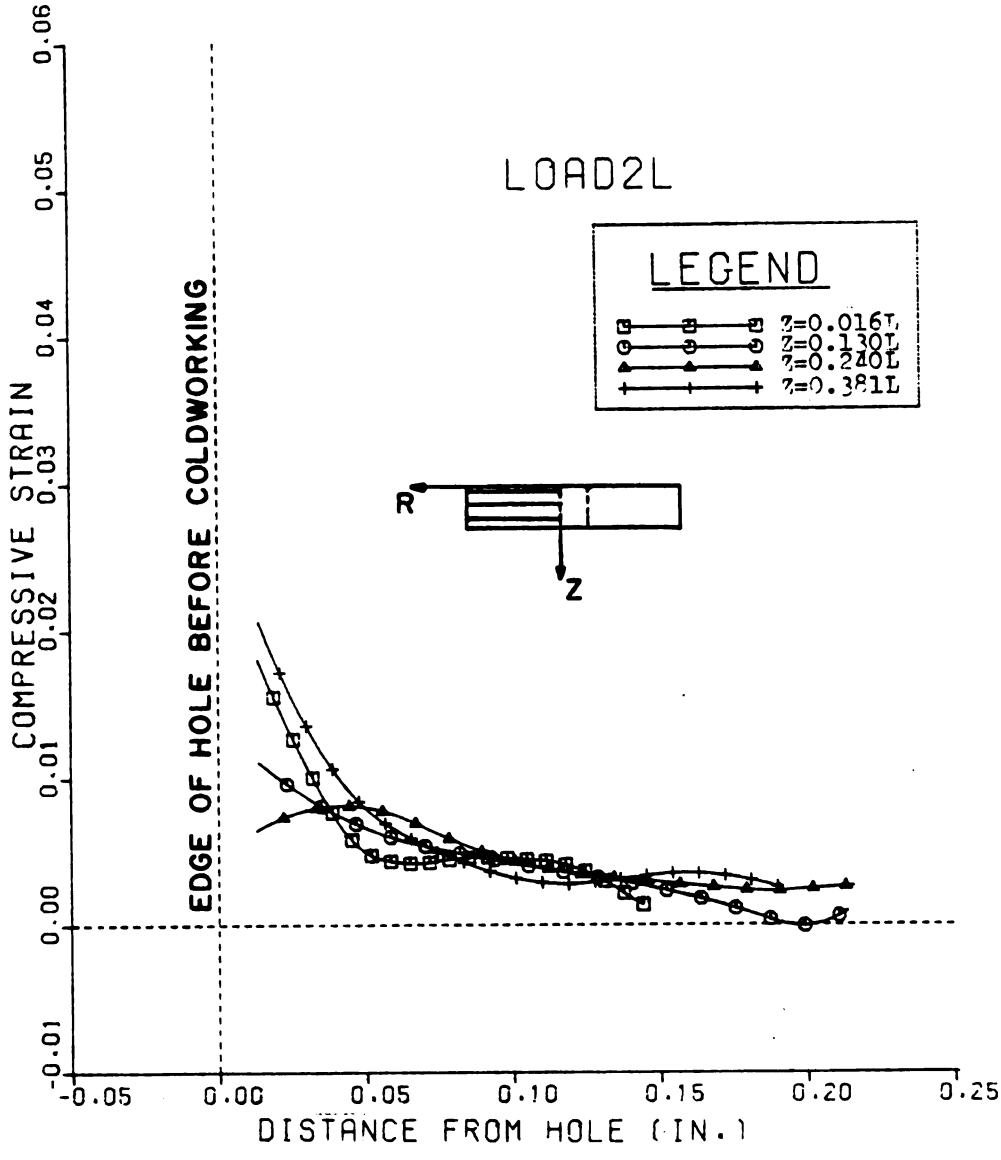

Figure 4.11.2 Radial Strain at Different Planes Along the Thickness on Left Side of Hole at 2nd Step.

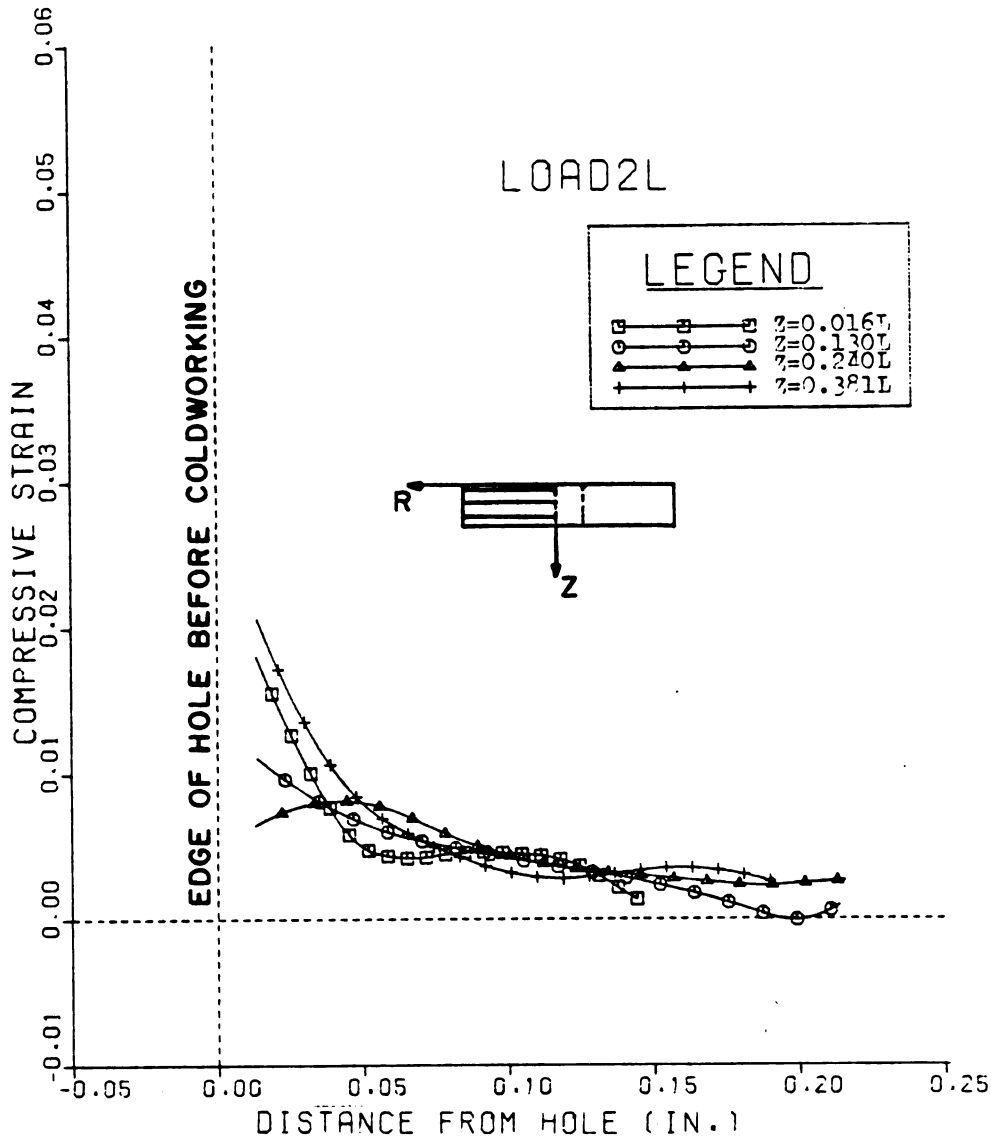

Figure 4.11.2 Radial Strain at Different Planes Along the Thickness on Left Side of Hole at 2nd Step.

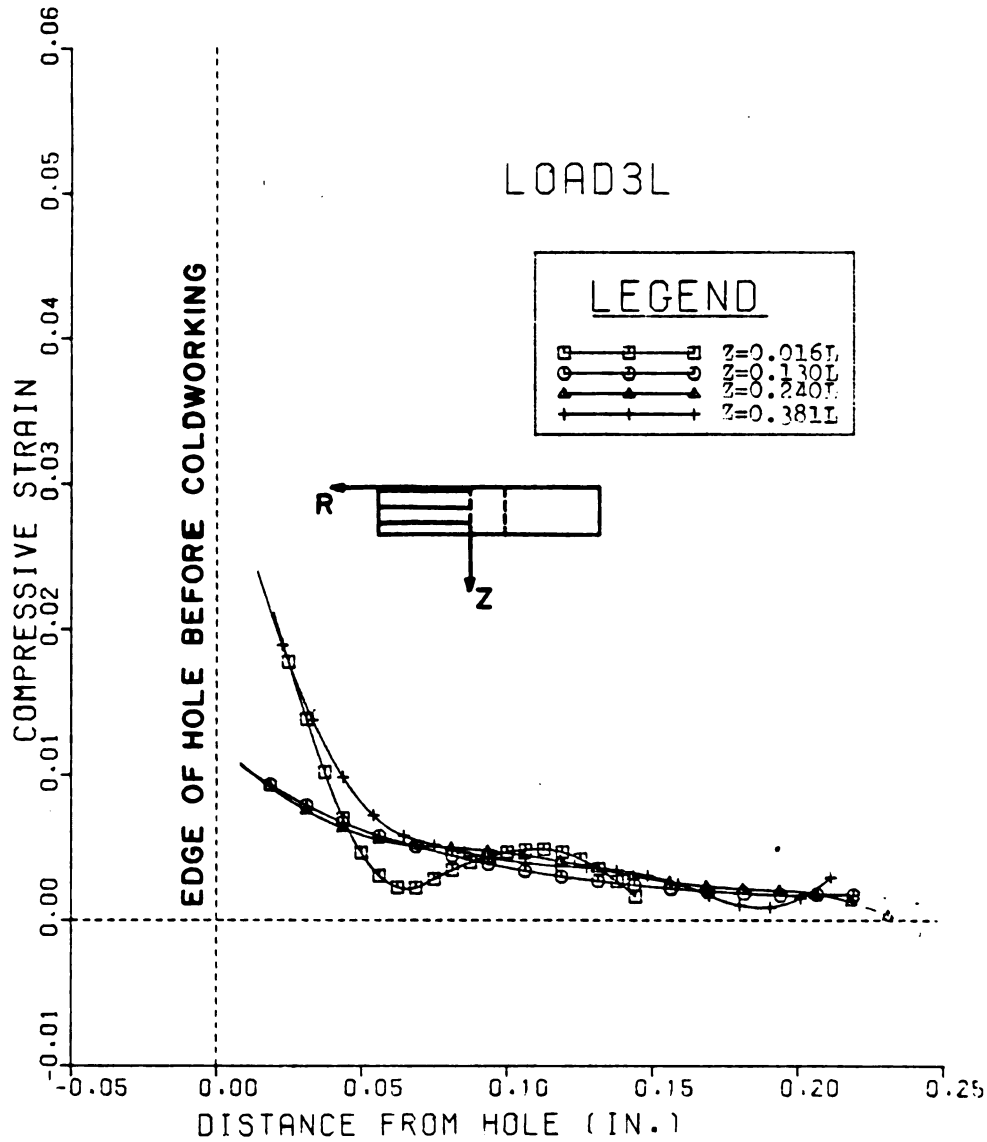

Figure 4.11.3 Radial Strain at Different Planes Along the Thickness on Left Side of Hole at 3rd Step.

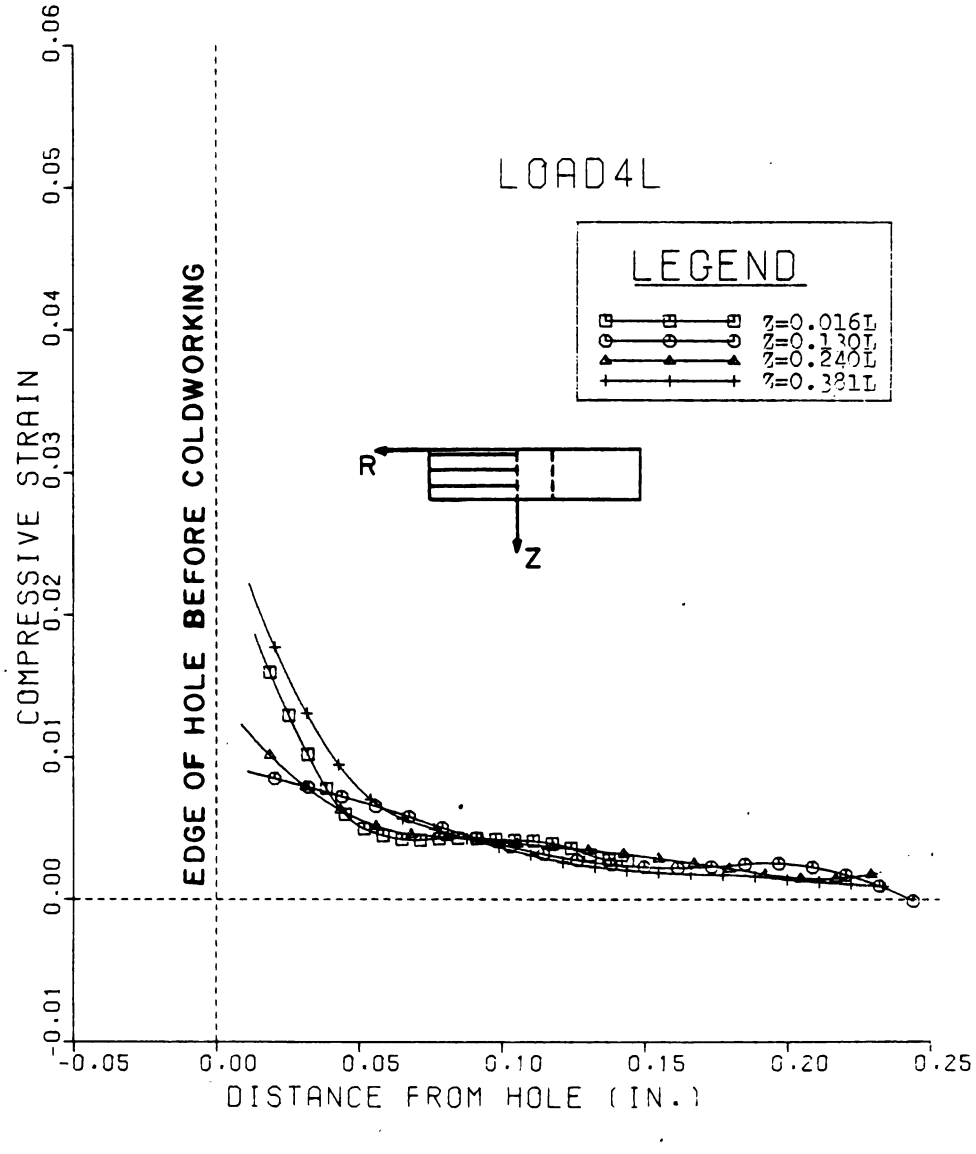

Figure 4.11.4 Radial Strain at Different Planes Along the Thickness on Left Side of Hole at 4th Step.

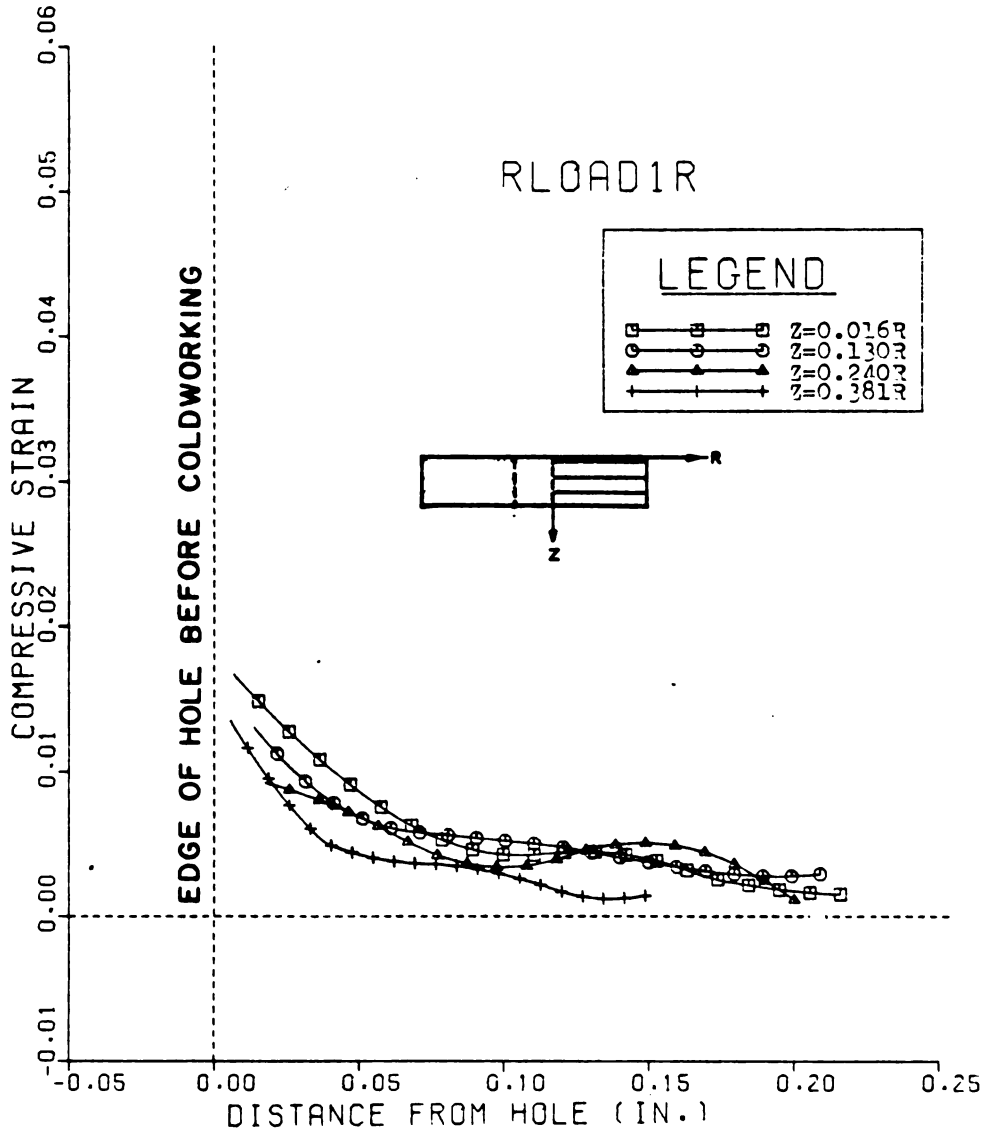

Figure 4.12.1 Radial Strain at Different Planes Along the Thickness on Right Side of Hole at 1st Step.

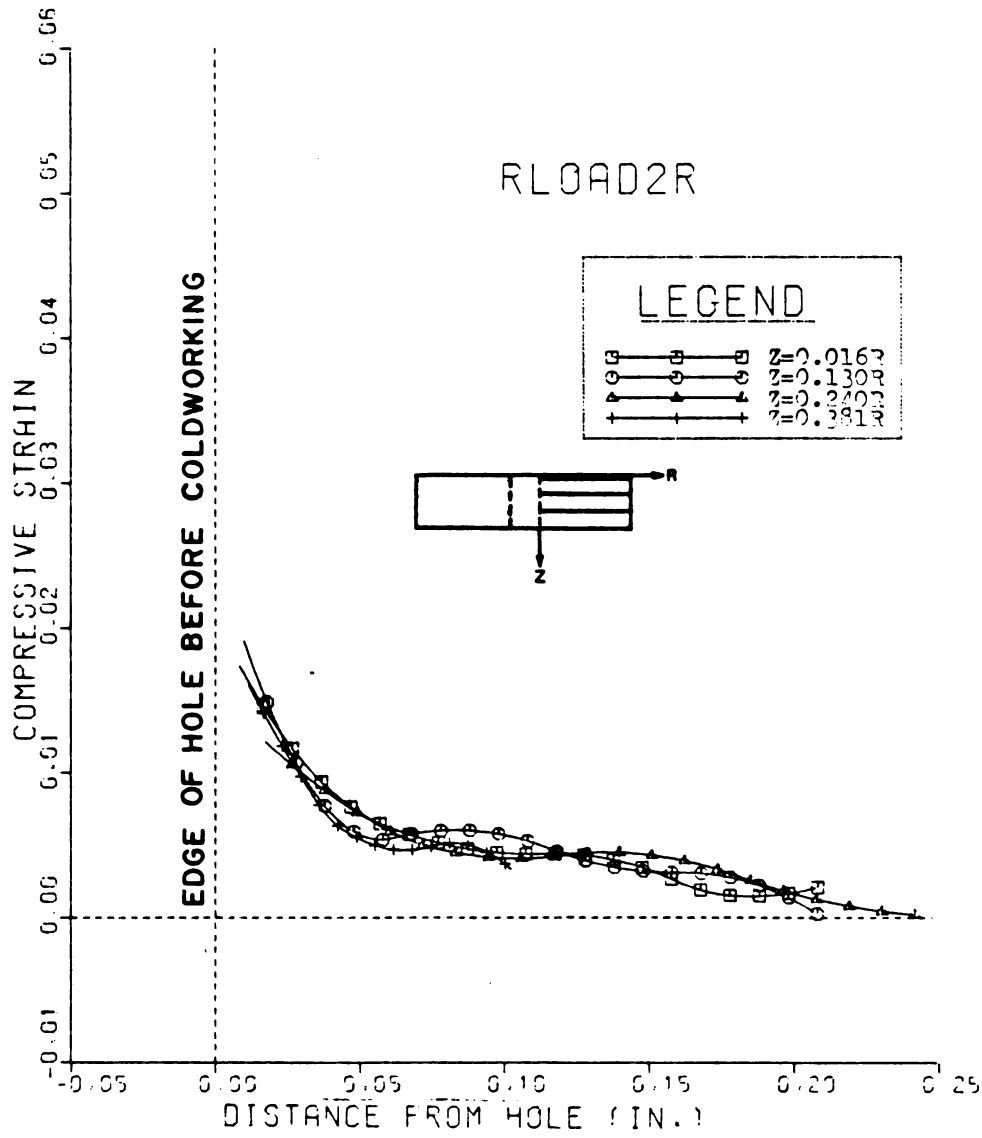

Figure 4.12.2 Radial Strain at Different Planes Along the Thickness on Right Side of Hole at 2nd Step.

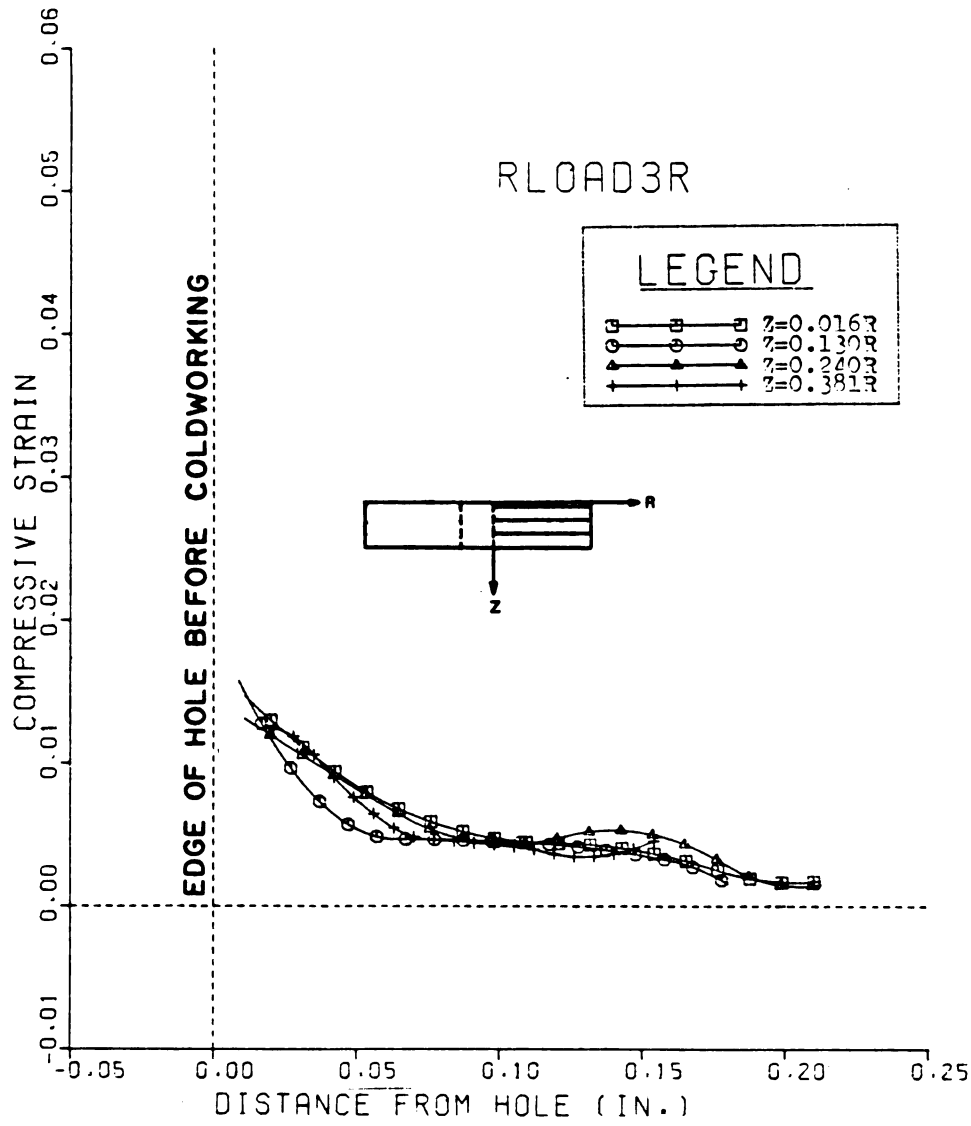

Figure 4.12.3 Radial Strain at Different Planes Along the Thickness on Right Side of Hole at 3rd Step.

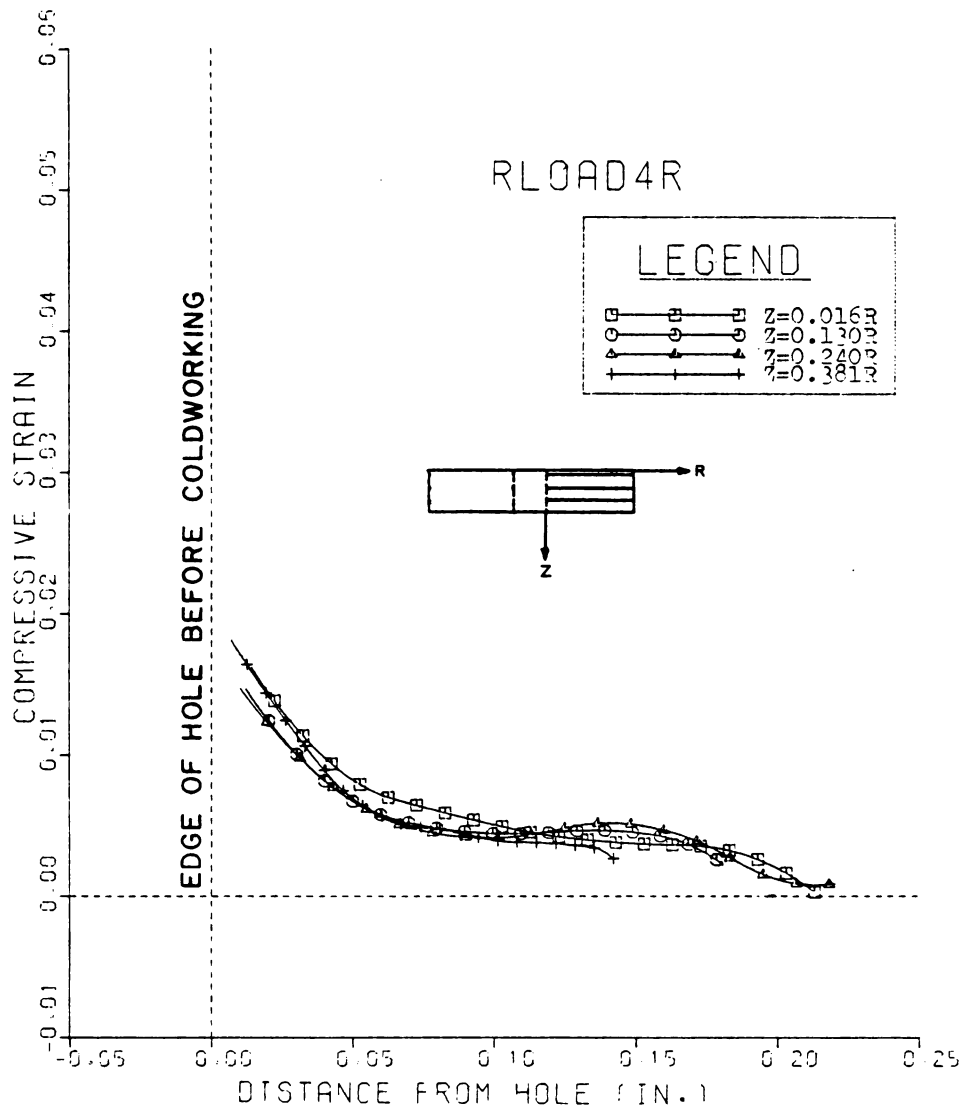

Figure 4.12.4 Radial Strain at Different Planes Along the Thickness on Right Side of Hole at 4th Step.

the radial direction was measured to within 0.01 inch (0.254 mm) of the edge of the hole. The results show that the largest strain occurred within 0.1 inch (2.54 mm) of the edge of the hole after the mandrel was pulled out. The strain is maximum at the top and decreases towards the bottom as shown in Figure 4.11.1 and Figure 4.12.1. The shape of the fringe line pattern obviously changes as the mandrel is pulled through. From Figures 4.10.3 and 4.10.4,one can see a modification of the fringe pattern near the top of the mandrel when the mandrel was pulled down for each step (the position of the top of the mandrel is shown by the arrow). When the tapered mandrel was pulled out, the strain on the bottom surface was slightly larger than at the top, and the strains inside the specimen were smaller than the surface strains, as shown in Figure 4.11.4 and 4.12.4, because the diametral expansion was smaller than on the surface.

The strain in the z-direction for the polyester specimen was measured from moire fringe patterns to within 0.05 inch (0.13 mm) of the edge of the hole after the tapered mandrel was pulled through and the sleeve was still in the hole. The photographs of moire fringe pattern from the horizontal grill (horizontal fringes) are shown in Figure 4.13.1 to Figure 4.13.5; and the plots of strain in the z-direction on the left side and the right side of the hole are shown in Figure 4.14.1 to Figure 4.14.4 and Figure 4.15.1

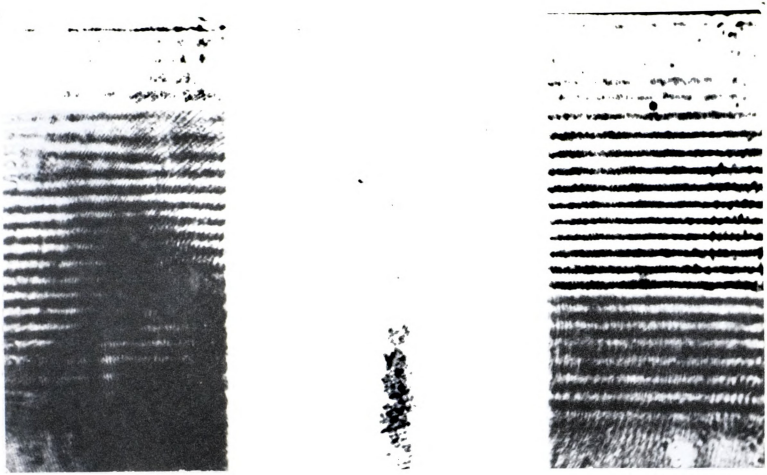

Figure 4.13.1 Photograph of Moire Fringe Pattern with Noloaded on Test Specimen of Mixed Polyester 60:40.

Figure 4.13.2 Photograph of Moire Fringe Pattern with 1st-Step Load on Test Specimen of Mixed Polyester 60:40.

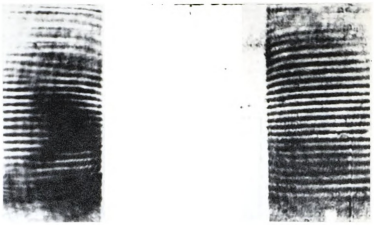

Figure 4.13.4 Photograph of Moire Fringe Pattern with 3rd-Step Load on Test Specimen of Mixed Polyester 60:40.

Figure 4.13.3 Photograph of Moire Fringe Pattern with 2nd-Step Load on Test Specimen of Mixed Polyester 60:40.

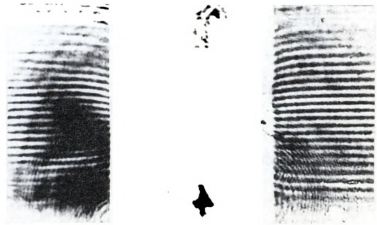

Figure 4.13.5 Photograph of Moire Fringe Pattern with 4th-Step Load on Test Specimen of Mixed Polyester 60:40.

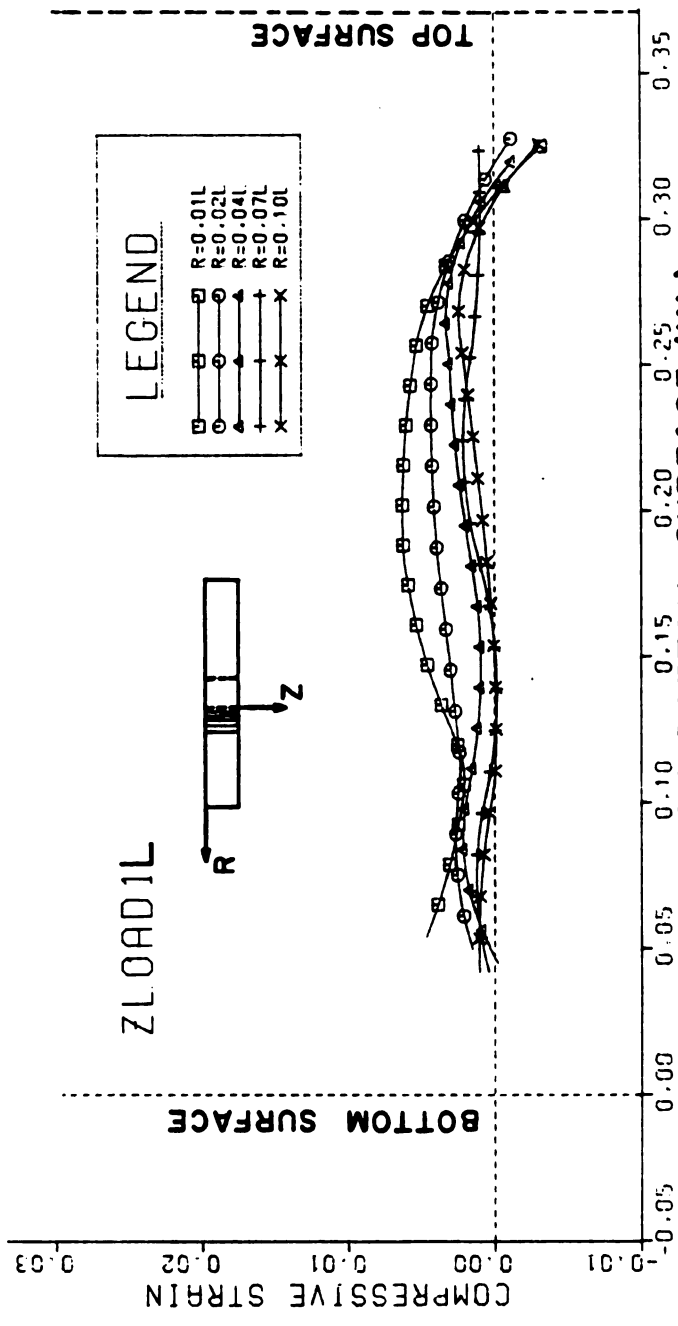

Figure 4.14.1 Strain in z-direction at Different Lines on Left Side of Hole at 1st Step.

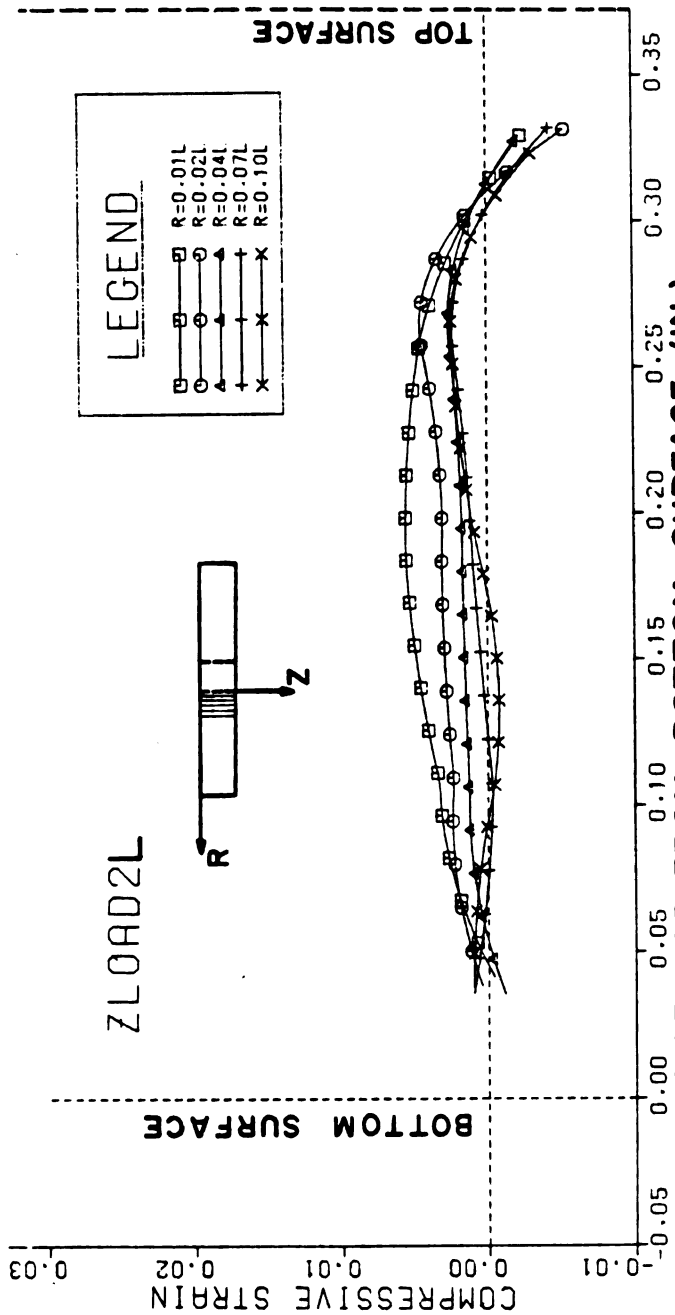

Figure 4.14.2 Strain in z-direction at Different Lines on Left Side of Hole in 2nd Step.

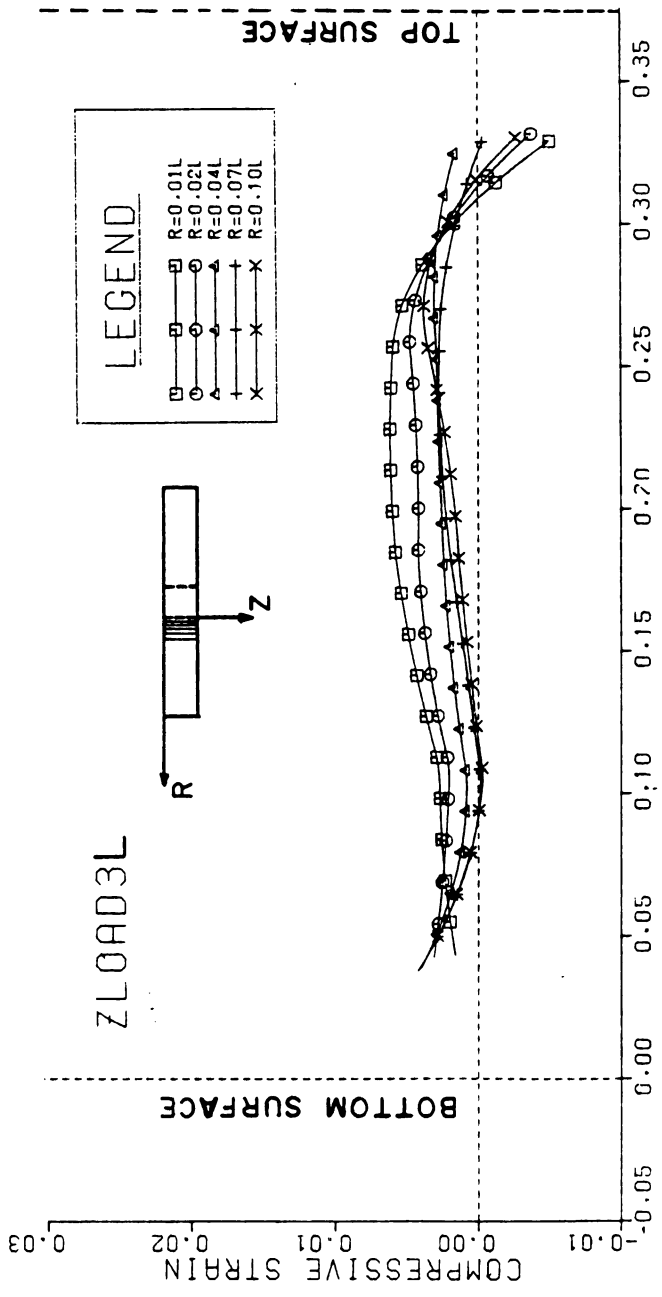

Figure 4.14.3 Strain in z-direction at Different Lines on Left Side of Hole at 3rd Step.

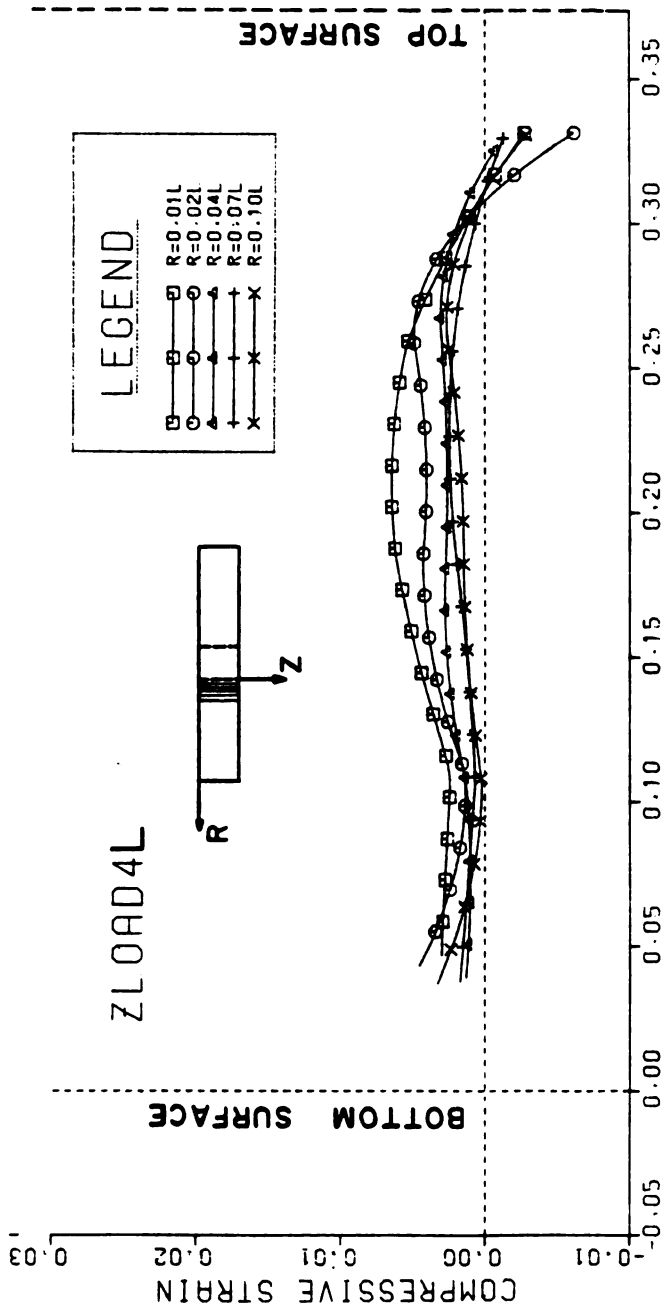

Figure 4.14.4 Strain in z-direction at Different Lines on Left Side of Hole at 4th Step.

to Figure 4.15.4 respectively. The results show that, after the specimen was loaded, the fringe near the edge of the hole moved toward the mid-plane. The distance between two fringes in the deformed specimen was smaller than the corresponding distance for the undeformed specimen. At the top of the specimen, the fringes near the edge of the hole moved toward the mid-plane but the distance between the two fringes is slightly larger than in the unloaded case. Such behavior occurs because the top layer of the speciemn near the edge of the hole is expanded. Unfortunately, the optical system could not record a good enough grating near the bottom surface, and thus, the bottom surface results could not be obtained because of lack of fringe resolution. The strain near the edge of the hole along the z-direction is tension near the top surface, but it changes to compressive strain farther than a few millimeters from the surface. The strain increases to a maximum compressive strain at about the mid-plane, decreases to near zero and then increases to compression again as the bottom surface is approached. These changes in sign result from the physical constraints of the process. When the tapered mandrel is pulled down, the bottom surface is supported by an anvil, and the area near the edge of the hole on the bottom surface cannot move down. This constraint causes increasing compressive strain near the bottom surface.

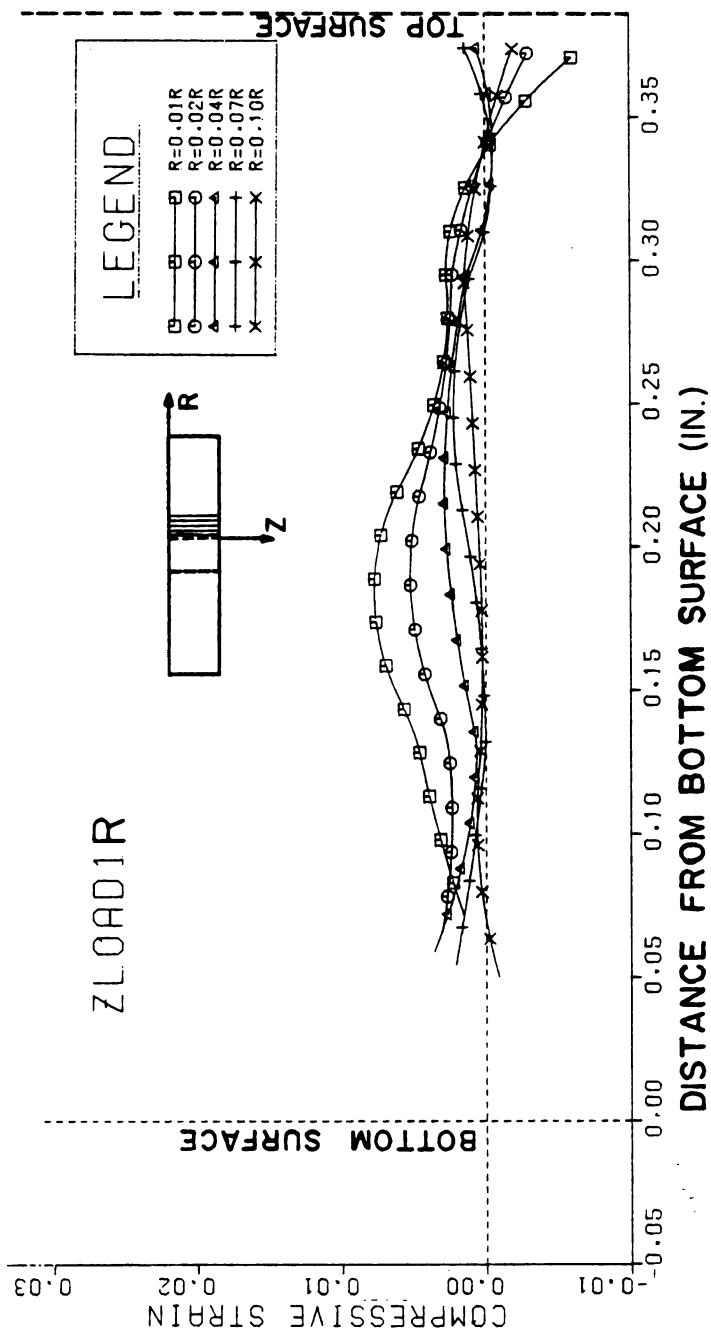

Figure 4.15.1 Strain in z-direction at Different Lines on Right Side of Hole at 1st Step.

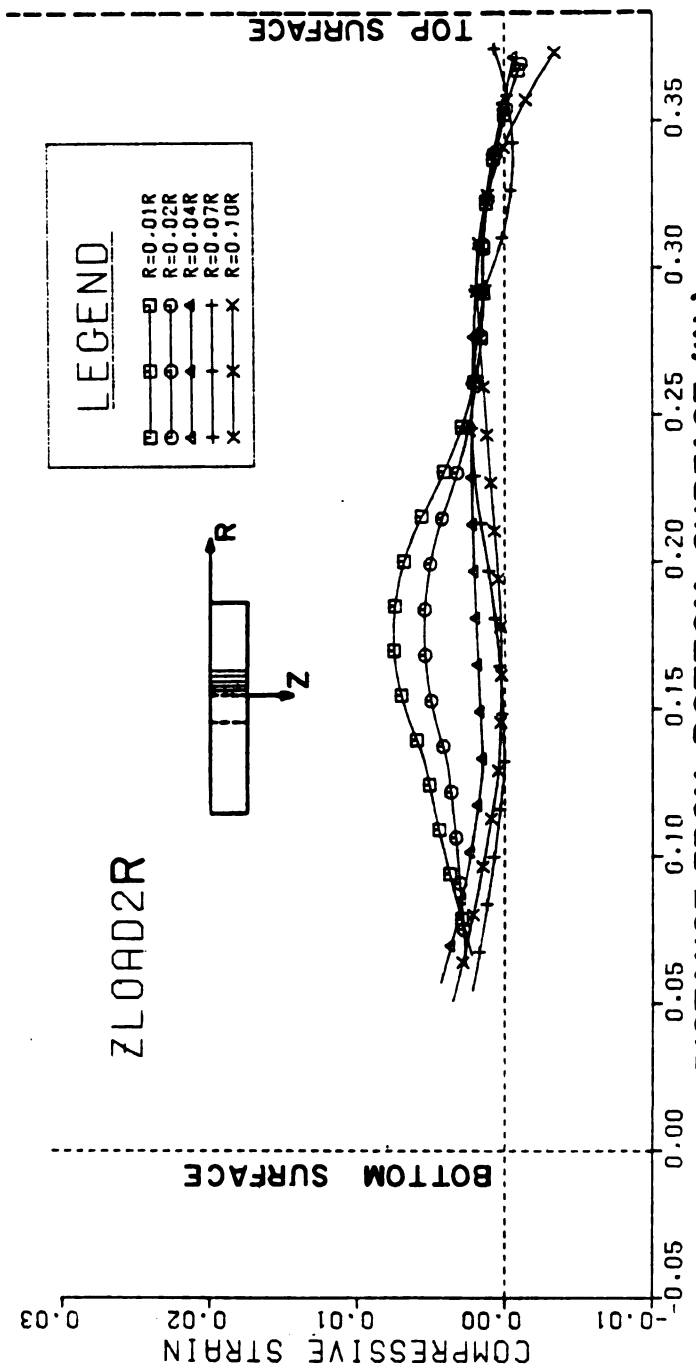

Figure 4.15.2 Strain in z-direction at Different Lines on Right Side of Hole at 2nd Step.

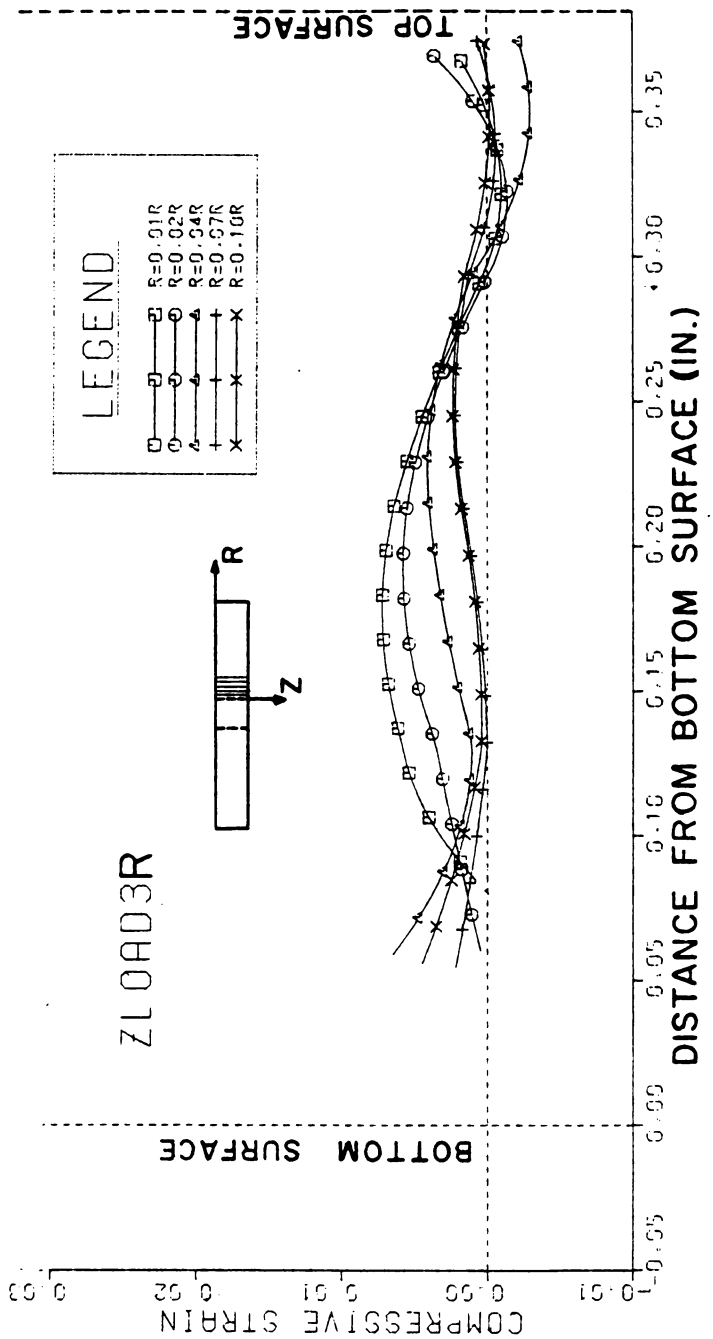

Figure 4.14.3 Strain in z-direction at Different Lines on Right Side of Hole at 3rd Step.

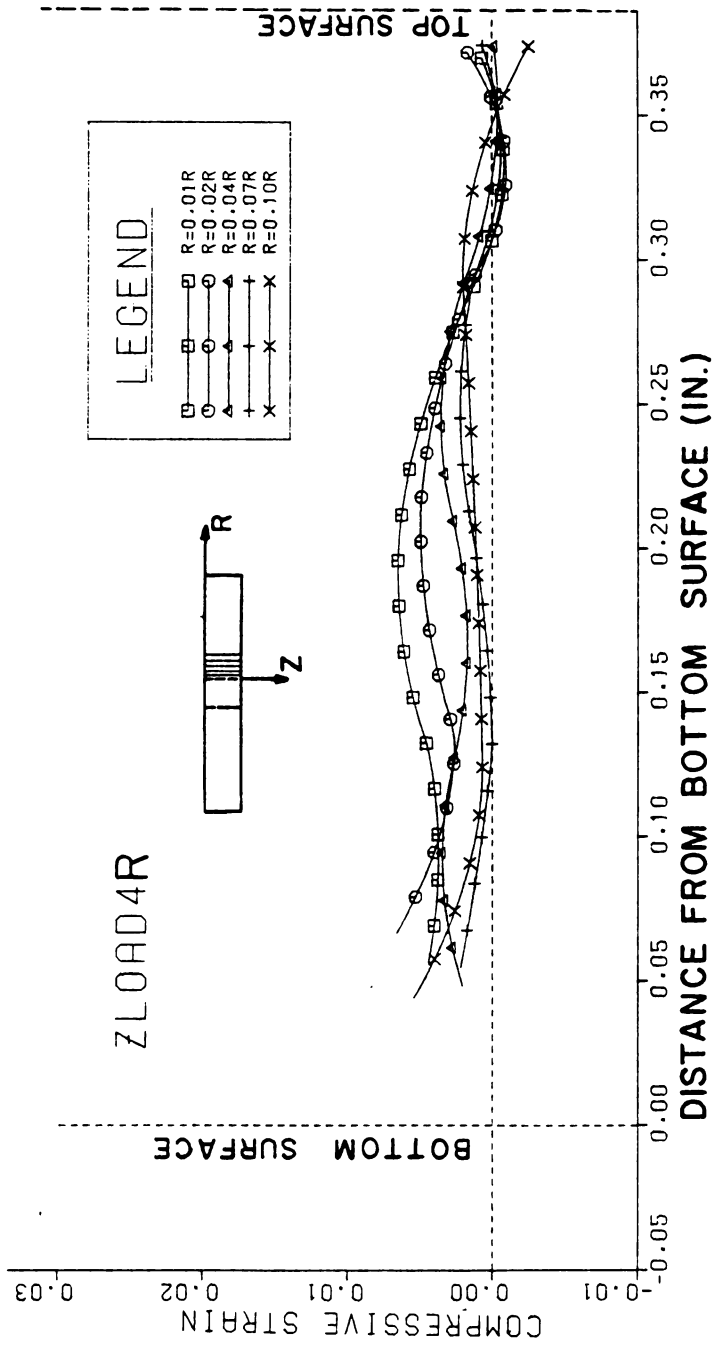

Figure 4.15.4 Strain in z-direction at Different Lines on Right Side of Hole at 4th Step.

The strain in the z-direction along the thickness is compression because the taper shape of the mandrel causes compressive force in the z-direction when the mandrel is pulled down. The maximum strain occurred at about mid-plane of the thickness. The vertical displacement near the edge of the hole results in tension strain for only a thin layer near the top surface. This result agrees with the experimental measurement of the thickness change near the edge of the hole on the top surface of a coldwork specimen by S. Poolsuk and W. N. Sharpe, Jr. (2). They showed that the thickness near the edge of the hole on the top surface was expanded after coldwork.

A plot of the strain in the z-direction versus distance from the edge of the hole on the midplane of the fully coldworked specimen is shown in Figure 4.16. The strain is maximum near the edge of the hole and then decreases with increasing distance from the hole.

4.3 Tangential Strain Measurement on Different Planes

4.3.1 Specimen Preparation

The tangential strain, or "hoop" strain, can be measured by using a unique multi-plane specimen having embedded gratings. For this study, polycarbonate was used to make a specimen. The specimen was made in a circular disk shape. It consisted of three pieces having different thicknesses. Two of the disks had half the thickness of the third one. The dimensions of the specimen are shown in

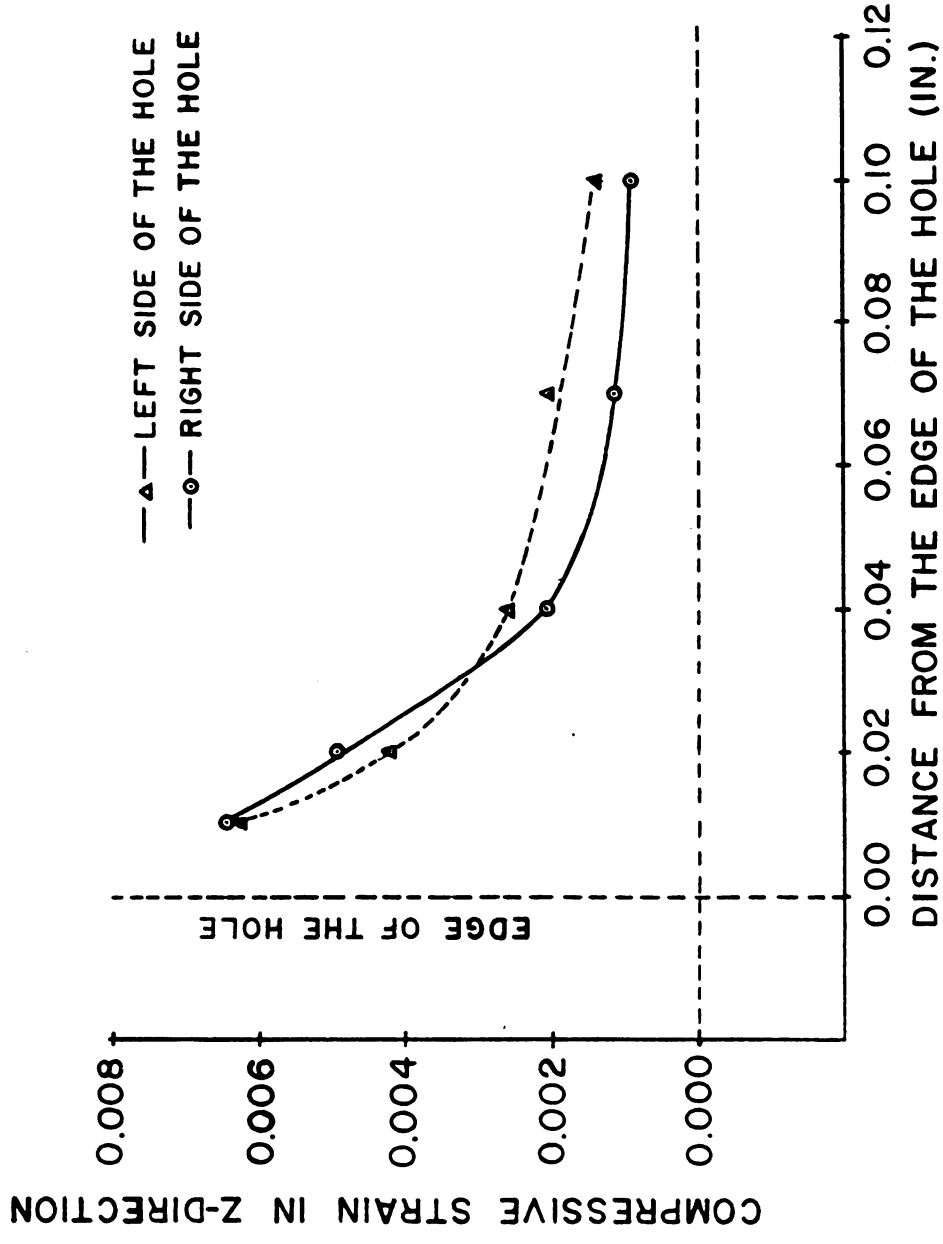

Figure 4.16 Strain in z-direction on the Midplane.

Figure 4.17. A copper grating was deposited on one side of each of the thinner pieces by using the stencil method, then, all three pieces were fastened together with epoxy (Epon 828 and Diethylene triamine 100:8 by weight) by bonding a grating side to a plain side. The resulting composite specimen had a copper grating on the quarter plane and on the midplane. The hole with diameter 0.25 inch (6.35 mm) was made at the center of the specimen. Finally, a copper grating was deposited on the top surface of the thinner piece. No grating was needed on the back surface because, when the specimen was coldworked, the anvil would destroy the grating around the hole. Before coldwork, the anvil was removed from the sleeve and the flange that supported the anvil was trimmed to be as small as possible in order to allow the light to pass through the specimen. This was done so that a photograph of the grating on each plane close to the edge of the hole could be made. The diameter of the flange of the sleeve was a little bigger than the diameter of the hole.

4.3.2 Photograph of Specimen Gratings

The specimen set-up was almost the same as before, the difference being that the specimen was placed on the specimen holder so as to let the light pass through the specimen in the direction parallel to the hole. A photographic process was developed so that each grating could be recorded individually even though it might be obstructed by other

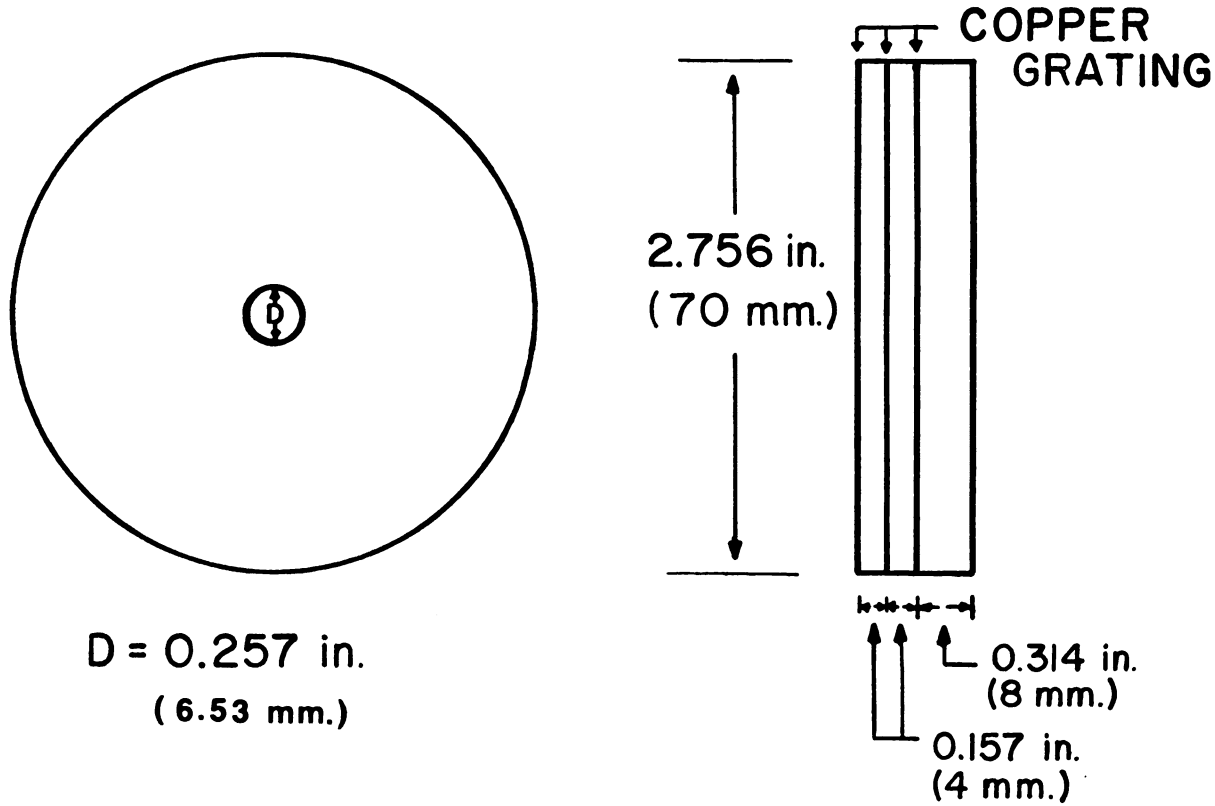

Figure 4.17 Specimen Dimension.

gratings. The first data plate was recorded by focusing on the surface grating. Then the specimen was moved closer to the lens to get a focus on the quarter plane and a second data plate was recorded. Finally the specimen was turned around, and after focusing the grating on the mid-plane, the third data plate was recorded. A schematic of the specimen set-up is shown in Figure 4.18.

4.3.3 Results and Discussion

For this study the specimen with no-load and the grating after mandrelizing were recorded on High Speed Holographic Plate (Kodak Type 131-02, 4x5 inch) for each plane of grating. The moire fringe pattern was extracted by using the optical processing technique. The photographs of the moire fringe pattern on each plane are shown in Figure 4.19.1 to Figure 4.19.3. The plots of hoop strain (0.0455 in from the edge of the hole of specimen before load) on each plane obtained from the moire fringe patterns are shown in Figure 4.20. The results show that the hoop strains near the edge of the hole on each plane are a little different. The hoop strain on the surface is slightly larger than the others, and the hoop strain on the midplane is the smallest. This agrees with the observation that the diametral expansion on the surface is slightly larger than in the interior of the specimen as was shown in Figure 4.7.

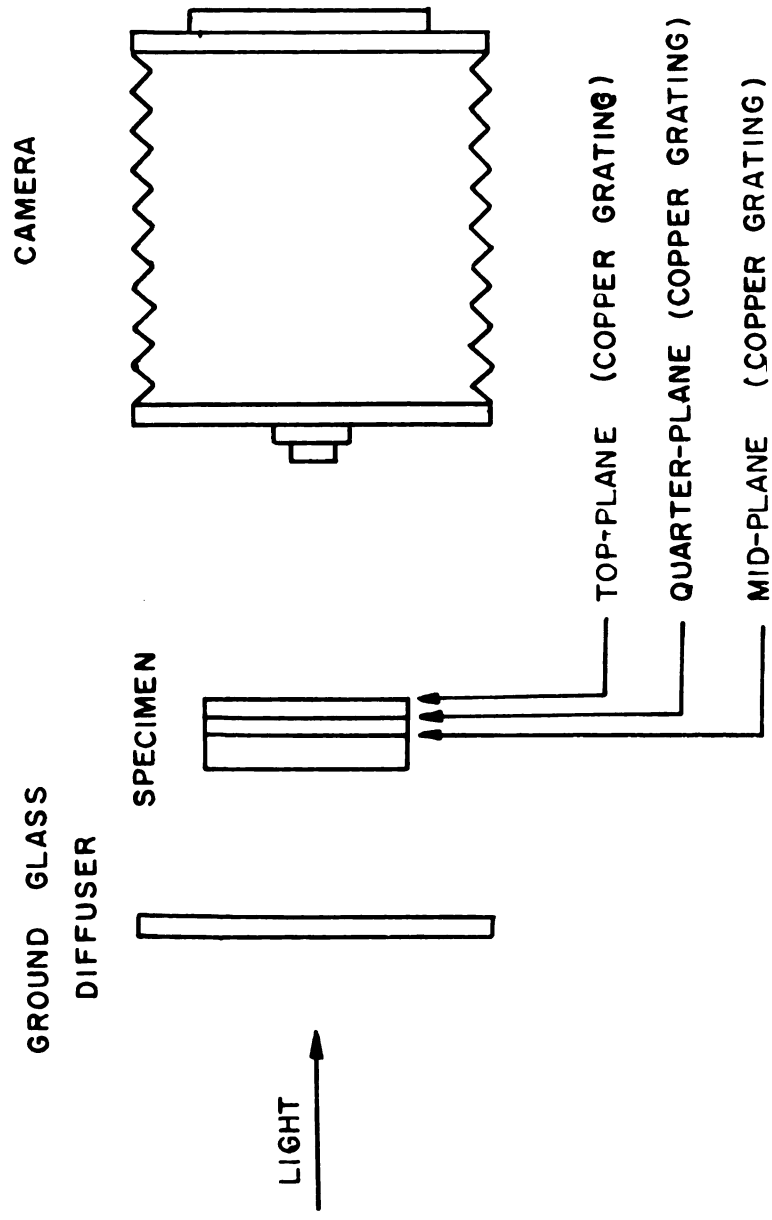

Figure 4.18 Schematic of the Photographic Data Recording.

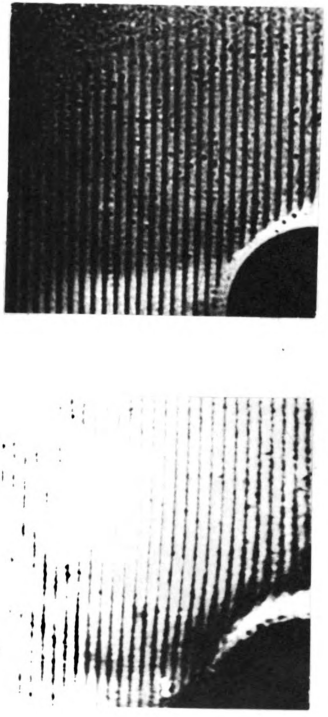

Figure 4.19.1 **The Moire Fringe Pattern of Specimen Before and After Load on Surface-Plane.**

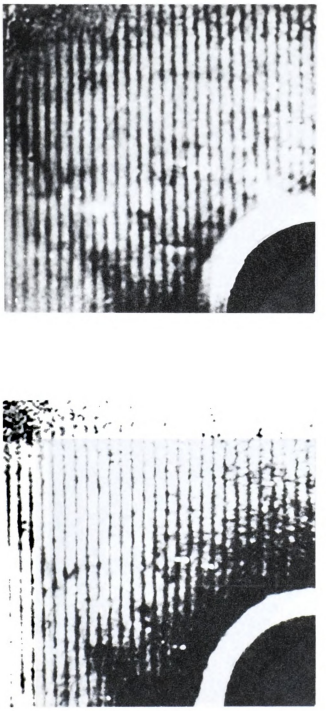

Figure 4.19.2 The Moire Fringe Pattern of Specimen Before and After Load on Quarter-Plane.

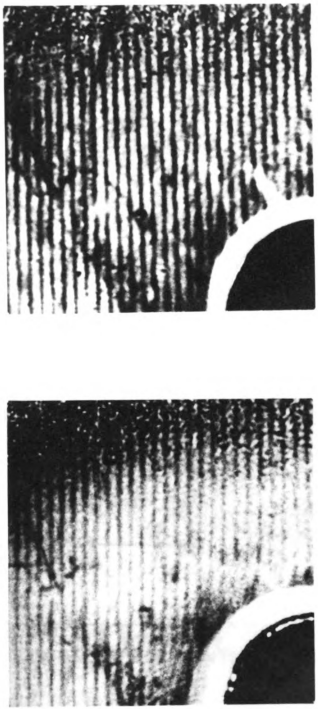

Figure 4.19.3 The Moire Fringe Pattern of Specimen Before and After Load on Mid-Plane.

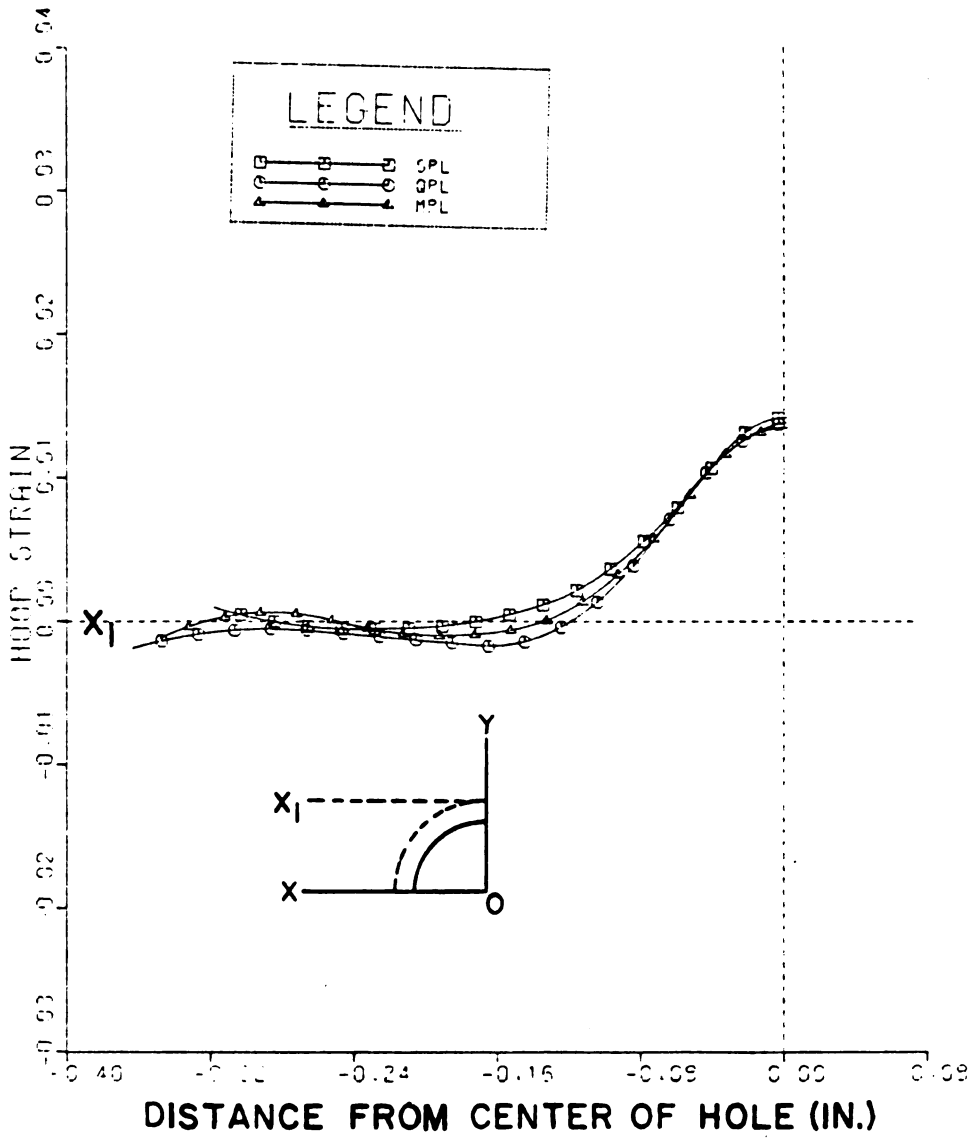

Figure 4.20 Hoop Strain Near the Edge of the Hole on Different Planes.

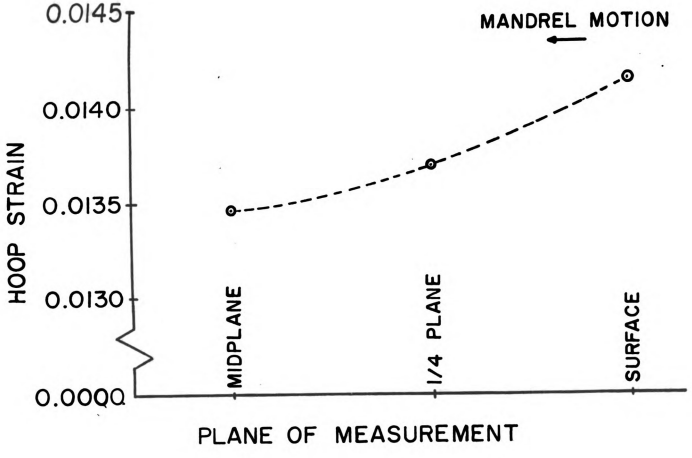

Figure 4.21 Comparison of Hoop Strain Near the Edge of the Hole on Each Plane.

4.4 Summary of Strain Field in Coldworked Specimen

The experimental results in this investigation are restricted to the strain maps along the thickness near the edge of the hole while the specimen is being coldworked and after coldwork is completed. The strain was measured by a moire technique which gave information about the radial, hoop, and transverse normal strain fields near the edge of the hole as a function of distance from specimen surface.

The moire fringe pattern near the edge of the hole along the thickness changes when the tapered mandrel was pulled down. The diametral expansion was found not to be uniform along the thickness. The expansion inside the specimen was smaller than on the surface.

While the specimen was being coldworked, the strain was different along the thickness depending on the thickness of the specimen and on the shape of the mandrel. The strains were not uniform along the specimen thickness, and the measured strains on both sides were not quite the same. The strain in the radial direction inside the specimen was smaller than on the surface after the specimen was coldworked. The maximum strain occurred near the edge of the hole and decreased with increasing distance from the hole. The strain in the z-direction was tension near the top surface and changed to compression along the thickness; the maximum occurred near the midplane, and the strain decreased towards the bottom. After passing through a

minimum, the transverse strain increased in compression again near the bottom. The hoop strain was a maximum on the top surface, decreased to a minimum at the midplane and appeared to increase towards the bottom surface.

The fact that the radial normal strain in the interior of the specimen on the hole boundary is small when compared with the surface strain is troubling from the view point of fatigue design with coldwork-type fasteners.

The creation of tensile transverse normal strain near the surface, however, is potentially more of a problem. It is recognized, however, that the transverse stress might be modified by installation of a fastener, such as a bolt, which induces compression in the material.

CHAPTER 5

STRAIN MEASUREMENT ON DIFFERENT PLANES NEAR A CRACK TIP IN THICK COMPACT TENSION SPECIMEN

5.1 Fundamentals of Fracture Mechanics

5.1.1 Linear Elastic Fracture Mechanics

Linear elastic fracture mechanics is based on an analytical procedure that relates the stress-field magnitude and distribution in the vicinity of a crack tip to the nominal stress applied to the structure, to the size, shape, and orientation of the crack, and to material properties.

The stress field near a crack tip can be described as one of three basic types, each associated with a local mode of deformation as illustrated in Figure 5.1. The three types of relative movements of the two crack surfaces are:

Mode I, called the opening mode, is characterized by local displacements that are symmetric with respect to x-y and x-z planes. The two fracture surfaces are displaced perpendicular to each other in opposite directions.

Mode II, the sliding or shearing mode is characterized by local displacements that are symmetric with respect to the x-y plane and skew-symmetric with respect to the x-z

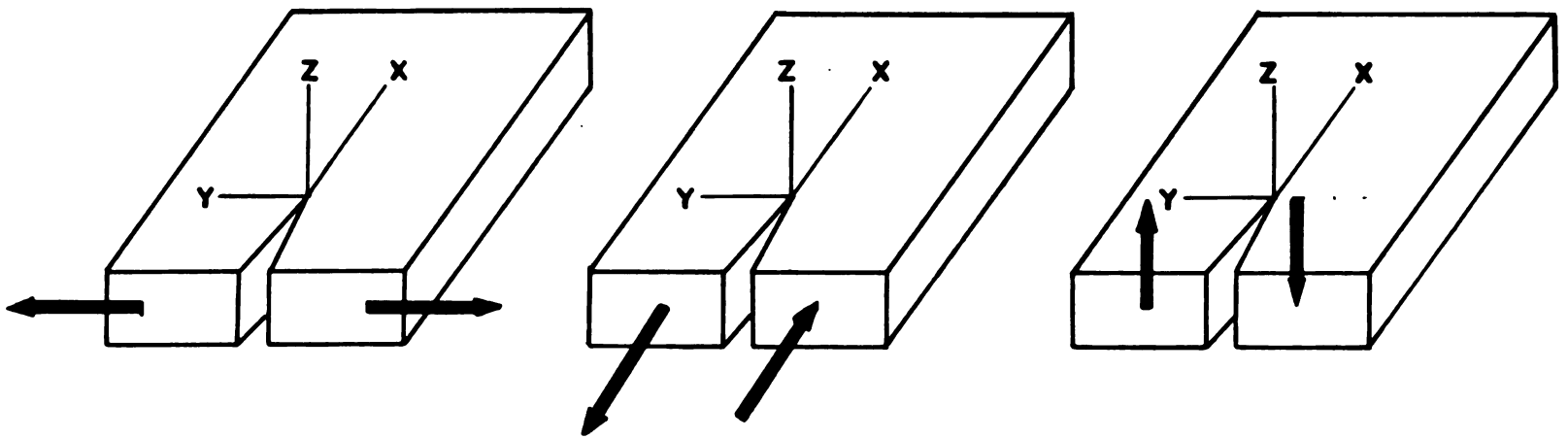

I) Opening or Tensile Mode

II) Sliding or Shearing Mode

III) Tearing or Anti-Plane Shear Mode

Figure 5.1 The Basic Modes of Loading the Crack Plate.

plane. The two fracture surfaces slide over each other in a direction perpendicular to the line of the crack tip.

Mode III, the tearing mode is associated with local displacements that are skew-symmetric with respect to both x-y and x-z planes. The two fracture surfaces slide over each other in the direction that is parallel to the line of the crack front.

5.1.2 The Relationship Between Stress, Strain and Displacement Near a Crack Tip

For a given plate thickness and a given material, a unique correspondence must exist between the stress intensity factor (K), the stresses (σ_{ij}), the strains (ε_{ij}), and the displacements (u_i) in the vicinity of a crack tip, even if there is a small plastic zone. Any one of these physical quantities completely characterizes all the others. In other words, if any one of these quantities is fixed, all the others are fixed with it. The correspondence between these physical quantities near a crack tip results from the fact that the crack tip stress and strain distributions are mainly determined by the unique geometry of the crack itself. This conclusion about the correspondence between K, σ_{ij}, ε_{ij}, and u_i is subject to the limitation of constant specimen thickness. The transition of the state of stresses and strains near a crack tip from that of plane stress on the surface of the specimen to

that of plane strain in the interior of the specimen is controlled by the specimen thickness. For a given specimen thickness, all the stresses, strains and displacements must be characterized by the stress intensity factor. It follows, then, that the critical value of stress intensity factor, K_c, must be a constant for a given material and specimen thickness. Because of the characteristic correspondence between K, σ_{ij}, ϵ_{ij}, and u_i near a crack tip, any one of these quantities can be used to define a fracture criterion in the case of small-scale yielding. If this characteristic correspondence between stresses, strains and displacements still exists in the case where extensive plastic deformation or even general yield occurs, the stress, strains, or displacements near a crack tip can be used as a ductile fracture criterion. Stress near a crack tip is difficult to measure, therefore its usefulness as a fracture criterion is limited. Indeed, crack opening displacement has been proposed as a ductile fracture criterion. Experimental technique to measure the crack opening displacement and the strain on the surface of a crack specimen have been pursued by many researchers, (22,26,49,70), but a technique to measure the crack opening displacement and strain in the interior of a crack specimen is yet to be developed.

The elastic solution for the stress, strain and displacement distribution around a crack tip has been obtained by William (30) and Irwin (31). The stress field equations for a cracked plate in tension (mode I) as derived by Irwin (31) using the methods of Westergaard (32) are:

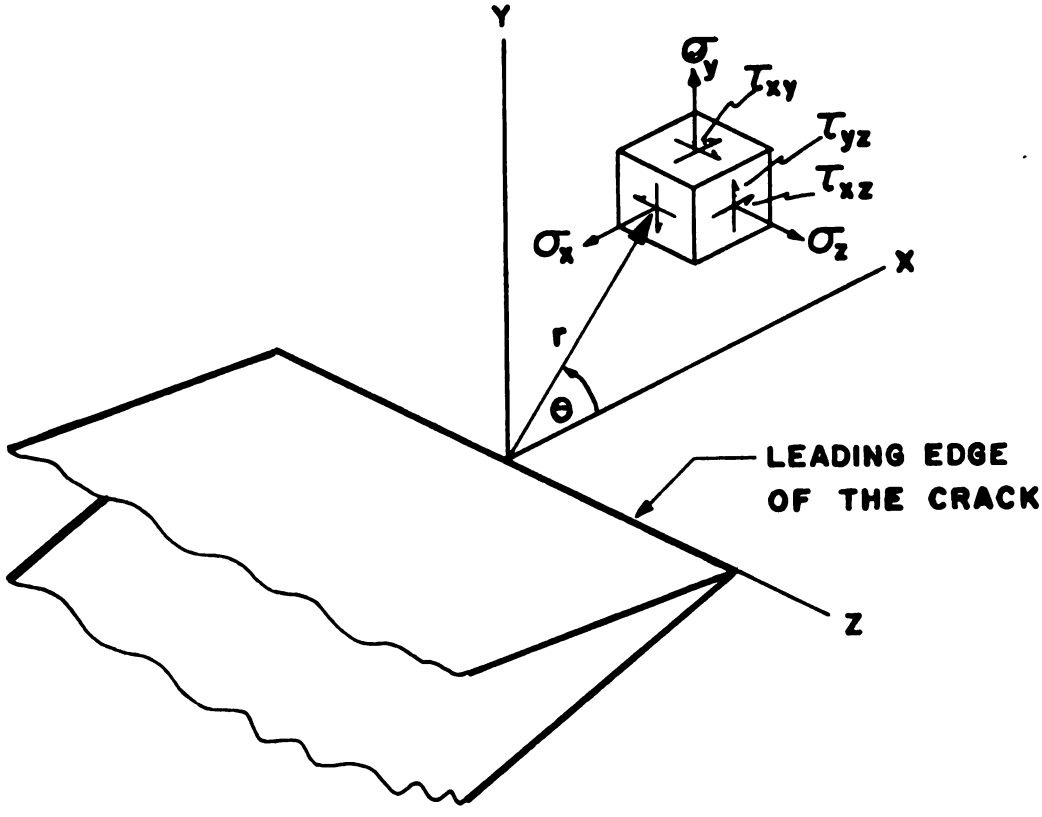

Figure 5.2 Coordinates Measured from the Leading Edge of a Crack and the Stress Components in the Crack Tip Stress Field.

Mode I

Elastic Stress

$$\left.\begin{aligned}
\sigma_{xx} &= \frac{K_I}{\sqrt{2\pi r}} \cos\frac{\theta}{2}\left[1 - \sin\frac{\theta}{2}\sin\frac{3\theta}{2}\right] + \ldots \\
\sigma_{yy} &= \frac{K_I}{\sqrt{2\pi r}} \cos\frac{\theta}{2}\left[1 + \sin\frac{\theta}{2}\sin\frac{3\theta}{2}\right] + \ldots \\
\sigma_{xy} &= \frac{K_I}{\sqrt{2\pi r}} \sin\frac{\theta}{2}\cos\frac{\theta}{2}\cos\frac{3\theta}{2} \\
\sigma_{xz} &= \sigma_{yz} = 0 \\
\sigma_{zz} &= \begin{cases} 0 & \ldots\ldots\text{Plane Stress} \\ \nu(\sigma_{xx} + \sigma_{yy}) = \dfrac{2\nu K_I}{\sqrt{2\pi r}}\cos\dfrac{\theta}{2} & \ldots\ldots\text{Plane Strain} \end{cases}
\end{aligned}\right\} \quad (5.1)$$

Strain in Terms of Stress

$$\varepsilon_{ij} = \frac{1}{\mu}\left[\sigma_{ij} - \frac{\nu}{1+\nu}\,\delta_{ij}\,\sigma_{kk}\right] \qquad (5.2)$$

Where μ is shear modulus

$$\mu = \frac{E}{2(1+\nu)}$$

$$\left.\begin{aligned}
\varepsilon_{yy} &= \frac{1}{E}\left[\sigma_y - \nu\sigma_x\right] \qquad \ldots\ldots\ldots \text{ plane stress} \\
\varepsilon_{yy} &= \frac{1}{E}\left[(1-\nu^2)\ \sigma_y - \nu(1+\nu)\,\sigma_x\right] \ldots \text{plane strain}
\end{aligned}\right\} \quad (5.3)$$

Elastic Strain

Strain in Plane Stress ($\sigma_{zz} = 0$)

$$\left.\begin{aligned}
\varepsilon_{xx} &= \frac{K_I}{E\sqrt{2\pi r}} \cos\frac{\theta}{2}\left[(1-\nu)-(1+\nu)\sin\frac{\theta}{2}\sin\frac{3\theta}{2}\right] + \ldots \\
\varepsilon_{yy} &= \frac{K_I}{E\sqrt{2\pi r}} \cos\frac{\theta}{2}\left[(1-\nu)+(1+\nu)\sin\frac{\theta}{2}\sin\frac{3\theta}{2}\right] + \ldots \\
\varepsilon_{zz} &= \frac{-2\nu}{E}\frac{K_I}{\sqrt{2\pi r}}\cos\frac{\theta}{2}
\end{aligned}\right\} \quad (5.4)$$

Strain in Plane Strain [$\sigma_{zz} = \nu(\sigma_{xx} + \sigma_{yy})$]

$$\left.\begin{aligned}
\varepsilon_{xx} &= \frac{K_I}{E\sqrt{2\pi r}} \cos\frac{\theta}{2}\left[(1-\nu-2\nu^2)-(1+\nu)\sin\frac{\theta}{2}\sin\frac{3\theta}{2}\right] + \ldots \\
\varepsilon_{yy} &= \frac{K_I}{E\sqrt{2\pi r}} \cos\frac{\theta}{2}\left[(1-\nu-2\nu^2)+(1+\nu)\sin\frac{\theta}{2}\sin\frac{3\theta}{2}\right] + \ldots \\
\varepsilon_{zz} &= 0
\end{aligned}\right\} \quad (5.5)$$

Displacement in Plane Strain

$$\left.\begin{aligned}
u &= \frac{K_I}{\mu}\sqrt{\frac{r}{2\pi}}\cos\frac{\theta}{2}\left[1-2\nu+\cos^2\frac{\theta}{2}\right] + \ldots. \\
v &= \frac{K_I}{\mu}\sqrt{\frac{r}{2\pi}}\sin\frac{\theta}{2}\left[2-2\nu-\cos^2\frac{\theta}{2}\right] + \ldots. \\
w &= 0
\end{aligned}\right\} \quad (5.6)$$

K_I is the stress intensity factor under tensile strain (mode I). The elastic stress equation shows that the stress intensity factor (K_I) characterizes the stress fields near the crack tip; i.e. for the same value of K_I, the same stress fields are obtained regardless of the crack length and/or the specimen geometry. But, the stress intensity factor itself is a function of applied stress, crack length and specimen geometry. In general the stress intensity factor has the form

$$K = \sigma\sqrt{\pi a}\ f(a/w)$$

where σ is the nominal stress

2a is the crack length

f(a/w) is a function of specimen geometry and

w is the specimen width.

When plastic deformation takes place at a crack tip, a correction to the stress field equations is necessary. Several suggestions have been made for such a correction. Irwin (66) suggests that the 'plastic enclave' is bounded by the surface on which the stress is equal to the uniaxial yield strength, σ_y of the material. The approximation of plastic zone size is

$$r_y = \frac{1}{2\pi}\left(\frac{K}{\sigma_y}\right)^2 \qquad \text{for plane stress}$$

$$r_y = \frac{1}{6\pi}\left(\frac{K}{\sigma_y}\right)^2 \qquad \text{for plane strain}$$

The full width of the plastic zone is $r_p = 2r_y$

Therefore, Irwin proposes that to take care of the effect of the plastic zone, an amount of r_y be added to each end of the real crack. This corrected value can be used as the effective crack length for the calculation of the stress intensity factor

$$K_{eff} = \sigma\sqrt{\pi(a+r_y)} \quad .$$

5.1.3 Crack Tip Deformation

The stress and strain fields near a crack tip in a thick plate are complicated. In a thick plate, the state of the stresses and strains change from that of plane strain in the interior to that of plane stress on the surface. This means that a triaxial stress condition exists in the interior, and biaxial stresses exist on the surface. This is true only if the plastic zone is small relative to the plate thickness (Reference 68).

For a triaxial state of stress where the three principal stresses, σ_x, σ_y, σ_z, are equal, there are no shearing stresses. This results in almost complete constraint against plastic flow, and the elastic stresses can be increased to extremely high values. In the case of most notched specimens, $\sigma_y > \sigma_x$ or σ_z, so the normal stresses are not equal, and some shearing stresses do exist.

Consider a notched thick plate loaded in tension to a low nominal stress level such that there is no local yielding at the notch root and the entire plate is elastic. The high longitudinal stresses $\sigma_{yy} \cong \sigma\sqrt{a/2r}$ set up at a distance, r,

ahead of the root (for $r > \rho$) cause the material there to extend elastically and consequently to contract because of the Poisson effect. This contraction is greatest near the notch root (Figure 5.3) where the longitudinal stresses are highest. The area, A, that has been cut by the notch does not want to contract because there are no longitudinal stresses acting along it, all of these are concentrated ahead of the root. Since the unstressed area, A, tries to maintain its original dimensions while the material ahead of the root is contracting, transverse tensile stresses, σ_{zz}, are set up in the contracting material. The stress σ_{zz} is a maximum at the center of the plate (z=0). Because the faces (xy-plane) of the plate are not loaded externally, σ_{zz} drop to zero at $z \pm B/2$, and σ_{zz} decreases with increasing distance, r, ahead of the root. In addition, transverse tensile stresses σ_{xx} are also set up ahead of the notch by the constraints which prevent contraction in the width (x) direction and by the cantilever type deflection induced by the presence of the notch itself. The variations of the longitudinal and transverse (elastic) stresses σ_{yy} and σ_{xx}, with distance, r, in the center of the plate (z=0), are shown in Figure 5.4. At any point

$$\sigma_{zz} = \nu \ (\sigma_{xx} + \sigma_{yy}).$$

Since $\sigma_{xx}=0$ at the root surface (r=0), local yielding will occur when the longitudinal stresses σ_{yy} are equal to the uniaxial tensile yield stress.

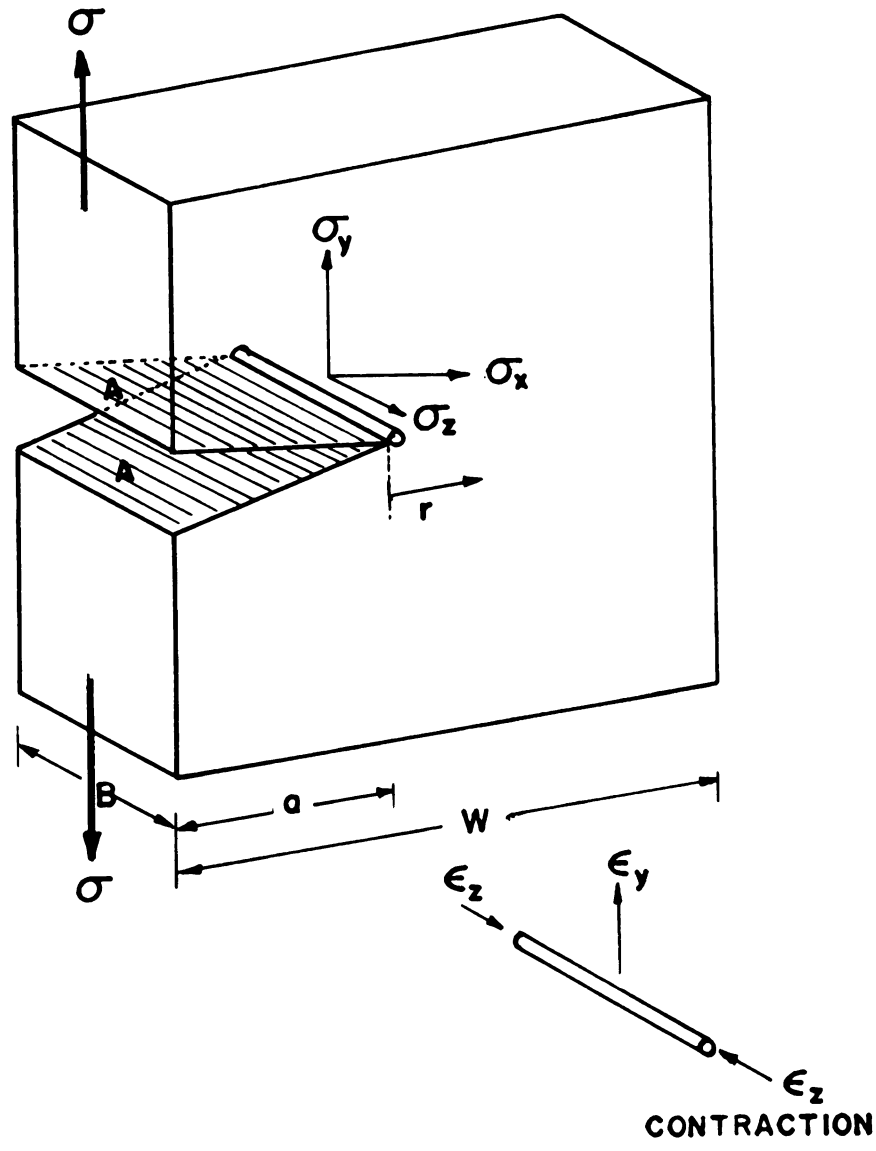

Figure 5.3 Transverse Contraction that Occurs Near the Crack Tip in a Thick Specimen. These Conditions are Opposed by the Unyielding Faces "A" of the Notch; Consequently Transverse Tensile Stresses σ_z and σ_x are set up Ahead of the Crack (Ref. 55).

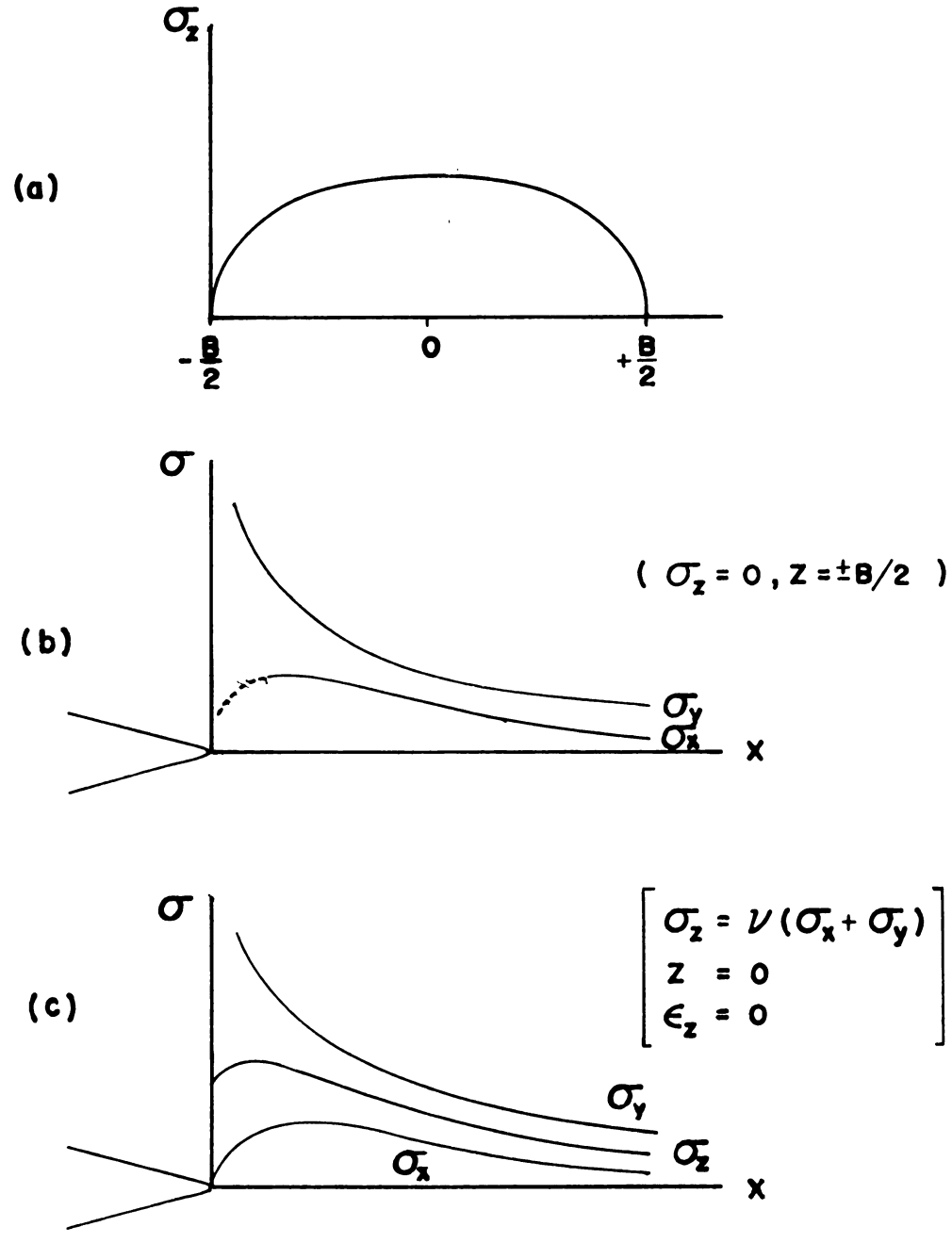

Figure 5.4 a) Variation of σ_z Across the Thickness, in z-direction at x=constant.

b) Variation of σ_y and σ_x with x on the Surface of a Notched Plate ($Z = \pm \frac{B}{2}$).

c) Variation of σ_y and σ_x with x at Mid-Thickness (z=0) of a Thick Notched Plate (Ref. 67).

When a notched piece is stressed elastically, it is possible to produce high stresses near the notch that may locally exceed the material's yield stress to produce a small plastic zone or 'enclave'. The stress distributions within this enclave depend very much on whether the deformation is occurring in plane stress or plane strain.

In plane stress, the smallest principal stress is that through the thickness, σ_{zz}, and yielding occurs on the plane at 45^{o} to the y and z axes. Yielding occurs when

$$\sigma_{yy} - \sigma_{zz} = 2\tau_{ys} = \sigma_{ys}$$

where $\sigma_{zz} = 0$, τ_{ys} = yield stress in shear, and σ_{ys} = yield stress. This condition is found throughout the plastic zone. Thus, the maximum stress in the plastic zone is equal to the material uniaxial yield stress.

In plane strain, the smallest principal stress is now σ_{xx} and the yield is consequently in the xy-plane, with

$$\sigma_{yy} - \sigma_{xx} = 2\tau_{ys} = \sigma_{ys}$$

$$\sigma_{yy} = \sigma_{ys} + \sigma_{xx}$$

Problems involving both elastic and plastic deformation around notches in plane strain becomes complicated because both elastic and plastic compatibility must be satisfied. Stress must be related to both elastic strain and to plastic strain increments.

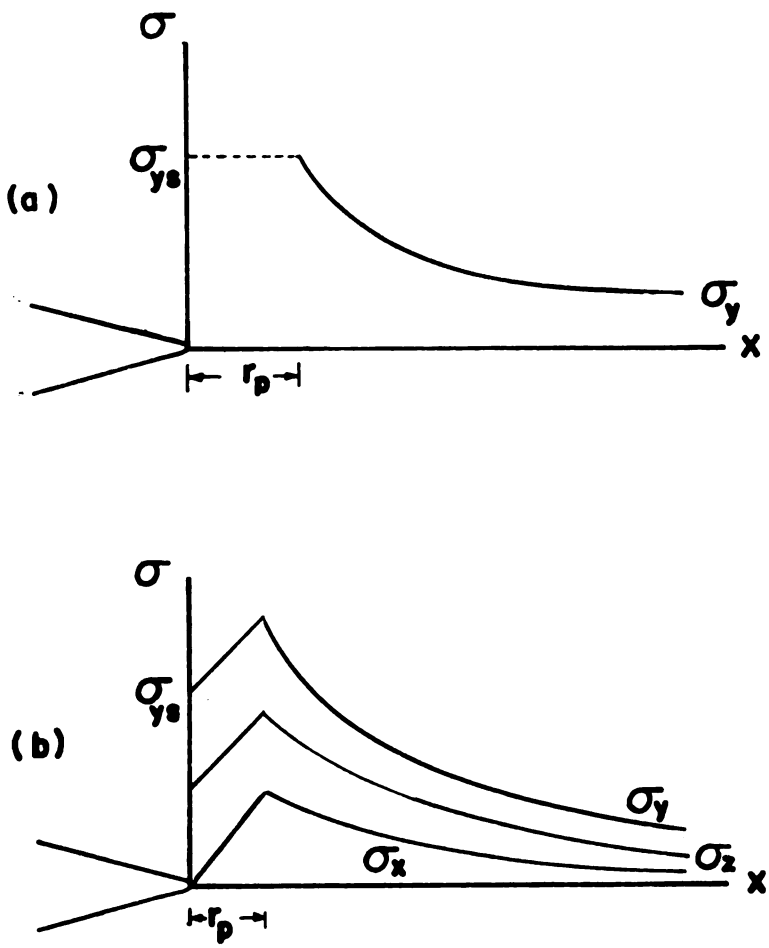

Figure 5.5 Stress Deformation In Front of a Crack Tip During Local Yielding for (a) Plane Stress, and (b) Plane Strain (Ref. 67).

5.1.4 Fracture Behavior of Thin and Thick Specimens

When plane stress conditions prevail and $r_y \geq B$, where r_y is the radius of the plastic zone and B is the specimen thickness, the fracture plane often assumes a $\pm$ 45 degree orientation with respect to the load axis and the plate thickness (Reference 57). This behavior may be rationalized in terms of failure occurring on those planes containing the maximum resolved shear stress (Figure 5.6b). (Since $\sigma_z = 0$ in plane stress, a Mohr circle construction will show that the plane of maximum shear will lie along $\pm$ 45 degree lines in the y-z plane).

In plane strain, where $\sigma_z = \nu(\sigma_y + \sigma_x)$ and $r_y << B$, the plane of maximum shear is found in the x-y plane (Figure 5.6a). Apparently, the fracture plane under the plane strain condition lies midway between the two maximum shear planes. This compromise probably also reflects the tendency for the crack to remain in a plane containing the maximum stress.

In very thick specimens, the plane-strain instability that occurs when $K = K_{IC}$ can cause the entire structure to fail so that $K_{IC} = K_C$ as in Figure 5.7a. However, in many structures, complete failure does not occur at $K = K_{IC}$ and a macroscopic slow crack growth precedes a complete failure (Figure 5.7b). In this instance, the plane-strain fracture tunnels ahead in the central portion of the structure where the degree of plane-strain loading is greatest (Figure 5.8). The material on either side of the tunnel is then loaded in plane stress and it eventually fracture by shear rupture.

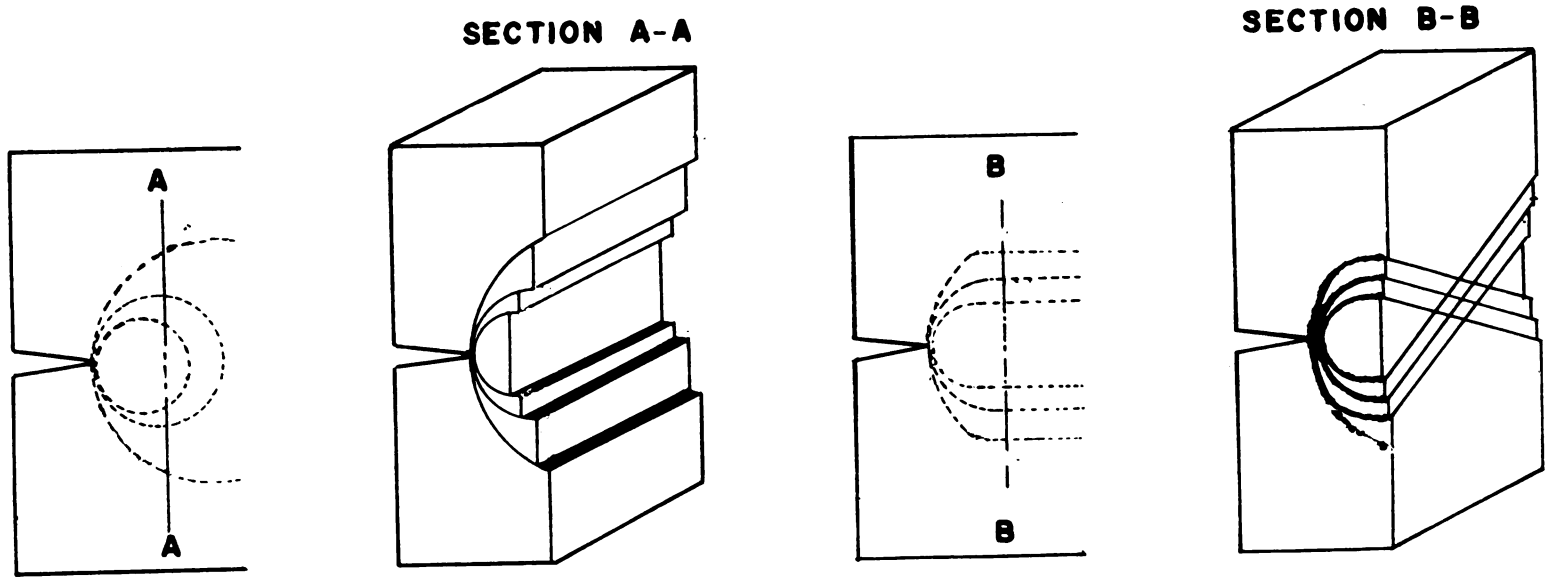

a) Hing Type
(Plane Strain)

b) Shear Type
(Plane Stress)

Figure 5.6 Schematic Drawing of the Types of Deformation Around a Crack (Ref. 69).

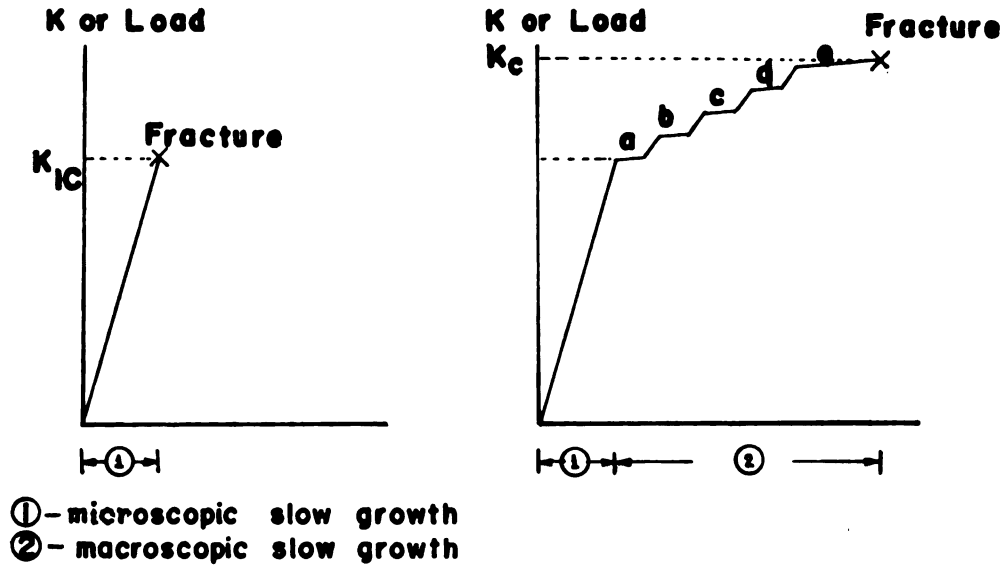

Figure 5.7 The Relationship Between Stress Intensity or Load and Change in Crack Length. (Ref. 56).

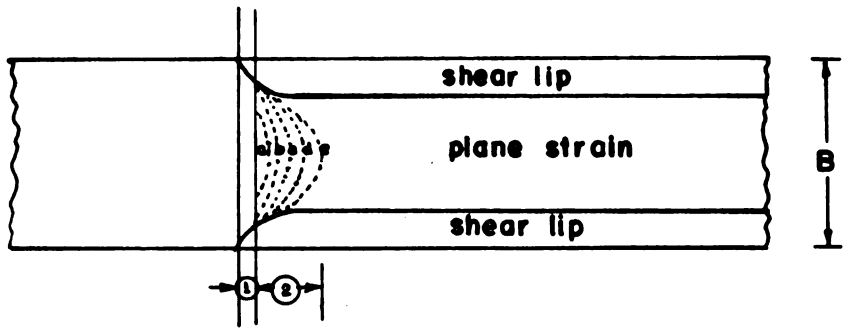

Figure 5.8 Schematic Diagram of Crack Propagation in a Plate Under Mode I Tensile Loading. Letters a, b, c, d, e, refer to Successive Positions of the Crack Part. (Ref. 56).

Each of the several "pops" lettered in Figure 5.7b result from the jumps taken by the crack front in Figure 5.8.

5.2 Specimen Preparation

Twenty rectangular shaped (3.9 in. x 4.0 in. (99 x 102 mm)) pieces were machined from a single sheet of 3/8 in. (9.5 mm) Merlon Polycarbonate. Copper gratings were printed on five of them by using the stencil method (see section 2.4). Five specimen blocks were made with four pieces. The pieces were fastened together with epoxy (Epon 828 and Diethylene Triamine 100:8 by weight) by bonding a grating side on the first piece to a plain side on the second piece. In addition, nickle mesh with 500 lpi (20 lpmm) and 0.008 in. (0.2 mm) in thickness was placed between the second piece and the third piece. Compact tension specimens were machined from these blocks. The dimensions of the compact tension specimens are shown in Figure 5.9. All specimens were polished on both sides to get smooth, clear and parallel surface which let the light pass through the specimen without scattering or creating optical distortion of the embedded grating. Finally, copper gratings were printed on the outside surfaces near the crack tip by using the stencil method. Five thick multi-layer tension specimens were made for this study. One of them had a fatigue crack to make a very sharp crack tip. The fatigue crack specimen did not give a straight crack front through the specimen thickness, and it thus did not give a good comparision of the

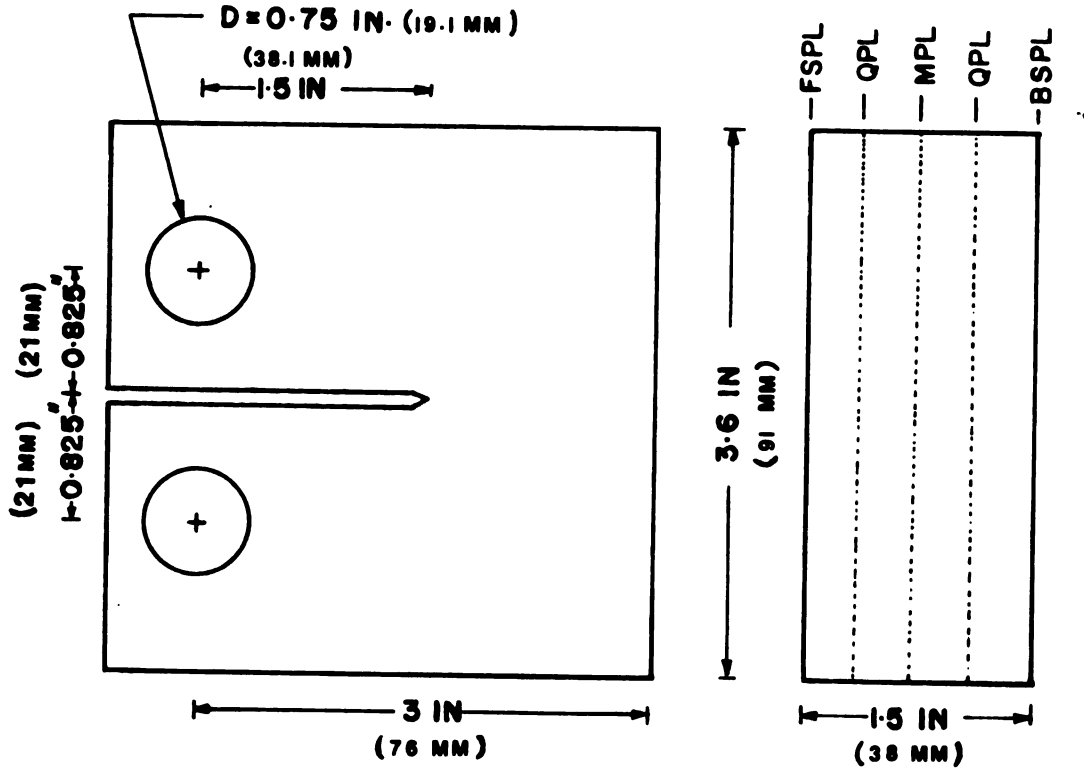

Figure 5.9 Specimen Dimensions of Compact Tension Specimens.

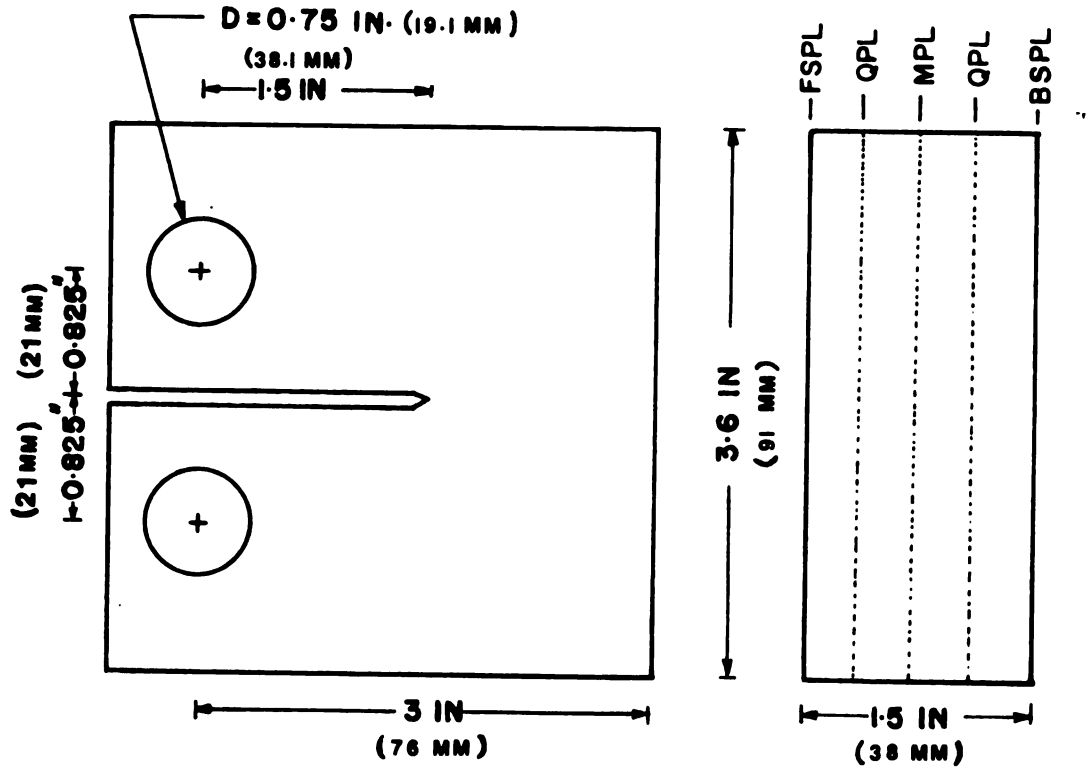

Figure 5.9 Specimen Dimensions of Compact Tension Specimens.

strain map around the crack tip in the interior and on the surface. For the rest of the specimens only a notch was used. In addition to the multi-layer thick specimen with embedded gratings, two similar specimens having embedded strain gages were made. Several thin specimens with gratings were also used.

5.3 Experimental Procedures

In this investigation, eleven compact tension specimens made from polocarbonate with the same dimensions were studied. They are:

i) one fatigue crack specimen (1.5 inches (38.1 mm) thick) with gratings on the surface-plane, the quarter-plane and the mid-plane.

ii) three notched specimens (1.5 inches (38.1 mm) thick) with gratings on the surface-plane, quarter-plane and mid-plane.

iii) two notched specimen (0.375 inch (9.525mm) thick) with gratings on the surface-plane only.

iv) two notched specimen (0.75 inch (19.05 mm) thick) with gratings on the surface-plane only.

v) one notched specimens (1.5 inches (38.1 mm) thick) with a grating on quarter-plane only.

vi) two notched specimens (1.5 inches (38.1 mm) thick) with strain gages on the surface-plane, the quarter-plane and the mid-plane.

All of these specimens were loaded in tension (Mode I). More details about each specimen are provided later.

The compact tension specimens were set up as shown in Figure 5.10. Each specimen was loaded by static loading on the hanger. A slide projector was used as a light source for this set up. Light-diffusing glass was placed in front of the light source to get a more uniform intensity on the area around the crack tip. Photographs of the specimen gratings were obtained in the same manner as before, the difference being that the lens was a Carl Zeiss N., S-Planer with a focal length of 120 mm. and a maximum aperture of f5.6. The camera was set up to get a magnification factor of 2. The specimens were placed to let the light pass through them in the direction parallel to the crack front. Each grating was imaged separately by focusing on each grating plane to get the maximum sharpness and contrast over the whole area near the crack tip.

The first data plate was recorded by focusing on the front surface and then the entire camera set up was moved closer to the specimen to get a focus on the quarter-plane and a second data plate was recorded. The specimen was then turned around and focused on the mid-plane and the third data plate was recorded. Finally, when the camera was focused on the back surface, the fourth data plate was recorded. For each specimen, four data plates were made for the unloaded specimen as the base line on each plane, and another four data plates were made for the loaded specimen.

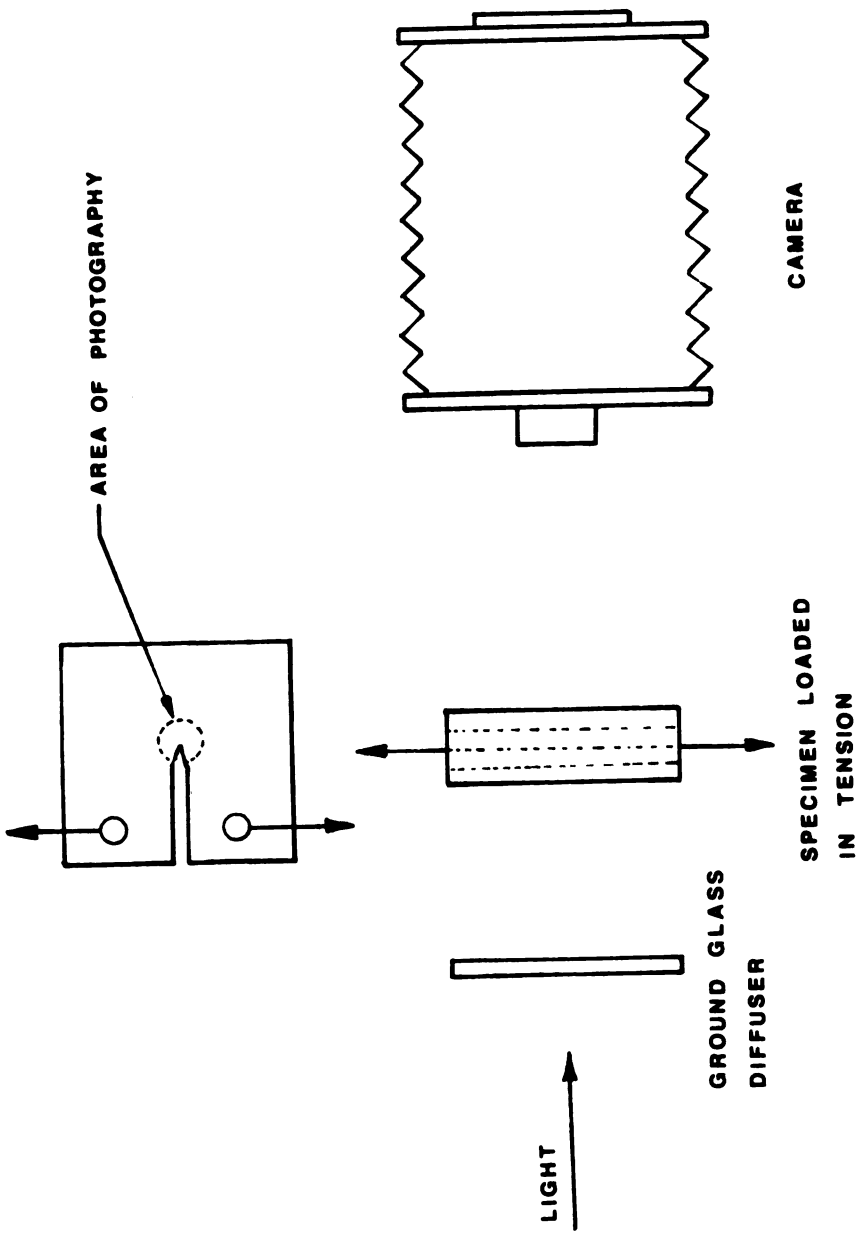

Figure 5.10. Schematic Drawing of the Specimen Set Up.

The specimen with the fatigue crack was loaded in tension up to 4.55 ksi (31.8 MPa), and the specimen gratings were recorded at 0.6 ksi, 2.6 ksi, and 4.5 ksi. (4.55, 18.2 and 31.8 MPa). When the specimen was loaded at about 5.20 ksi (36.4 MPa), the compact tension specimen split on the bond plane in a small area around the crack tip. This effect was the result of the triaxial stress which occured near the crack tip in the interior of specimen; the maximum tensile stress in the direction of specimen thickness occured at the crack tip on the mid-plane, and it decreased to zero on the surface of the specimen.

In addition to applying a load on the fatigue crack specimen, a small load (9.1 MPa) was applied in tension on the notched specimen. The moire fringe patterns of the unloaded and loaded specimen on each plane of the specimen were obtained by using optical processing as explained in section 2.6. Moire fringe were produced by the interference between the specimen grills and a master grill on a glass plate. The density of the specimen grill is nominally 238 lpi (9.4 lpmm), and the density of master grills used were 215 lpi, 230 lpi, 260 lpi and 507 lpi (8.5, 9.1, 10.2 and 20 lpmm). The fringe patterns were recorded by a zoom lens with a focal range 95-205 mm which fitted a Nikon F camera; Kodak Plus-X film was used. The fringe pattern was recorded in both directions, perpendicular and parallel to the crack line. The strain plots in the direction perpendicular and parallel to the crack line on each plane (the

surface-plane, the quarter-plane and the mid-plane) are obtained by using the data reduction technique explained in section 2.8.

5.4 Experimental Results

5.4.1 First Experimental Results

Moire fringe patterns of the area around the crack tip of the polycarbonate compact tension specimen were obtained from the data plates on each plane. At the beginning, the fatigue crack specimen was studied. Three steps of loading 0.6, 2.6 and 4.5 ksi; (4.55, 18.2 and 31.9 MPa) were applied to this specimen. The moire fringe patterns for the surface plane obtained at each step loading with two different submasters are shown in Figure 5.11 and Figure 5.12. Figure 5.11 was obtained from the data plate with a submaster having 270 lpi. This fringe pattern given tensile strain when the fringe lines are close together. Figure 5.12 was obtained from the same data plate with a submaster of 230 lpi (9.1 lpmm). The fringe pattern here gives compressive strain when the fringe lines are close together. The plots of the surface strain in the directions perpendicular (ε_y) and parallel (ε_x) to the crack line are shown in Figures 5.13 and Figure 5.14. The comparison of strain plots along the crack line in both directions (ε_x and ε_y) are shown in Figure 5.15. The results show that ε_y at the crack tip is very large (when compared with ε_x) and that it decreases with increasing

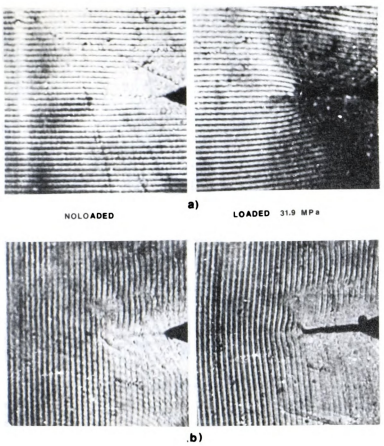

Figure 5.11 Moire Fringe Pattern on the Surface of the Specimen with Fatigue Crack Obtained From Dataplate with Submaster 10.6 lpmm in the Direction
a) Parallel and b) Perpindicular to the Crack Line.

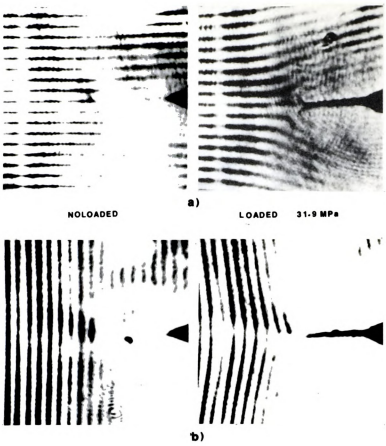

Figure 5.12 Moire Fringe Pattern on the Surface of the Specimen with Fatigue Crack Obtained from Data Plate with Submaster 9.1 lpmm in the Direction
a) Parallel and b) Perpindicular to the Crack Line.

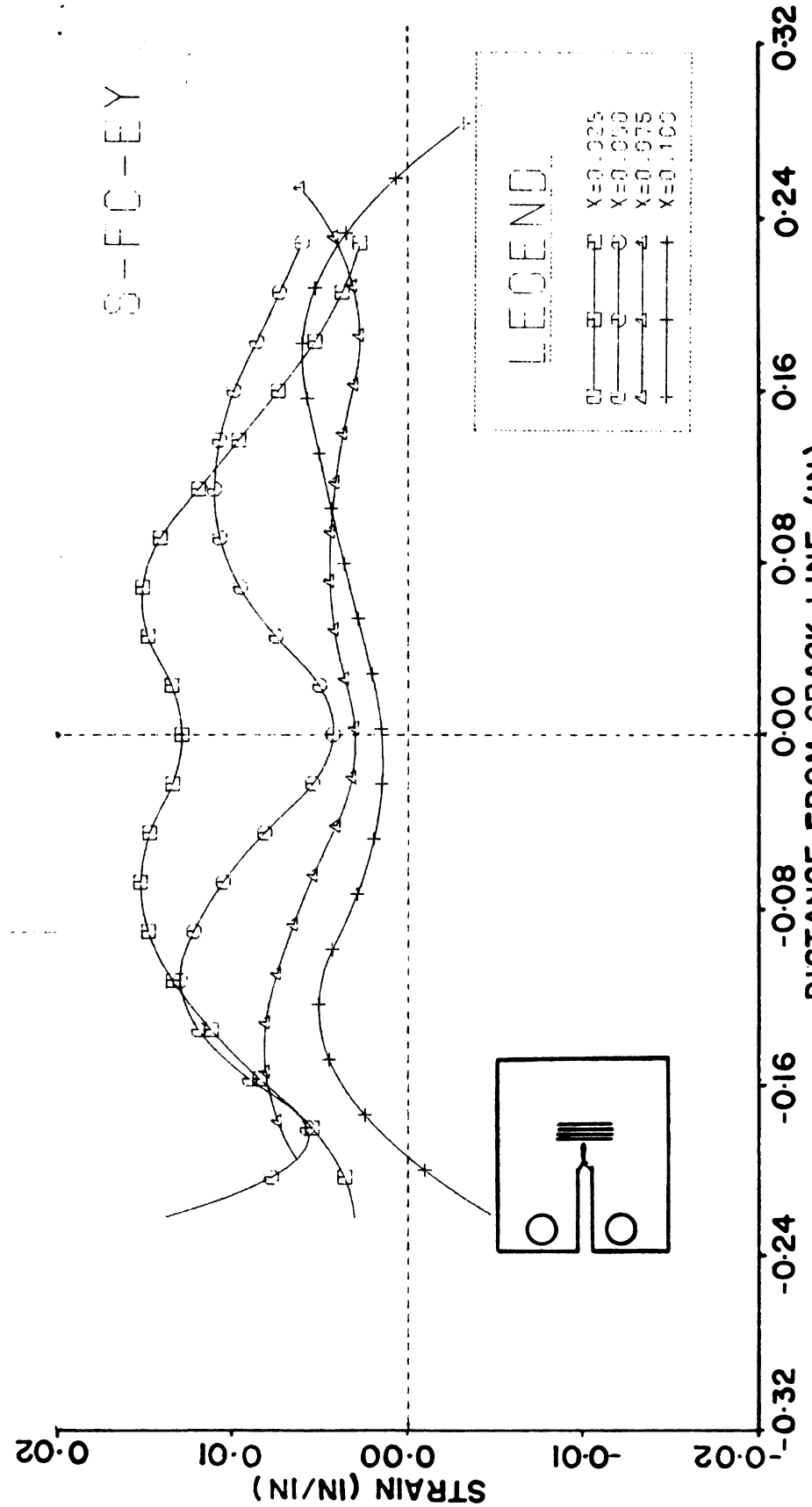

Figure 5.13 The Plot of Surface Strain ε_y in the Direction Perpendicular to the Crack Line for Various Distances from Crack Tip in the Fatigue Crack Specimen.

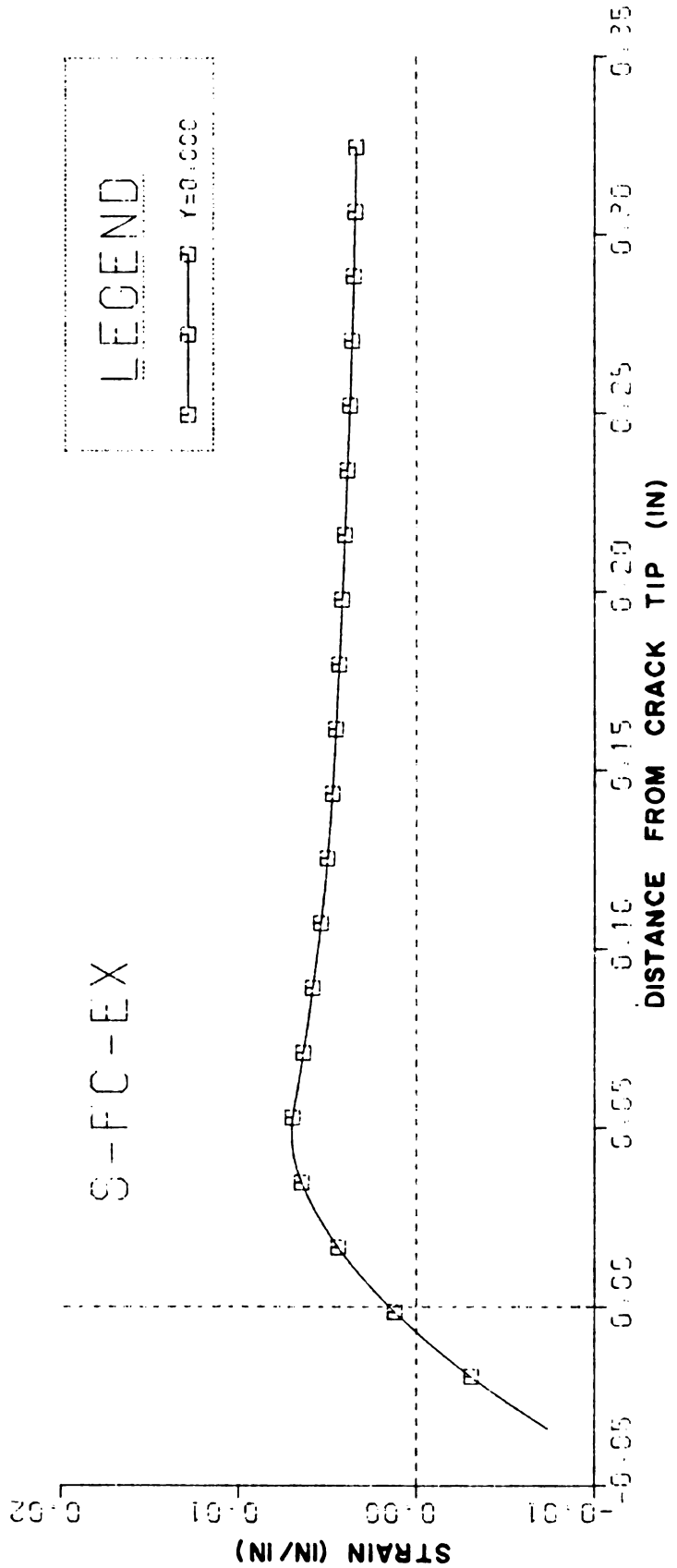

Figure 5.14 The Surface Strain in the Direction Parallel to the Crack Line of a Fatigue Crack Specimen.

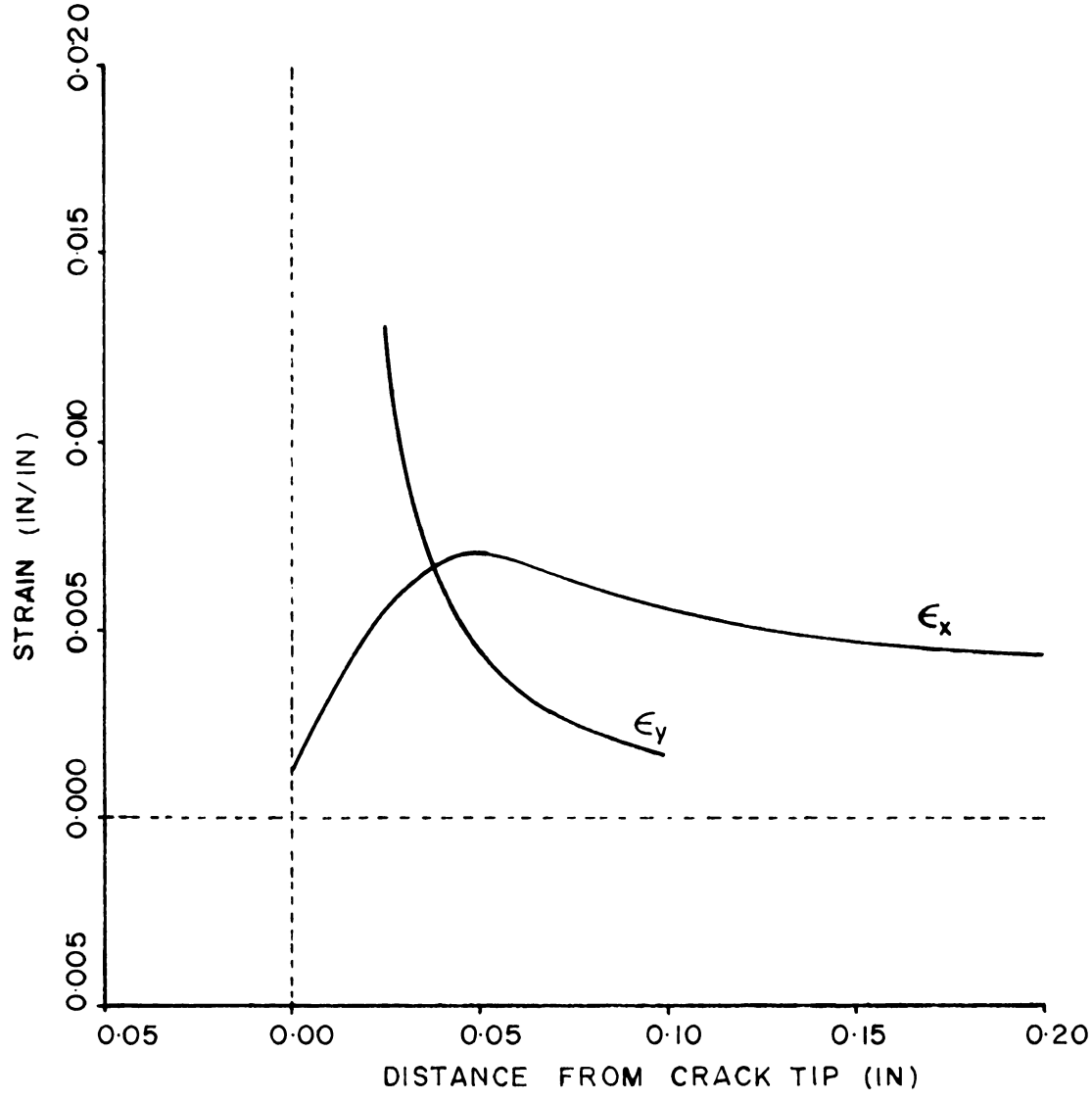

Figure 5.15 Comparison of the Plot of Surface Strain ε_x and ε_y from the Crack Tip Along the Crack Line of the Specimen with Fatigue Crack.

distance from the crack tip. ε_x is small at the crack tip; it increases to a maximum and then decreases with increasing distance from the crack tip.

Moire fringe patterns for the first interior plane (quarter-plane) of the fatigue crack specimen in the direction parallel and perpendicular to the crack line are shown in Figure 5.16.1. They are obtained from a data plate with a submaster having 507 lpi (20 lpmm). At the early stage, a small dark zone occured at the crack tip and the fringe pattern near the crack tip changed from parallel fringes to a small dilatation zone as shown in Figure 5.16.1b. The schematic of this zone is shown in Figure 5.16.2. The results were recorded while increasing the load to 0.6, 2.6 and 4.5 ksi (4.55, 18.2 and 31.8 MPa). Under these conditions, the dark zone at crack tip was bigger and the fringe pattern near the crack tip was changed to show a larger dilatation zone as shown in Figure 5.16.1c and 5.16.1d. The rate of change of strain ε_y at the crack tip increased markedly while the specimen was being loaded, and this effect caused the change of the dilatation zone. The moire fringe patterns in the interior of the fatigue cracked specimen support the idea that, while increasing the load on the specimen, the fringe patterns at the crack tip were changed from a small dilatation zone to a larger one. The dilatation zone obtained from the moire method in this study corresponds to the decohesion enclave in a thick plate which was described by Boyd (72). The decohesion enclave is a

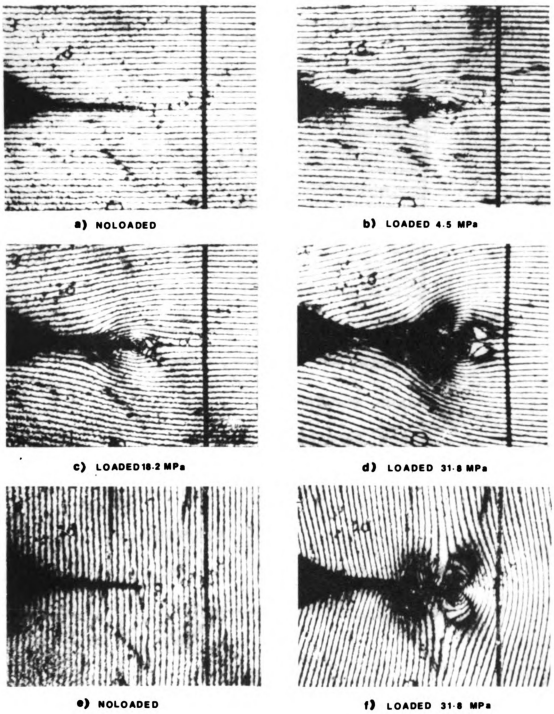

Figure 5.16.1 Moire Fringe Patterns in the Interior (Quarter-plane) of a Fatigue Crack Specimen in the Direction Parallel to the Crack Line (a,b,c,d) and Perpendicular to the Crack Line (e,f) Which Obtained from a Submaster Having 19.96 lpmm.

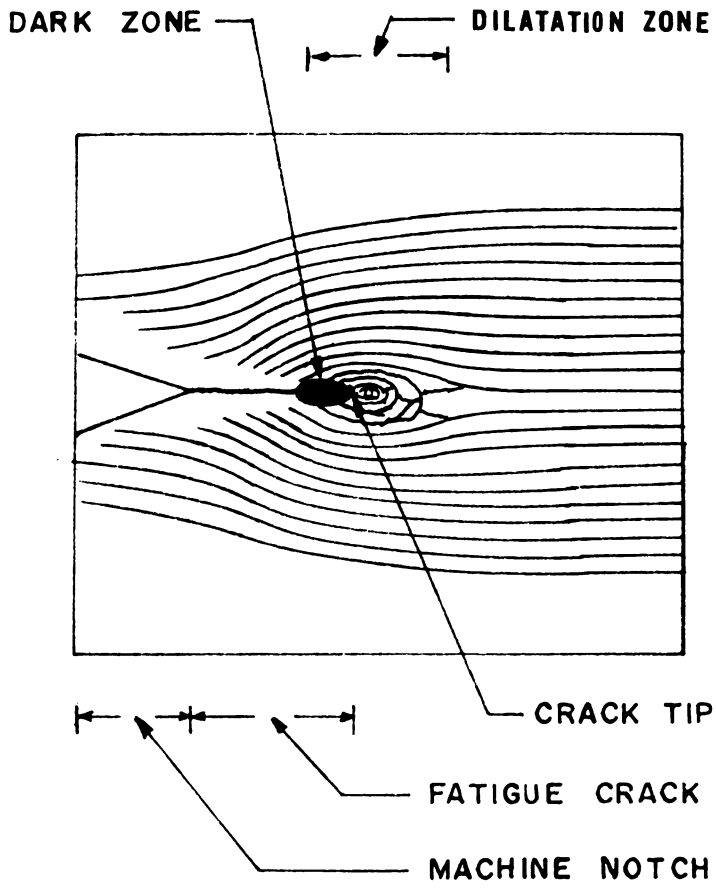

Figure 5.16.2 The Schematic of the Deformation Zone Near Crack Tip.

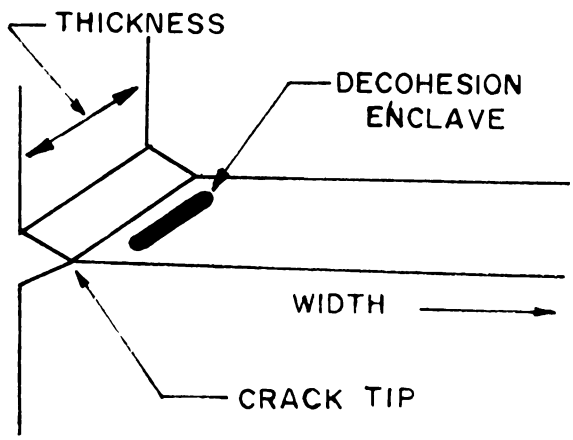

Figure 5.16.3 The Decohesion Enclave in a Thick Plate [after Boyd (72)]

small zone that is developed at some finite distance ahead of the crack and away from the specimen sides. This small region (see Figure 5.16.3) will strongly favor the initiation of brittle fracture by quasi-cleavage and the spread of square fracture (Reference 72).

Unfortunately, the calculation of strain near the crack tip cannot be obtained from these photographs because the fringe patterns near the crack tip are not continuous nor are they clear enough to be interpreted. To solve this problem, the same data plate was used with a submaster having 230 lpi (9.1 lpmm) to obtain a more easily digitized form of the moire fringe pattern as shown in Figure 5.17. Because the crack front of the crack specimen is not straight through the specimen thickness, the comparison of the strain on each plane cannot be obtained from this specimen.

A comparison of the strain results on the surface and in the interior near the crack tip was obtained by using the notched specimen. Three specimens were used, only the specimen that gave the best results on the surface and in the interior is discussed here.

The moire fringe patterns on the surface plane of a notched specimen with and without load are shown in Figure 5.18. The plots of ε_y and ε_x and the constant strain contours on the surface plane are shown in Figure 5.19 to Figure 5.22. The results are typical of all specimens (three specimens were used for this test). They show that on the surface plane, ε_y is tensile around the crack tip, and that the

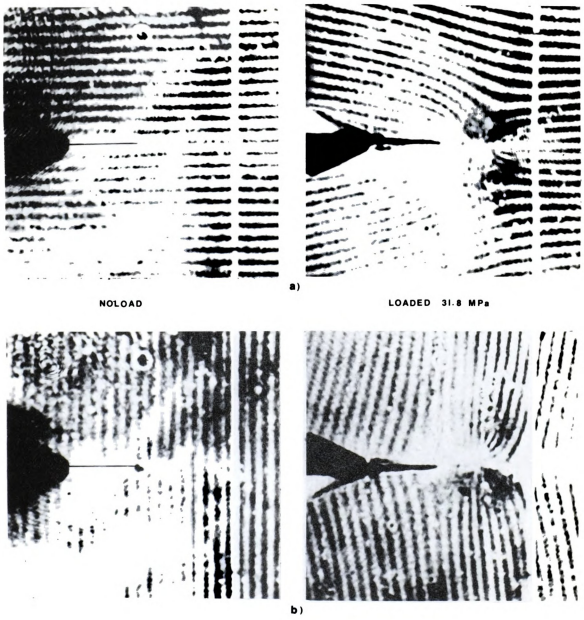

Figure 5.17 The Moire Fringe Pattern in the Interior (quarter-plane) of a Fatigue Crack Specimen in the Direction (a) Parallel, and (b) Perpendicular to the Crack Line Obtained From a Submaster Having 9.1 lpmm.

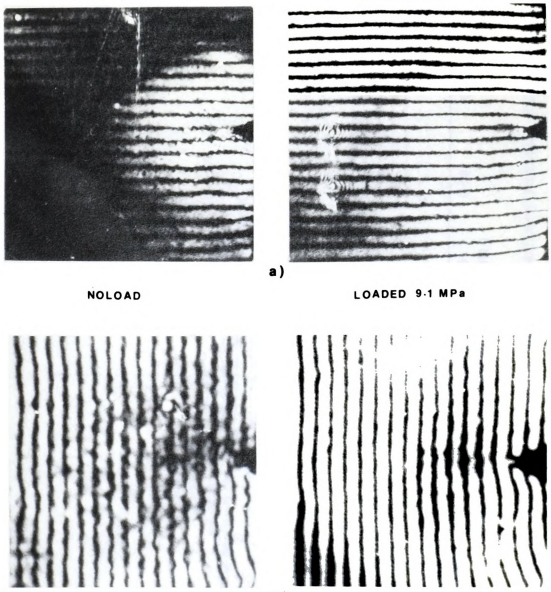

Figure 5.18 Moire Fringe Pattern or the Surface of Specimen without Fatigue Crack in the Direction a) Parallel and b) Perpendicular to the Crack Line.

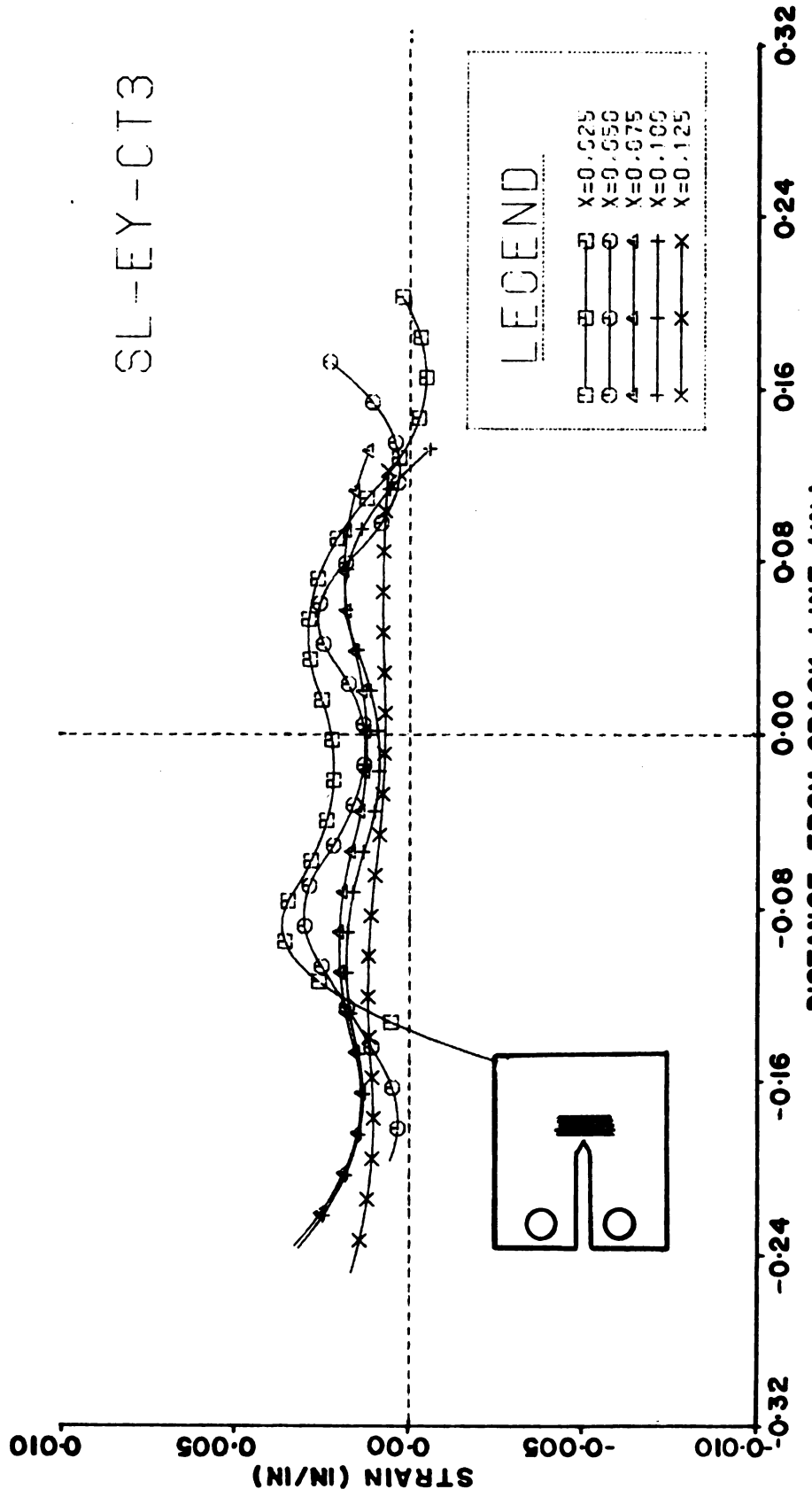

Figure 5.19 Strain ε_y on the Surface Plane of the Specimen Without Fatigue Crack.

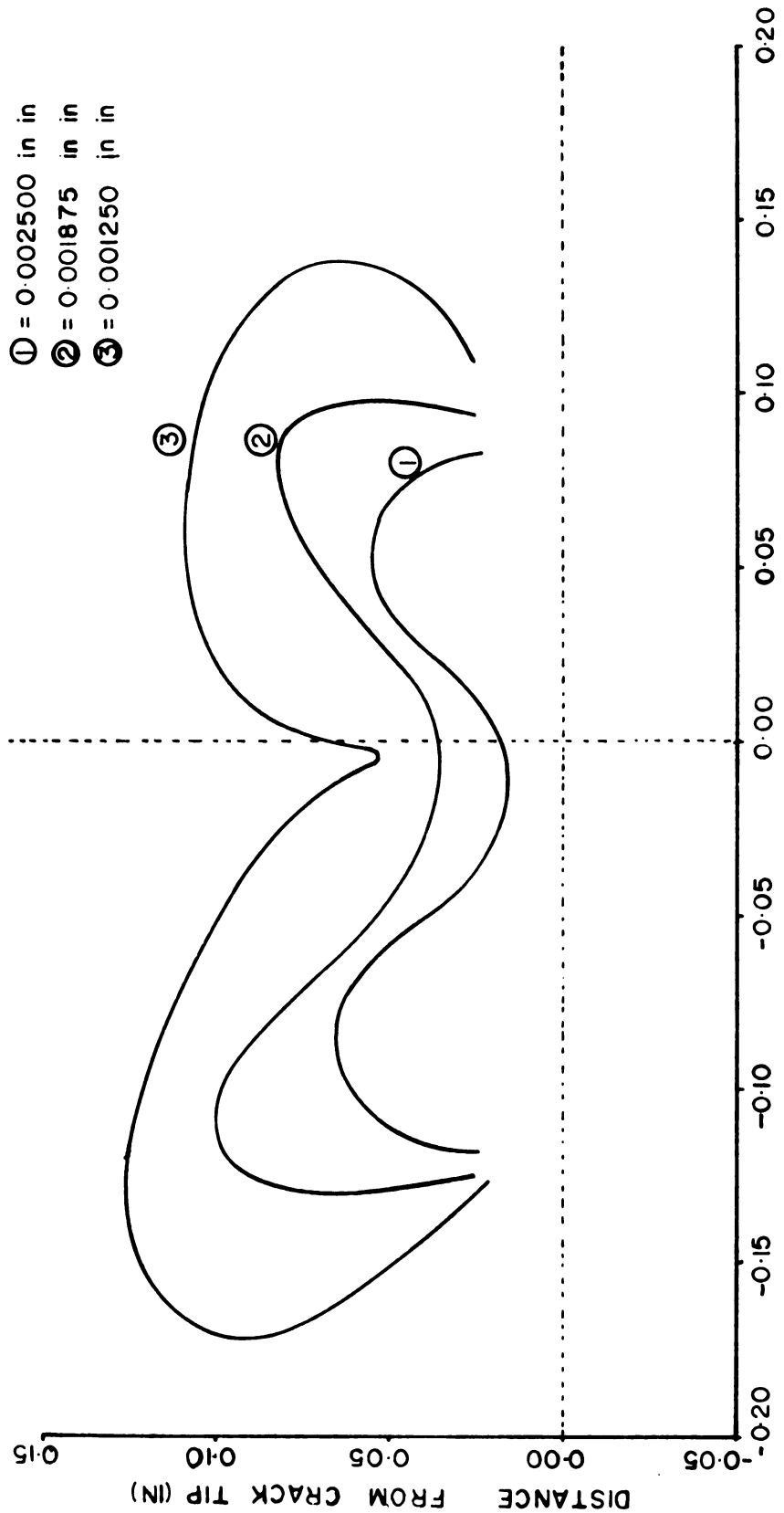

Figure 5.20 The Constant Strain Contours ε_y Around Crack Tip on the Surface Plane.

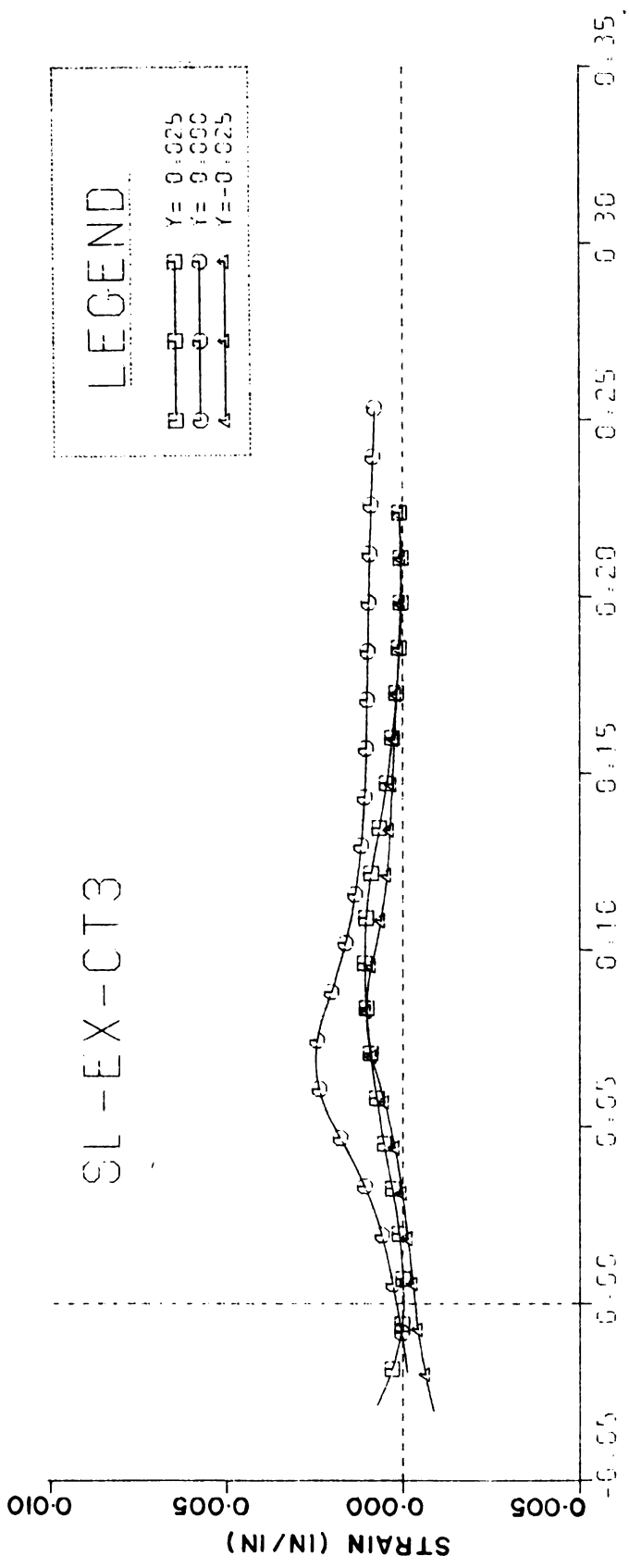

Figure 5.21 Strain ε_x on the Surface Plane of Specimen Without Fatigue Crack.

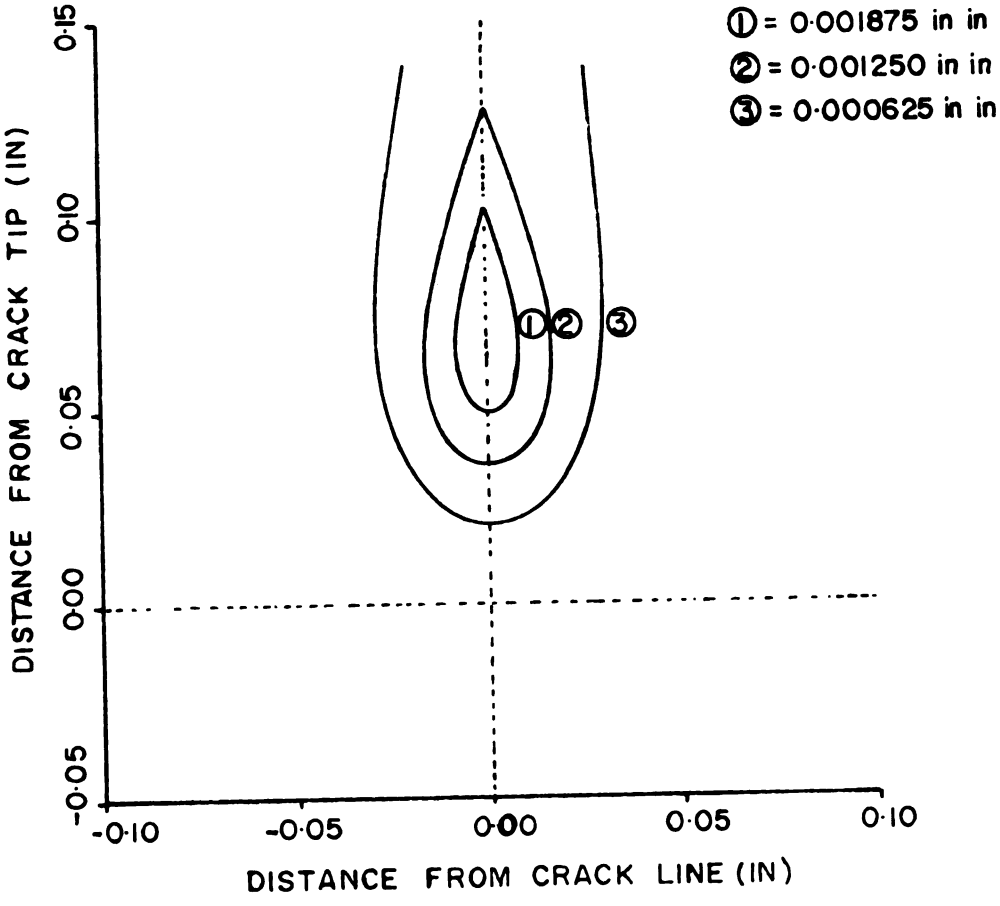

Figure 5.22 The Constant Strain Contours ε_x Around Crack Tip on Surface Plane.

maximum strain occurred near the crack tip. Near the crack tip ε_y has a high strain gradient, the gradient decreasing with distance from the crack tip. Along the crack line, ε_x is tensile. Comparisons of the strains, ε_y and ε_x, along the crack line are shown in Figure 5.23. The results show that near the crack tip the strain ε_x is much smaller than the strain ε_y while the specimen was loaded. The same phenomenon has also been observed by Liu and Ke (34), Underwood et al. (35) and W. Gerberich (36). The major difference between this study and those mentioned above is that they study the central crack of a thin plate with a tension load by using aluminum and steel. In this study, a thick compact tension specimen of polycarbonate was used. Under these circumstances, it is reasonable to expect that the magnitude of ε_y on the surface plane is a more valuable indicator of the severity of the deformation in front of the crack tip than is ε_x.

For the specimen with a notch, the moire fringe patterns of the quarter-plane and the mid-plane are shown in Figures 5.24, 5.25, 5.26 and 5.27. The resulting strain plots of ε_y and ε_x are shown in Figures 5.28, 5.29 and 5.30, and 5.31. The results show that ε_y around the crack tip in the interior of the specimen is compressive strain. From the available theory of interior stress and strain as described in section 5.1 , however, the stress σ_y in the interior along the crack line is tensile. By using the relationship between stress and strain (eq. 5.2) the interior

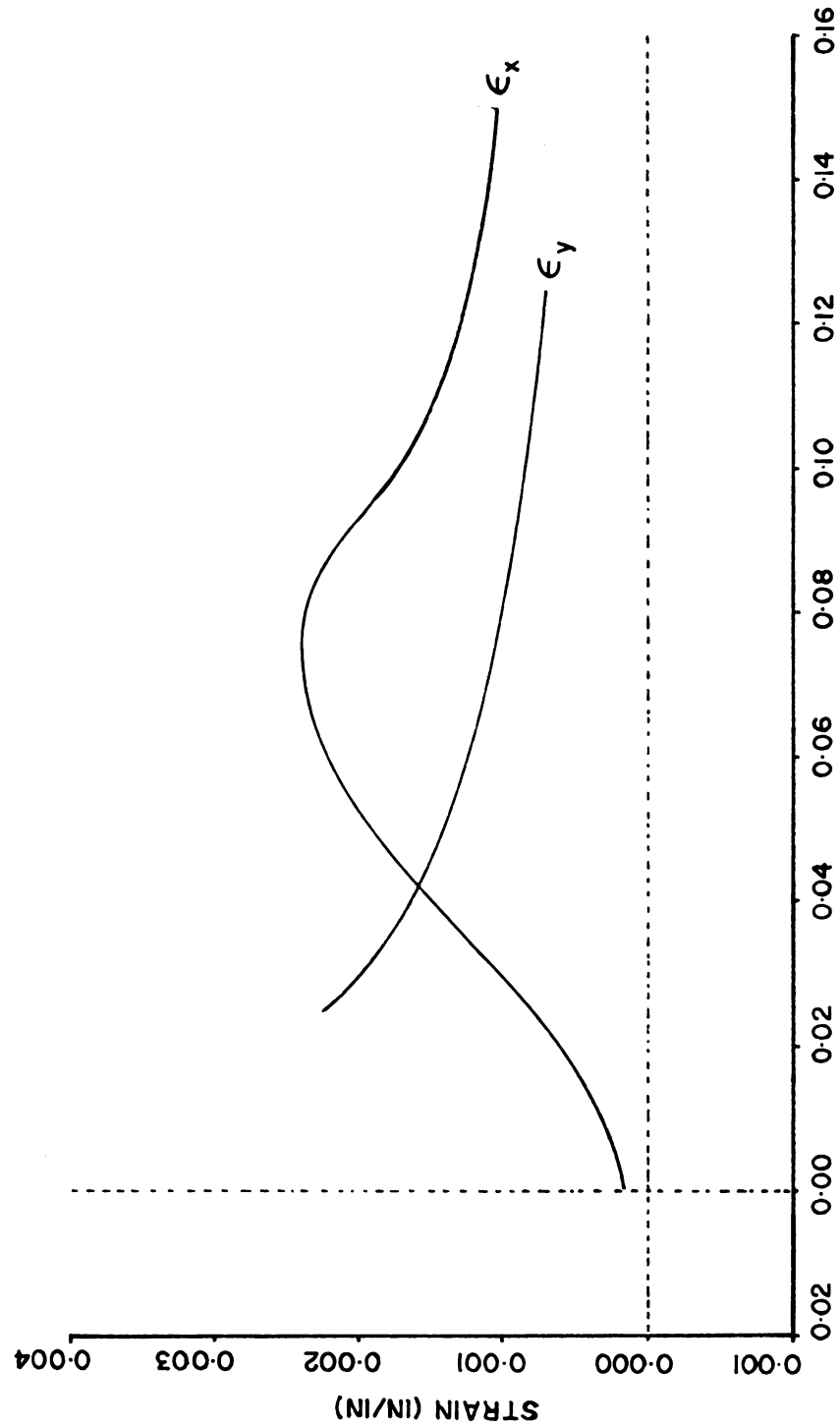

Figure 5.23 Comparison of the Strains ε_x and ε_y along the Crack Line on the Surface Plane.

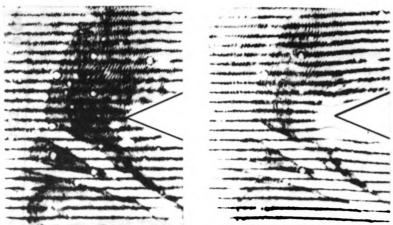

Figure 5.24 The Moire Fringe Patterns of Loaded and Unloaded on the Quarter Plane of the Notched Specimen in the Direction Parallel to the Crack Line.

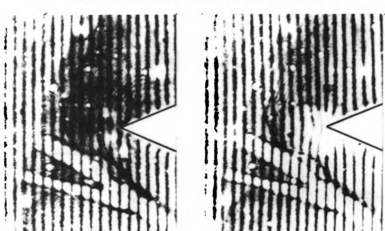

Figure 5.25 The Moire Patterns of Loaded and Unloaded on the Quarter Plane of the Notched Specimen in the Direction Perpendicular to the Crack Line.

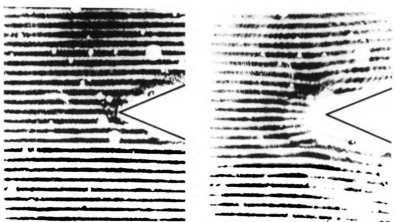

Figure 5.26 The Moire Fringe Patterns of Unloaded and Loaded on the Mid-Plane of the Notched Specimen in the Direction Parallel to the Crack Line.

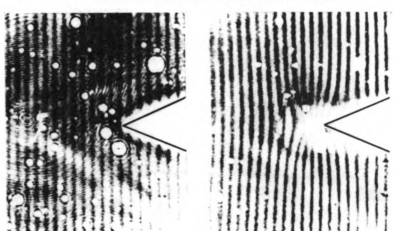

Figure 5.27 The Moire Fringe Patterns of Unloaded and Loaded on the Mid-Plane of the Notched Specimen in the Direction Perpendicular to the Crack Line.

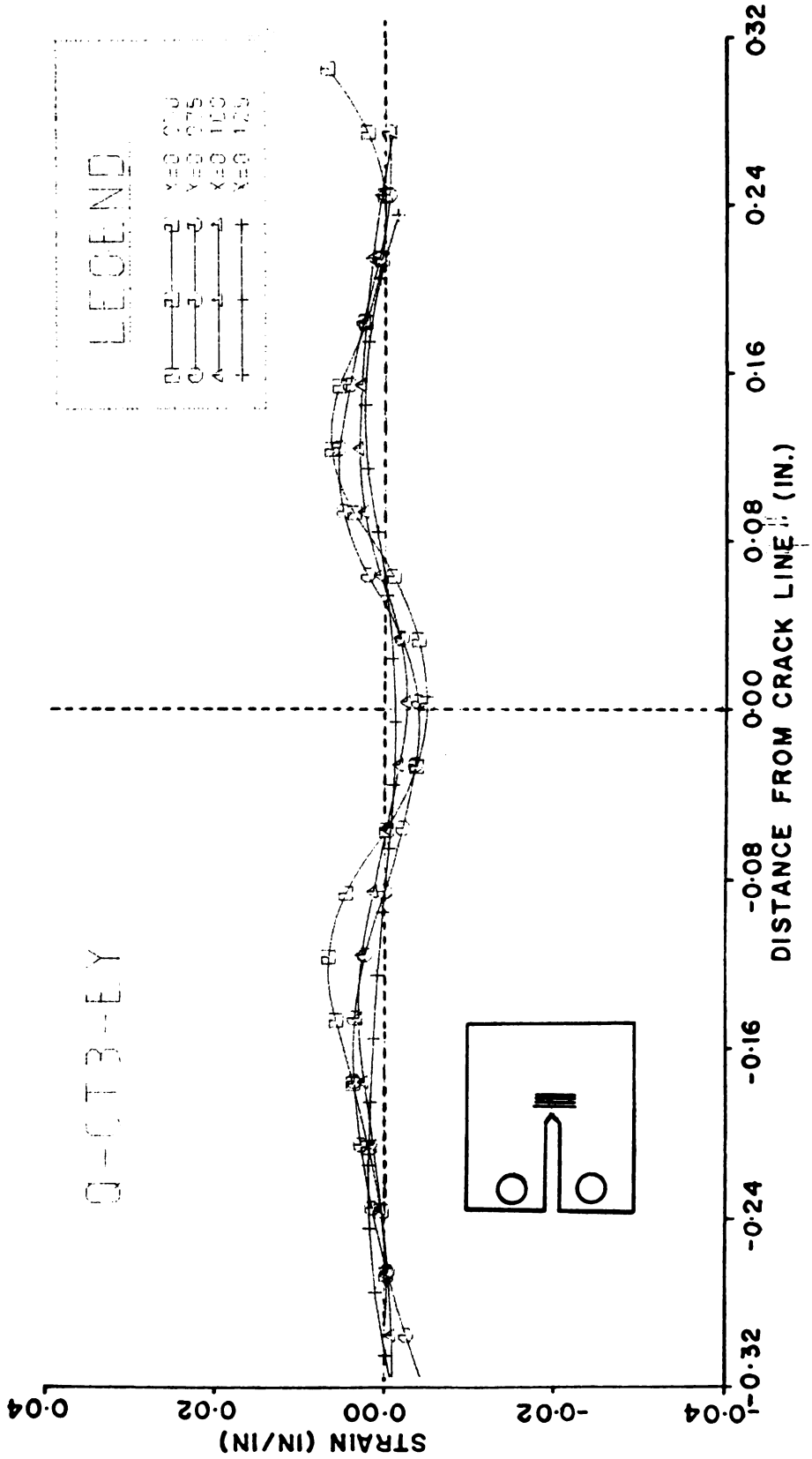

Figure 5.28 The Strain Plot of ε_y on the Quarter-Plane of a Notched Specimen.

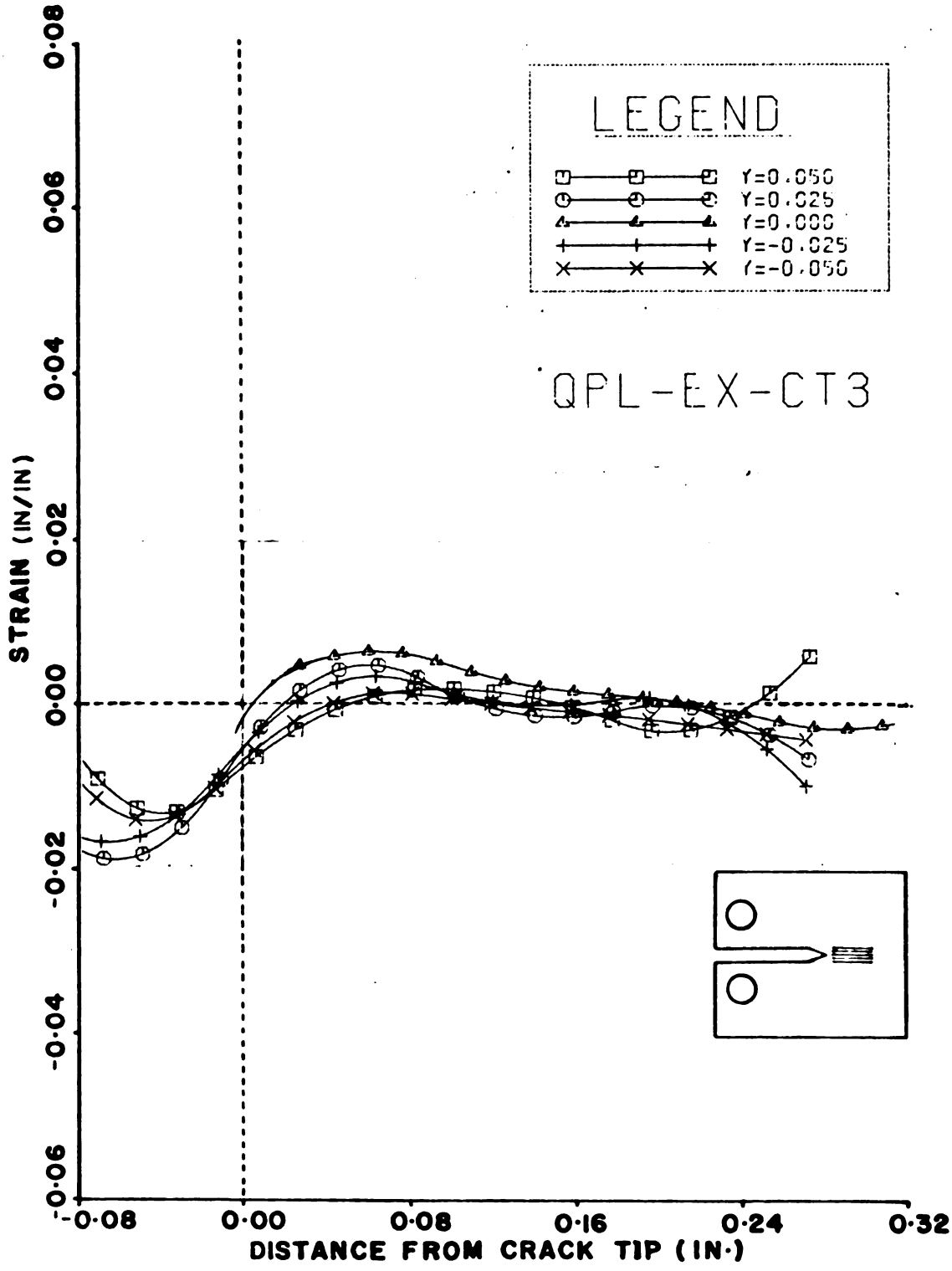

Figure 5.29 Strain ε_x on the Quarter Plane of a Notched Specimen.

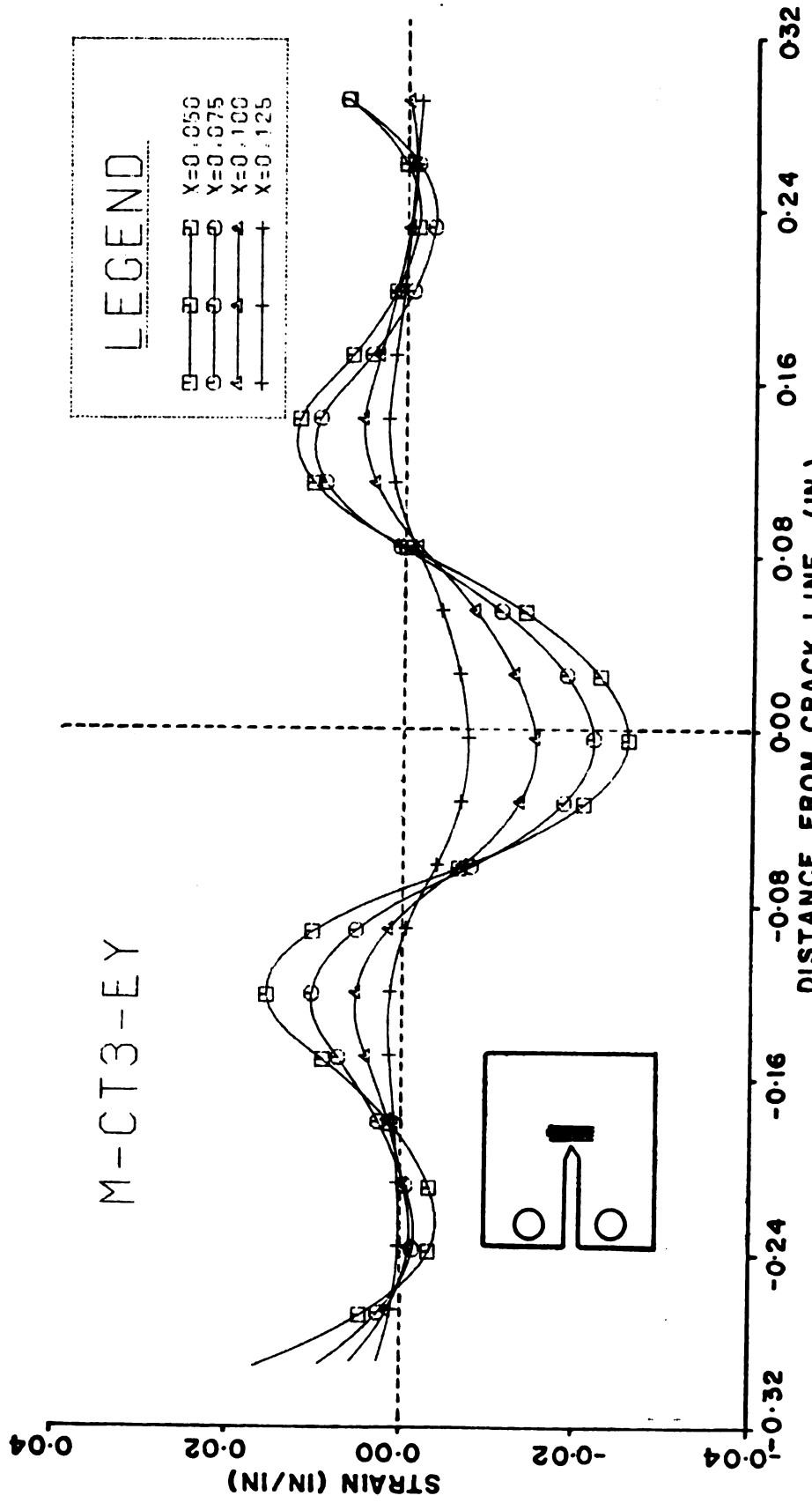

Figure 5.30 The Strain Plot of ε_y on the Mid-plane of a Notched Specimen.

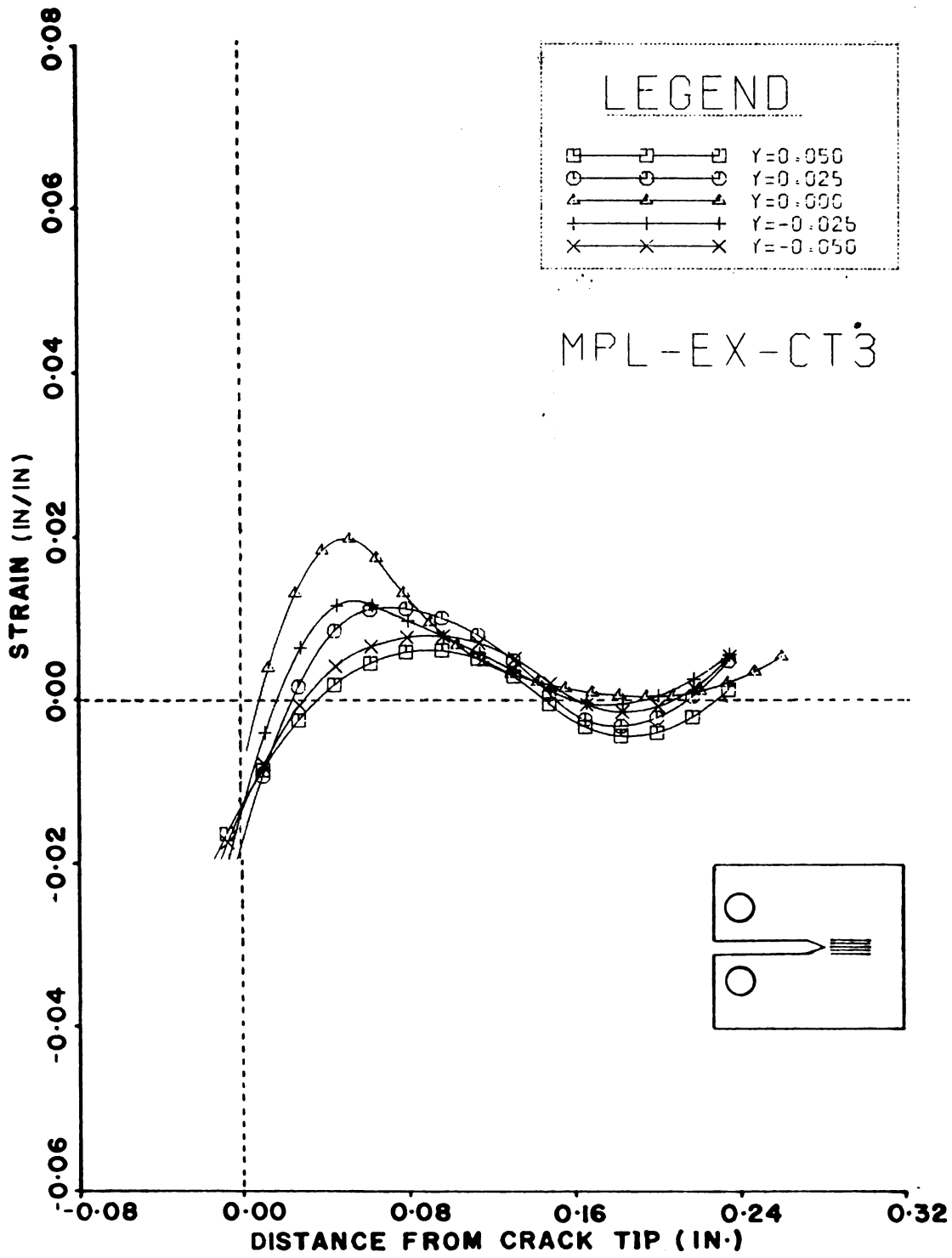

Figure 5.31 Strain ε_x on the Mid-plane of a Notched Specimen.

strain ε_y along crack line is found to be tensile strain. At this point the results of the strain in the interior of specimen obtained from the experiment do not agree with theory. The interior strain from the experimental results needs to be considered and a correction of these results have to be made.

R. C. Kerber and J. S. Whittier (37) suggested that the embedded grid measurements of internal motion in transparent models, in some cases, can be seriously in error owing to the internal optical refraction caused by stress gradients within the model. For this study these errors were created by both the change of index of refraction and the changed of thickness of the specimen. While the specimen was being loaded large strains occurred near the crack tip and changed the index of refraction of the specimen. Furthermore, due to the strain of contraction, ε_z, the thickness close to the crack tip is changed.

As pointed out by R. P. Kambour (38) crack propagation in polymers do not behave as it would in the simple elastic, ideal brittle solids for which the original formulation of the theories was intended. In fact, it is known today that in these materials, crack propagation occurs by the formation of more or less substantial amounts of craze material followed by failure. R. P. Kambour (38) and D.

Hull (39) concluded that the main characteristics of a craze in transparent, isotropic polymers are:

1. A craze is a highly localized region of plastic deformation.
2. Crazes formed in a uniaxial tensile stress field have a similar shape to a crack, and the plane of a craze is at a right angle to the stress axis.
3. The craze volume has a lower density than the surrounding material. Because the crazing creates holes smaller than the wavelength of light, the craze behaves as an optically homogeneous medium and has a refractive index considerably lower than that of the normal polymer.

As pointed out by Vincent (42), the development of a plastic zone in a polycarbonate is more complex than in the other polymers. While increasing the load, the development of a plastic zone at the crack tip of a polycarbonate specimen is not the same as in the other types of polyester such as PMMA. This notion was explained in an experimental work by Vincent (42). For PMMA the kidney-shape (or butterfly-shape) that occurs at the crack tip becomes larger and larger with increasing load. This corresponds to the development of a plastic zone in almost all materials. This kind of development is seen in a polycarbonate specimen in the early stages too. While applying a small load, the local strains are below the yield strain and the zone is

kidney-shaped (or butterfly-shaped). In the second stage, however, the local strains are above the yield strain, and the zone becomes wedge shaped. Finally, at higher strains, there is a kidney-shaped zone within the wedge. The schematic of the development of a plastic zone of a polycarbonate crack specimen is shown in Figure 5.32. In this investigation, while the specimen was loaded, it was possible to have a local yield strain at the crack tip higher than the material yield strain, and a wedge shaped plastic zone (the second stage of development of plastic zone in a polycarbonate specimen) formed near the crack tip. A craze occurred within this zone and caused the index of refraction to change near the crack tip.

Clearly, the results that were obtained by taking a photograph of the interior grating through a portion of the specimen will be erroneous. This effect was demonstrated by making two compact tension specimens with the same dimensions from the same sheet of polycarbonate but with thicknesses a quarter (0.375 in) and a half (0.750 in) that of the test specimens (1.50 in.). Copper gratings were applied on one side by using the stencil method. Specimen gratings were recorded by taking photographs on the same surface plane with two types of set-ups. First a photograph was taken directly of the specimen surface by putting the grating side near the camera lens. Then, the specimen was turned around and the photograph of the specimen grating was taken through the specimen thickness.

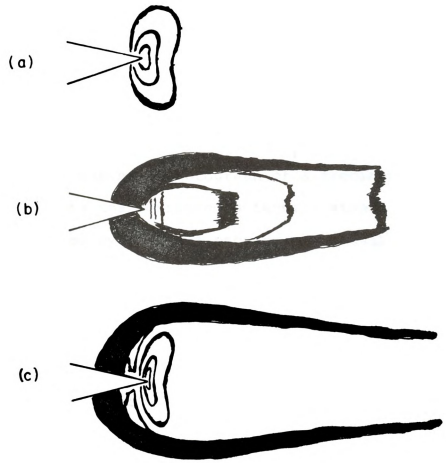

Figure 5.32 Development of Plastic Zone Size on the Surface of Polycarbonate Crack Specimen (Ref 42).

a) Kidney-shaped Zone of Deformation Near the Tip at Small Load.
b) Wedge-shaped Zone at Higher Extension.
c) Internal Kidney Within the Wedge of Still Higher Extension.

The moire fringe patterns that were obtained from these set-ups are shown in figure 5.33 and Figure 5.34. The plots of ε_y are shown in Figure 5.35 and Figure 5.36. The results show that the strain, ε_y, on the same surface plane obtained from different sides of the specimen are totally different. The strain ε_y near the crack tip obtained by taking a photograph of a specimen grating directly from the near surface is tensile strain; but the strain ε_y obtained by taking a photograph through the specimen thickness is compressive strain. The magnitude of the strain ε_y near crack tip obtained by taking a photograph through the specimen thickness is much larger than that obtained directly from the surface grating.

The interior strains obtained by simple means are shown to be in serious error due to internal refraction. For the observation to be valid, the measured strains in the interior must be corrected. It was necessary to develop a suitable correction procedure.

5.4.2 Correction Procedure

From previous sections, the measurements on the same surface plane obtained from different sides were found to be a lot different. The observed difference depends on specimen thickness. Assume the strain difference of a very thin specimen is zero. A plot of the strain difference (strain error) of the very thin ($\approx$ zero thickness) specimen, the quarter thickness (0.375 in. thick) specimen, and the half-thickness (0.750 in. thick) specimen (see Figures 5.35

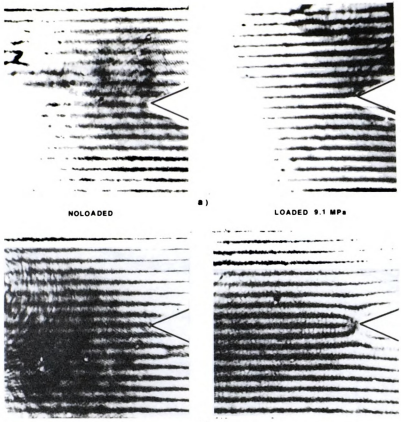

Figure 5.33 The Moire Fringe Patterns Observed on the Surface of a Quarter Thickness Specimen (0.375 in) in the Direction Parallel to the Crack Line by Taking a Photograph

a) Directly of the Grating on the Surface Plane and
b) by a Pass Through the Specimen Thickness.

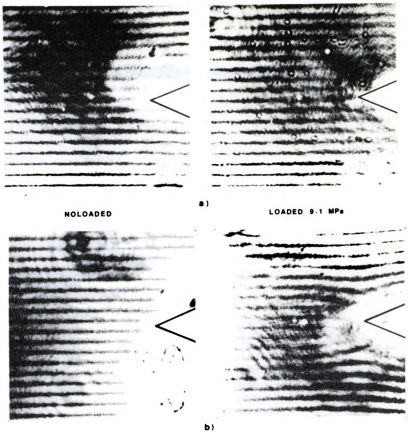

Figure 5.34 The Moire Fringe Patterns Observed on the Surface Plane of a Half Thickness Specimen (0.750 in) in the Direction Parallel to the Crack Line by Taking a Photograph

a) Directly to the Grating on Surface Plane and
b) by a Pass Through the Specimen Thickness.

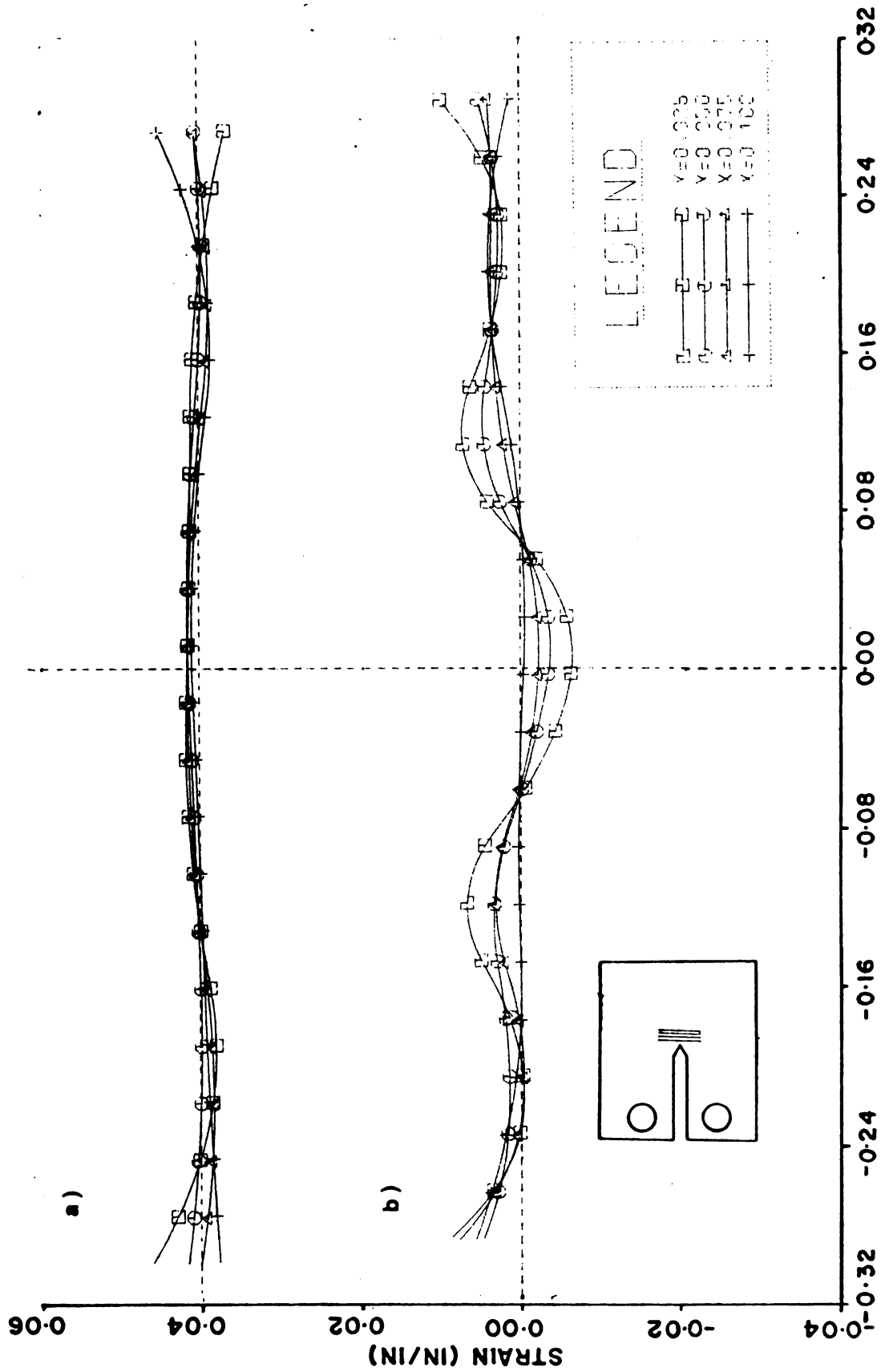

Figure 5.35 The Strain Observed in the Direction Perpendicular to a Crack Line (ε_y) of a Specimen Thickness of 3/8 in. by Taking a Photograph (a) Directly of the Surface, and (b) Through the Thickness of the Specimen.

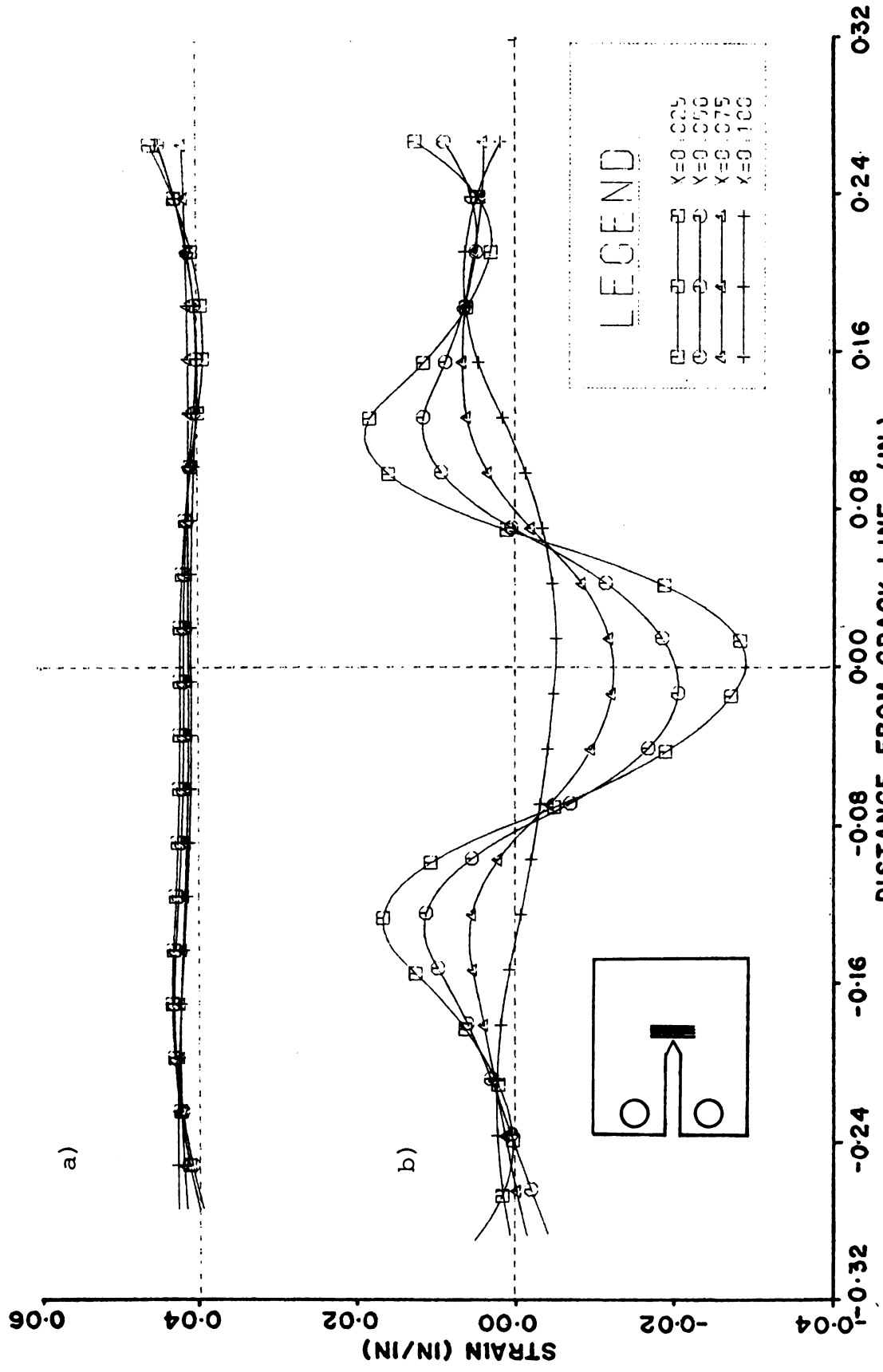

Figure 5.36 The Strain Observed in the Direction Perpendicular to the Crack Line (ε_y) of the Specimen Thickness of 3/4 in. by taking a Photograph (a) Directly of the Surface and (b) Through the Thickness of the Specimen.

and 5.36) at various distances ahead of crack tip along the crack plane versus specimen thickness is shown in Figure 5.37. The results show that the curves of the strain difference give approximately

$$\Delta\varepsilon = \delta\ x^2$$

where $\Delta\varepsilon$ is the strain difference or strain error

δ is a material property to be determined

x is the specimen thickness

The plots of the strain difference (strain error) at various distances along the plane perpendicular to the crack plane (y_1, y_2, y_3, where y_i are the distance from the crack plane) versus the specimen thickness are shown in Figure 5.38. The results show that only a small region near the crack plane satisfied this approximation. In this investigation, therefore, the correction of the interior strain will be obtained only for the region near the crack plane.

The information needed to correct the results in the interior were obtained by making a compact tension specimen from the same sheet of polycarbonate with the same dimensions and thickness as the test specimen. A piece of Nickel mesh grating was applied on the quarter plane only. One strain gage was applied at a distance 0.3 in. from the crack tip along the crack line to measure strain, ε_y, on the quarter plane. The position of the Nickel mesh grating and the strain gage of this correction specimen are shown

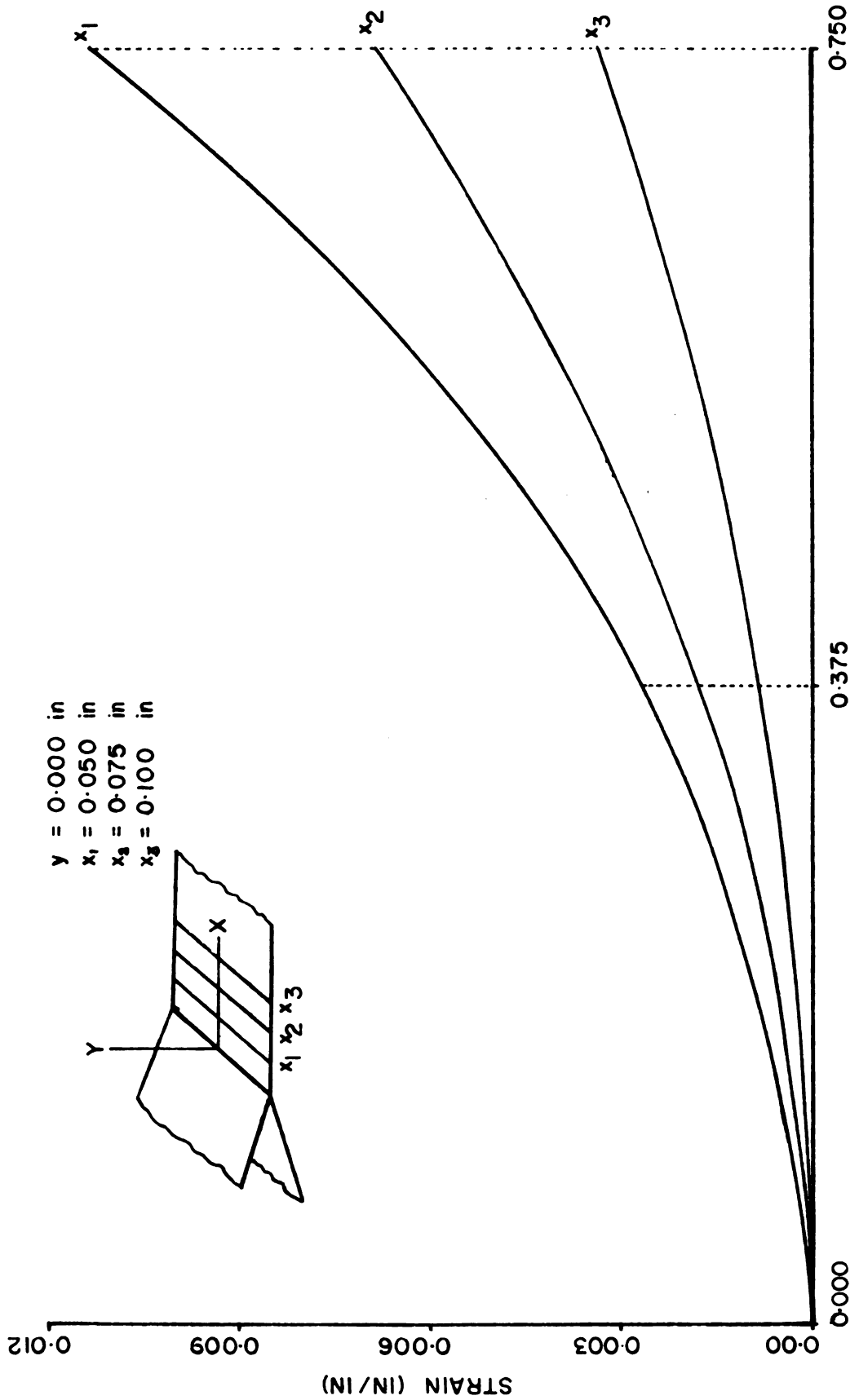

Figure 5.37 The Plot of Strain Error on Different Lines (x_1, x_2, x_3) in the Crack Plane.

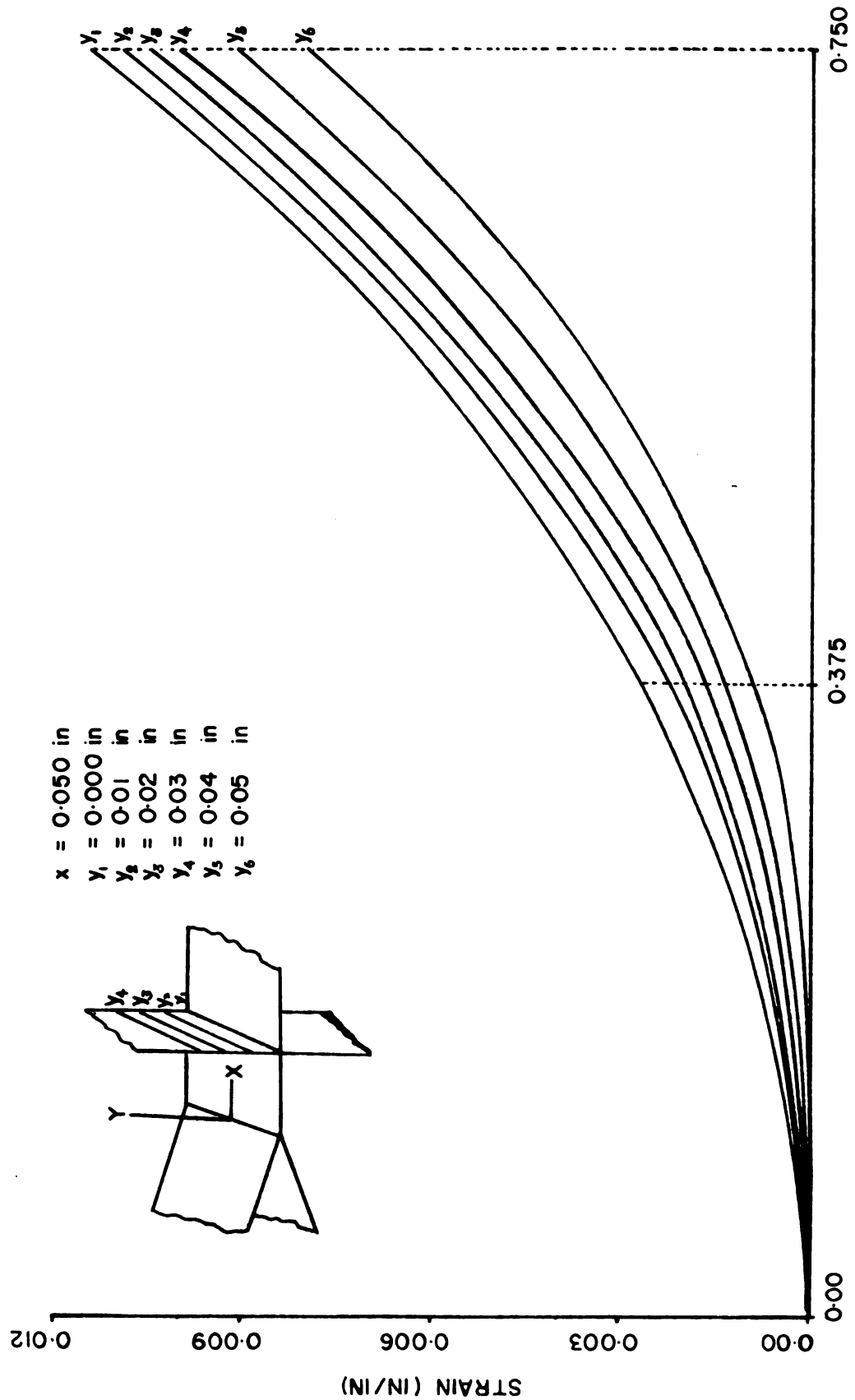

Figure 5.38 The Plot of Strain Error on Different Lines ($y_1, y_2, \ldots y_6$) in the Plane Perpendicular to Crack Plane at x=0.050 in.

schematically in Figure 5.40. The photoplates of the specimen grating on the same plane were recorded from both sides of the specimen. One was recorded through a quarter of the specimen thickness and the other was recorded through three-quarters of specimen thickness. While the specimen was loaded the strain measurement obtained from the strain gage was a small tensile strain. Moire fringe patterns obtained from both sides are shown in Figure 5.41 and Figure 5.42 The strain ε_y obtained from both sides is shown in Figure 5.43 and Figure 5.45. The results from each side can be expressed as:

$$\varepsilon_{1M} = \varepsilon_{1R} + \Delta\varepsilon_1$$

$$\varepsilon_{3M} = \varepsilon_{3R} + \Delta\varepsilon_3$$

where ε_{1M} is a measure of the strain on the quarter-plane by taking a photograph through one-quarter of the specimen thickness.

ε_{3M} is a measure of the strain on the quarter-plane by taking a photograph through three-quarters of the specimen thickness.

ε_{1R} and ε_{3R} are the real strain on the quarter-plane, $\varepsilon_{1R} = \varepsilon_{3R}$, since it is the same plane.

$\Delta\varepsilon_1$ is the strain error on the quarter-plane obtained from a quarter thickness side.

$\Delta\varepsilon_3$ is the strain error on the quarter-plane obtained from a three-quarters thickness side.

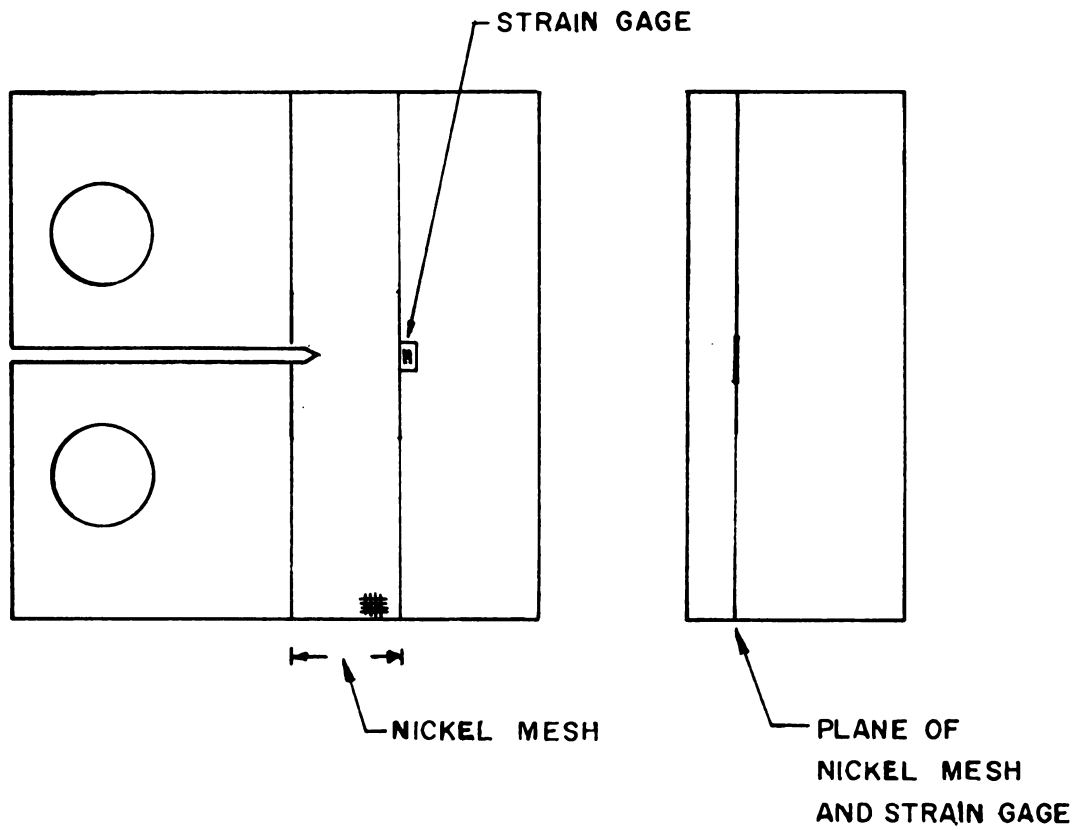

Figure 5.39 Schematic Showing the Positon of Nickel Mesh and Strain Gage on the Quarter Plane of Specimen.

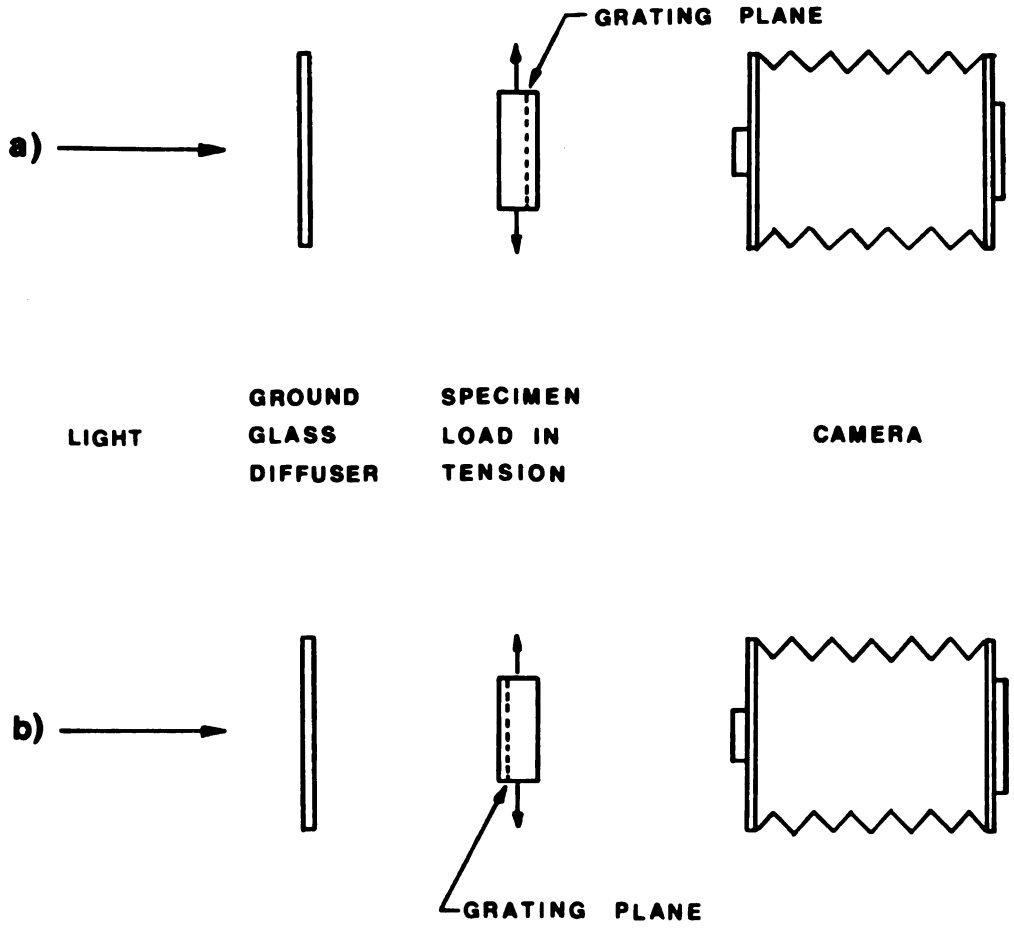

Figure 5.40 Schematic of Photography Process
a) Through one-quarter Thickness Side and
b) Through three-quarter Thickness Side.

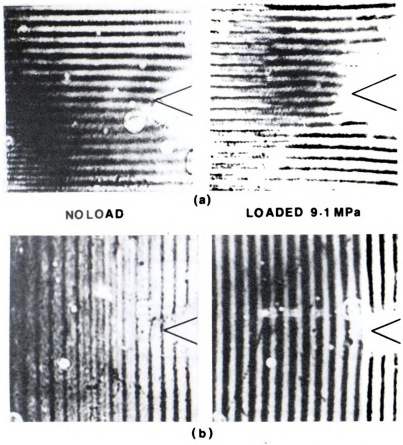

Figure 5.41 Moire Fringe Pattern in the Interior of the Specimen with one Plane Grating by Taking a Photograph Pass Through a Quarter Thickness Side in the Direction a) Parallel and b) Perpendicular to the Crack Line.

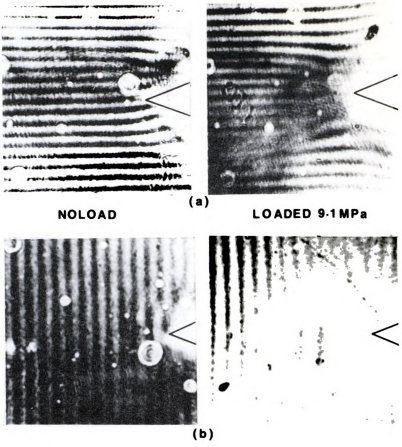

Figure 5.42 Moire Fringe Pattern in the Interior of Specimen with one Plane Grating by Taking a Photograph Pass Through Three-quarter Thickness Side in the Direction a) Parallel and b) Perpendicular to the Crack Line.

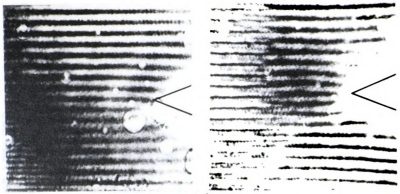

Figure 5.41 Moire Fringe Pattern in the Interior of the Specimen with one Plane Grating by Taking a Photograph Pass Through a Quarter Thickness Side in the Direction a) Parallel and b) Perpendicular to the Crack Line.

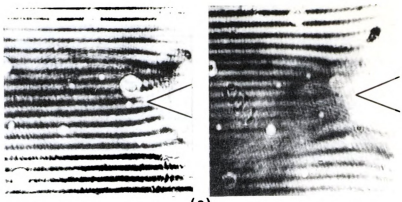

Figure 5.42 Moire Fringe Pattern in the Interior of Specimen with one Plane Grating by Taking a Photograph Pass Through Three-quarter Thickness Side in the Direction a) Parallel and b) Perpendicular to the Crack Line.

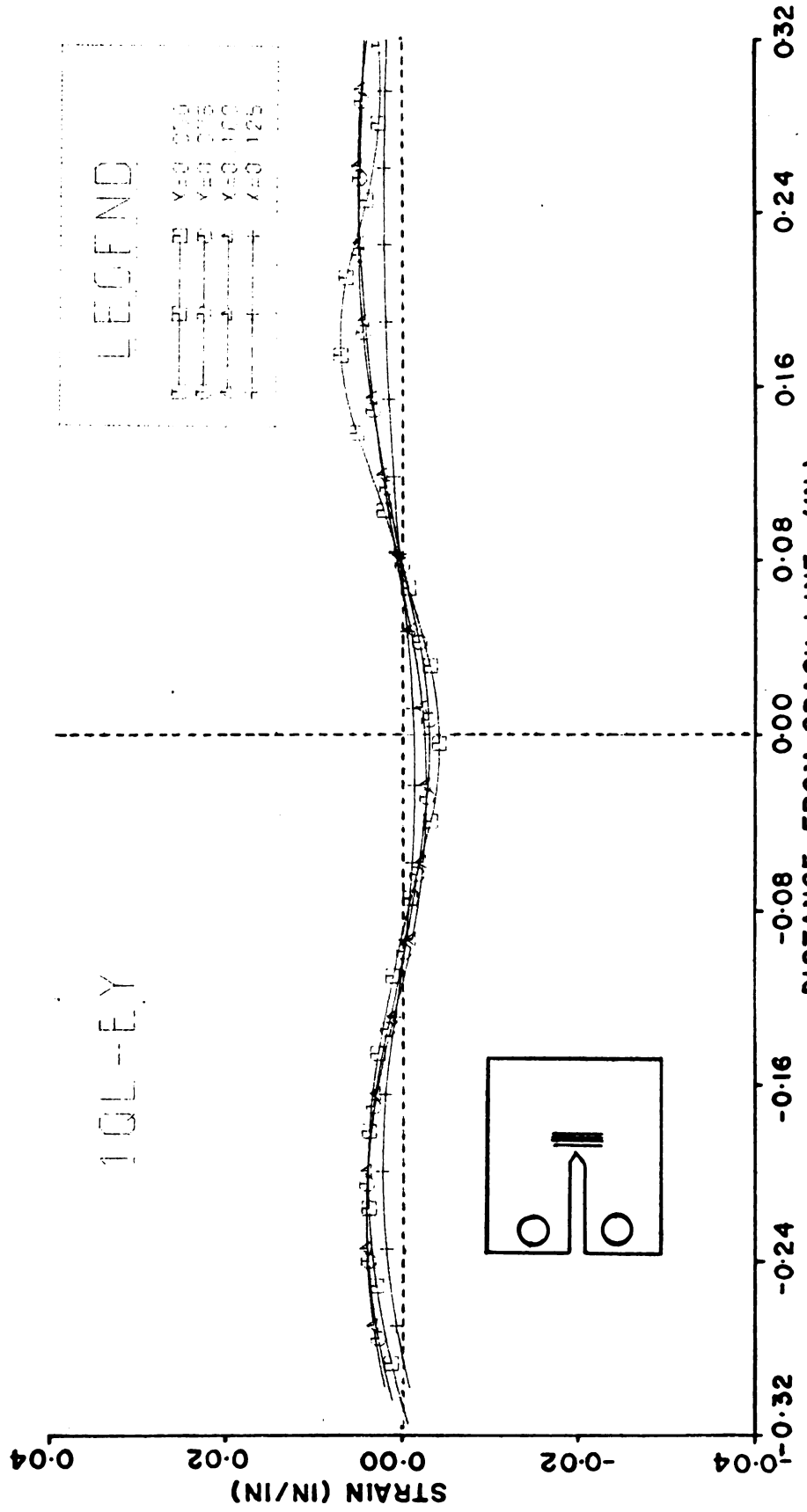

Figure 5.43. The Strain Plot of ε_y in the Interior Obtained from the Moire Fringe Pattern by Taking a Photograph Through the One-Quarter Side of the Specimen.

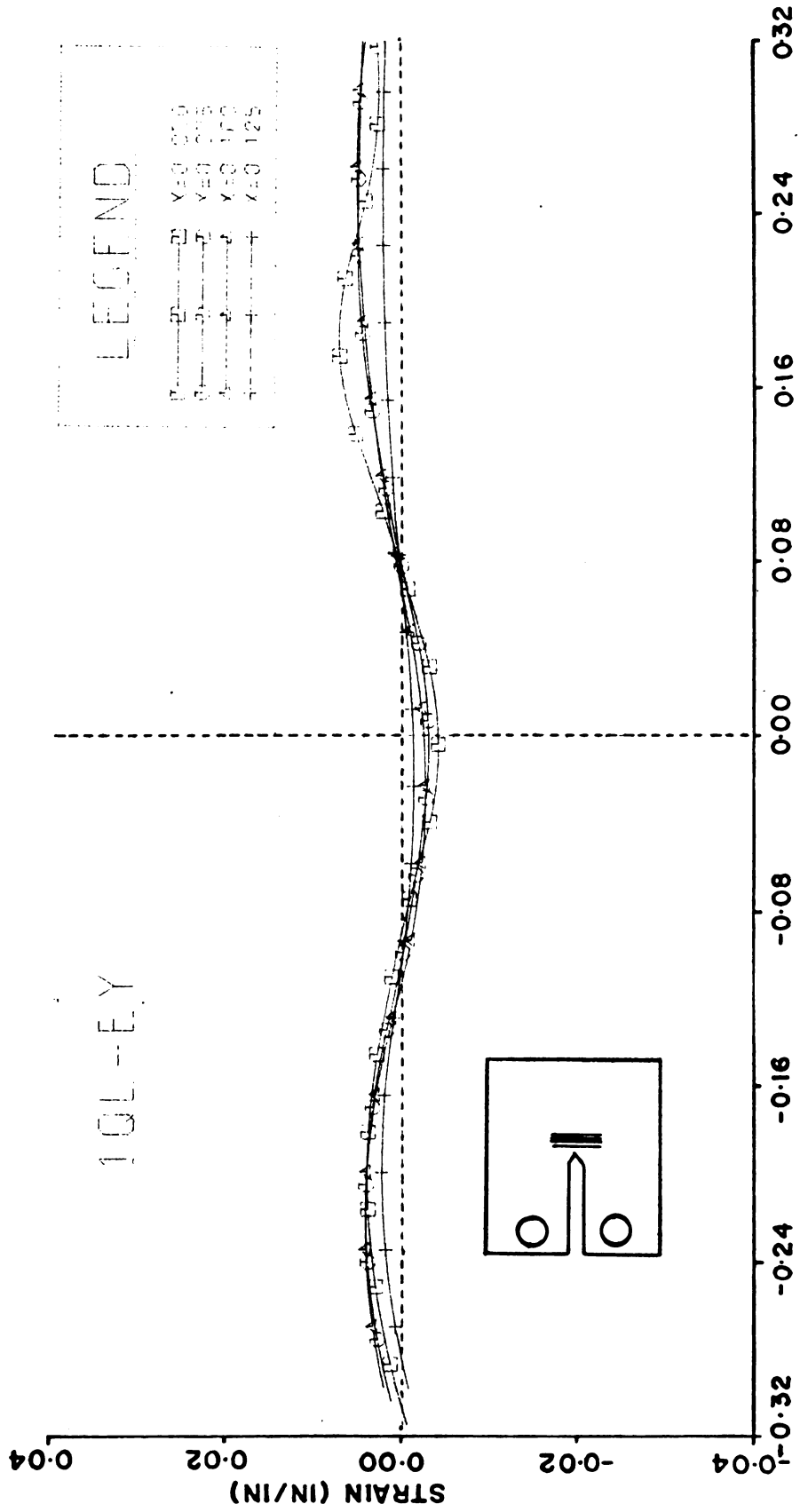

Figure 5.43. The Strain Plot of ε_y in the Interior Obtained from the Moire Fringe Pattern by Taking a Photograph Through the One-Quarter Side of the Specimen.

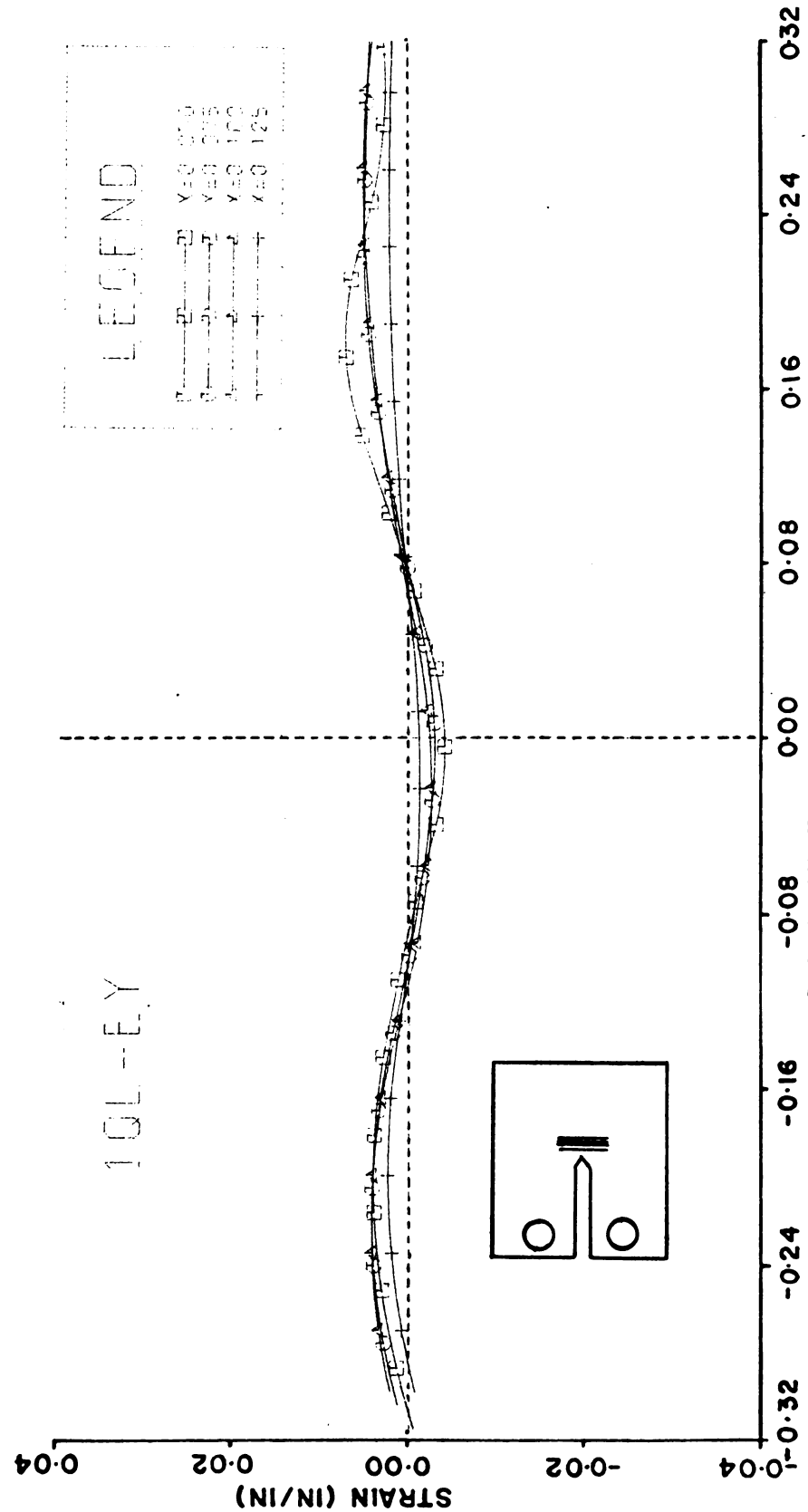

Figure 5.43. The Strain Plot of ε_y in the Interior Obtained from the Moire Fringe Pattern by Taking a Photograph Through the One-Quarter Side of the Specimen.

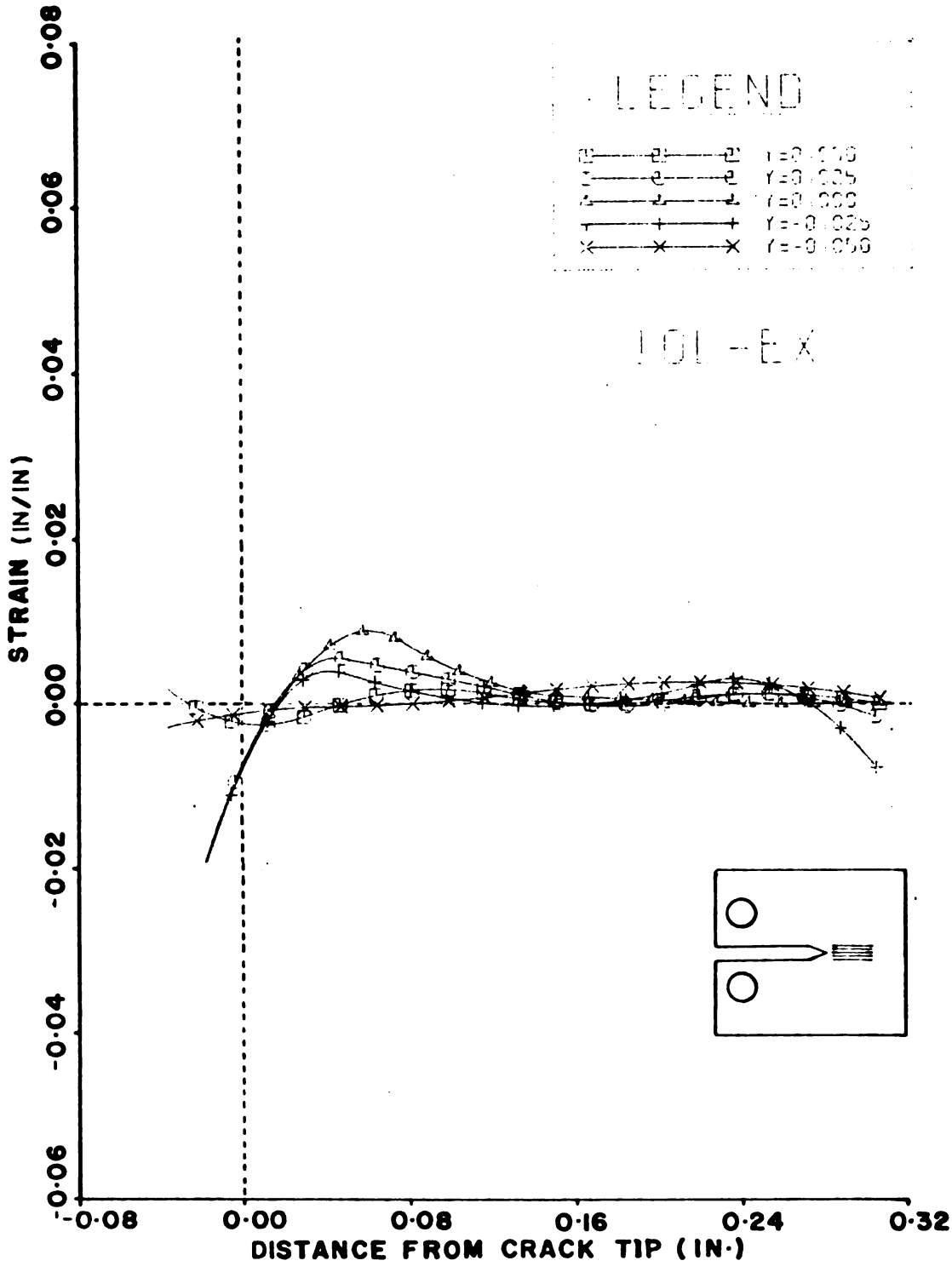

Figure 5.44. The Strain Plot of ε_x in the Interior Obtained from the Moire Fringe Pattern by Taking a Photograph Through a Quarter-Thickness Side.

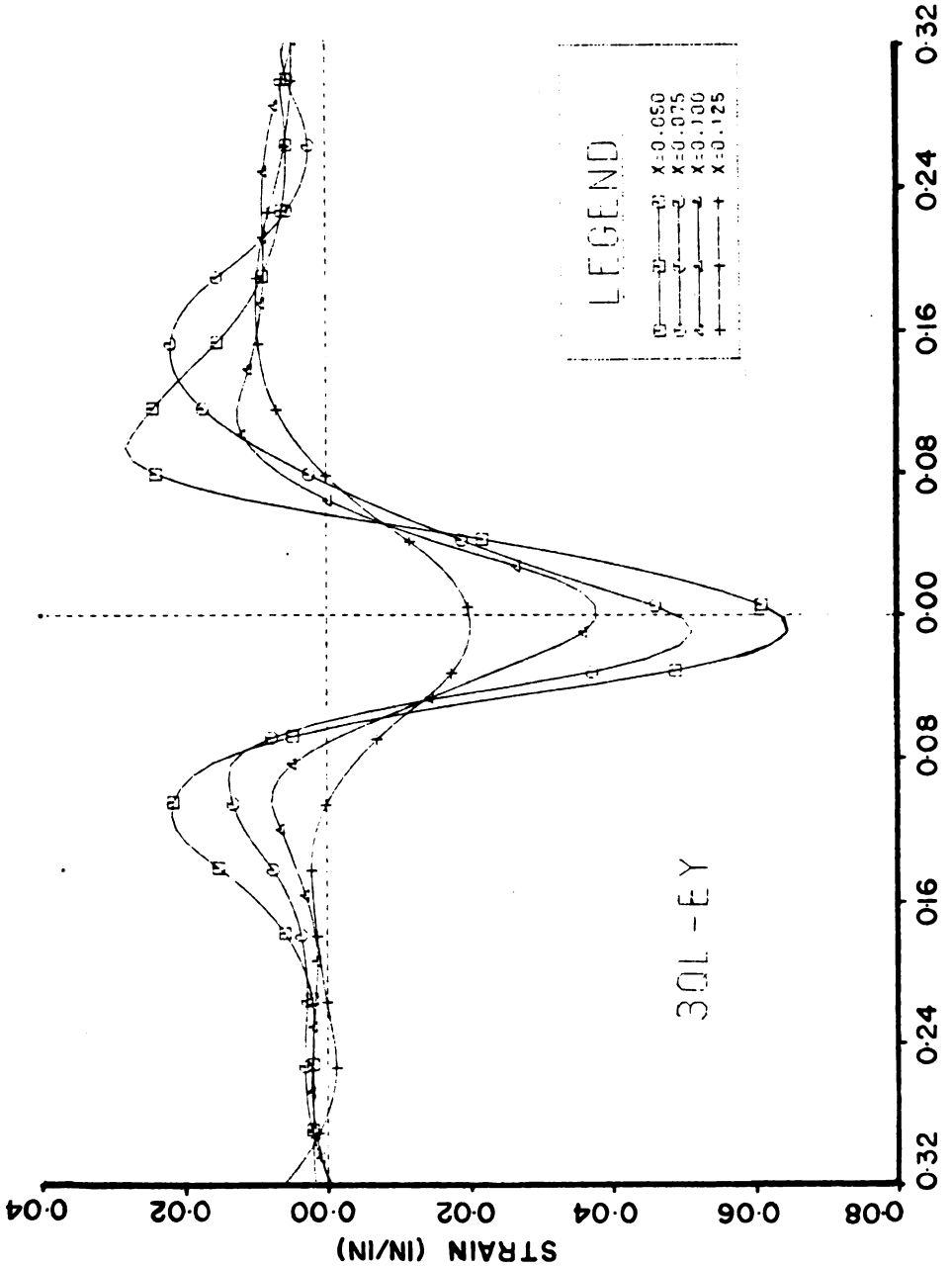

Figure 5.45 The Strain Plot of ε_y in the Interior Obtained from the Moire Fringe Pattern by Taking a Photograph Through the Three-quarter Side of the Specimen.

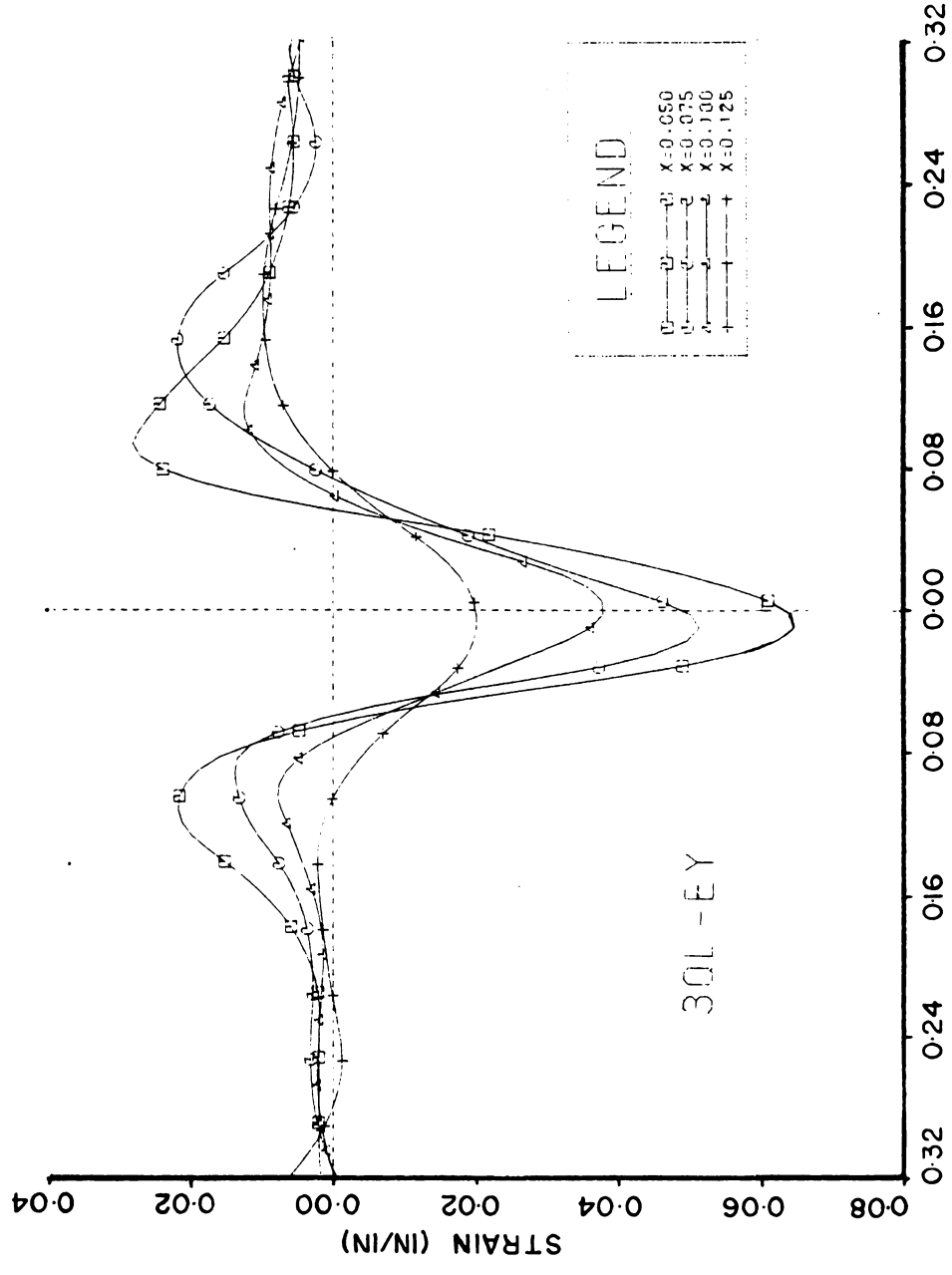

Figure 5.45 The Strain Plot of ε_y in the Interior Obtained from the Moire Fringe Pattern by Taking a Photograph Through the Three-quarter Side of the Specimen.

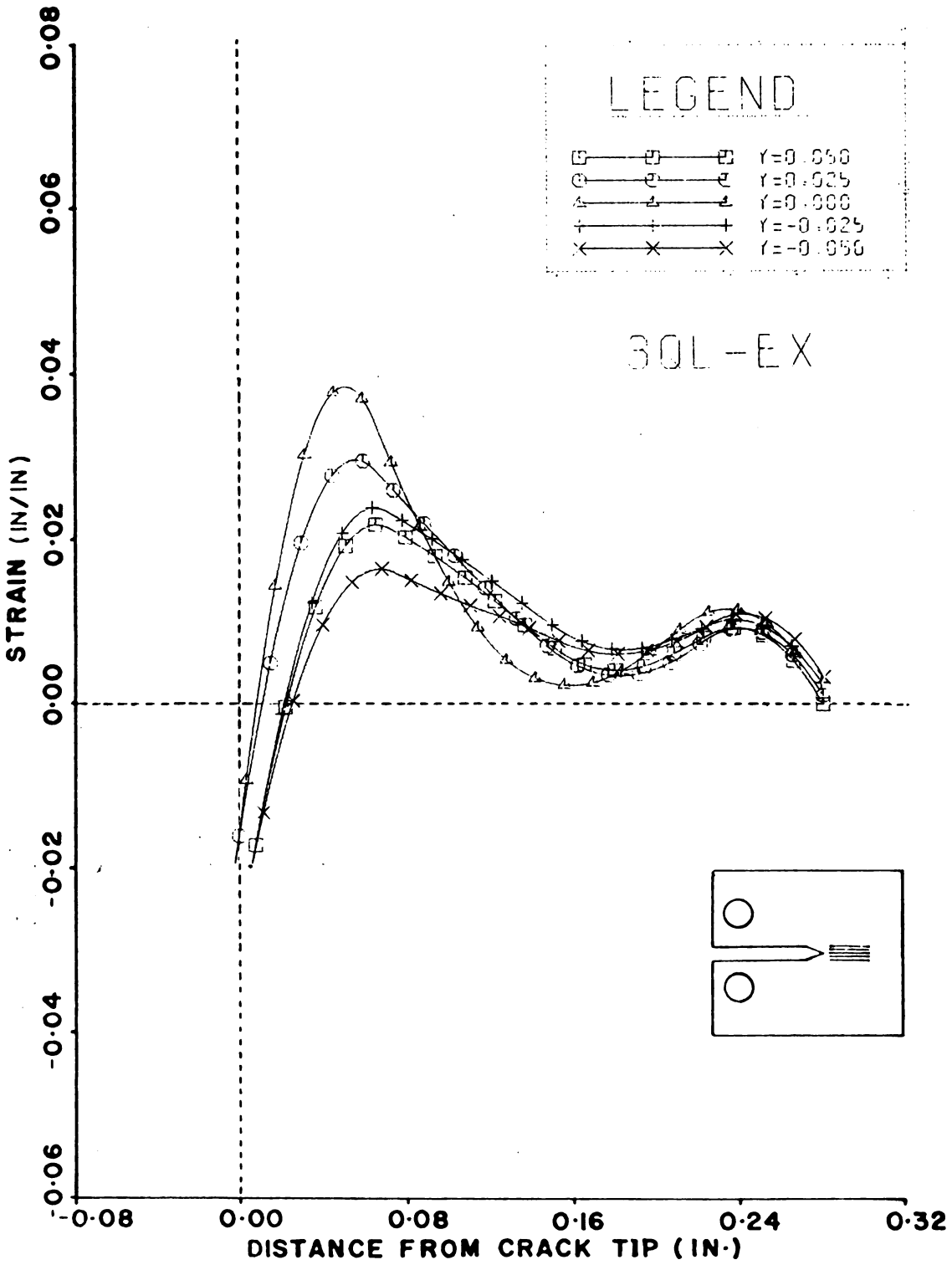

Figure 5.46 The Strain Plot of ε_x in the Interior Obtained from the Moire Fringe Pattern by Taking a Photograph Through Three-quarter Side of the Specimen.

To find the strain error, the difference of strain measurement from both sides is given by

$$\varepsilon_{3M} - \varepsilon_{1M} = \Delta\varepsilon_3 - \Delta\varepsilon_1$$

At this point, assume that the strain error, $\Delta\varepsilon$, is a function of material property, δ, and the thickness of the specimen. The observation that the error is proportional to the square of thickness leads to the expression,

$$\Delta\varepsilon = \left(\frac{d}{t}\right)^2 \delta$$

where δ is the material property that affects the index of the refraction while the specimen is loaded.

d is the distance from the grating plane to the surface plane on the camera side.

t is the specimen thickness.

The strain errors from both sides are

$$\Delta\varepsilon_1 = \left(\frac{\frac{1}{4}t}{t}\right)^2 \delta = \left(\frac{1}{4}\right)^2 \delta$$

$$\Delta\varepsilon_3 = \left(\frac{(3/4)t}{t}\right)^2 \delta = (3/4)^2 \delta$$

$$\varepsilon_{3M} - \varepsilon_{1M} = (3/4)^2\delta - (1/4)^2\delta = 1/2\delta$$

so,

$$\delta = 2(\varepsilon_{3M} - \varepsilon_{1M})$$

Finally the real strain on the quarter-plane is

$$\varepsilon_{1R} = \varepsilon_{3R} = \frac{1}{8}(9\,\varepsilon_{1M} - \varepsilon_{3M}) \quad \ldots\ldots \text{(I)}$$

The real strain on the mid-plane can be obtained in terms of the correction factor found from the quarter-plane observations by extending this idea.

$$\varepsilon_{2R} = \varepsilon_{2M} - \Delta\varepsilon_2$$

$$= \varepsilon_{2M} - \left(\frac{1/2t}{t}\right)^2 \delta$$

$$= \varepsilon_{2M} - \frac{1}{2}\left(\varepsilon_{3M} - \varepsilon_{1M}\right) \quad \ldots\ldots \text{(II)}$$

The real strain in the interior of specimen is calculated by using eq. (I) and eq. (II) to correct the data from moire fringe patterns. The strains ε_{1M} and ε_{2M} were obtained from the test specimen with two gratings in the interior, but ε_{3M} was obtained from the specimen with one grating in the quarter plane of the specimen.

5.4.3 Final Experimental Results

5.4.3.1 Experimental Results from the Moire Method

The results given in Section 5.4.1 for the specimen which gave the best results on the surface-plane, quarter-plane and mid-plane were corrected by using eq (I) and (II) in Section 5.4.2. For this specimen, the data plate of the quarter-plane grating obtained by taking a photograph through a three-quarter thickness side did not record a good grating, due to the camera lens having to focus through the copper grating on the surface plane and the nickle mesh grating on the mid-plane before getting to the grating on the quarter-plane (three-quarter thickness side). Consequently, the moire fringe patterns and the strain plot from the three-quarter thickness side could not be obtained from this specimen. The final results for the specimen with gratings on the quarter and mid-plane were corrected by using the results from

two different specimens. The quarter-plane (ε_{1M}), and the mid-plane, ε_{2m}, results obtained from the first experiment, and the quarter-plane, ε_{3M}, results obtained from the three-quarter thickness side from the specimen with one plane grating (quarter-plane) in the interior were substituted in eq. (I) and eq. (II) in Section 5.4.2. The corrected strain plots and constant strain contours on the quarter-plane and the mid-plane are shown in Figure 5.47 to Figure 5.50. The results show that the strain ε_y around the crack tip on the quarter-plane and mid-plane is tensile strain and the magnitude of the strain ε_y on the mid-plane near the crack tip is larger than on the quarter-plane. The plots of the strain ε_y along crack line on the surface-plane, quarter-plane and mid-plane are shown in Figure 5.51. The results show that the strain ε_y in the interior along the crack line near the crack tip is larger than the surface strain. The difference of the strain ε_y on the quarter-plane and the mid-plane is small. At the same distance from the crack tip through the specimen thickness, the strain ε_y near the crack tip is maximum on the mid-plane and decreases to a minimum on the surface-plane. Consider the strain plot and the constant strain contours of ε_y in the interior and on the surface. The peak of the maximum strain in the interior is on the crack line. The peak of the maximum strain on the surface (see Figure 5.20), however, does not lie on the crack line. There are, instead, two symmetrically located strain peaks above and below the crack line along

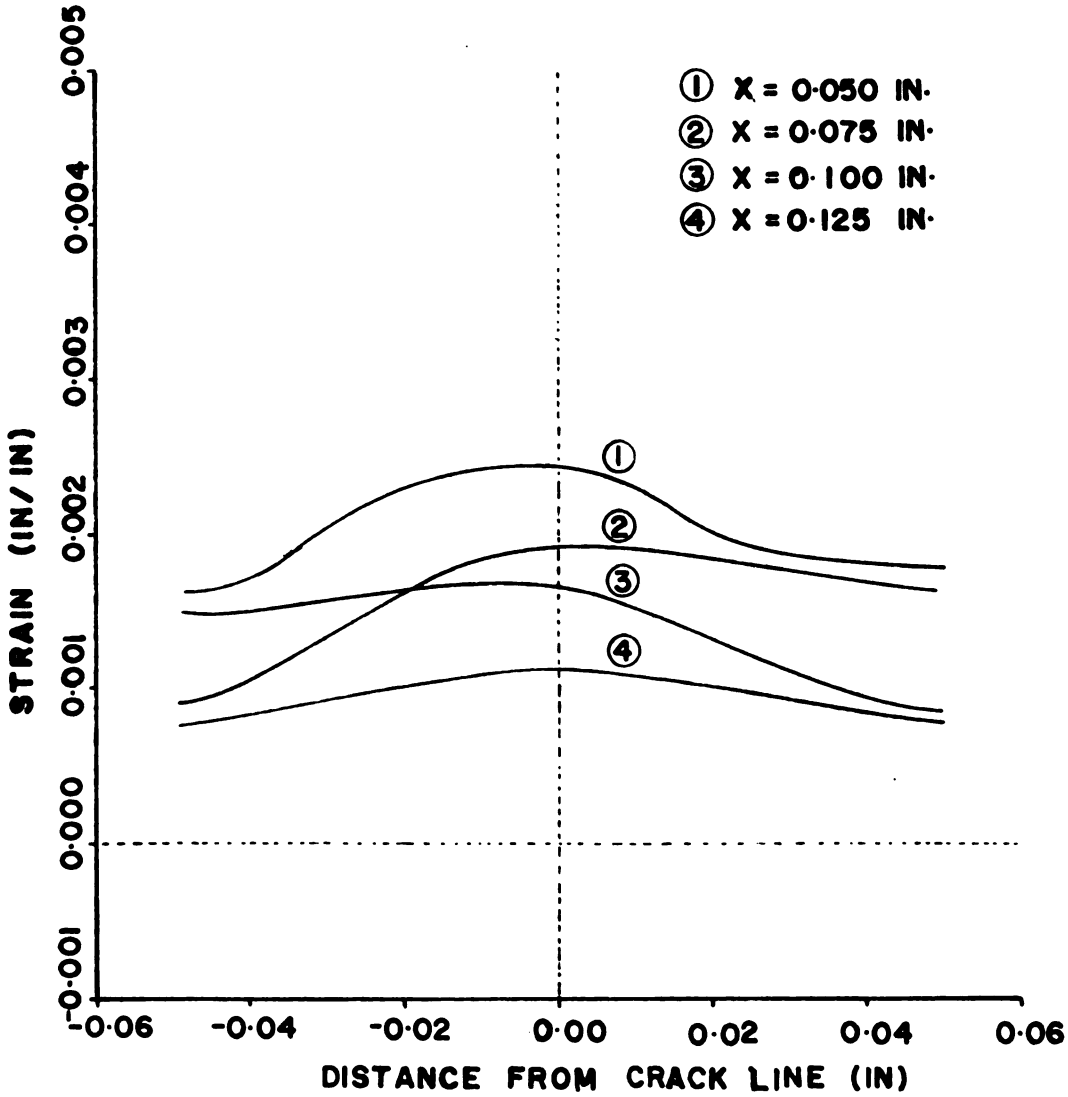

Figure 5.47 A Plot of Strain ε_y on the Quarter-plane.

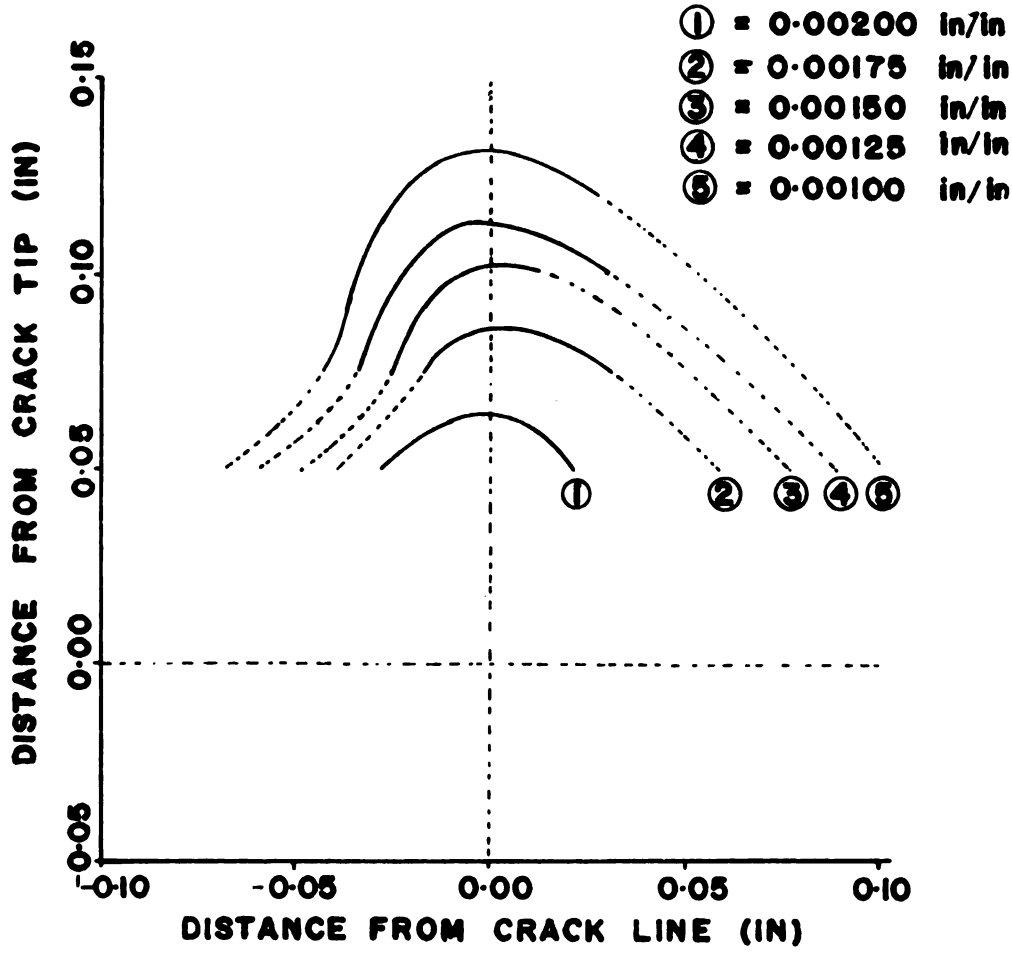

Figure 5.48 The Constant Strain Contours ε_y on the Quarter-plane.

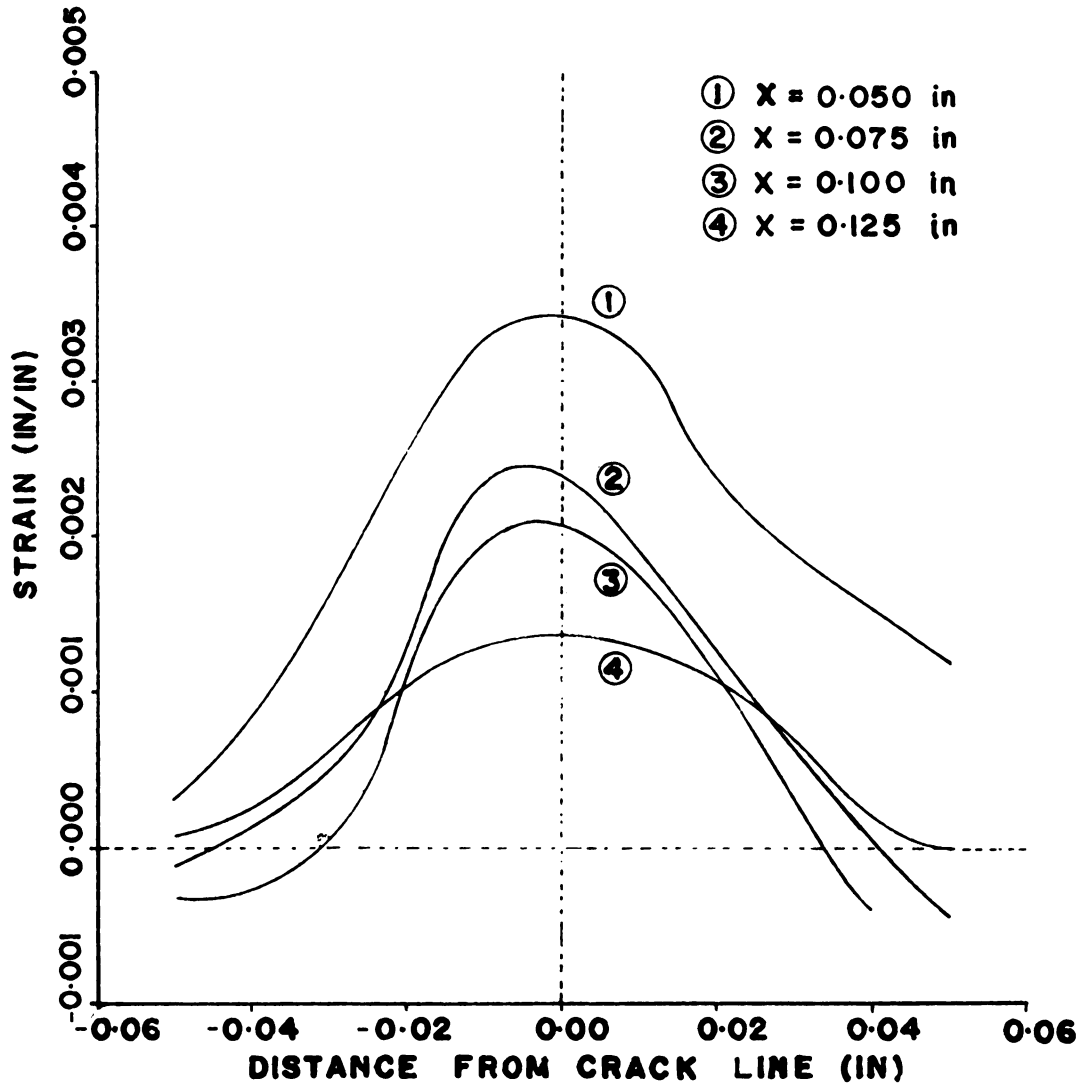

Figure 5.49 A Plot of Strain ε_y on the Mid-plane.

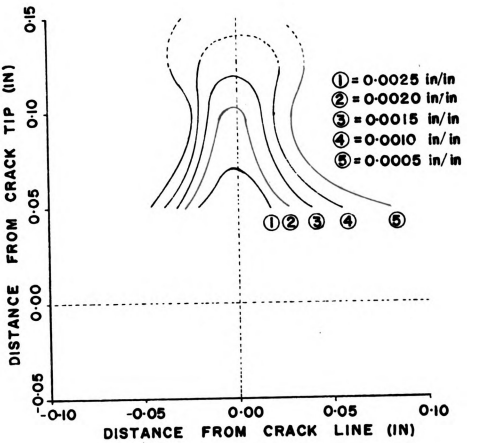

Figure 5.50 The Constant Strain Contours ε_y on the Mid-plane.

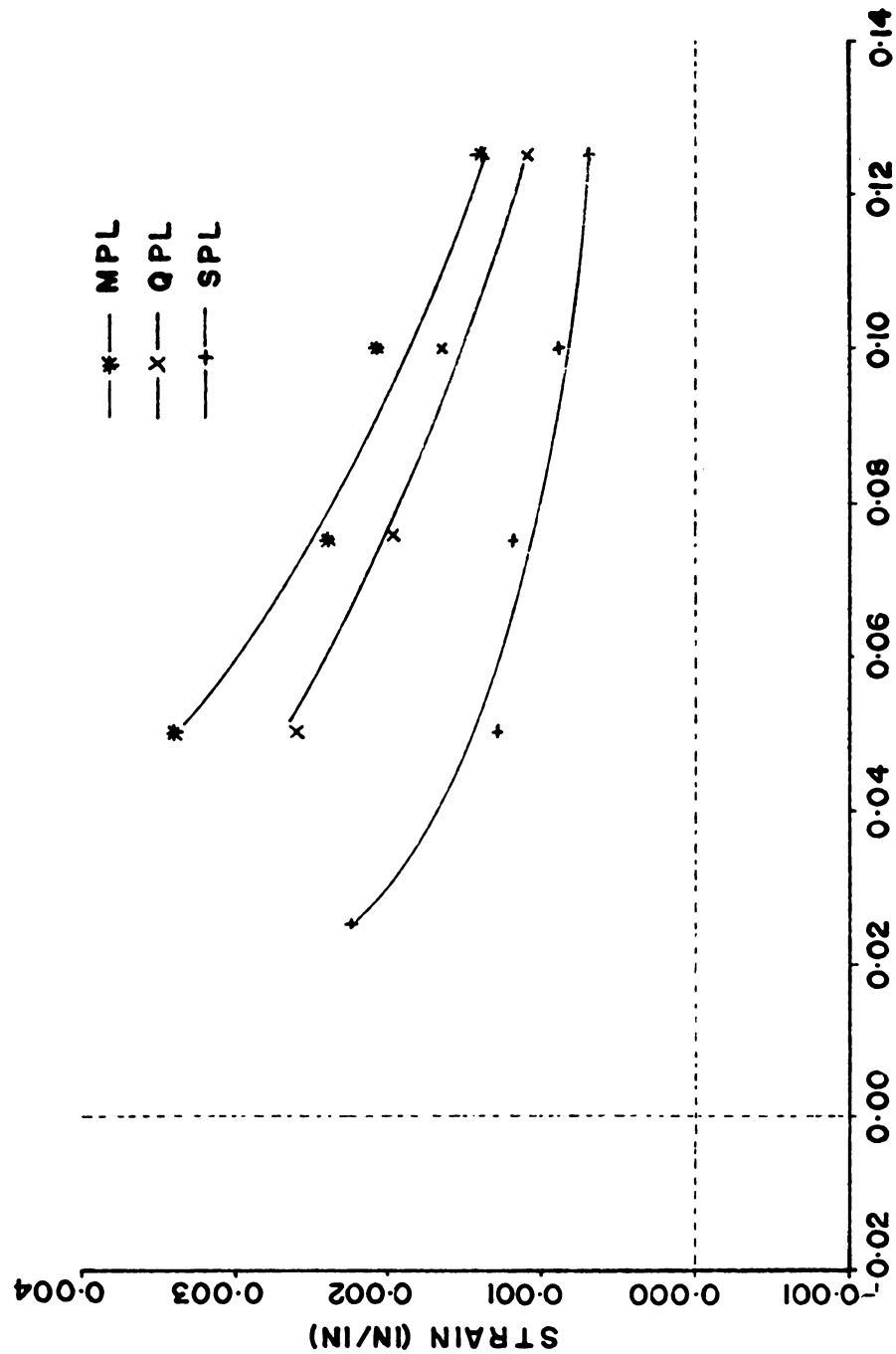

Figure 5.51 A Comparison of ε_y on the Surface, Quarter and Mid-planes Along the Crack Line.

each curve. The distance between these peaks is small near the crack tip, but gradually increases with distance from the crack. On the surface-plane, the contour lines of constant ε_y start out at the crack tip and fan out. These general characteristics of strain contours are similar to those observed by Gerberich (36), Kobayashi (40) and Lui and Ke (34), but all of these experimentors studied aluminum plate and/or steel plate with a central crack. In the interior the contour lines of constant ε_y seem to start out at the crack tip and spread out, and then they come close to forming a complete loop on each of the contour lines. From these results in the interior, the maximum strain starts out at the crack tip and lies on the crack plane. In contrast, the maximum strain on the surface is split into two lines corresponds to the shear lip on the surface.

The final results of the strain in the direction parallel to the crack line, ε_x, were corrected by using the same procedure as before. The strain plots and the constant strain contours of ε_x on the quarter-plane and the mid-plane are shown in Figure 5.52 to Figure 5.55. Near the crack tip, strain ε_x is very small when compared with strain ε_y. Therefore, the strain ε_y is more important than the strain ε_x on any plane along the thickness. The shapes of the constant strain contours on the surface-plane, the quarter-plane and the mid-plane are basically the same, differing slightly in magnitude. A comparison of the strain ε_x on the surface-plane, the quarter-plane and the mid-plane along the crack

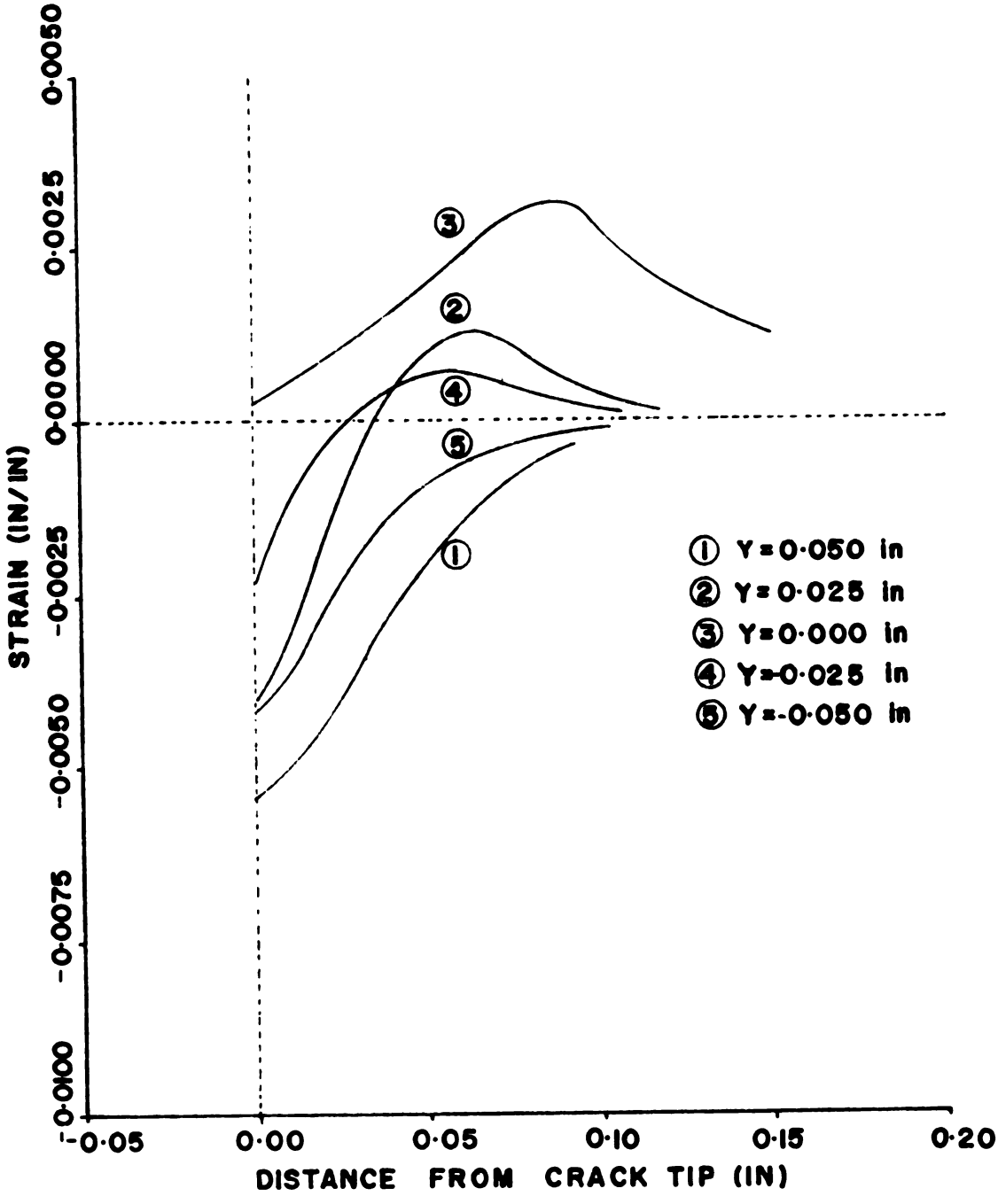

Figure 5.52 The Plot of the Strain ε_x on the Quarter-plane Along the Crack Line After Correction.

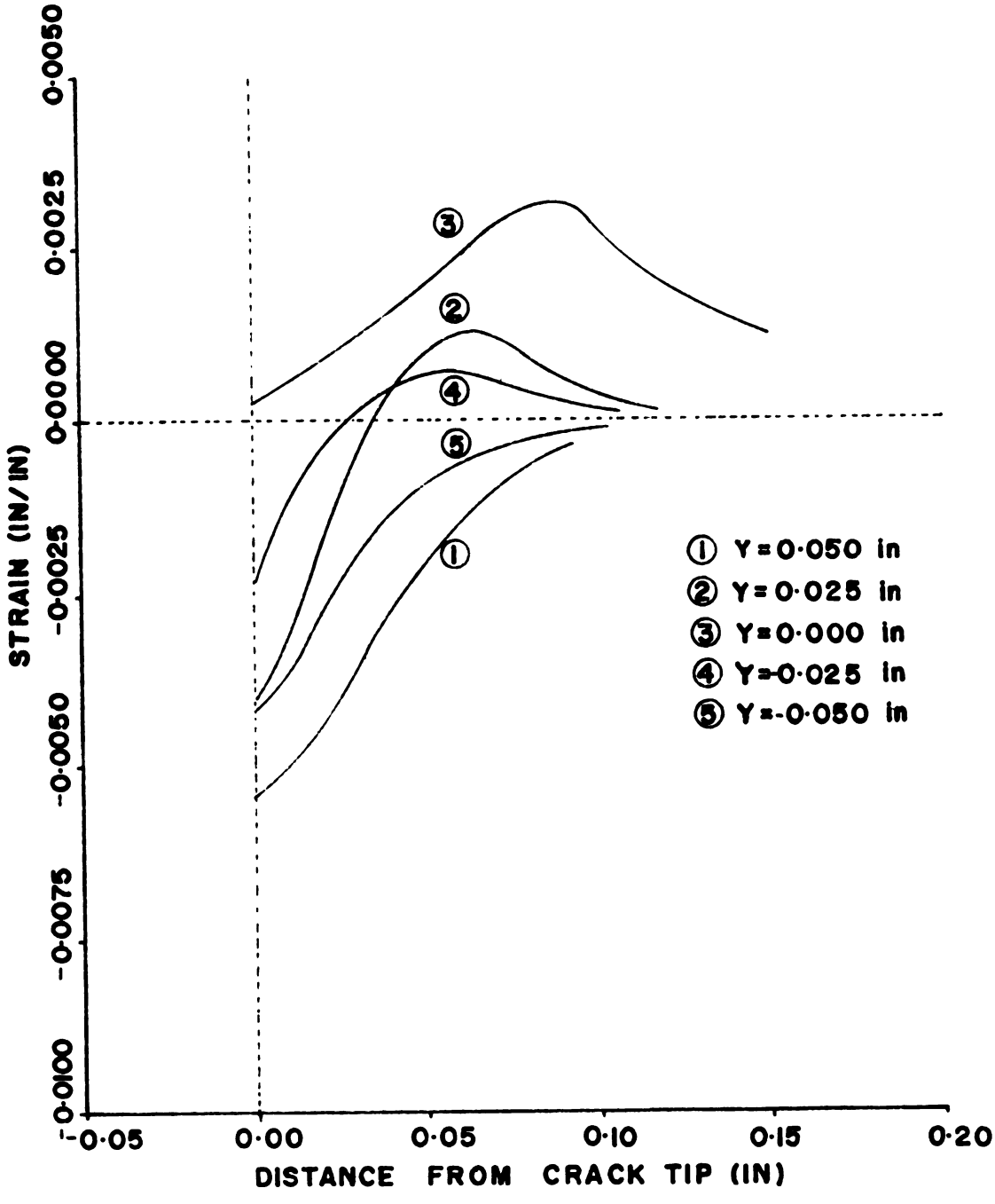

Figure 5.52 The Plot of the Strain ε_x on the Quarter-plane Along the Crack Line After Correction.

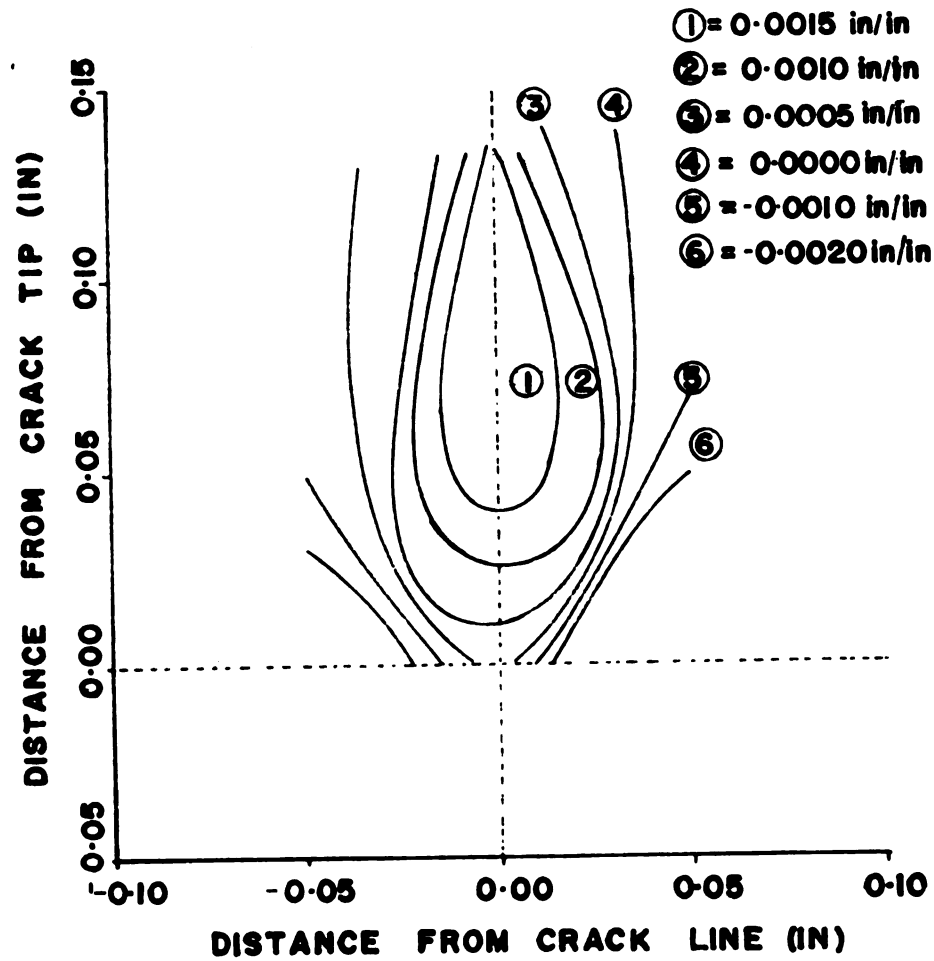

Figure 5.53 The Constant Strain Contours ε_x on the Quarter Plane.

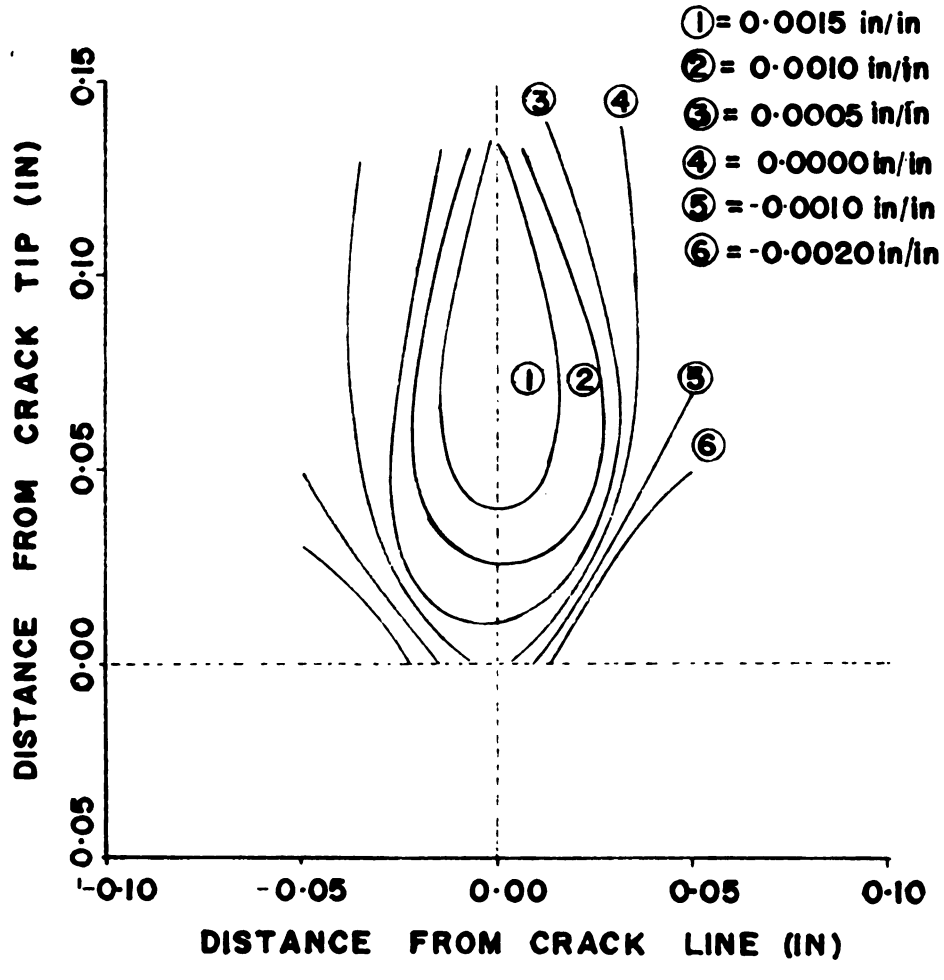

Figure 5.53 The Constant Strain Contours ε_x on the Quarter Plane.

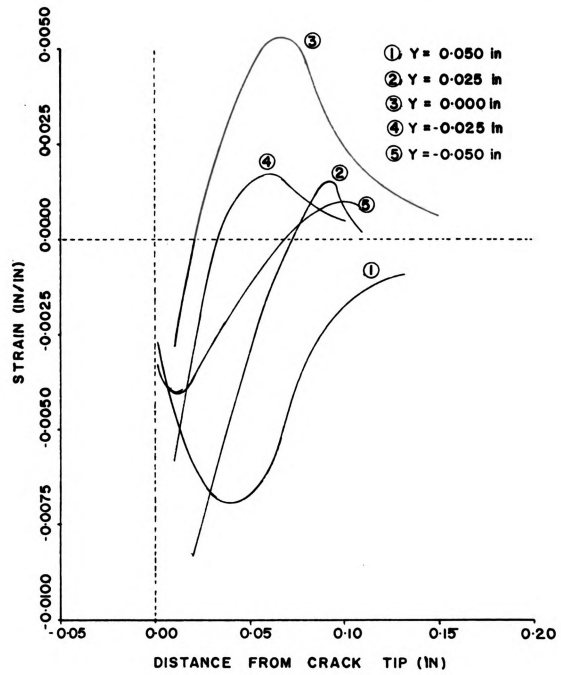

Figure 5.54 The Plot of Strain ε_x on the Mid-Plane Along the Crack Line After Correction.

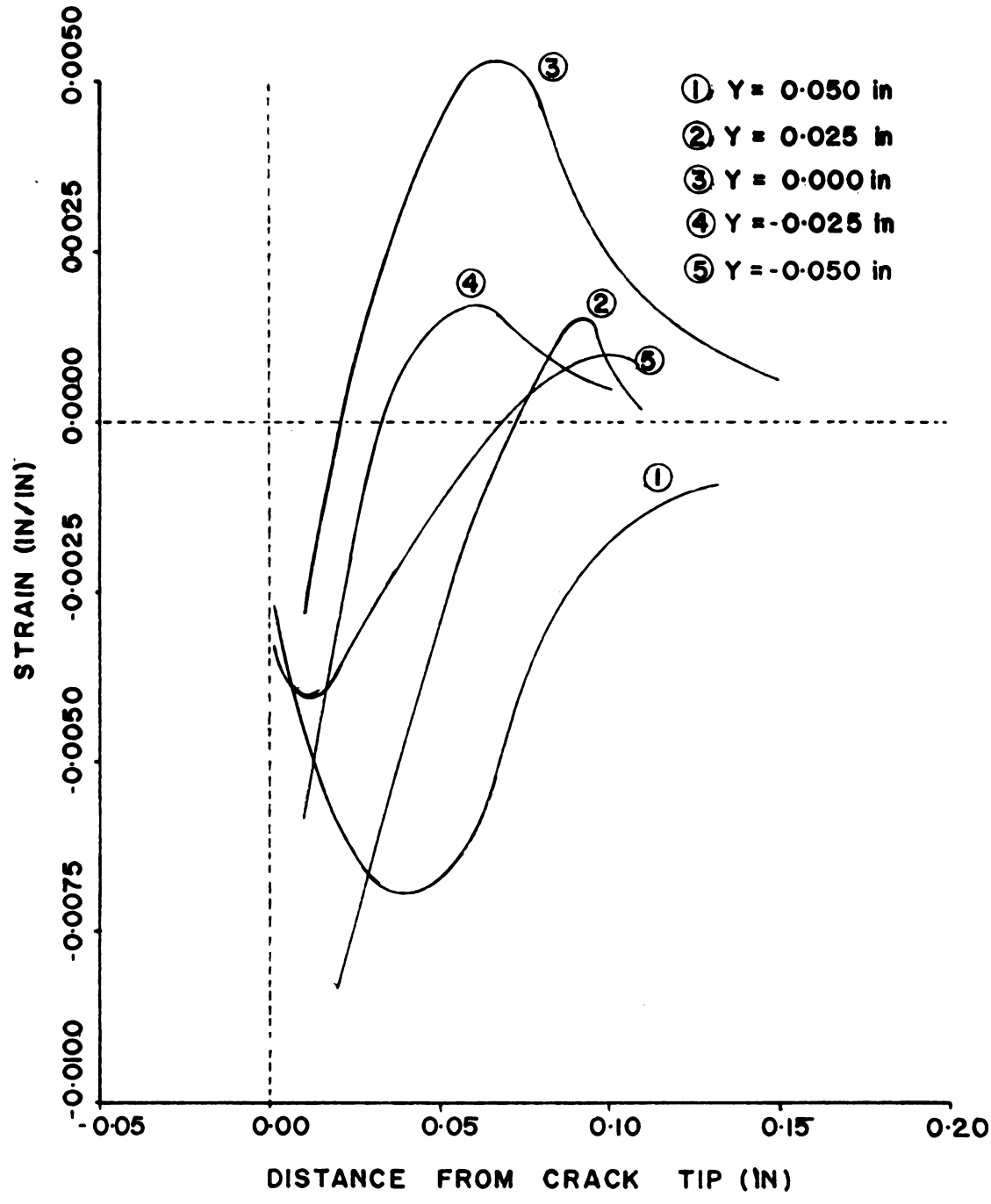

Figure 5.54 The Plot of Strain ε_x on the Mid-Plane Along the Crack Line After Correction.

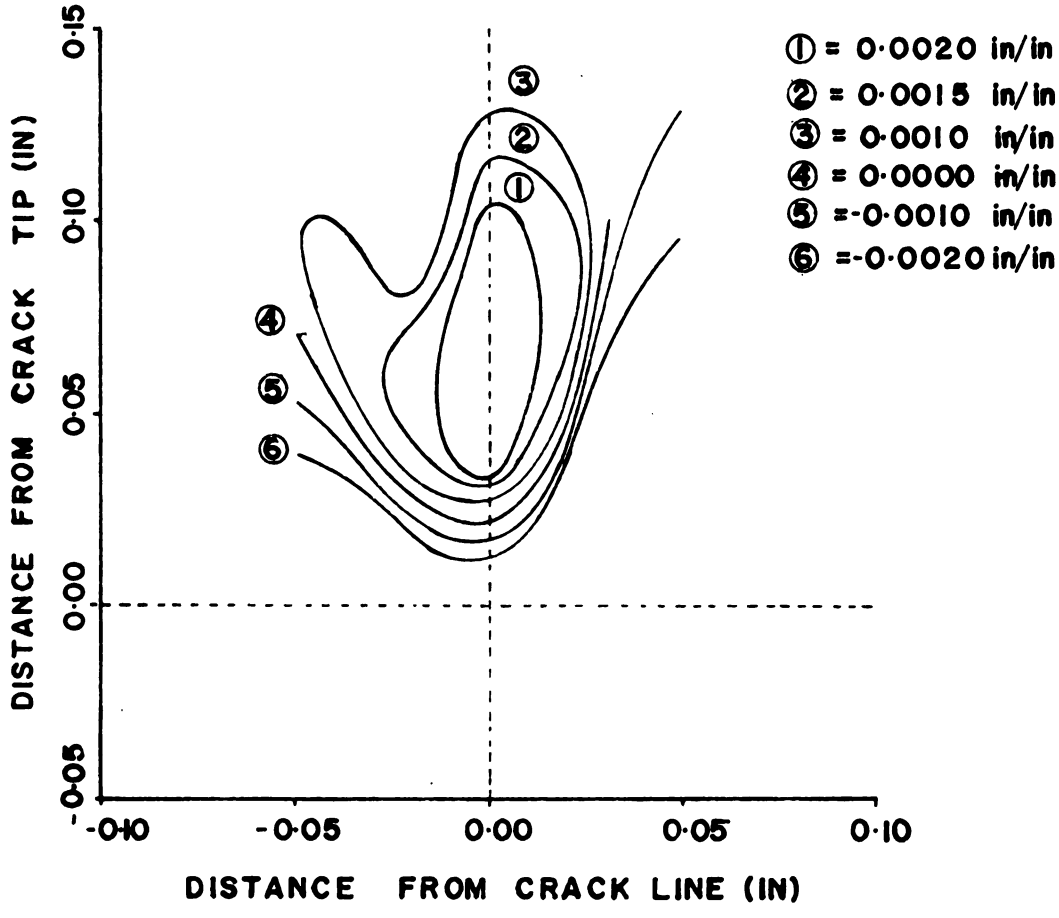

Figure 5.55 The Constant Strain Contours ε_x on the Mid-plane.

line is shown in Figure 5.56. The constant strain contours show that tensile strain ε_x only occurrs along the crack line, compressive strain occurring above and below a small area along the crack line.

5.4.3.2 Experimental Results From Strain Gages

The interior strain measurements obtained by the moire technique are subject to question because of the necessity to use an empirical procedure to correct for the apparent strain caused by refraction. The results obtained from the moire method were compared with another experimental method in order to verify them. A specimen with strain gages was used to verify the strains in both directions (ε_x and ε_y) along the crack line near the crack tip. Two compact tension specimens with strain gages were studied. Many gages were installed on the surface and in the interior of each specimen. Each specimen was made from four rectangular pieces (3.9 x 4.0 in (99 x 102 mm)) cut from the same polycarbonate sheet as before.

For specimen no. 1, four gages were installed along the crack line on both the quarter-plane and the mid-plane (the first piece and the second piece) to measure the strain, ε_y, in the direction perpendicular to the crack line. On the three-quarter plane (the third piece), four gages were installed to measure the strain ε_x in the direction parallel to the crack line. Then, all four pieces were fastened together with epoxy to make a block. A compact tension

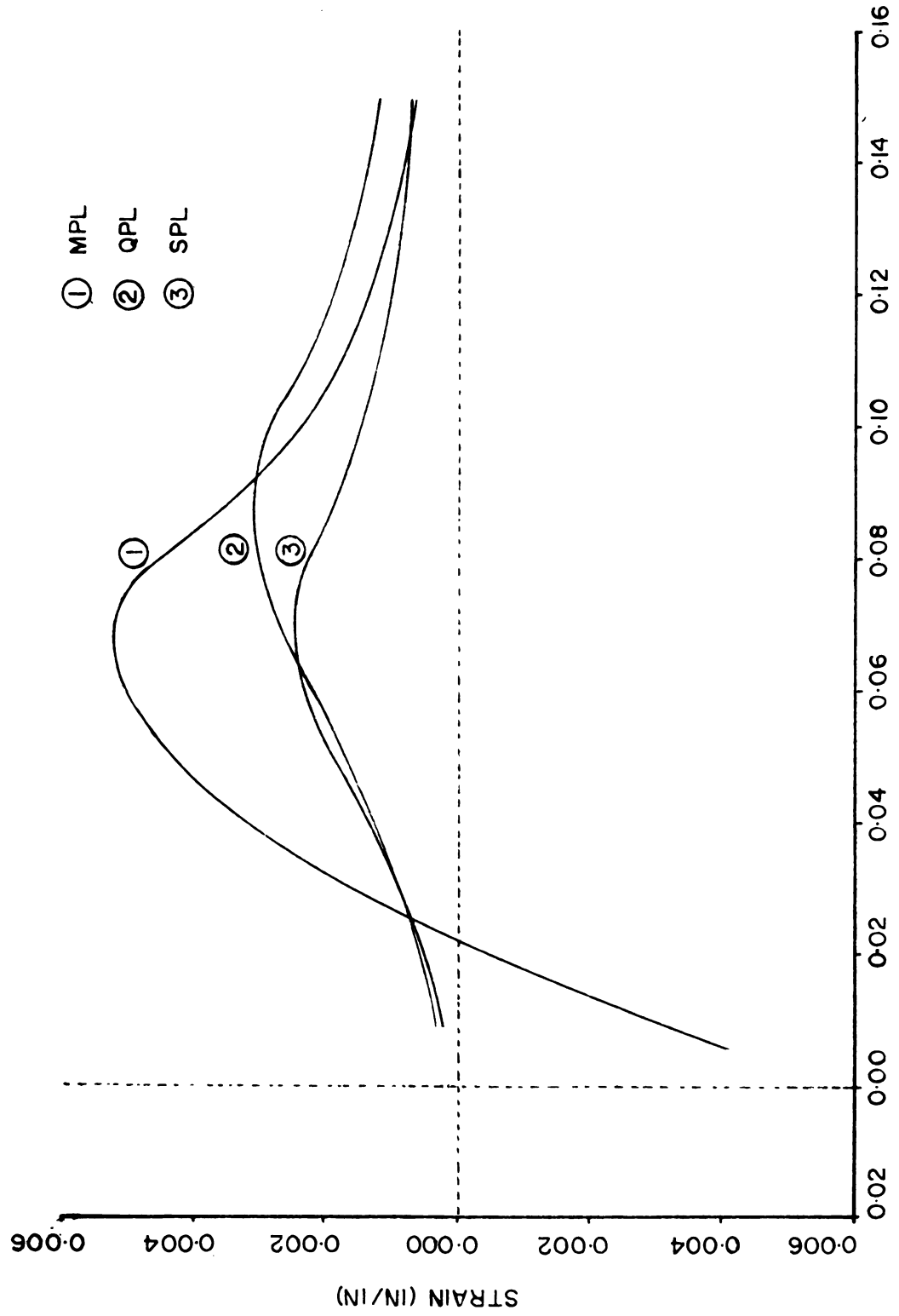

Figure 5.56 A Comparison of the Strain ε_x on the Surface, Quarter and Mid-plane Along the Crack Line.

specimen was made from this block. Finally three gages were installed to measure the strain ε_y on one surface and four gages were installed to measure the strain ε_x on the other surface. All strain gages were installed in front of the crack tip along the crack line. The schematic of the position of the strain gage on each plane is shown in Figure 5.57. The distances between each gage and from the crack tip are shown in Table 5-1a. Strain gage types EA-06-015DJ-120 and EP-08-030LB-120 (Micromeasurements, Inc.) were used to measure strains, ε_y and ε_x, respectively.

The schematic of the position of the strain gages on each plane for specimen No. 2 is shown in Figure 5.58. For this specimen, four strain gages were installed on the quarter-plane and the mid-plane (the first and the second piece) to measure the strain in the direction perpendicular to the crack line, ε_y. On each plane, three gages were installed along the crack line and one gage was installed on the line perpendicular to the crack line near the crack tip as shown in Figure 5.58. Then all four pieces were fastened together with epoxy to make a block. A compact tension specimen was made from this block. Finally, six gages were installed on one surface and three gages were installed on the other surface. The distance between each gage is shown in Table 5.2a. All gages used on this specimen are Micromeasurements type EP-08-015-CK-120.

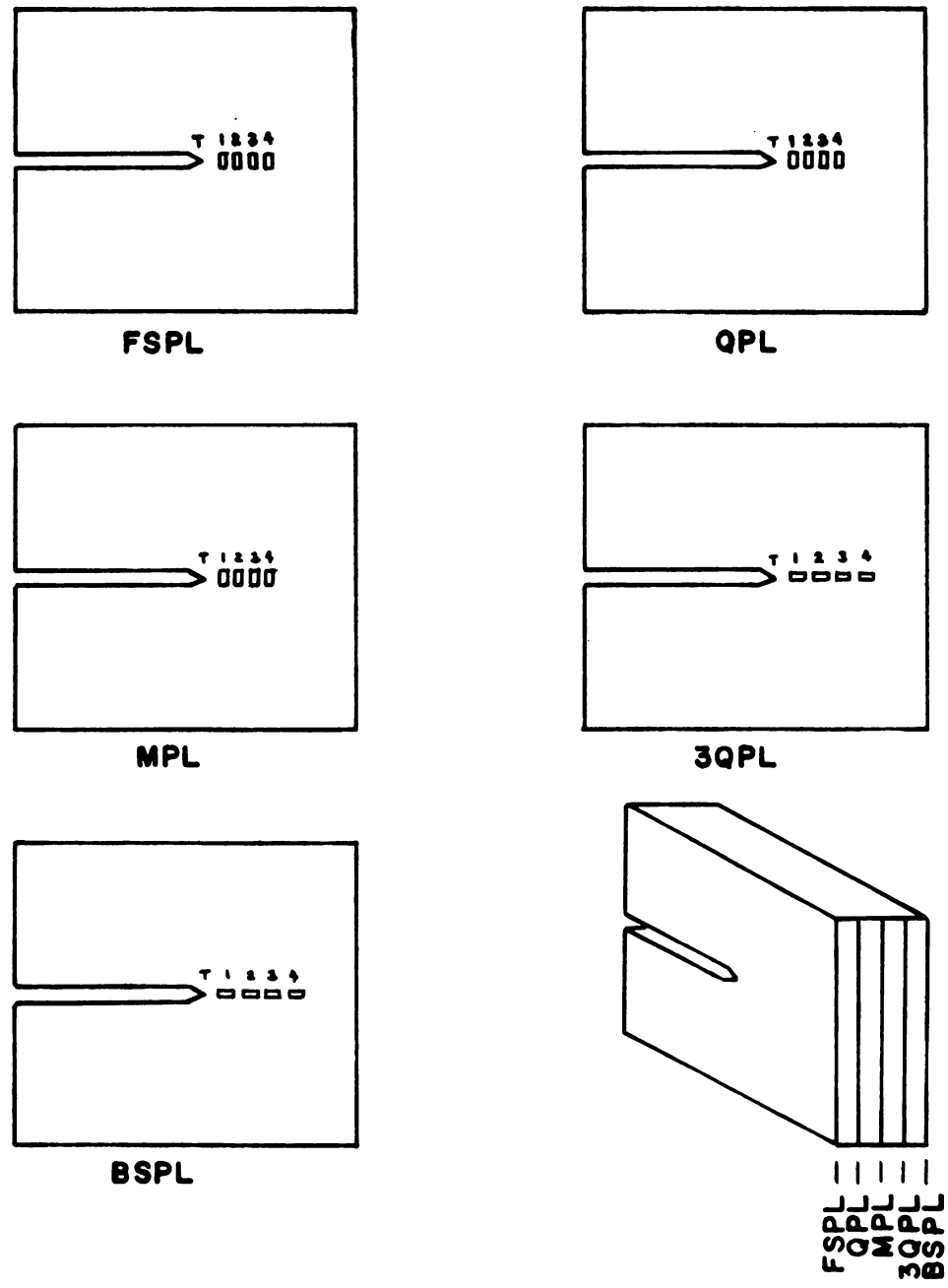

Figure 5.57 Positions of the Strain Gage Installed on Each Plane of Specimen No. 1.

NOTE: FSPL = Front Surface Plane; QPL = Quarter Plane, MPL = Mid Plane; 3QPL = Three-Quarter Plane; BSPL = Back Surface Plane; T = Crack Tip; E = The End of the Specimen Width.

Table 5.1a The Position of Strain Gages on Specimen No. 1.

Gage Position	DISTANCE (IN)				
	FSPL	QPL	MPL	3QPL	BSPL
T-1	0.09	0.06	0.09	0.03	0.03
1-2	0.20	0.20	0.20	0.15	0.15
2-3	0.20	0.20	0.20	0.15	0.15
3-4	-	0.20	0.20	0.15	0.15

Table 5.1b The Strain Results From Specimen No. 1.

Gage Number	STRAIN (IN/IN)				
	FSPL	QPL	MPL	3QPL	BSPL
1	0.00091	0.00210	0.00197	0.00129	0.00092
2	0.00020	0.00053	0.00065	0.00129	0.00111
3	-0.00024	0.00014	0.00011	0.00096	0.00082
4	-	-0.00029	....	0.00065	0.00065

Note: - Means strain gage was not installed on that plane.
.... Means strain gage does not work.

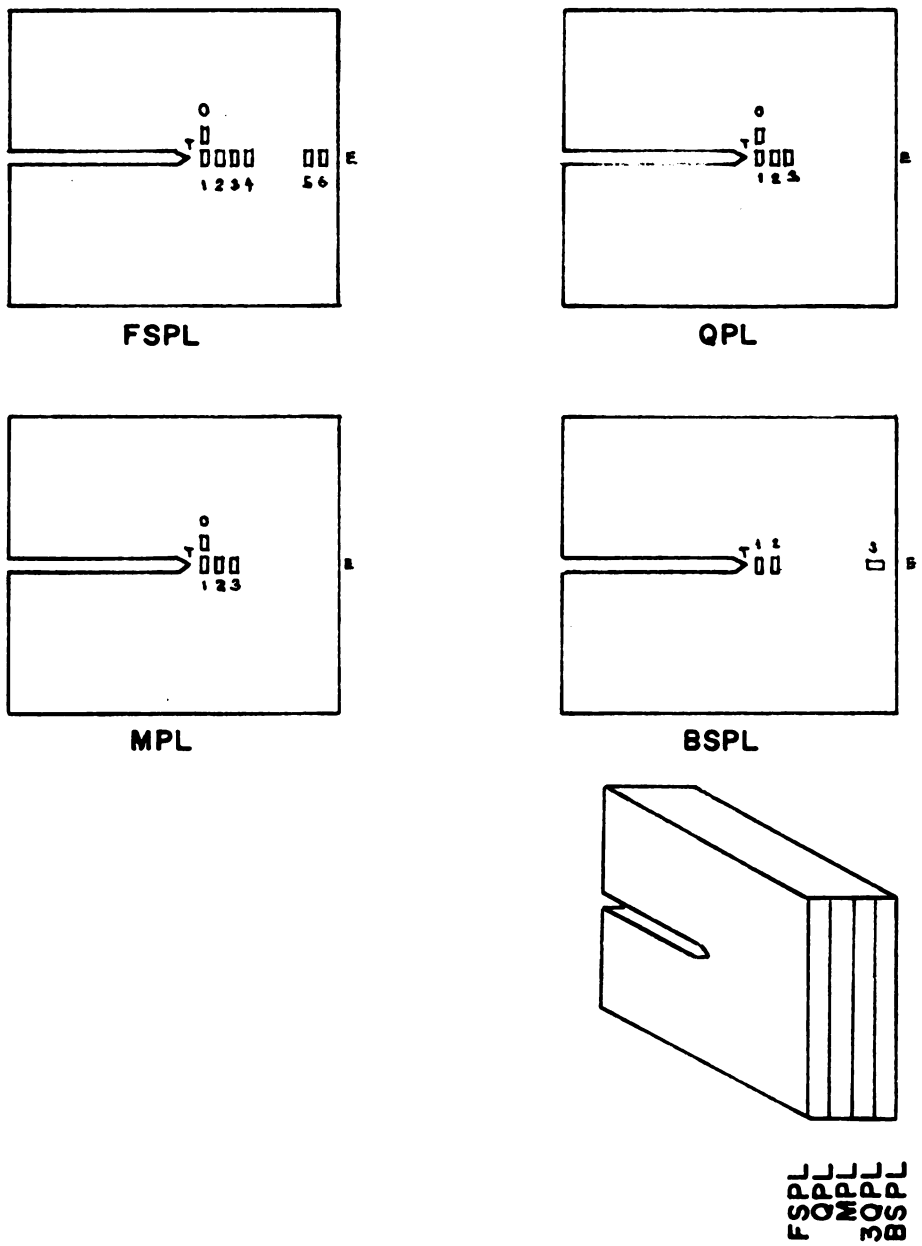

Figure 5.58 Positions of the Strain Gage Installed on Each Plane of Specimen No. 2.

NOTE: FSPL = Front Surface Plane; QPL = Quarter Plane; MPL = Mid Plane; 3QPL = Three-Quarter Plane; BSPL = Back Surface Plane; T = Crack Tip; E = The End of the Specimen Width.

Table 5.2a Position of Strain Gages on Specimen No. 2

Gage Position	DISTANCE (IN)			
	FSPL	QPL	MPL	BSPL
0-1	0.065	0.054	0.054	-
T-1	0.067	0.058	0.050	0.038
1-2	0.124	0.102	0.114	0.120
2-3	0.118	0.098	0.126	1.164
3-4	0.140	-	-	-
4-5	0.906	-	-	-
5-6	0.114	-	-	-
6-E	0.061	-	-	-
3-E	-	1.272	1.240	0.208

Table 5.2b Strain Results From Specimen No. 2

Gage Position	STRAIN (IN/IN)			
	FSPL	QPL	MPL	BSPL
0	0.00264	....	0.00283	-
1	0.00079	0.00191	0.00315	0.00132
2	0.00022	0.00072	....	0.00038
3	0.00003	....	0.00052	0.00058*
4	-0.00010	-	-	-
5	-0.00100	-	-	-
6	-0.00138	-	-	-

* The strain values of ε_x.

The differences between these two specimens are:

i) On specimen no. 1 all gages were installed to measure the strain along the crack line only, but on specimen no. 2 gage no. 0 was installed to measure the strain ε_y near the crack tip but not on the crack line (see Figure 5.58).

ii) On specimen no. 1 all gages were installed to measure strain near the crack tip only, but on specimen no. 2 two gages (gage no. 5 and no. 6) were installed to measure the strain ε_y near the end of the width of the specimen on one surface. On the other surface, one gage (gage no. 3) was installed to measure the strain ε_x near the end of the width of the specimen (see Figure 5.58).

The dimensions of the compact tension specimen with the strain gages are the same as those of the test specimens with the gratings. The set-up of the specimen with the strain gage is the same as before except that no light source and no camera were used. Each gage was connected to a VISHAY 1011 (Vishay Instruments, Inc.) portable strain indicator A photograph of specimen set up is shown in Figure 5.59. Each specimen was loaded in tension to 1.3 ksi (9.10 MPa) the same as the specimen with the grating. The strain results on each plane were obtained from the strain indicators. The strain results from all gages on specimen no. 1 and no. 2 are shown in Table 5.1b and 5.2b, respectively. The plots of ε_y on each plane are shown in Figure 5.60.

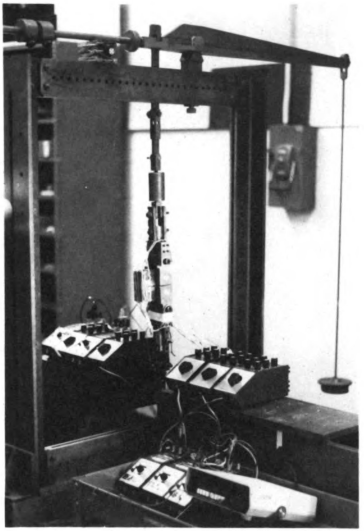

Figure 5.59 Overall View of the Specimen Set Up.

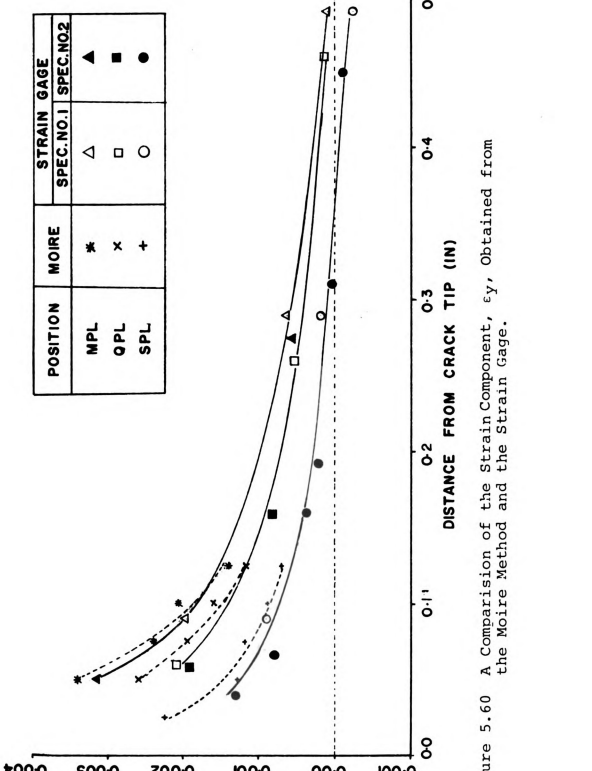

Figure 5.60 A Comparision of the Strain Component, ε_y, Obtained from the Moire Method and the Strain Gage.

The results show that close to the crack tip, the strains ε_y in the interior and on the surface are very large tensile strains when compared with those at a distance farther away from the tip. A high strain gradient occurred near the crack tip. The strain ε_y is a maximum on the mid-plane and decreases to a minimum on the surface plane. On the quarter-plane, strain ε_y changed to a compressive strain at about 0.55 in. (14 mm) from the crack tip. On the mid-plane, gage no. 4 did not work, but it seemed that the strain ε_y changed to a compressive strain somewhere between 0.5 in. to 0.6 in. (12.7 mm to 15.2 mm). On the surface plane, large tensile strain occurred near the crack tip then decreased and became a compressive strain at about 0.375 in. (9.5 mm) from the crack tip until the end of the width of specimen.

As pointed out by Irwin, Tada and Paris (43) applied stress on a compact tension specimen has both tensile and bending components.

From $$K_I = \sigma_N \ (\sqrt{W-a}) \quad F(\frac{a}{W}, \frac{h}{W}, \frac{d}{W})$$

where $$\sigma_N = \sigma_{N_{(\text{tension})}} + \sigma_{N_{(\text{bending})}}$$

$$= \frac{P}{W-a} + \frac{6P(a+(W-a)/2)}{(W-a)^2}$$

if $W = 2a$

$$\sigma_N = \frac{P}{a} + 9\frac{P}{a}$$

Because the bending stress is much larger than the pure tensile stress, the bending stress causes the compressive strain from the end of the width of the specimen. Tensile strain near the crack tip was caused by both applied tensile stress and bending stress.

The strain plot of ε_x is shown in Figure 5.61. From Table 5.1a, strain ε_x on gage no. 1 is slightly smaller than strain ε_x on gage no. 2. Therefore, tensile strain ε_x increased with distance from the crack tip and the maximum strain occurred somewhere between gage no. 1 and gage no. 2. It then slightly decreased until the end of the width of specimen. The strain plots of ε_x and ε_y on the surface plane from the crack tip to the end of the width of the specimen along the crack line are shown in Figure 5.62. The results show that the strain ε_y is tensile strain in only a small area near the crack tip, but ε_x is tensile strain from near the crack tip to the end of the width of specimen. Strain ε_x close to the crack tip is much smaller than ε_y, therefore, strain ε_y is more important than ε_x in studying deformation in front of the crack tip.

From Table 5.2b the strain ε_y of gage no. 0 on the surface plane is larger than that of gage no. 1 that lies on the crack line. Because the maximum strain ε_y on the surface-plane did not lie along the crack line, there were two symmetrically located strain peaks above and below the crack line. This result is consistent with the result obtained from the moire method. On the mid-plane, the

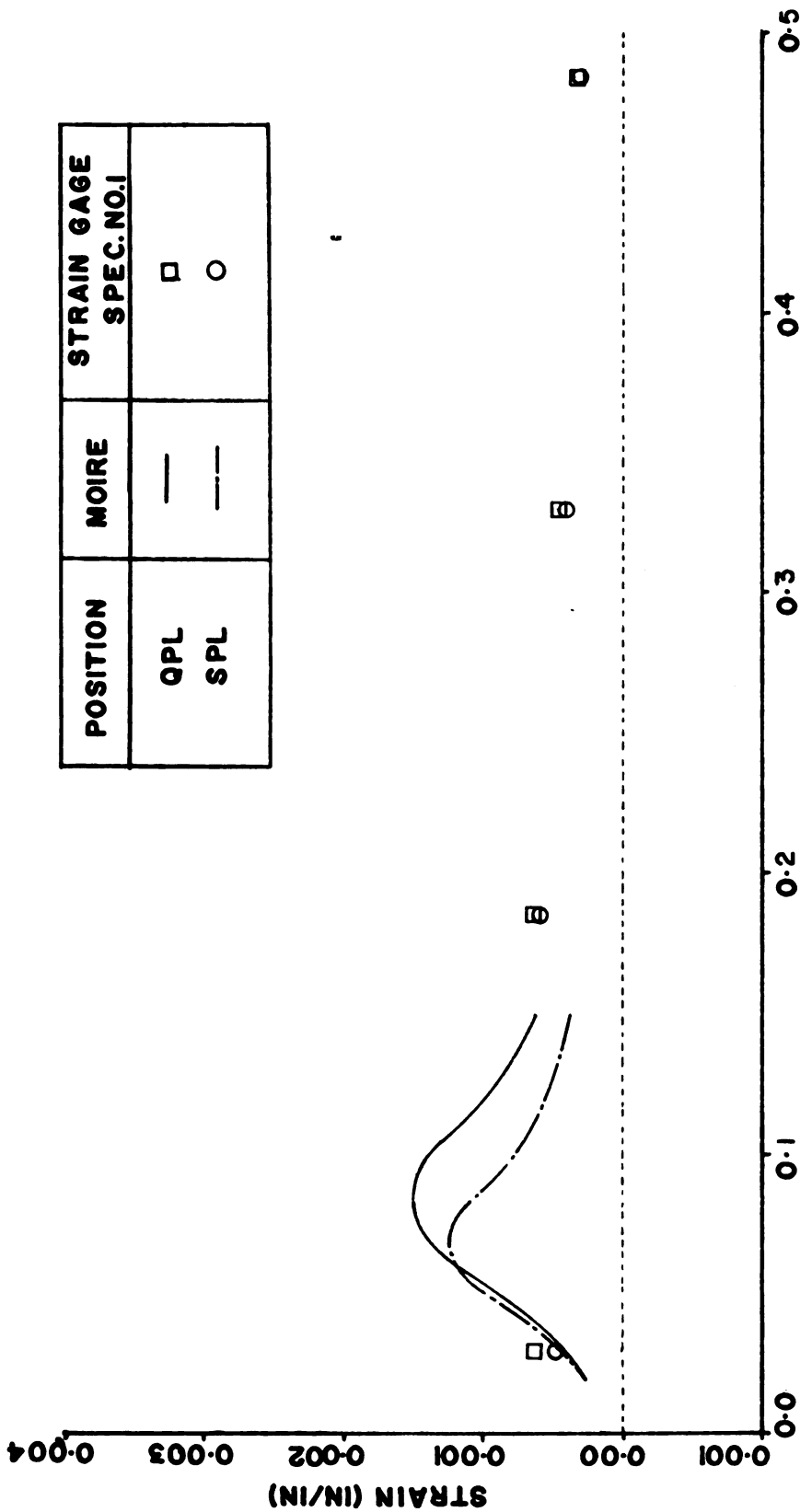

Figure 5.61 A Comparison of the Strain Component, ε_x, that Obtained from the Moire Method and the Strain Gage.

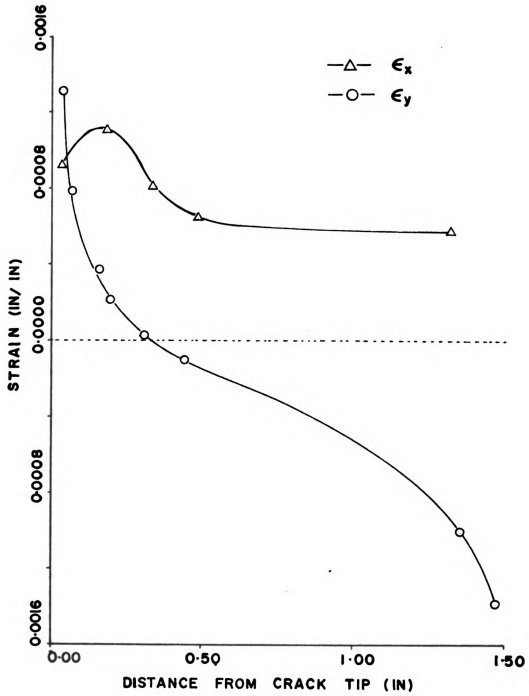

Figure 5.62 The Plot of ε_x and ε_y From the Crack Tip to the End of the Width on the Surface Plane of the Specimen with the Strain Gages.

resultant strain on gage no. 0 (at 0.054 in. (1.37 mm) from the crack tip, see Figure 5.58 and Table 5.2a) is about 7% smaller than that of gage no. 1 on the crack line. Therefore the peak of maximum strain in the interior lies on the crack line. This result is again consistent with the result obtained from the moire method, but the strain difference of these two positions obtained from the moire method is about 60%. The strain ε_y obtained from gage no. 0 on the mid-plane is about 50% larger than that obtained from the moire method at the same position because the correction strain from the moire method is accurate only on the area close to the crack line (within 0.02 in (0.51 mm) from the crack line). At a distance farther away from the crack line, the result is not quite as good because the curve of the strain error does not satisfy the equation ($\Delta\varepsilon = \delta x^2$) that is used for correcting the interior strain (as shown in Figure 5.38). More data would be needed to get a good-fitting curve for each line. Many specimens would be required to get an equation for the curve of the strain error along the thickness for each point. The purpose of this research, however, is to study the strain close to the crack tip that causes severe deformation. The result then shows that in the interior of the specimen, the maximum strain occurred along the crack line. Because we are only concerned with the analysis of the strain along the crack line near the crack tip, it is not necessary to make more specimens to get better results for the area away from the crack line.

The measurements of strain ε_y from the strain gages on the surface-plane, the quarter-plane and the mid-plane were compared with those values obtained from the moire method (see Figure 5.60). The moire method gives good results only from 0.025 in. (0.635 mm) on the surface plane and 0.05 in (1.27 mm) on the quarter and mid-planes to 0.125 in (3.175 mm) away from the crack tip. The strain values from the moire method are slightly higher (about 1%) than those from the strain gage, but the two methods agree quite well.

The measurements of the strain ε_x obtained from the strain gages on the surface-plane and the quarter-plane were also compared with the moire method measurements (see Figure 5.61). The results show that, for both methods, the magnitude of the strain ε_x on the quarter-plane is slightly higher than on surface-plane. The results obtained from strain gage can not give a good strain plot near the crack tip along the crack line because the distance between the gages is too large. Only the results from the first gage from both the quarter-plane and the mid-plane were compared with the strain from the moire method. The magnitude of the strain gage value is in a good agreement with that of the moire method.

5.5 Discussions

In this investigation, strain deformation was studied close to the crack tip along the thickness of a polycarbonate crack specimen. Experimental results are compared with

available theory. From the theory of linear elastic fracture mechanics and the stress-strain relation as described in Section 5.1.2, the strain ε_y on the surface is predicted to be larger than on the mid-plane. The strain measurements from the moire method are found to be in disagreement with the theory of linear elastic fracture mechanics because, in almost every case, higher strain was measured near the crack tip in the interior, even though only a small load was applied to the specimen.

Vincent (41) suggested that in some cases such as for the fracture of notched specimens of isotropic polyestyrene at room temperature, the zone of plastic deformation is small. It is possible, then, to calculate stress distributions and to derive the stress intensity factor assuming linear material behavior. On the other hand, in many practical cases, the size of the zone of plastic deformation is not negligible and theories based on the assumption of Hooke's law can be in significant disagreement with experimental values (42). Liu (33) pointed out that when the plastic zone size is small the elastic relationships may no longer be valid, but unique relationships between the stress intensity factor, stress and strain do exist. It follows, then, that the theory of linear elastic fracture mechanics cannot be applied in this case. Several researchers (74, 75, 76, 77) have now determined the variation of the stress intensity factors along a straight crack in the

standard compact tension specimen defined in ASTM E 399-74 by using elastic three-dimensional finite element programs. All of their results show that the stress intensity factor is a maximum at the center of the specimen and a minimum at the surface. For the same condition, Schroedl and Smith (50) used photoelasticity techniques to study the stress intensity variation between the full thickness and a center slice of a compact tension specimen made from PLM-4B. In the center slice, K_I was found to be 5 to 10% higher than average through the thickness. From these results and the relation between local stress and the stress intensity factor, the stress on the mid-plane is shown to be larger than on the surface plane. Experimental study of the deformation at the crack tip on the surface plane and the mid-plane of specimens made of steel were carried out by Lequear and Lubahn (48) and by Robinson and Tetleman (49). Lequear and Lubahn found that the radius of curvature of the notch in the bent specimen was greater at the specimen mid-section than at the outside. Robinson and Tetleman measured crack tip opening displacement at the tip of bent specimens by using the rubber infiltration technique. A low alloy pressure vessel steel, A533B, was used to make the specimen (0.394 in thick). The technique consisted of filling the crack or notch with a catalytically hardening silicone rubber. After the rubber had hardened, the casting was removed and examined in the scanning electron microscope. They found the crack opening displacement at the tip on the

mid-section of the specimen to be larger than on the surface. Considering all of these results, because the stress intensity factor (K_1), stress (σ_y) and crack tip opening displacement (CTOD) on the mid-plane are larger than on the surface plane, and because fracture initiates at the mid-plane, then the deformation on mid-plane near the crack tip should be larger than on the surface plane. Thus, strain on the mid-plane along the crack line near the crack tip must be larger than on the surface. The reason why strain ε_y in the interior near the crack tip along the crack line is larger than on the surface was thought to be that, while the specimen was loaded, the contraction strain occurrs near the crack tip on the surface of the specimen. The contraction strain increases while increasing the load. This effect causes reduction of the crack tip opening displacement and ε_y near the crack tip on the surface plane. In the mid-plane, however, the transverse strain is zero. No contraction affects the mid-plane, and the crack tip opens easier than on the surface. At the same time, no strain reduction occurs on the mid-plane. Therefore strain deformation on the mid-plane is larger than on the surface, and it causes fracture initiation on the mid-plane.

The elastic solution (Boyd (72)) predicted that, <u>at the crack tip</u> ($r \approx 0$), $\sigma_x = 0$ and σ_y on the mid-plane is larger than σ_y on the surface. This prediction agrees with the experimental result reported by Martoff, Leven, Ringler and Johnson (73). It is possible to have σ_y on the

mid-plane larger than ε_y on the surface plane right at the crack tip.

For $r < 0$, that is, within a small but finite region near the crack tip, Irwin (78) and Cotterel and Rice (79) suggested that,

$$\sigma_y\ (r,0) = \frac{K_I}{\sqrt{2\pi r}} + 0\ (r^{\frac{1}{2}})$$

$$\sigma_x\ (r,0) = \frac{K_I}{\sqrt{2\pi r}} - \sigma_{ox} + 0(r^{\frac{1}{2}}) \qquad (5.7)$$

The added term, σ_{ox}, corresponds to local stress acting parallel to the crack center at its tip. $0(r^{\frac{1}{2}})$ are higher order terms which customarily are assumed to be negligible

If eq. (5.7) is substituted into eq. (5.3) (page 107) one obtains

$$\varepsilon_y\ (r,o) = \frac{1}{E}\left[(1-\nu)\ \frac{K_I}{\sqrt{2\pi r}} + \nu\sigma_{ox}\right] \text{ for plane stress}$$

$$\varepsilon_y\ (r,0) = \frac{1}{E}\left[(1-\nu-2\nu^2)\ \left(\frac{K_I}{\sqrt{2\pi r}}\right) + \nu(1+\nu)\ \sigma_{ox}\right] \text{ for plane strain}$$

For the material used in this study, $\nu = 0.45$. For the thick specimens used it is assumed that the surface-plane is in a state of plane stress, and the mid-plane is in plane strain. If K_I on the mid-plane is larger than on the surface-plane, and if σ_{ox} is a large value, then it is possible to have ε_y on the mid-plane larger than on the surface plane for $r > 0$. It follows that the strain ε_y along the crack line on the mid-plane must be larger than

ε_y on the surface-plane. This conclusion is supported by the results obtained in this study. The σ_{ox} seems to be an important factor for the conditions of this investigation.

5.6 Summary of Strain Field in Thick Compact Tension Specimens

The embedded grid moire method was used to measure the strain near the crack tip on the surface and in the interior of a compact tension specimen that was made of polycarbonate. Strain error was found in the interior resulting from the fact that the specimen thickness changed and its index of refraction changed near the crack tip. The results obtained from the moire method in the interior of the compact tension specimens were not real strain. Other specimens were made and studied correct these interior results. Finally, compact tension speciemns with internal and external strain gages were made. The results of the strain plots from the crack tip along the crack line for both ε_x and ε_y on the surface and in the interior from the strain gage and the moire method were compared and found to be in good agreement.

Near the crack tip the strain gradient of ε_y is high. This strain near the crack tip is tensile strain which decreases and changes to a compressive strain at some distance from the crack tip. The maximum compressive strain occurs at the end of the specimen width. On the mid-plane the strain ε_x is compressive strain at the crack tip. It increases to a maximum tensile strain at about 0.07 in.

(1.8mm) from the crack tip, then decreases until the end of the specimen width. Strains ε_x on the quarter-plane and on the surface-plane are tensile strain from the crack tip to the end of the width. ε_x on the quarter-plane and on the surface-plane increases from the crack tip to a maximum at about 0.09 and 0.07 in. (2.3 and 1.8 mm) from the crack tip, then slightly decreases until the end of the specimen width. Near the crack tip, tensile strain ε_y is much larger than ε_x, and therefore, the strain value ε_y is more important than ε_x. The severe deformation near the crack tip is due to strain ε_y.

Near the crack tip maximum tensile strain ε_y occurs on the mid-plane and decreases to a minimum on the surface-plane. Therefore, the crack front will grow on the mid-plane first, then extend to the surface-plane. In the interior, the maximum strain ε_y starts out from the crack tip and lies on the crack-plane, but on the surface, maximum ε_y splits and lies along two lines radiating from the crack tip.

CHAPTER 6

CONCLUSIONS

In this study, the embedded grid moire method was developed. The specimen gratings in the interior and on the surface formed moire fringe patterns of comparable quality. This successful technique was successfully employed to measure the strain in the interior of coldworked specimens and compact tension specimens. Two types of transparent material, 60:40 of flexible-rigid polyester resins and polycarbonate, were used to make the specimens. Strain gages were used to measure the strain in the compact tension specimen. The results were compared with the moire method and found to be in good agreement.

First, the strain around the coldworked specimen was studied. Radial strain, transverse strain and hoop strain were measured by using the embedded grid moire method. Good results were obtained by this method. The strain was different along the thickness depending on the thickness of specimen and the shape of the mandrel while the specimen was being coldworked. The strain was not uniform along the thickness and the strain measurements on both sides were not quite the same. The strain in the radial direction

inside the specimen was smaller than on the surface after the specimen was coldworked. The maximum strain occurred near the edge of the hole and decreased with distance from the hole. The strain in the z-direction, or transverse strain, was tension near the top surface and changed to compression along the thickness; the maximum occured near the mid-plane and it decreased towards the bottom. After passing through a minimum, the transverse strain increased in compression again near the bottom (about 0.08 in (2 mm) from the bottom). The hoop strain was maximum on the top surface and decreased slightly to the minimum at mid-plane. The change in this component is only about four percent of maximum value. It then appeared to increase toward the bottom surface.

Second, the compact tension specimens that were made of polycarbonate with the gratings on the surface and in the interior were studied. The moire method was used to measure the strain around the crack tip on the surface and in the interior. Good results were obtained directly on the surface plane. The interior results were corrected by making one specimen with gratings on the quarter-plane only to provide data for a new correction procedure. Two polycarbonate compact tension specimens with strain gages were made to validate the results obtained from the moire method. The strain measurements near the crack tip along the crack line from both methods are in good agreement. The strain gradient of ε_y is very high near the crack tip. Strain ε_y was tensile in only a small area near the crack tip, then changed to a

compressive strain at a distance father away from the crack tip. The characteristics of the plot of ε_x along the crack line from the crack tip are the same for both types of test specimens (the specimen with the grating and the specimen with the strain gages) on the surface and in the interior. Close to the crack tip, strain ε_y along the specimen thickness was maximum on the mid-plane and decreased to a minimum on the surface plane. ε_x on the quarter-plane and on the surface-plane was small tension at the crack tip. It increased to a maximum and then decreased at distances further away from the crack tip. On the mid-plane the strain ε_x was a compressive strain at the crack tip and increased to become the overall maximum tensile strain at about 0.07 in. (1.8 mm) from the crack tip. It decreased, like ε_x, on the quarter-plane, with distance from the crack tip. In this investigation, at the crack tip, ε_y was much greater than ε_x on both the surface and the interior planes. The severe deformation at the crack tip will, therefore, be caused primarily by the strain ε_y. It is possible, then, to start fracture at the mid-plane while loading in tension, because a larger strain occurs on the mid-plane.

It is not possible to present here a complete analysis of the three-dimensional strain around the crack tip. It is important to briefly mention, though, some basic observations made in using the embedded grid moire method in the study of interior displacement and strain. The experimental

measurement by the embedded grid moire method of the internal strain in the transparent compact tension specimen of the area around the crack tip was found to be in very serious error due to the non-uniformity of the index of refraction caused by a craze zone (high strain gradient) and because the thickness changed around the crack tip. In such instances, the embedded grid appeared better suited to measure the development of the dilatation near the crack tip rather than to measure the occurring strains and displacements. For the study of coldworking, on the other hand, no correction was necessary. Most of the resultant strain from the coldworked specimen was found to be compressive strain (the craze zone does not form by compressive strain) and the specimen that was used to measure hoop strain is a lot thinner than compact tension specimen. No serious error was found in the coldworked specimen. It is shown that in some cases, however, static problems can be very seriously in error. In order to gain confidence in such techniques, further experimentation with known theoretical solutions is needed.

One physical phenomenon observed during the experimental measurement of the strain around the crack tip on the surface and in the interior of the compact tension specimen was a crack tip opening displacement in the interior of the specimen. It was thought that the crack tip opening displacement measurement in the interior could be obtained by using the moire technique as has been done on the

surface (44). The results illustrated in Figure 5.16.1, however, show that the grating record could not give good enough fringes for the interior immediately behind and ahead of the crack tip. Because of an optical problem, while the compact tension specimen was loaded diffusion occurred at the crack tip in the interior, the density was changed, the thickness was changed, and thus the index of refraction changed. Consequently, the moire fringe pattern in the immediate vicinity of the crack tip in the interior cannot be used for measuring crack tip opening displacement. At this time, there is no technique to correct this problem. It follows that the crack tip opening displacement in the interior cannot be measured by this technique. It seems possible, however, the interior crack tip openind displacement could be measured by the embedded grid moire method provided that one can find a transparent material that will not change its index of refraction at the crack tip during specimen loading.

REFERENCES

REFERENCES

1. Post, D., "The Moire Grid Analyzer Method for Strain Analysis", Exp. Mechs. 5 (11), 368-377 (1965).

2. Durelli and Daniel, "A Nondestructive Three-Dimensional Strain Analysis Method", J. of Appl. Mech., 83-86 (March 1961).

3. Sciammarella, C. A., and Fu-pen Chiang, "The Moire Method Applied to Three-Dimensional Elastic Problem", Exp. Mechs., 4, 11, 313-319 (Nov. 1964).

4. Gran, R. J., Orazio, F. D., Paris, P. C., Irwin, G. R., and Hertzberg, R., "Investigation and Analysis Development of Early Life Aircraft Structural Failures", Technical Report AFFDL-TR-70-149, Wright-Patterson AFB, Ohio, March 1971.

5. Adler, W. F., and Dupree, D. M., "Stress Analysis of Coldworked Fastener Holes," AFML-TR-74-44, Air Force Material Laboratory, Wright-Patterson AFB, July 1974.

6. Sharpe, W. N., Jr., "Measurement of Residual Strains Around Coldworked Fastener Holes", Scientific Report, AFOSR Grant 75-28117, Bolling AFB, Washington D. C., April 1976.

7. Chandawanich, N., and Sharpe, W. N., Jr., "An Experimental Study of Crack Initiation and Growth From Coldworked Holes", Proc. 1978 SESA, Spring Meeting, Wichita, Kansas, May 1978.

8. Poolsuk, S., and Sharpe, W. N., Jr., "Measurement of the Elastic-Plastic Boundary Around Coldworked Holes", J. Appl. Mech., Paper 78-WA/APM2.

9. Cloud, G. L., "Residual Surface Strain Distributions Near Holes Which are Coldworked to Variuos Degrees", Technical Report, AFML-TR-78, Wright-Patterson AFB, Ohio, 1978.

10. Cloud, G. L., and Tipton, M., "An Experimental Study of the Interaction of Strain Fields Between Coldworked Fastener Holes," Technical Report AFWAL-TR-80-4205, Wright-Patterson AFB, Ohio, March 1980.

11. Cloud, G. L., and Sulaimana, R., "An Experimental Study of Large Compressive Loads Upon Residual Strain Fields and the Interaction Between Surface Strain Fields Created by Coldworking Fastener Holes," Technical Report AFWAL-TR-80, Wright-Patterson AFB, Ohio, September 1980.

12. Evans, W. T. and Luxmoore, A., "Measurement of In-plane Displacement Around Crack Tips by a Laser Speckle Method", Eng. Fract. Mech. 6, 735-743 (1974).

13. Somer, E., "An Optical Method for Determining the Crack Tip Stress Intensity Factor", Eng. Fract. Mech. 1, 705-718 (1970).

14. Closeley, P. B., Mostovey, S., and Eipling, E. J., "An Optical Method for Experimental Stress Analysis of Crack Structures", Eng. Fract. Mech. 3, 421-433 (1971).

15. Marloff, R. H., Leven, M. M., Ringler, T. N., and Johnson, R. L., "Photoelastic Determination of Stress Intensity Factors", Exp. Mech. 11, 12, 529 (Dec. 1971).

16. Brinson, H. F., "The Ductile Fracture of Anisotropic Materials", Exp. Mech. 12, 12, 557 (Dec. 1972).

17. Villarreal, G., Sih, G. C., and Hartranjt, R. J., "Photoelastic Investigation of a Thick Plate with a Transverse Crack", J. Appl. Mech. 42, 1, 9 (Mar. 1975).

18. Mills, N. J., "Dugdale Yielded Zones in Cracked Sheets of Glassy Polymers", Eng. Fract. Mech. 6, 537-549 (1974).

19. Post, D., "Photoelastic Analysis for an Edge Crack in a Tensile Field", Proc. SESA, XII, No. 1, 1954.

20. Barker, D. B., and Fourney, M. E., "Three-Dimensional Interferometric Investigation of the Stress Intensity Factor Along a Crack Front", Eng. Mech. 17, 7, 241-247 (July 1977).

21. Hahn, G. T., and Rosenfield, A. R., "Sources of Fracture Toughness; The Relation Between K_{IC} and the Ordinary Tensile Properties of Metals", ASTM STP 432, 5-32 (1968).

22. Underwood, J. H., and Kandell, D. P., "Measurement of Microscopic Plastic-Strain Distributions in the Region of a Crack Tip", Exp. Mech., 296-304 (July 1969).

23. Pitoniak, F. J., Grandt, A. F., Montulli, L. T., and Packman, P. F., "Fatigue Crack Retardation and Closure in Polymethymetheralate", Eng. Fract. Mech. 6, 663-670 (1974).

24. "An Engineering Handbook on Merlon Polycarbonate", Mobay Chemical Company, Pittsburgh, Pennsylvania.

25. Cloud, G. L., "Mechanical Properties of Polycarbonate Resin and some Relations with Material Structure", Exp. Mech. 9, 11, 489-499 (Nov. 1969).

26. Morris, D. H., and Riley, W. F., "A Photomechanic Material for Elastic Stress Analysis", Exp. Mech. 12, 10, 448-453 (Oct. 1972).

27. Walker, C. A., and McKelvie, J., "The Measurement of Residual Stress by a Moire Fringe Method", SPIE Vol. 136, 1st European Congress on Optics Applied to Metrology (1977).

28. Luxmoore, A. R., and Hermann, R., "The Rapid Deposition of Moire Grids", Exp. Mech. 11, 8, 375-377 (Aug. 1971).

29. Holister, G. S., and Luxmoore, A. R., "The Production of High-Density Moire Grids", Exp. Mech. 8, 5, 210-216 (May 1968).

30. William, M. L., "On the Stress Distribution at the Base of a Stationary Crack", J. Appl. Mech, Vol. 24, No. 1, (1957).

31. Irwin, G. R., "Analysis of Stress and Strain Near the End of a Crack Traversing a Plate", J. Applied Mechanics, Vol. 24, No. 3, (1957).

32. Westergard, H. M., "Bearing Pressure and Cracks", Transactions, Am. Society Mechanical Engrs., J. of Appl. Mech. (1939).

33. Liu, H. W., "Discussion to a Critical Appraisal of Fracture Mechanics", STP 381, ASTM-NASA, 23-26 (1965).

34. Liu, H. W., and Ke, J. S., "The Measurements of Fracture Toughness of Ductile Materials", Engrg. Fract. Mech., 5, 187-202 (1973).

35. Underwood, J. H. and Kendall, D. P., "Measurement of the Strain Distribution in the Region of a Crack", Presented to ASTM Committee E-24, (March 1967).

36. Gerberich, W. W., "Plastic Strains and Energy Density in Crack Plates, Part 1 - Experimental Technique and Results", Exp. Mech., 335-344 (Nov. 1964).

37. Kerber, R. C. and Whittier, J. S., "Moire Interferometry with Embedded Grids-Effect of Optical Refraction" Exp. Mech., (May 1969).

38. Kambour, R. P., "Stress-Strain Behavior of the Craze", Polymer Engineering and Science, Vol. 8, No. 4, 281-289 (Oct. 1968).

39. Hull, D., "The Microstructure and Properties of Crazes", Deformation and Fracture of High Polymers, Edited by Kauch, Hassell, and Jeffee, Plenum Press, pp. 171-189.

40. Kobayashi, A. S., Engstorn, E. L., and Simon, B. R., "Crack Opening Displacements and Normal Strains in Centrally Notched Plates", Exp. Mech. Vol. 9, No. 4, 163-170 (1969).

41. Vincent, P. I., "Ductile Crack Growth in Poly (Ethylene Terephthalate) Film, Polymer, 12, 534-536 (1971).

42. Vincent, P. I., "Load-Extension Curves and Fracture Toughness", Deformation and Fracture of High Polymers, Edited by Kausch, Hassell and Jaffee, Plenum Press, 287-300 (1972).

43. Tada, H., Paris, P., and Irwin, G., "The Stress Analysis of Crack Handbook", Del Research Corporation, Hellertown, Pennsylvania.

44. Luxmoore, A., and Wyatt, P. J., "Application of the Moire Technique to Fracture-Toughness Tests on Zirconium Alloys", J. of Strain Analysis, (Oct. 1970).

45. Polymer Fracture, Edited by H. H. Kauseh, Springer-Verlag Berlin Heidelberg, Germany, (1978).

46. Fatigue of Engineering Plastics, Edited by R. W. Hertzberg and J. A. Manson, Academic Press, (1980).

47. Hahn, G. T., Sarate, M. and Rosenfield, A. R., "Plastic Zones in Fe-3Si Steel Double Cantilever-Beam Specimens", Int. J. of Fract. Mech., 7, 435-446 (1971).

48. Lequear, H. A., and Lubahn, J. D., "Root Conditions in a V-Notch Charpy Impact Specimen", Weld. Res. Suppl., 33, pp. 585-S to 588-S, (1954).

49. Robinson, J. N. and Tetelman, A. S., "The Relationship Between Crack Tip Opening Displacement, Local Strain and Specimen Geometry", Int. J. of Fracture, 11, 453-468 (1975).

50. Schroedl, M. A. and Smith, C. W., "Influence of Three-Dimensional Effect on the Stress Intensity Factors for Compact Tension Specimen", Fract. Anal. ASTM STP 560, 64-80 (1974).

51. Theory of Flow and Fracture of Solids", Edited by A. Nadai, McGraw-Hill Book Company, Inc. 1950.

52. Plasticity, Edited by A. Nadai, McGraw-Hill Book Company, Inc. 1931.

53. Theory of Plasticity, Edited by O. Hoffman and G. Sachs, McGraw-Hill Book Company, Inc. 1953.

54. Fracture Process in Polymeric Solid, Edited by B. Rosen, Interscience Publishers, John Wiley and Sons, Inc., 1964.

55. Fracture and Fatigue Control in Structures, Edited by S. T. Rolfe and J. M. Barsom, Prentice-Hall, Inc., 1977.

56. Fracture of Structural Materials, Edited by A. S. Tetelman and A. J. McEvily, Jr., John Wiley and Sons, Inc. 1967).

57. Deformation and Fracture Mechanics of Engineering Materials, Edited by R. W. Hertzberg, John Wiley and Sons, 1976.

58. The Physics of Glassy Polymers, Edited by R. N. Haward, Applied Science Publishers, Ltd. 1973.

59. Elementary Engineering Fracture Mechanics, Edited by David Broek, Sijthoff and Noordhoff, International Publishers B. V., 1978.

60. Experimental Techniques in Fracture Mechanics, 2, Edited by A. S. Kobayashi, The Iowa Stress Press, SESA, 1975.

61. Numerical Methods in Fracture Mechanics, Edited by A. R. Luxmoore and D. R. J. Owen, Proceedings of the First International Conference held at the University of College Swansea, Swansea SA2 8PP, West Glamorgan, U.K. (Jan. 1978).

62. Experimental Stress Analysis, Edited by J. W. Dally and W. F. Riley, McGraw-Hill Book Company, Inc., (1978).

63. Kambour, R. P., "A Review of Crazing and Fracture in Thermoplastics", Macromolecular Reviews, Vol. 7, J. of Polymer Science, Edited by A. Peterlin, John Wiley and Sons, pp. 1-154 (1973).

64. Moire Fringes in Strain Analysis, edited by P. S. Theoearis, Pergamon Press (1969).

65. Cloud, G. L., "Simple Optical Processing of Moire Grating Photographs", Experimental Mechanics, V. 20, No. 8 (August 1980).

66. Irwin, G. R., "Plastic Zone Near a Crack and Fracture Mechanics", Seventh Sagamore Ordnance Material Research Conference, (1960).

67. Fundamentals of Fracture Mechanics, edited by J. F. Knott, John Wiley and Sons, 1973.

68. Liu, H. W., "Analysis of Fatigue Crack Propagation", NASA Contract Report, NASA CR-2032, National Aeronautics and Space Administration Washington, D. C., May (1972).

69. G. T. Hahn and A. R. Rosenfield, Acta. Met., 13, p. 293 (1965).

70. Sharpe, W. N., Jr., and Paleebut, S., "An Experimental Study of Dugdale Model", the Fifth International Conference on Fracture ICFS at Cannes (France), March 1981.

71. Dally, J. W., and Mulc, A., "Polycarbonate as a Model Material for Three-Dimensional Photoplasticity", Transaction of the ASME, J. of Applied Mechanics, 600-605 (June 1973).

72. Boyd, G. M., "From Griffith to COD and Beyond", Engineering Fracture Mechanics, 172, Vol. 4, pp. 459-482.

73. Marloff, R. H., Leven, M. M., Ringler, T. N., and Johnson, R. L., "Photoelastic Determination of Stress-intensity Factors", Experimental Mechanics, pp. 529-539 (Dec. 1971).

74. Tracey, D. M., "Three-Dimensional Elastic Crack Analysis," Nucl. Eng. and Design, Vol. 26, No. 2, pp. 282-290, 1974.

75. Reynen, J., "On the Use of Finite Elements in Fracture Analysis of Pressure Vessel Components," Trans. ASME J. Press. Vess. Tech., No-75-PVP-20, pp. 1-9, 1975.

76. Raju, I. S. and Newman, J. C., "Three-Dimensional Finite Element Analysis of Finite Thickness Fracture Specimens. NASA Technical Note, No. NASA TN D-8414, 1977.

77. Neale, B. K., "The Stress Intensity Factors Associated with Curve Crack Fronts in a Compact Tension Specimen." Numerical Methods in Fracture Mechanics, edited by A. R. Luxmoore and D. R. J. Owen, Proceedings of the First International Conference held at the University of College Swansea, Swansea SA2 8PP, West Glamorgan, U. K. (Jan. 1978).

78. Irwin, G. R., "Analysis of Stresses and Strains Near the End of a Crack Traversing a Plate," J. of Appl. Mechs. (Sept. 1957), pp. 361-364.

79. Cotterell, B. and Rice, J. R., "Slightly Curved or Kinked Cracks," Int. J. of Fracture, 16 (1980) 155-169.

APPENDIX

Computer Program and Subroutines

```
      PROGRAM MOIRE (INPUT, OUTPUT=65)

C
C
      COMMON /INTP/ YINT(101.2)
      COMMON /DIFY/ YDIF(101)DY(100)
      COMMON /STNAM/ ISTNAM(9),IST
      COMMON /PLOTER/ XRAY(900),YRAY(900),INUM
      COMMON X(80,2),Y(80,2)NPTS(2),XPL(101),XL,XJ,YL,YH,XMIN,
     1       XMAX
      REAL M
      LOGICAL FIN
C
      FIN=.FALSE.
      IC=0
      INUM=0
C
C ---ENTER RUN DATA
C
100   IC=IC+1
      CALL READIN(P,M,C,XO,IPR,FIN)
      IF (FIN) GO TO 1000
      ISET=ISTNAM(IST)
C
C ---DETERMINE X-RANGE FOR INTERPOLATION & DELTA VALUE
C
      CALL RANGE(DEL)
C
C ---COMPUT INTERPOLATED "SMOOTH" CURVES THRU DATA & BASE SETS
C
      CALL INTERP(DEL)
C
C ---PLOT INPUT & SMOOTHED DATA
C
      CALL PLOTM(1,ISET)
C
C ---COMPUTE CURVE DIFFERENCE & DERIVATIVES
C
      PMC=P*M*C
      CALL DIFF(PMC,DEL)
C
C ___CORRECT ABSCISSA ARRAY
C
      CALL CORRECT (XO)
C
C ---PLOT DIFFERENCE CURVE
C
      CALL PLOTM(2,ISET)
C
C ---PLOT STRAIN CURVE
C
      CALL PLOTM(3,ISET)
```

```
C
C ---PRINT OUTPUT IF DESIRED
C
      IF(IPR.NE.1) GOTO 100
      CALL WRITEOUT(IC,DEL)
      GO TO 100
1000 CONTINUE
      STOP
      END
```

```
            PROGRAM CLOUD(INPUT,OUTPUT=65)

C
      COMMON /INTP/ YINT(101,2)
      COMMON /DIFY/ YDIF(101),DY(100)
      COMMON /PLOTER/ XRAY(900),YRAY(900),INUM
      COMMON X(80,2),Y(80,2),NPTS(2),XPL(101),XL,XH,YL,
             YH, XMIN, XMAX
      REAL M
      LOGICAL FIN
C
      FIN=.FALSE.
      IC=0
      INUM=0
C
C ---ENTER RUN DATA
C
      READ 1, ISET
1     FORMAT(A10)
100   CALL READIN(P,M,C,XO,IPR,PIN)
      IF(FIN)GO TO 500
C
C ---DETERMINE X-RANGE FOR INTERPOLATION & DELTA VALUE
C
      CALL RANGE(DEL)
C
C ---COMPUTE INTERPOLATED 'SMOOTH' CURVES THRU DATA AND BASE
     SETS
C
      CALL INTERP(DEL)
C
C ---CORRECT ABSCISSA ARRAY
C
      CALL CORRECT(X0)
C
C ---COMPUTE CURVE DIFFERENCES & DERIVATIVES
C
      PMC=P*M*C
      CALL DIFF(PMC,DEL)
C
      IC=IC+1
      IF(IPR.EQ.1) CALL WRITOUT(1C,DEL)
      GO TO 100
500   CALL PLOTR(IC,ISET)
      STOP
      END
```

```
            PROGRAM HOOP (INPUT, OUTPUT = 65)


C
C
      COMMON /INTP/ TINT (101,2)
      COMMON /DIFY/ YDIF (101), DY (100)
      COMMON /PLOTER/ XRAY (900), YRAY (900), INUM
      COMMON X (80,2), Y (80,2), NPTS (2), XPL (101),
            XL,XH,YL, YH, XMIN, XMAX
      REAL M
      LOGICAL FIN
C
      FIN=. FALSE.
      IC = 0
      INUM = 0
C
C ---ENTER RUN DATA
C
      READ 1, ISET
1     FORMAT (A10)
100   CALL READIN (P,M,C,XO,IPR,FIN)
      IF (FIN) GO TO 500
      XO=.2
C
C ---DETERMINE X-RANGE FOR INTERPOLATION & DELTA VALUE
C
      CALL RANGE (DEL)
C
C ---COMPUTE INTEROLATED SMOOTH CURVES THRU DATA AND BASE
     SETS
C
      CALL INTERP (DEL)
C
C ---CORRECT ABSCISSA ARRAY
C
      CALL CORRECT (XO)
C
C ---COMPUTE CURVE DIFFERENCES & DERIVATIVES
C
      PMC=P*M*C
      CALL DIFF (PMC,DEL)
C
      IC=IC+1
      GO TO 100
500   CALL PLOTH (IC,ISET)
      STOP
      END
```

```
      SUBROUTINE READIN (P,M,C,XO,IPR,FIN)
      COMMON /STNAM/ ISTNM(9),IST
      COMMON X(80,2),Y(80,2),NPTS(2),XPL(101),XL,XH,YL,YH,XMIN,XMAX
      REAL M
      LOGICAL FIN
      DATA IST/0/
C
C  ----INPUT RUN CONSTANTS
C
      IST=IST+1
      READ 1, ISTNM(IST)
1     FORMAT(A10)
      IF(EOF(5LINPUT).NE.0) GO TO 50
      READ *,P,M,C,XO,IPR
      IF(P.LT.10. .OR. P.GT.100000.) GO TO 999
      IF(M.LT.0.  .OR. M.GT.5.) GO TO 999
      IF(C.LT.0.  .OR. C.GT.5.) GO TO 999
      IF(XO.LT.0. .OR. XO.GT.1.) GO TO 999
C
C  ----INPUT DATA VALUES
C
      READ *,NPTS(1),Y(1,1)
      IF(NPTS(1).LE.0) GO TO 999
      IF(ABS(Y(1,1)).GT.3) GO TO 999
      N=NPTS(1)
      READ *,(X(J,1),J=1,N)
      PRINT 9002
      DO 3 I=1,N
      PRINT 9001,X(I,1)
3     CONTINUE
      XLAST=-.25
      DO 5 I=1,N
      IF(X(I,1).GT.1. .OR. X(I,1).LT.XLAST) GO TO 999
      XLAST=X(I,1)
5     CONTINUE
C
C  ----COMPUTE REMAINING DATA Y-VALUES
C
      DO 10 I=2,N
      Y(I,1)=Y(I-1,1)+1.0
10    CONTINUE
C
C  ----INPUT BASELINE VALUES
C
```

```
      READ *,NPTS(2),Y(1,2)
      IF(NPTS(2).LE.0) GO TO 999
      IF(ABS(Y(1,2)).GT.3.) GO TO 999
      N=NPTS(2)
      READ *,(X(J,2),J=1,N)
      PRINT 9002
      DO 13 I=1,N
      PRINT 9001,X(I,2)
13    CONTINUE
      XLAST=-.15
      DO 15 I=1,N
      IF(X(I,2).GT.1. .OR. X(I,2).LT.XLAST) GO TO 999
      XLAST=X(I,2)
15    CONTINUE
C
C ----COMPUTE REMAINING BASE Y-VALUES
C
      DO 20 I=2,N
      Y(I,2)=Y(I-1,2)+1.0
20    CONTINUE
C
C
      RETURN
C
50    FIN=.TRUE.
      RETURN
999   PRINT 9000
9000  FORMAT(1X,"INPUT DATA DOES NOT CONFORM -- PLS CK")
9001  FORMAT(5X,F8.6)
9002  FORMAT(1X,"DATA VALUES")
9003  FORMAT(1X,"BASE VALUES")
      STOP 77
      END
      SUBROUTINE RANGE(DEL)
      COMMON X(80,2),Y(80,2),NPTS(2),XPL(101),XL,XH,YL,YH,XMIN,XMAX
C
      N1=NPTS(1)
      N2=NPTS(2)
C
      IF(X(1,1).LE.X(1,2)) GO TO 20
      XMIN=X(1,1)
      XL=X(1,2)
      GO TO 40
C
```

```
      XMIN=X(1,2)
      XL=X(1,1)
C
      IF(X(N1,1).GE.X(N2,2)) GO TO 60
      XMAX=X(N1,1)
      XH=X(N2,2)
      GO TO 80
C
60    XMAX=X(N2,2)
      XH=X(N1,1)
C
80    DEL=(XMAX-XMIN)/100.0
C
      YL=Y(1,2)
      IF(Y(1,1).LT.Y(1,2)) YL=Y(1,1)
      YH=Y(N2,2)
      IF(Y(N1,1).GT.Y(N2,2)) YH=Y(N1,1)
C
      RETURN
      END
      SUBROUTINE INTERP(DEL)
      COMMON /INTP/ YINT(101,2)
      COMMON X(80,2),Y(80,2),NPTS(2),XPL(101),XL,XH,YL,YH,XMIN,XMAX
      DIMENSION WD(80),RD(80),XN(80),FN(80),GN(80),DN(80),THETA(80),
     +W(1200)
      DIMENSION XD(80),YD(80)
      DATA WD/80*1.0/
      DATA RD/80*0.0/
      DATA XN/80*0.0/
      DATA FN/80*0.0/
      DATA GN/80*0.0/
      DATA DN/80*0.0/
      DATA THETA/80*0.0/
      DATA W/1200*0.0/
C
C
      DO 10 I=1,101
      XPL(I)=XMIN+DEL*(I-1)
10    CONTINUE
C
      DO 40 I=1,2
      DO 15 J=1,80
      XD(J)=X(J,I)
      YD(J)=Y(J,I)
```

```
15      CONTINUE
        CALL SPLIN1(NPTS(I),KNOTS,XD,YD,WD,RD,XN,FN,GN,DN,THETA,W,
       +0,0)
        DO 20 K=1,101
        YINT(K,I)=SPLIN2(XPL(K),KNOTS,XN,FN,GN,1)
2C      CONTINUE
4C      CONTINUE
C
C
        RETURN
        END
        SUBROUTINE CORRECT(X0)
        COMMON X(80,2),Y(80,2),NPTS(2),XPL(101),XL,XH,YL,YH,XMIN,XMAX
C
C  ----THIS ROUTINE COMPUTES CORRECTION FOR DISTANCE FROM HOLE
C
        DO 10 I=1,101
        XPL(I)=X0-XPL(I)
1C      CONTINUE
C
        RETURN
        END
        FUNCTION SPLIN2(X,N,XN,FN,GN,ITYPE)
C
C   *  *  *  *  *  *  *  *  *  *  *  *  *  *  *  *  *  *  *  *  *  *  *  *
C
C
C  - -  A FUNCTION UTILITY TO BE USED IN CONJUNCTION WITH THE SPLINE
C       ROUTINES SPLIN4 OR SPLIN1.
C
C            X =  THE VALUE OF THE INDEPENDENT VARIABLE AT WHICH THE SPLINE
C                 OR ITS DERIVATIVE ARE TO BE EVALUATED. X MUST BE BETWEEN
C                 XN(1) AND XN(N) FOR CORRECT RESULTS.
C            N =  THE NUMBER OF KNOTS (RETURNED BY SPLINING ROUTINES)
C           XN =  ARRAY OF KNOTS POSITIONS (RETURNED BY SPLINING ROUTINES)
C           FN =  ARRAY OF SPLINE VALUES (RETURNED BY SPLINE ROUTINES)
C           GN =  ARRAY OF DERIVATIVE VALUES (RETURNED BY SPLINE ROUTINES)
C       ITYPE =  1 RETURNS SPLINE VALUE AT X
C                2 RETURNS THE DERIVATIVE VALUE AT X.
C
C
C   *  *  *  *  *  *  *  *  *  *  *  *  *  *  *  *  *  *  *  *  *  *  *  *
C
        DIMENSION XN(80),FN(80),GN(80)
```

```
15      CONTINUE
        CALL SPLIN1(NPTS(I),KNOTS,XD,YD,WD,RD,XN,FN,GN,DN,THETA,W,
       +0.0)
        DO 20 K=1,101
        YINT(K,I)=SPLIN2(XPL(K),KNOTS,XN,FN,GN,1)
20      CONTINUE
40      CONTINUE
C
C
        RETURN
        END
        SUBROUTINE CORRECT(XO)
        COMMON X(80,2),Y(80,2),NPTS(2),XPL(101),XL,XH,YL,YH,XMIN,XMAX
C
C  ----THIS ROUTINE COMPUTES CORRECTION FOR DISTANCE FROM HOLE
C
        DO 10 I=1,101
        XPL(I)=XO-XPL(I)
10      CONTINUE
C
        RETURN
        END
        FUNCTION SPLIN2(X,N,XN,FN,GN,ITYPE)
C
CC   *  *  *  *  *  *  *  *  *  *  *  *  *  *  *  *  *  *  *  *  *  *  *  *  *
CCC
CCC
CC  - -  A FUNCTION UTILITY TO BE USED IN CONJUNCTION WITH THE SPLINE
CC       ROUTINES SPLIN4 OR SPLIN1.
CCC
CCC           X = THE VALUE OF THE INDEPENDENT VARIABLE AT WHICH THE SPLINE
CCC               OR ITS DERIVATIVE ARE TO BE EVALUATED. X MUST BE BETWEEN
CCC               XN(1) AND XN(N) FOR CORRECT RESULTS.
CCC           N = THE NUMBER OF KNOTS (RETURNED BY SPLINING ROUTINES)
CCC          XN = ARRAY OF KNOTS POSITIONS (RETURNED BY SPLINING ROUTINES)
CCC          FN = ARRAY OF SPLINE VALUES (RETURNED BY SPLINE ROUTINES)
CCC          GN = ARRAY OF DERIVATIVE VALUES (RETURNED BY SPLINE ROUTINES)
CCC       ITYPE = 1 RETURNS SPLINE VALUE AT X
CCC               2 RETURNS THE DERIVATIVE VALUE AT X.
CCC
CCC  *  *  *  *  *  *  *  *  *  *  *  *  *  *  *  *  *  *  *  *  *  *  *  *  *
C
        DIMENSION XN(80),FN(80),GN(80)
```

```
15      CONTINUE
        CALL SPLIN1(NPTS(I),KNOTS,XD,YD,WD,RD,XN,FN,GN,DN,THETA,W,
       +0.0)
        DO 20 K=1,101
        YINT(K,I)=SPLIN2(XPL(K),KNOTS,XN,FN,GN,1)
2C      CONTINUE
4C      CONTINUE
C
C
        RETURN
        END
        SUBROUTINE CORRECT(X0)
        COMMON X(80,2),Y(80,2),NPTS(2),XPL(101),XL,XH,YL,YH,XMIN,XMAX
C
C  ----THIS ROUTINE COMPUTES CORRECTION FOR DISTANCE FROM HOLE
C
        DO 10 I=1,101
        XPL(I)=X0-XPL(I)
1C      CONTINUE
C
        RETURN
        END
        FUNCTION SPLIN2(X,N,XN,FN,GN,ITYPE)
C
CC   *  *  *  *  *  *  *  *  *  *  *  *  *  *  *  *  *  *  *  *  *  *  *  *
CCC
CCC
CC  - -  A FUNCTION UTILITY TO BE USED IN CONJUNCTION WITH THE SPLINE
CC       ROUTINES SPLIN4 OR SPLIN1.
CC
CC            X = THE VALUE OF THE INDEPENDENT VARIABLE AT WHICH THE SPLINE
CC                OR ITS DERIVATIVE ARE TO BE EVALUATED. X MUST BE BETWEEN
CC                XN(1) AND XN(N) FOR CORRECT RESULTS.
CC            N = THE NUMBER OF KNOTS (RETURNED BY SPLINING ROUTINES)
CC           XN = ARRAY OF KNOTS POSITIONS (RETURNED BY SPLINING ROUTINES)
CC           FN = ARRAY OF SPLINE VALUES (RETURNED BY SPLINE ROUTINES)
CC           GN = ARRAY OF DERIVATIVE VALUES (RETURNED BY SPLINE ROUTINES)
CC        ITYPE = 1 RETURNS SPLINE VALUE AT X
CC                2 RETURNS THE DERIVATIVE VALUE AT X.
CC
CCC
CC   *  *  *  *  *  *  *  *  *  *  *  *  *  *  *  *  *  *  *  *  *  *  *  *
C
        DIMENSION XN(80),FN(80),GN(80)
```

```
      IF(X.LT.XN(1)) GOTO 100
      IF(X.GT.XN(N)) GOTO 110
      DO 8 K=1,N
      IF(X.NE.XN(K)) GOTO 8
      KK=K
      GO TO 120
8     CONTINUE
      DO 10 K=2,N
      IF(X.GT.XN(K)) GOTO 10
      JK=K
      GO TO 20
10    CONTINUE
20    HH=XN(JK)-XN(JK-1)
      HH3=HH**3
      T1=HH*GN(JK-1)+FN(JK-1)-FN(JK)
      T2=HH*GN(JK)+FN(JK-1)-FN(JK)
      T3=XN(JK)-X
      T4=X-XN(JK-1)
      IF(ITYPE.EQ.2) GOTO 201
      SPLIN2=(T3*FN(JK-1)+T4*FN(JK))/HH+T3*T4*(T3*T1-T4*T2)/HH3
      RETURN
201   SPLIN2=(FN(JK)-FN(JK-1))/HH-T3*T4*(HH*(GN(JK-1)+GN(JK))+2.*(FN(JK-
     +1)-FN(JK)))/HH3+(XN(JK-1)+XN(JK)-2.*X)*(T3*T1-T4*T2)/HH3
      RETURN
100   JK=2
      GO TO 20
110   JK=N
      GO TO 20
120   IF(ITYPE.EQ.2) GOTO 301
      SPLIN2=FN(KK)
      RETURN
301   SPLIN2=GN(KK)
      RETURN
      END
      SUBROUTINE SPLIN3(M,N,XD,YD,WD,RD,XN,FN,GN,DN,THETA,W,IPRINT)
C
      DIMENSION W(1200),XD(80),YD(80),WD(80),RD(80),XN(80),FN(80),GN(80)
     +  ,DN(80),S(7),THETA(80)
C
C     TRANSFER KNOTS TO W, AND INSERT EXTRA KNOTS AT ENDS OF RANGE
C
      XN(N)=AMAX1(XN(N),XD(M))
      DO 1 I=1,N
    1 W(I+3)=XN(I)
```

```
      DO 2 J=1,3
      K=4-J
      W(K)=W(K+1)+W(K+1)-W(K+2)
      K=J+N
    2 W(K+3)=W(K+2)+W(K+2)-W(K+1)
C
CC    SET UP THE LEAST SQUARES EQUATIONS IN W
C
      I=1
      J=2
      K=N+13
      AA=1.0/((W(3)-W(4))*(W(3)-W(5))*(W(3)-W(6))*(W(3)-W(7)))
      D=1.0/((W(5)-W(1))*(W(5)-W(2))*(W(5)-W(3))*(W(5)-W(4)))
    3 A=AA
      AA=1.0/((W(J+2)-W(J+3))*(W(J+2)-W(J+4))*(W(J+2)-W(J+5))*
     1   (W(J+2)-W(J+6)))
      B=AA*(W(J+2)-W(J+6))/(W(J+2)-W(J+1))
      DD=D
      D=1.0/((W(J+4)-W(J))*(W(J+4)-W(J+1))*(W(J+4)-W(J+2))*
     1  (W(J+4)-W(J+3)))
      C=DD*(W(J+3)-W(J-1))/(W(J+3)-W(J+4))
      FN(J-1)=K-7
      IF(J-2) 4,4,5
    4 W(K-6)=-DD
      W(K-5)=-C-D
      W(K-4)=A+B
      W(K-3)=AA
      W(K-2)=0.
      IF(I-M) 6,6,7
    6 W(K-1)=1.
      W(K)=0.
      GO TO 8
    5 W(K-4)=-AW*(W(K-4)+C+D)
      W(K-3)=AW*B
      W(K-2)=AW*AA
    8 K=K+7
      IF(I-M) 9,9,12
    9 IF(W(J+3)-XD(I)) 11,10,10
   10 W(K-6)=DD*WD(I)*(W(J+3)-XD(I))**3
      W(K-5)=WD(I)*(C*(W(J+3)-XD(I))**3+D*(W(J+4)-XD(I))**3)
      W(K-4)=WD(I)*(A*(XD(I)-W(J+1))**3+B*(XD(I)-W(J+2))**3)
      W(K-3)=WD(I)*AA*(XD(I)-W(J+2))**3
      W(K-2)=WD(I)*YD(I)
      W(K-1)=0.
```

```
      W(K)=0.
      I=I+1
      GO TO 8
   12 IF(J-N) 11,4,4
   11 J=J+1
      AW=6.*THETA(J-1)
      W(K-6)=AW*DD
      W(K-5)=AW*C
      W(K-4)=A+B
      GO TO 3
    7 W(K-1)=0.
      W(K)=1.
      FN(J)=K
C
CC    APPLY HOUSEHOLDER ORTHOGONAL TRANSFORMATIONS TO OBTAIN AN UPPER
CC    TRIANGULAR LEAST SQUARES MATRIX
C
      KUMAX=K
      I=1
      IPR=N-1
      NPINIT=7
   13 I=I+1
      IPP=IPR+7
      NP=NPINIT
      J=I+NP
      KL=MAX0(IPR+8,IFIX(FN(J-8)+1.5))
      KU=IFIX(FN(J-7)+0.5)
      IF(NP-3) 14,14,15
   14 W(IPR+1)=0.
      W(IPR+2)=0.
      W(IPR+3)=0.
      W(IPR+4)=0.
   15 IF(KU-KL) 25,25,17
   17 NPINIT=MAX0(3,NPINIT-1)
      GO TO 18
   16 NP=NP+1
      J=IPR+NP
      W(J)=W(J-1)
      W(J-1)=W(J-2)
      W(J-2)=W(J-3)
      W(J-3)=0.
      KL=KU+1
      J=I+NP
      KU=IFIX(FN(J-7)+0.5)
```

```
18 DO 19 J=1,NP
   JP=IPR+J
19 S(J)=W(IPR+1)*W(JP)
   KPIV=0
   PIVMAX=ABS(W(IPR+1))
   DO 20 K=KL,KU,7
   DO 21 J=1,NP
   JJ=K+J
21 S(J)=S(J)+W(JJ-1)*W(K)
   IF(PIVMAX-ABS(W(K))) 70,20,20
70 PIVMAX=ABS(W(K))
   KPIV=K
20 CONTINUE
   IF(KPIV) 71,71,72
72 DO 73 J=1,NP
   JJ=IPR+J
   A=W(JJ)
   W(JJ)=W(KPIV)
   W(KPIV)=A
   KPIV=KPIV+1
73 CONTINUE
71 AA=SIGN(SQRT(S(1)),W(IPR+1))
   B=W(IPR+1)+AA
   A=1.0/(AA*B)
   DO 22 J=2,NP
   JP=IPR+J
   S(J)=A*(S(J)+AA*W(JP))
22 W(JP)=W(JP)-B*S(J)
   W(IPR+1)=-AA
   DO 23 K=KL,KU,7
   A=W(K)
   DO 24 J=2,NP
   JJ=K+J
   W(JJ-2)=W(JJ-1)-A*S(J)
24 CONTINUE
23 CONTINUE
   IF(KU-KUMAX) 25,26,26
25 IF(NP-7) 16,27,27
27 GN(I)=SQRT(W(IPR+1)**2+W(KU+1)**2)
   A=W(IPR+1)/GN(I)
   B=W(KU+1)/GN(I)
   C=W(KU+5)
   DO 28 J=1,3
   JP=IPR+J
```

```
      JJ=KU+J
      W(JP)=A*W(JP+1)+B*W(JJ+1)
      W(JJ)=A*W(JJ+1)-B*W(JP+1)
      W(JJ+4)=-B*W(JP+4)
   28 W(JP+4)=A*W(JP+4)
      W(IPR+4)=B*C
      W(KU+4)=A*C
      GO TO 13
   26 IF(NP-4) 29,29,13
C
C     BACK-SUBSTITUTION TO OBTAIN MULTIPLIERS OF FUNDAMENTAL SPLINES
C
   29 K=KUMAX
      DO 30 J=1,4
      K=K-3
      JJ=IPR+J
      DO 31 I=1,3
      KK=K+I
      JK=JJ+I
      W(KK)=W(JK)
      L=IPP+1
      LK=KK
   32 IF(L-JJ) 33,34,34
   33 L=L+1
      LK=LK+3
      W(KK)=W(KK)-W(LK)*W(L)
      GO TO 32
   34 W(KK)=W(KK)/W(IPR+1)
   31 CONTINUE
      IPR=IPR-7
   30 CONTINUE
      L=N
   35 IF(IPR-N) 36,36,37
   37 K=K-3
      L=L-1
      DO 38 I=1,3
      KK=K+I
      JJ=IPR+I
   38 W(KK)=(W(JJ+4)-W(IPR+1)*W(KK+3)-W(IPR+2)*W(KK+6)-W(IPR+3)*W(KK+9)
     1       -W(IPR+4)*W(KK+12))/GN(L)
      IPR=IPR-7
      GO TO 35
   36 KRES=K
C
```

```
C     CALCULATE SPLINE VALUES AT THE DATA POINTS, AND SCALAR PRODUCTS
C
      KSDATA=KRES-3*M
      I=1
      J=1
      DO 43 L=1,5
   43 S(L)=0.
      KK=KSDATA
      AA=1.0/((W(3)-W(4))*(W(3)-W(5))*(W(3)-W(6))*(W(3)-W(7)))
      D=1.0/((W(5)-W(1))*(W(5)-W(2))*(W(5)-W(3))*(W(5)-W(4)))
   39 J=J+1
      K=K+3
      A=AA
      AA=1.0/((W(J+2)-W(J+3))*(W(J+2)-W(J+4))*(W(J+2)-W(J+5))*
     1    (W(J+2)-W(J+6)))
      B=AA*(W(J+2)-W(J+6))/(W(J+2)-W(J+1))
      DD=D
      D=1.0/((W(J+4)-W(J))*(W(J+4)-W(J+1))*(W(J+4)-W(J+2))*
     1   (W(J+4)-W(J+3)))
      C=DD*(W(J+3)-W(J-1))/(W(J+3)-W(J+4))
   40 IF(XD(I)-XN(J)) 41,41,39
   41 DO 42 L=1,3
      LK=L+K
      KU=L+KK
   42 W(KU)=A*W(LK+3)*(XD(I)-W(J+1))**3+(B*W(LK+3)+AA*W(LK+6))*
     1       (XD(I)-W(J+2))**3+(C*W(LK)+DD*W(LK-3))*(W(J+3)-XD(I))**3
     2       +D*W(LK)*(W(J+4)-XD(I))**3
      RD(I)=YD(I)-W(KK+1)
      AS=WD(I)*RD(I)
      BS=WD(I)*W(KK+2)
      CS=WD(I)*W(KK+3)
      S(1)=S(1)+BS*BS
      S(2)=S(2)+BS*CS
      S(3)=S(3)+CS*CS
      S(4)=S(4)+AS*BS
      S(5)=S(5)+AS*CS
      I=I+1
      KK=KK+3
      IF(I-M) 40,40,44
C
C     CALCULATE THE RESIDUALS AND PARAMETERS OF THE REQUIRED SPLINE
C
   44 DET=S(1)*S(3)-S(2)*S(2)
      A=(S(3)*S(4)-S(2)*S(5))/DET
```

```
      B=(S(1)*S(5)-S(2)*S(4))/DET
      K=KSDATA
      DO 45 I=1,M
      K=K+3
   45 RD(I)=RD(I)-A*W(K-1)-B*W(K)
      KL=KRES+1
      DO 46 K=KL,KUMAX,3
   46 W(K)=W(K)+A*W(K+1)+B*W(K+2)
C
CC    COMPUTE ELEMENTS OF FN,GN AND DN
C
      K=KRES
      AA=1.0/((W(2)-W(3))*(W(2)-W(4))*(W(2)-W(5))*(W(2)-W(6)))
      DN(1)=0.
      DO 47 J=1,N
      A=AA*W(K+4)*(XN(J)-W(J+1))**2
      AA=1.0/((W(J+2)-W(J+3))*(W(J+2)-W(J+4))*(W(J+2)-W(J+5))*
     1   (W(J+2)-W(J+6)))
      B=AA*(W(K+7)+W(K+4)*(W(J+2)-W(J+6))/(W(J+2)-W(J+1)))*
     1  (XN(J)-W(J+2))**2
      DD=W(K+1)*(W(J+4)-XN(J))/((W(J+4)-W(J))*(W(J+4)-W(J+1))*
     1   (W(J+4)-W(J+2)))
      FN(J)=A*(XN(J)-W(J+1))+B*(XN(J)-W(J+2))+DD*(W(J+4)-XN(J))
      GN(J)=3.0*(A+B-DD)
      IF(J-1) 48,48,49
   49 DN(J)=6.0*(GN(J-1)+GN(J)+2.0*(FN(J-1)-FN(J))/(XN(J)-XN(J-1)))/
     1(XN(J)-XN(J-1))**2
      DN(J-1)=DN(J)-DN(J-1)
   48 K=K+3
   47 CONTINUE
C
CC    PROVIDE PRINT IF REQUESTED
C
      IF(IPRINT) 50,50,51
   50 RETURN
C
   51 PRINT 52
   52 FORMAT(1H1,35X,*SPLINE APPROXIMATION OBTAINED BY SPLIN3*//4X,1HI,
     19X,5HXN(I),18X,5HFN(I),18X,5HGN(I),13X,16H3RD DERIV CHANGE,11X,
     28HTHETA(I)//)
      I=1
      PRINT 63,I,XN(I),FN(I),GN(I)
   54 I=I+1
      IF(I-N) 55,56,56
```

```
   55 PRINT 63,I,XN(I),FN(I),GN(I),DN(I),THETA(I)
      GO TO 54
   56 PRINT 63,I,XN(I),FN(I),GN(I)
      PRINT 57
   57 FORMAT(///4X,1HI,9X,5HXD(I),18X,5HYD(I),18X,5HWD(I),19X,3HFIT,
     118X,8HRESIDUAL//)
      J=2
      DO 58 I=1,M
   59 IF(XD(I)-XN(J)) 60,60,61
   61 PRINT 62
   62 FORMAT(5X)
      J=J+1
      GO TO 59
   60  YDRD = YD(I)-RD(I)
      PRINT 63,I,XD(I),YD(I),WD(I),YDRD        ,RD(I)
   63 FORMAT(I5,5E23.14)
   58 CONTINUE
      GO TO 50
      END
      SUBROUTINE DIFF(PMC,DEL)
      COMMON /INTP/ YINT(101,2)
      COMMON /PLOTER/ XRAY(900),YRAY(900),INUM
      COMMON /DIFY/ YDIF(101),DY(100)
      COMMON X(80,2),Y(80,2),NPTS(2),XPL(101),DUM6(6)
C
C  ----COMPUTE DIFFERENCES AND DIVIDE BY PMC
C
      DO 20 K=1,101
      YDIF(K)=(YINT(K,1)-YINT(K,2))/PMC
20    CONTINUE
C
C  ----COMPUTE DERIVATIVES
C
      DO 40 K=2,101
      DY(K-1)=(YDIF(K)-YDIF(K-1))/DEL
      INUM=INUM+1
      XRAY(INUM)=XPL(K)
      YRAY(INUM)=DY(K-1)
40    CONTINUE
      RETURN
      END
      SUBROUTINE PLOTR(IC,ISET)
      COMMON /STNAM/ ISTNAM(9),IST
      COMMON /PLOTER/ X(900),Y(900),II
```

```
      DIMENSION IBUF(257),XRAY(102),YRAY(102)
      DIMENSION XLEG(5),YLEG(5)
      NC=IC*100
      DO 1 I=1,NC
1     CONTINUE
C
C ----INIT PLOTTING PARAMETERS
C
      CALL PLOTS(IBUF,257,0)
      XRAY(101)=-0.05
      XRAY(102)=0.05
      YRAY(101)=-0.01
      YRAY(102)=0.01
C
C ----PRINT AXES AND TITLES
C
      CALL AXIS(0.,0.,"DISTANCE FROM HOLE (IN.)",-24,9.0,0.0,
     +XRAY(101),XRAY(102))
      CALL AXIS(0.,0.,"COMPRESSIVE STRAIN",18,7.0,90.0,
     +YRAY(101),YRAY(102))
      CALL DASHLN(0.,1.,9.,1.,.042,.042)
      CALL DASHLN(1.0,1.,1.,7.,.042,.042)
      CALL SYMBOL(1.2,6.,0.2,"HOLE NO. ",0.,9)
      CALL SYMBOL(3.0,6.,0.2,ISET,0.,10)
C ----LEGEND INITIALIZATION
      CALL SYMBOL(7.2,6.6,0.2,"LEGEND",0.,6)
      CALL DASHLN(7.2,6.56,8.4,6.56,.014,.014)
      HTD=6.45
      XLEG(1)=7.0
      XLEG(2)=7.45
      XLEG(3)=7.9
      XLEG(4)=0.0
      XLEG(5)=1.0
      YLEG(4)=0.0
      YLEG(5)=1.0
C
C ----PRINT PLOT LINES
C
      DO 30 I=1,IC
      K=I-1
      N=100*K
      DO 20 J=1,100
      XRAY(J)=X(J+N)
      YRAY(J)=Y(J+N)
```

```
20      CONTINUE
        CALL LINE(XRAY,YRAY,100,1,5,K)
C ----PRINT LEGEND
        HTD=HTD-0.14
        YLEG(1)=HTD
        YLEG(2)=HTD
        YLEG(3)=HTD
        CALL LINE(XLEG,YLEG,3,1,1,K)
        CALL SYMBOL(8.1,HTD-.042,0.084,ISTNAM(I),0.,10)
30      CONTINUE
C ----COMPLETE LEGEND
        HTD=HTD-0.14
        CALL DASHLN(6.8,7.0,6.8,HTD,.014,.014)
        CALL DASHLN(6.8,HTD,9.0,HTD,.014,.014)
        CALL DASHLN(9.0,HTD,9.0,7.0,.014,.014)
        CALL DASHLN(9.0,7.0,6.8,7.0,.014,.014)
C
C ----EXIT PLOT ROUTINE
C
        CALL PLOT(12.0,0.0,999)
        RETURN
        END
        SUBROUTINE SPLIN1(M,N,XD,YD,WD,RD,XN,FN,GN,DN,THETA,W,IPRINT,IFIT)
C
CCC  *  *  *  *  *  *  *  *  *  *  *  *  *  *  *  *  *  *  *  *  *  *
CCC
CCC
CC  - - A ROUTINE TO FIT THE SMOOTHEST CURVE THRU A GIVEN SET OF DATA
CCC     USING CUBIC SPLINES
CCC
CCC          M = TOTAL NUMBER OF DATA POINTS.
CCC          N = NUMBER OF KNOTS USED (INPUT OR OUTPUT DEPENDING ON IFIT)
CCC         XD = X-COOR. DATA ARRAY (INPUT)
CCC         XD = X-COOR. DATA ARRAY (INPUT)
CCC         YD = Y-COOR. DATA ARRAY (INPUT)
CCC         WD = WEIGHT FOR EACH DATA POINT (GENERALLY = 1.0, IF W(I) = 0.
CCC              THEN THE ITH POINT WILL BE OMITTED FROM THE FIT) (INPUT)
CCC         RD = AN ARRAY CONTAINING YD(I)-S(XD(I)) (OUTPUT)
CCC         XN = AN ARRAY CONTAINING THE KNOT POSITIONS (INPUT OR OUTPUT
CCC              DEPENDING ON IFIT)
CCC         FN = AN ARRAY CONTAINING THE VALUES OF THE SPLINE AT THE KNOTS
CCC              (OUTPUT)
CCC         GN = AN ARRAY CONTAINING THE VALUES OF THE DERIVATIVE OF THE
C                SPLINE AT THE KNOTS (OUTPUT)
```

```
C         DN = AN ARRAY CONTAINING THE VALUES OF THE 3RD DERIVATIVE
C              DISCONTINUITIES OF THE SPLINE ACROSS THE KNOTS (ROUGH
C              ESTIMATE OF THE ERROR IN THE FIT) (OUTPUT)
C      THETA = WORKING ARRAY
C          W = WORKING ARRAY (MUST BE DIMENSIONED ATLEAST 7*M+8*N+6)
C     IPRINT = PRINT OPTION
C              1 PRINT RESULTS AFTER EACH ITERATION
C              0 NO PRINT PRODUCED
C             -1 PRINT RESULTS FOR BEST FIT ONLY
C       IFIT = FIT OPTION
C              0  PROGRAM WILL AUTOMATICALLY SELECT KNOT POSITIONS
C              1 CALCULATE THE SPLINE WITH THE INPUT SET OF KNOT
C                POSITIONS **CAUTION N MUST BE .GE. 5 AND XN(1)=XD(1),
C                XN(N)=XD(M) FOR CORRECT RESULTS.
C
C
C     THE NORMAL MODE OF OPERATION IS TO ALLOW THE PROGRAM TO
C     AUTOMATICALLY SELECT THE OPTIMAL KNOT POSITIONS BASED ON
C     STATISTICAL ERROR TESTS. IN THIS MODE OF OPERATION IT IS DIFFICULT
C     TO PREDICT THE REQUIRED DIMENSION FOR THE ARRAYS XN, FN, GN, DN,
C     THETA, AND W. THE PROGRAM WILL NEVER MAKE N GT M SO A SAFE
C     DIMENSIONALITY FOR THESE ARRAYS WOULD BE M. SPLIN1 CALLS SPLIN3
C     TO CALCULATE THE LEAST SQUARES SPLINE APPROXIMATION.
C
C  *  *  *  *  *  *  *  *  *  *  *  *  *  *  *  *  *  *  *  *  *  *  *
C
      DIMENSION XD(80),YD(80),WD(80),RD(80),XN(80),FN(80),GN(80),DN(80),
     1          THETA(80),W(1200)
C
C     OMIT DATA WITH ZERO WEIGHTS
C
      MM=1
      J=1
      DO 1 I=2,M
      IF(WD(I)) 3,2,3
    2 IF(I-M) 4,3,3
    4 W(J)=XD(I)
      W(J+1)=YD(I)
      W(J+2)=FLOAT(I)
      J=J+3
      GO TO 1
    3 MM=MM+1
```

```
C         DN = AN ARRAY CONTAINING THE VALUES OF THE 3RD DERIVATIVE
C              DISCONTINUITIES OF THE SPLINE ACROSS THE KNOTS (ROUGH
C              ESTIMATE OF THE ERROR IN THE FIT) (OUTPUT)
C      THETA = WORKING ARRAY
C          W = WORKING ARRAY (MUST BE DIMENSIONED ATLEAST 7*M+8*N+6)
C     IPRINT = PRINT OPTION
C              1 PRINT RESULTS AFTER EACH ITERATION
C              0 NO PRINT PRODUCED
C             -1 PRINT RESULTS FOR BEST FIT ONLY
C       IFIT = FIT OPTION
C              0  PROGRAM WILL AUTOMATICALLY SELECT KNOT POSITIONS
C              1 CALCULATE THE SPLINE WITH THE INPUT SET OF KNOT
C                POSITIONS **CAUTION N MUST BE .GE. 5 AND XN(1)=XD(1),
C                XN(N)=XD(M) FOR CORRECT RESULTS.
C
C
C     THE NORMAL MODE OF OPERATION IS TO ALLOW THE PROGRAM TO
C     AUTOMATICALLY SELECT THE OPTIMAL KNOT POSITIONS BASED ON
C     STATISTICAL ERROR TESTS. IN THIS MODE OF OPERATION IT IS DIFFICULT
C     TO PREDICT THE REQUIRED DIMENSION FOR THE ARRAYS XN, FN, GN, DN,
C     THETA, AND W. THE PROGRAM WILL NEVER MAKE N GT M SO A SAFE
C     DIMENSIONALITY FOR THESE ARRAYS WOULD BE M. SPLIN1 CALLS SPLIN3
C     TO CALCULATE THE LEAST SQUARES SPLINE APPROXIMATION.
C
C  *  *  *  *  *  *  *  *  *  *  *  *  *  *  *  *  *  *  *  *  *  *  *
C
C
      DIMENSION XD(80),YD(80),WD(80),RD(80),XN(80),FN(80),GN(80),DN(80),
     1          THETA(80),W(1200)
C
C     OMIT DATA WITH ZERO WEIGHTS
C
      MM=1
      J=1
      DO 1 I=2,M
      IF(WD(I)) 3,2,3
    2 IF(I-M) 4,3,3
    4 W(J)=XD(I)
      W(J+1)=YD(I)
      W(J+2)=FLOAT(I)
      J=J+3
      GO TO 1
    3 MM=MM+1
```

```
      XD(MM)=XD(I)
      YD(MM)=YD(I)
      WD(MM)=WD(I)
    1 CONTINUE
      J=1
      K=MM
    7 IF(K-M) 5,6,6
    5 K=K+1
      XD(K)=W(J)
      YD(K)=W(J+1)
      WD(K)=W(J+2)
      J=J+3
      GO TO 7
C
C     INITIALIZATION OF ITERATIONS
    6 IF(IFIT .EQ. 1) GO TO 110
      JA=1
      IF(WD(1)) 9,8,9
    8 JA=2
    9 N=5
      XN(1)=XD(1)
      XN(5)=XD(MM)
      XN(3)=0.5*(XN(1)+XN(5))
      XN(2)=0.5*(XN(1)+XN(3))
      XN(4)=0.5*(XN(3)+XN(5))
  110 IW=7*MM+8*N+6
      DO 10 I=1,N
      J=IW+I
   10 W(J)=XN(I)
      IP=-IPRINT
C
CC    CALCULATE THE HISTOGRAMS FOR NEW SCALE FACTORS
C
   11 J=0
      K=1
      SA=0.
   12 SA=SA+WD(K)**2
      K=K+1
      IF(XD(K)-XD(1)) 12,12,13
   13 SA=(SA+0.5*WD(K)**2)/(XD(K)-XD(1))
   14 J=J+1
      IF(XD(K)-XN(J+1)) 15,15,16
   16 GN(J)=SA*(XN(J+1)-XN(J))
      GO TO 14
```

```
   15 GN(J)=SA*(XD(K)-XN(J))+0.5*WD(K)**2
   17 K=K+1
      IF(K-MM) 18,18,19
   18 IF(XD(K)-XN(J+1)) 20,20,21
   20 GN(J)=GN(J)+WD(K)**2
      GO TO 17
   21 SA=0.5*(WD(K-1)**2+WD(K)**2)/(XD(K)-XD(K-1))
      GN(J)=GN(J)-0.5*WD(K-1)**2+SA*(XN(J+1)-XD(K-1))
      GO TO 14
C
C     CALCULATE THE NEW SCALE FACTORS
C
   19 K=IW+2
      GN(1)=0.00025216*GN(1)*(W(K)-W(K-1))**8/(XN(2)-XN(1))
      DO 22 J=3,N
      IF(XN(J)-W(K)) 23,23,24
   24 K=K+1
   23 GN(J-1)=0.00025216*GN(J-1)*(W(K)-W(K-1))**8/(XN(J)-XN(J-1))
   22 GN(J-2)=ALOG(GN(J-2)+GN(J-1))
      NN=N-2
      HS=1.386294
      DO 97 J=2,NN
   97 GN(J)=AMIN1(GN(J),GN(J-1)+HS)
      J=NN-1
   98 GN(J)=AMIN1(GN(J),GN(J+1)+HS)
      J=J-1
      IF(J) 99,99,98
   99 DO 25 J=3,N
   25 THETA(J-1)=SQRT(EXP(GN(J-2))/(XN(J)-XN(J-2)))
C
C     CALCULATE THE SPLINE APPROXIMATION WITH CURRENT KNOTS
C
      CALL SPLIN3(MM,N,XD,YD,WD,RD,XN,FN,GN,DN,THETA,W,IP)
      IF(IFIT .EQ. 1) GO TO 41
C
C     APPLY STATISTICAL TEST FOR EXTRA KNOTS
C
      J=IW+1
      JJ=C
      K=JA
      TMAX=0
      IIS=1
   26 KC=-1
      SW=0.
```

```
      SR=0.
      RP=0.
      J=J+1
      JJ=JJ+1
      W(JJ)=0.
   27 IF(W(J)-XD(K)) 28,29,30
   30 KC=KC+1
      SW=SW+RD(K)**2
      SR=SR+RP*RD(K)
      RP=RD(K)
      K=K+1
      GO TO 27
   29 IF(WD(K)) 31,28,31
   31 KC=KC+1
      SW=SW+RD(K)**2
      SR=SR+RP*RD(K)
   28 IF(SR) 32,32,33
   33 SW=(SW/SR)**2
      RP=SQRT(SR/FLOAT(KC))
      IF (FLOAT(KC)-SW) 32,32,34
   34 IF (IIS .EQ. 3) GO TO 37
      IF (IIS .EQ. 2) GO TO 36
      PRP=RP
      IIS=3
      IF(FLOAT(KC)-2.*SW) 38,38,39
   37 W(JJ-1)=PRP
      TMAX=AMAX1(TMAX,PRP)
   39 IIS=2
   36 W(JJ)=RP
      TMAX=AMAX1(TMAX,RP)
      GO TO 38
   32 IIS=1
   38 IF(W(J)-XN(N)) 26,40,40
C
CC    TEST WHETHER ANOTHER ITERATION IS REQUIRED
C
   40 IF(TMAX) 41,41,42
C
CC    CALCULATE NEW TREND ARRAY, INCLUDING LARGER TRENDS ONLY
C
   42 TMAX=0.5*TMAX
      I=0
      J=1
      JW=1
```

```
      K=IW+1
      THETA(JW)=W(K)
   43 I=I+1
      K=K+1
      IF(W(I)-TMAX) 44,44,45
   44 JW=JW+1
      THETA(JW)=W(K)
   46 FN(J)=0.
      J=J+1
      IF(W(K)-XN(J)) 47,47,46
   45 JW=JW+2
      THETA(JW-1)=0.5*(W(K-1)+W(K))
      THETA(JW)=W(K)
      IF(XN(J+1)-THETA(JW-1)) 46,46,48
   48 FN(J)=1.
      J=J+1
   47 IF(J-N) 43,49,49
C
CC    MAKE KNOT SPACINGS BE USED FOUR TIMES
C
   49 IK=1
      KL=1
      FN(2)=AMAX1(FN(1),FN(2))
   50 K=KL+3
   51 IF(FN(K)) 52,52,53
   52 K=K-1
      IF(K-KL) 54,54,51
   53 K=K-1
      FN(K)=1.
      IF(K-KL) 54,54,53
   54 K=K+1
      IF(K-N) 55,56,56
   55 IF(XN(K+1)-XN(K)-1.5*(XN(K)-XN(K-1))) 54,54,56
   56 KU=K
      FN(K-2)=AMAX1(FN(K-2),FN(K-1))
   57 KKU=K
   58 K=K-1
      IF(K-KL) 59,59,60
   60 IF(XN(K)-XN(K-1)-1.5*(XN(K+1)-XN(K))) 58,58,61
   61 FN(K+1)=AMAX1(FN(K),FN(K+1))
   59 KKL=K
      KZ=4
      IF(FN(K)) 62,62,63
   63 K=K+1
```

```
      IF(K-KKU) 64,65,65
   64 IF(FN(K)) 66,66,63
   66 KZ=0
   62 KZ=KZ+1
      K=K+1
      IF(K-KKU) 67,65,65
   67 IF(FN(K)) 62,62,68
   68 IF(KZ-3) 69,69,70
   69 J=K-KZ
   71 FN(J)=1.
      J=J+1
      IF(J-K) 71,63,63
   70 IF(K+1-KKU) 72,65,65
   72 K=K+1
      FN(K)=1.
      GO TO 63
   65 IF(KL-KKL) 73,74,74
   73 FN(KKL-2)=AMAX1(FN(KKL-2),FN(KKL+1))
      FN(KKL-1)=AMAX1(FN(KKL-1),FN(KKL+3))
   75 K=KKL-4
   78 IF(FN(K)) 76,76,77
   76 K=K+1
      IF(K-KKL) 78,79,79
   77 FN(K)=1.
      K=K+1
      IF(K-KKL) 77,79,79
   79 IF (IK .EQ. 1) GO TO 57
      IF (IK .EQ. 2) GO TO 80
   74 IF(KU-N) 81,82,82
   81 KL=KU
      FN(KL+1)=AMAX1(FN(KL+1),FN(KL-2))
      FN(KL)=AMAX1(FN(KL),FN(KL-4))
      GO TO 50
   82   IK = 2
      KKL=N
      GO TO 75
C
C     INSERT EXTRA KNOTS FOR NEW APPROXIMATION
C
   80 DO 83 J=1,N
   83 GN(J)=XN(J)
      NN=1
      DO 84 J=2,N
      IF(FN(J-1)) 85,85,86
```

```
   86 NN=NN+1
      XN(NN)=0.5*(GN(J-1)+GN(J))
   85 NN=NN+1
      XN(NN)=GN(J)
   84 CONTINUE
      N=NN
      IW=7*MM+8*N+6
      DO 87 J=1,JW
      I=IW+J
   87 W(I)=THETA(J)
      GO TO 11
C
C     RESTORE DATA WITH ZERO WEIGHTS
C
   41 IF(MM-M) 88,89,89
   89 IF(IPRINT) 90,90,91
   88 J=-2
      K=MM
   92 J=J+3
      K=K+1
      W(J)=XD(K)
      W(J+1)=YD(K)
      W(J+2)=WD(K)
      IF(K-M) 92,93,93
   93 I=INT(W(J+2)+0.1)
   94 IF(K-I) 95,95,96
   96 XD(K)=XD(MM)
      YD(K)=YD(MM)
      WD(K)=WD(MM)
      K=K-1
      MM=MM-1
      GO TO 94
   95 XD(K)=W(J)
      YD(K)=W(J+1)
      WD(K)=0.
      K=K-1
      J=J-3
      IF(J) 91,91,93
   91 CALL SPLIN3(M,N,XD,YD,WD,RD,XN,FN,GN,DN,THETA,W,IABS(IPRINT))
   90 RETURN
      END
      SUBROUTINE WRITOUT(IC,DEL)
      COMMON /INTP/ YINT(101,2)
      COMMON /DIFY/ YDIF(101),DY(100)
```

```
      COMMON X(80,2),Y(80,2),NPTS(2),XPL(101),XL,XH,YL,YH,XMIN,XMAX
C
C
      PRINT 100, IC
      PRINT 105, XMIN,XMAX,DEL
      PRINT 110
      PRINT 115, XPL(1),YINT(1,1),YINT(1,2),YDIF(1)
      DO 50 K=2,101
      PRINT 115, XPL(K),YINT(K,1),YINT(K,2),YDIF(K),DY(K-1)
50    CONTINUE
C
      PRINT 120
C
100   FORMAT(1H1,//,5X,"OUTPUT -- MOIRE DATA ANALYSIS -- SET #",I2,//)
105   FORMAT(5X,"COMPUTED VALUES USED -",//10X,"XMIN = ",E17.9/10X,
     +"XMAX = ",E17.9/7X,"DELTA X = "E17.9//)
110   FORMAT(4X,"DISTANCE FROM HOLE",10X,"Y1",19X,"Y2",15X,
     +"DISPLACEMENT",12X,"STRAIN",/)
115   FORMAT(4X,5(E16.9,5X))
120   FORMAT(1H1)
      RETURN
      END
      SUBROUTINE PLOTM(IP,ISET)
      COMMON /INTP/ YINT(101,2)
      COMMON /DIFY/ YDIF(101),DY(100)
      COMMON X(80,2),Y(80,2),NPTS(2),XPL(101),XL,XH,YL,YH,XMIN,XMAX
      DIMENSION IBUF(257),HOLDX(103),HOLDY(103)
C
C ----INITIALIZE PLOT PARAMETERS
C
      CALL PLOTS(IBUF,257,0)
C
C ----DETERMINE PLOT TYPE
C
      IF(IP-2) 100,200,300
C
C ----BASIC PLOT
C
100   CALL AXIS(0.,0.,"X",-1,8.0,0.0,0.0,0.05)
      CALL AXIS(0.,0.,"FRINGE ORDER",12,8.0,90.0,0.0,4.0)
      N=NPTS(1)
      DO 110 I=1,N
      HOLDX(I)=X(I,1)
      HOLDY(I)=Y(I,1)
```

```
110   CONTINUE
      HOLDX(N+1)=0.0
      HOLDX(N+2)=0.05
      HOLDY(N+1)=0.0
      HOLDY(N+2)=4.0
      CALL LINE(HOLDX,HOLDY,N,1,5,1)
      N=NPTS(2)
      DO 120 I=1,N
      HOLDX(I)=X(I,2)
      HOLDY(I)=Y(I,2)
120   CONTINUE
      HOLDX(N+1)=0.0
      HOLDX(N+2)=0.05
      HOLDY(N+1)=0.0
      HOLDY(N+2)=4.0
      CALL LINE(HOLDX,HOLDY,N,1,5,2)
      GO TO 500
C
C ----DIFFERENCE PLOT
C
200   CALL AXIS(0.,0.,"DISTANCE FROM HOLE (IN.)",-24,9.,0.,-.05,.05)
      CALL AXIS(0.,0.,"DISPLACEMENT",12,7.,90.,-.001,.001)
      DO 210 I=1,101
      HOLDX(I)=XPL(I)
      HOLDY(I)=YDIF(I)
210   CONTINUE
      HOLDX(102)=-0.05
      HOLDX(103)=0.05
      HOLDY(102)=-0.001
      HOLDY(103)=0.001
      CALL LINE(HOLDX,HOLDY,101,1,0,0)
      CALL DASHLN(0.,1.,9.1,.042,.042)
      CALL DASHLN(1.,0.,1.,7.,.042,.042)
      GO TO 500
C
C ----STRAIN PLOT
C
300   CALL AXIS(0.,0.,"DISTANCE FROM HOLE (IN.)",-24,9.,0.,-.05,.05)
      CALL AXIS(0.,0.,"COMPRESSIVE STRAIN",18,7.,90.,-.01,.01)
      DO 310 I=1,100
      HOLDX(I)=XPL(I+1)
      HOLDY(I)=DY(I)
310   CONTINUE
      HOLDX(101)=-0.05
```

```
110   CONTINUE
      HOLDX(N+1)=0.0
      HOLDX(N+2)=0.05
      HOLDY(N+1)=0.0
      HOLDY(N+2)=4.0
      CALL LINE(HOLDX,HOLDY,N,1,5,1)
      N=NPTS(2)
      DO 120 I=1,N
      HOLDX(I)=X(I,2)
      HOLDY(I)=Y(I,2)
120   CONTINUE
      HOLDX(N+1)=0.0
      HOLDX(N+2)=0.05
      HOLDY(N+1)=0.0
      HOLDY(N+2)=4.0
      CALL LINE(HOLDX,HOLDY,N,1,5,2)
      GO TO 500
C
C ----DIFFERENCE PLOT
C
200   CALL AXIS(0.,0.,"DISTANCE FROM HOLE (IN.)",-24,9.,0.,-.05,.05)
      CALL AXIS(0.,0.,"DISPLACEMENT",12,7.,90.,-.001,.001)
      DO 210 I=1,101
      HOLDX(I)=XPL(I)
      HOLDY(I)=YDIF(I)
210   CONTINUE
      HOLDX(102)=-0.05
      HOLDX(103)=0.05
      HOLDY(102)=-0.001
      HOLDY(103)=0.001
      CALL LINE(HOLDX,HOLDY,101,1,0,0)
      CALL DASHLN(0.,1.,9.,1.,.042,.042)
      CALL DASHLN(1.,0.,1.,7.,.042,.042)
      GO TO 500
C
C ----STRAIN PLOT
C
300   CALL AXIS(0.,0.,"DISTANCE FROM HOLE (IN.)",-24,9.,0.,-.05,.05)
      CALL AXIS(0.,0.,"COMPRESSIVE STRAIN",18,7.,90.,-.01,.01)
      DO 310 I=1,100
      HOLDX(I)=XPL(I+1)
      HOLDY(I)=DY(I)
310   CONTINUE
      HOLDX(101)=-0.05
```

```
      HOLDX(102)=0.05
      HOLDY(101)=-0.01
      HOLDY(102)=0.01
      CALL LINE(HOLDX,HOLDY,100,1,0,0)
      CALL DASHLN(0.,1.,9.,1.,.042,.042)
      CALL DASHLN(1.,0.,1.,7.,.042,.042)
C
C
500   CALL SYMBOL(1.2,6.,.2,"SET NO. ",0.,8)
      CALL SYMBOL(2.8,6.,.2,ISET,0.,10)
      CALL PLOT(10.,8.,999)
      RETURN
      END
      SUBROUTINE PLOTH(IC,ISET)
      COMMON /STNAM/ ISTNAM(9),IST
      COMMON /PLOTER/ X(900),Y(900),II
      DIMENSION IBUF(257),XRAY(102),YRAY(102)
      DIMENSION XLEG(5),YLEG(5)
      NC=IC*100
      DO 1 I=1,NC
1     CONTINUE
C
C  ----INIT PLOTTING PARAMETERS
C
      CALL PLOTS(IBUF,257,0)
      XRAY(101)=-0.40
      XRAY(102)=0.08
      YRAY(101)=-0.03
      YRAY(102)=0.01
C
C  ----PRINT AXES AND TITLES
C
      CALL AXIS(0.,0.,"DISTANCE FROM HOLE (IN.)",-24,9.0,0.0,
     +XRAY(101),XRAY(102))
      CALL AXIS(0.,0.,"HOOP STRAIN",11,7.0,90.0,
     +YRAY(101),YRAY(102))
      CALL DASHLN(0.,3.,9.,3.,.042,.042)
      CALL DASHLN(5.,0.,5.,7.,.042,.042)
      CALL SYMBOL(1.2,6.,.2,"HOLE NO. ",0.,9)
      CALL SYMBOL(3.0,6.,.2,ISET,0.,10)
C  ----LEGEND INITIALIZATION
      CALL SYMBOL(7.2,6.6,0.2,"LEGEND",0.,6)
      CALL DASHLN(7.2,6.56,8.4,6.56,.014,.014)
      HTD=6.45
```

```
      XLEG(1)=7.0
      XLEG(2)=7.45
      XLEG(3)=7.9
      XLEG(4)=0.0
      XLEG(5)=1.0
      YLEG(4)=0.0
      YLEG(5)=1.0
C
C ----PRINT PLOT LINES
C
      DO 30 I=1,IC
      K=I-1
      N=100*K
      DO 20 J=1,100
      XRAY(J)=X(J+N)
      YRAY(J)=Y(J+N)
20    CONTINUE
      CALL LINE(XRAY,YRAY,100,1,5,K)
C ----PRINT LEGEND
      HTD=HTD-0.14
      YLEG(1)=HTD
      YLEG(2)=HTD
      YLEG(3)=HTD
      CALL LINE(XLEG,YLEG,3,1,1,K)
      CALL SYMBOL(8.1,HTD-.042,0.084,ISTNAM(I),0.,10)
30    CONTINUE
C ----COMPLETE LEGEND
      HTD=HTD-0.14
      CALL DASHLN(6.8,7.0,6.8,HTD,.014,.014)
      CALL DASHLN(6.8,HTD,9.0,HTD,.014,.014)
      CALL DASHLN(9.0,HTD,9.0,7.0,.014,.014)
      CALL DASHLN(9.0,7.0,6.8,7.0,.014,.014)
C
C ----EXIT PLOT ROUTINE
C
      CALL PLOT(12.0,0.0,999)
      RETURN
      END
      SUBROUTINE TPLOTR(IC,ISET)
      COMMON /STNAM/ ISTNAM(9),IST
      COMMON /PLOTER/ X(900),Y(900),II
      DIMENSION IBUF(257),XRAY(102),YRAY(102)
      DIMENSION XLEG(5),YLEG(5)
      NC=IC*100
```

```
      DO 1 I=1,NC
1     CONTINUE
C
C ----INIT PLOTTING PARAMETERS
C
      CALL PLOTS(IBUF,257,0)
      XRAY(101)=-0.05
      XRAY(102)=0.05
      YRAY(101)=-0.1
      YRAY(102)=0.025
C
C ----PRINT AXES AND TITLES
C
      CALL AXIS(0.,0.,"DISTANCE FROM HOLE (IN.)",-24,9.0,0.0,
     +XRAY(101),XRAY(102))
      CALL AXIS(0.,0.,"COMPRESSIVE STRAIN",18,7.0,90.0,
     +YRAY(101),YRAY(102))
      CALL DASHLN(0.,4.,9.,4.,.042,.042)
      CALL DASHLN(1.0,1.,7.,.042,.042)
      CALL SYMBOL(1.2,6.,0.2,"HOLE NO. ",0.,9)
      CALL SYMBOL(3.0,6.,0.2,ISET,0.,10)
C ----LEGEND INITIALIZATION
      CALL SYMBOL(7.2,6.6,0.2,"LEGEND",0.,6)
      CALL DASHLN(7.2,6.56,8.4,6.56,.014,.014)
      HTD=6.45
      XLEG(1)=7.0
      XLEG(2)=7.45
      XLEG(3)=7.9
      XLEG(4)=0.0
      XLEG(5)=1.0
      YLEG(4)=0.0
      YLEG(5)=1.0
C
C ----PRINT PLOT LINES
C
      DO 30 I=1,IC
      K=I-1
      N=100*K
      DO 20 J=1,100
      XRAY(J)=X(J+N)
      YRAY(J)=Y(J+N)
20    CONTINUE
      CALL LINE(XRAY,YRAY,100,1,5,K)
C ----PRINT LEGEND
```

```
      HTD=HTD-0.14
      YLEG(1)=HTD
      YLEG(2)=HTD
      YLEG(3)=HTD
      CALL LINE(XLEG,YLEG,3,1,1,K)
      CALL SYMBOL(8.1,HTD-.042,0.084,ISTNAM(I),0.,10)
30    CONTINUE
C ----COMPLETE LEGEND
      HTD=HTD-0.14
      CALL DASHLN(6.8,7.0,6.8,HTD,.014,.014)
      CALL DASHLN(6.8,HTD,9.0,HTD,.014,.014)
      CALL DASHLN(9.0,HTD,9.0,7.0,.014,.014)
      CALL DASHLN(9.0,7.0,6.8,7.0,.014,.014)
C
C ----EXIT PLOT ROUTINE
C
      CALL PLOT(12.0,0.0,999)
      RETURN
      END
      SUBROUTINE TPLOTM(IP,ISET)
      COMMON /INTP/ YINT(101,2)
      COMMON /DIFY/ YDIF(101),DY(100)
      COMMON X(80,2),Y(80,2),NPTS(2),XPL(101),XL,XH,YL,YH,XMIN,XMAX
      DIMENSION IBUF(257),HOLDX(103),HOLDY(103)
C
C ----INITIALIZE PLOT PARAMETERS
C
      CALL PLOTS(IBUF,257,0)
C
C ----DETERMINE PLOT TYPE
C
      IF(IP-2) 100,200,300
C
C ----BASIC PLOT
C
100   CALL AXIS(0.,0.,"X",-1,8.0,0.0,0.0,0.05)
      CALL AXIS(0.,0.,"FRINGE ORDER",12,6.0,90.0,0.0,4.0)
      N=NPTS(1)
      DO 110 I=1,N
      HOLDX(I)=X(I,1)
      HOLDY(I)=Y(I,1)
110   CONTINUE
      HOLDX(N+1)=0.0
      HOLDX(N+2)=0.05
```

```
      HOLDY(N+1)=0.0
      HOLDY(N+2)=4.0
      CALL LINE(HOLDX,HOLDY,N,1,5,1)
      N=NPTS(2)
      DO 120 I=1,N
      HOLDX(I)=X(I,2)
      HOLDY(I)=Y(I,2)
120   CONTINUE
      HOLDX(N+1)=0.0
      HOLDX(N+2)=0.05
      HOLDY(N+1)=0.0
      HOLDY(N+2)=4.0
      CALL LINE(HOLDX,HOLDY,N,1,5,2)
      GO TO 500
C
C ----DIFFERENCE PLOT
C
200   CALL AXIS(0.,0.,"DISTANCE FROM HOLE (IN.)",-24,9.,0.,-.05,.05)
      CALL AXIS(0.,0.,"DISPLACEMENT",12,7.,90.,-.001,.001)
      DO 210 I=1,101
      HOLDX(I)=XPL(I)
      HOLDY(I)=YDIF(I)
210   CONTINUE
      HOLDX(102)=-0.05
      HOLDX(103)=0.05
      HOLDY(102)=-0.001
      HOLDY(103)=0.001
      CALL LINE(HOLDX,HOLDY,101,1,0,0)
      CALL DASHLN(0.,1.,9.,1.,.042,.042)
      CALL DASHLN(1.,0.,1.,7.,.042,.042)
      GO TO 500
C
C ----STRAIN PLOT
C
300   CALL AXIS(0.,0.,"DISTANCE FROM HOLE (IN.)",-24,9.,0.,-.05,.05)
      CALL AXIS(0.,0.,"COMPRESSIVE STRAIN",18,7.,90.,-.01,.01)
      DO 310 I=1,100
      HOLDX(I)=XPL(I+1)
      HOLDY(I)=DY(I)
310   CONTINUE
      HOLDX(101)=-0.05
      HOLDX(102)=0.05
      HOLDY(101)=-0.1
      HOLDY(102)=0.025
```

```
      CALL LINE(HOLDX,HOLDY,100,1,0,C)
      CALL DASHLN(0.,4.,9.4,.042,.042)
      CALL DASHLN(1.,C.,1.,7.,.042,.042)
C
C
500   CALL SYMBOL(1.2,6..2,"SET NO. ",0.,8)
      CALL SYMBOL(2.8,6..2,ISET,0.,10)
      CALL PLOT(10.,8.,999)
      RETURN
      END
```

MICHIGAN STATE UNIVERSITY LIBRARIES
3 1293 03142 6822